ON THE DYNAMICS AND CONTROL OF MANIPULATORS WITH SLEWING AND DEPLOYABLE LINKS

Yuan Chen

B.Eng., Shanghai Jiao-Tong University, China, 1982
M.A.Sc., The University of British Columbia, Canada, 1993

A THESIS SUBMITTED IN PARTIAL FULFILMENT OF
THE REQUIREMENT FOR THE DEGREE OF

DOCTOR OF PHILOSOPHY

in

The Faculty of Graduate Studies
Department of Mechanical Engineering

We accept this thesis as conforming
to the required standard

The University of British Columbia

June 1999

In presenting this thesis in partial fulfillment of the requirements for an advanced degree at the University of British Columbia, I agree that the Library shall make it freely available for reference and study. I further agree that permission for extensive copying of this thesis for scholarly purposes may be granted by the head of my department or by his or her representatives. It is understood that copying or publication of this thesis for financial gain shall not be allowed without my written permission.

Department of Mechanical Engineering

The University of British Columbia

Vancouver, B.C. CANADA

Date: June 1999

ABSTRACT

Space manipulators present several features uncommon to ground-based robots: they are highly flexible, often mobile, and have a degree of redundancy. As space robots become more complex, effective formulation procedures and efficient algorithms are required to evaluate their performance. The present study aims at development of some basic tools and their application to assess dynamics and control of a novel, flexible, multi-module manipulator with slewing and deployable links. To begin with, a rather general three-dimensional, order N, Lagrangian formulation for the system is developed which accounts for interactions between orbital, librational, slew, deployment and elastic degrees of freedom. The versatile character of the formulation makes it applicable to a large class of manipulator systems of contemporary interest. Validity of the formulation and associated computer code is established through conservation of energy in the absence of dissipation.

A planar parametric study follows which provides better appreciation as to the influence of several important system variables, initial disturbances and maneuver profiles. Behaviour of a two-unit gross and fine manipulator is also discussed. Results suggest that the system flexibility could significantly affect the manipulator's performance, which may not be acceptable. This suggests a need for control.

A nonlinear controller based on the Feedback Linearization Technique (FLT) is developed to regulate rigid degrees of freedom which proves to be quite effective. Flexible generalized coordinates, though not actively controlled, are regulated through coupling. Optimal trajectory design for the gross-fine manipulator system with redundant degrees of freedom is also investigated.

Finally, the general formulation is reduced to represent the ground-based two-unit prototype manipulator thus demonstrating its wide scope of application. Simulation results for the ground-based system are obtained with the FLT control and compared with those given by the prototype. Considering the friction and backlash effects for the prototype, the correlation may be considered satisfactory.

Such a comprehensive investigation involving a novel configuration of the space-based manipulator, three-dimensional formulation, dynamics and controlled performance, as well as ground-based experiments on a prototype system is indeed rare. It should prove useful in the design of this new class of manipulators.

TABLE OF CONTENTS

LIST OF SYMBOLS

$C^L_{u,i}, C^L_{v,i}, C^L_{w,i}$	equivalent viscous damping coefficients for the longitudinal and transverse modes of vibration for the i^{th} body (module), respectively
$\boldsymbol{d}_i$	translation vector of the frame F_i from the tip of the (i^{th} - 1) body, Fig. 2-2
$\boldsymbol{D}_i$	inertial position vector to the frame F_i, Fig. 2-2
dm_i	mass of the infinitesimal element located on the i^{th} body, Fig. 2-2
e	energy conservation error, $(E_t - E_0)/E_0 = \Delta E/E_0$
$\boldsymbol{e}_i$	displacement of the frame F_i caused by the elastic deformation of the (i^{th} - 1) body, Fig. 4-2
E_0	initial total energy
E_t	instantaneous total energy
EA_i	product of the Young's modulus of the i^{th} body with its cross-sectional area
EI_d, EI_s	Flexural rigidity of deployable and slewing links, respectively
EI_p	Flexural rigidity of the platform
EI_i	flexural rigidity of the i^{th} body
$\boldsymbol{f}_i(\boldsymbol{r}_i)$	displacement of the mass element located at $\boldsymbol{r}_i$ due to body flexibility, Fig. 2-2
F	vector containing the terms associated with the centrifugal, Coriolis, gravitational, elastic, and internal dissipative forces, Eq. (1.1)
F_0	inertial reference frame
F_i	reference frame attached to the i^{th} body
$\mathcal{F}_i$	force provided by the linear actuator responsible for the deployment and retrieval of the i^{th} body

F_r	orbital reference frame, Fig. 2-1
$\boldsymbol{g}_i$	position vector to a mass element relative to the frame F_i accounting for deformation of the body i
h	altitude of the system
$\mathbf{I}^n$	$n \times n$ identity matrix
K	Stiffness of the revolute joint
$\mathbf{KA}_i$	matrix of admissible functions representing flexibility of body i
$\mathbf{KAD}_i$	matrix in which KA_i takes a derivative with respect to $\boldsymbol{d}_i$
$\mathbf{KAL}_i$	matrix in which KA_i takes a derivative with respect to l_i
$\mathbf{K}_p$, $\mathbf{K}_v$	diagonal control matrices containing the proportional and derivative gains, respectively
l_d, l_s	length of deployable and slewing links, respectively
l_i	length of the i^{th} body
l_p	length of the platform
LH, LV	local horizontal and local vertical, respectively
m_d, m_s	mass of deplyable and slewing links, respectively
m_i	mass of the i^{th} body
m_j	mass of the revolute joint
m_p	mass of the platform
$\mathbf{M}$	coupled system mass matrix
$\widetilde{\mathbf{M}}$	decoupled system mass matrix
$\widetilde{\mathbf{M}}_i$	decoupled mass matrix of the i^{th} body
$\mathbf{M}_r$, $\mathbf{F}_r$	respective values taken by $\mathbf{M}$ and $\mathbf{F}$ when the bodies are taken to be rigid

n_a	number of system actuators
n_c	number of system constraints
n_p	number of generalized coordinates describing the dynamics of the platform
n_u	number of generalized coordinates describing the dynamics of each unit
N	number of bodies (i.e. platform and manipulator units) in the system
$\boldsymbol{o}_j$	vector from frame F_{i-1} to frame F_i without the effect of flexibility
$O(N)$	order N
$\mathbf{P}^c$	matrix assigning the Lagrange multipliers to the constrained equations
$\boldsymbol{q}$	set of generalized coordinates leading to the coupled mass matrix $\mathbf{M}$, Eq. (1.1)
$\tilde{\boldsymbol{q}}$	set of generalized coordinates leading to the decoupled mass matrix $\tilde{\mathbf{M}}$
$\boldsymbol{q}_c$	controlled component of $\boldsymbol{q}$
$\boldsymbol{q}_d$	desired value of $\boldsymbol{q}_c$
$\tilde{\boldsymbol{q}}_i$	set of generalized coordinates, associated with the i^{th} body, leading to the decoupled mass matrix $\tilde{\mathbf{M}}_i$
$\boldsymbol{q}_s$	specified component of $\boldsymbol{q}$
$\boldsymbol{q}_u$	uncontrolled component of $\boldsymbol{q}$
$\mathbf{Q}$	vector containing the external non-conservative generalized forces, Eq. (1.1)
$\mathbf{Q}^d$	matrix assigning inputs to the actuated variables
$\mathbf{Q}_{LQR}$	LQR state weighting matrix
r, s	number of modes considered for the elastic deformation of the i^{th} body in the longitudinal and transverse directions, respectively
r_0	instantaneous distance of the platform's center of mass from the inertial reference frame F_0

r_i	position vector of the elemental mass dm_i with respect to F_i in absence of deformation of the body i
$\boldsymbol{R}_{a_i}$	inertial position vector of the actuator located at the i^{th} joint
R_d	Rayleigh dissipation function for the whole system
$\boldsymbol{R}_{dm_i}$	inertial position vector to the mass element dm_i located on the i^{th} body
$\mathbf{R}$, $\mathbf{R}^n$, $\mathbf{R}^v$	transformation matrices relating $\dot{\boldsymbol{q}}$ and $\dot{\tilde{\boldsymbol{q}}}$, Eqs. (2-46), (2-47), and (2-56)
t	time
T	total kinetic energy of the system
T_0, T_i	torques provided by control momentum gyros for attitude control and vibration suppression, respectively
$\mathbf{T}_i$	rotation matrix mapping F_0 onto F_i
T_i	torque provided by the slew-actuator located at the i^{th} joint
$\boldsymbol{u}$	vector containing the FLT control inputs
u_i, v_i	longitudinal and transverse components of $\boldsymbol{f}_i$, respectively
V_e	total strain energy of the system
V_g	total gravitational potential energy of the system
x_e, y_e	manipulator tip position with respect to F_1
x_i, y_i, z_i	cartesian components of $\boldsymbol{r}_i$
$\boldsymbol{x}_L$	state vector for the flexible subsystem

Greek Symbols

α_i, β_i, γ_i	rotations of the frame F_i caused by the control action of the actuator located at the i^{th} joint

$\chi_{i1}, \chi_{i2}, \chi_{i3}$ angular motion contributed by joint flexibility in three rotation directions defined by Fig. 2-3

δ_i vector containing time dependent generalized coordinates describing elastic deformation of the i^{th} body

ϕ_i actuator rotor angle of the revolute joint i with respect to F_{i-1}

$\Delta\tau$ time taken for maneuver

η_i inertial orientation of the actuator rotor on the i^{th} joint

θ true anomaly of the system

λ_i rotation of the i^{th} frame relative to the (i^{th} - 1) frame

λ_{ij} eigenvalue corresponding to the j^{th} vibrational mode of the i^{th} body

Λ vector containing the Lagrange multipliers

μ Earth's gravitational parameter

ξ_i rotation of F_i caused by the elastic deformation the (i^{th} - 1) body, Fig. 2-3

τ time from start of maneuver

$\Phi_i(x_i, l_i)$ matrix containing spatially varying shape functions for the i^{th} body

ψ platform's pitch angle

ψ_i inertial orientation of the frame F_i defined by the Euler angles

$\zeta_{i1}, \zeta_{i2}, \zeta_{i3}$ angles between F_i and F_{i-1}, Fig. 2-3

A dot above a character refers to differentiation with respect to time.

A boldface italic character denotes a vector quantity.

A boldface character denotes a matrix quantity.

Subscripts 'p' and 'd' correspond to the platform and deployable link, respectively. Subscript 's' refers to the slewing link or a specified coordinate.

LIST OF FIGURES

LIST OF TABLES

ACKNOWLEDGEMENT

I wish to express my sincere appreciation to those who directly or indirectly helped me during my involvement with the present research.

First, I wish to thank my supervisor Prof. Vinod J. Modi for his guidance and support throughout my graduate studies. His invaluable insight on wide variety of subjects greatly enriched my knowledge and took me to a new level.

I wish to thank my supervisor Prof. C. W. de Silva. I have known him in person since the fist day I arrived in Canada. His help and encouragement guided me through many difficulties and obstacles.

I wish to express my sincere appreciation to Prof. Seiya Ueno from Yokohama National University, Japan. During his stay at UBC during 1997-1998 (10 months), we had many valuable discussions which gave me further understanding in control and optimization issues.

Thanks are also due to my past and present colleagues and friends from all around the world. In the alphabetical order I wish to thank: Mr. Yang Cao, Mr. Mathieu Caron, Mr. Jooyeol Choi, Mr. Mark Chu, Mr. Vijay Deshpande, Mr. Jean-François Goulet, Mr. Vincent Den Hertog, Dr. Shinji Hokamoto, Mr. Spiros Kalantzis, Dr. Sandeep Munshi, Dr. Alfred Ng, Mr. Behara Patnaik, Dr. Satyabrata Pradhan, Dr. Mae Seto, Dr. Afzel Suleman, Mr. Kenneth Wong, and Mr. Jian Zhang. They have shared their knowledge, experience, and culture with me and have thus broadened my horizons. They have made my stay in the University of British Columbia very enjoyable.

Funding for this research has been provided through a Strategic Research Grant from the Natural Sciences and Engineering Research Council of Canada jointly held by Dr. de Silva and Dr. Modi at the University of British Columbia, and Dr. A.K. Misra at McGill University. Further funding for parts of the work has been received from the IRIS Network of Centres of Excellence Program, Part II.

To My Parents 陈欣生，经稚英.

To My Lovely Wife Liana Chen (陈超英)

and

Daughter Cheney Chen (陈辰).

1. INTRODUCTION

1.1 Preliminary Remarks

The term robot is derived from the Czech word robota, meaning "compulsory labor." It was first used in the 1921 play "Rossum's Universal Robots" by the Czech novelist and playwright Karel Capek. The word described a mechanical device that looked human but, lacking human sensibility, could perform only automatic, mechanical operations. Ever since, engineers have tried to adapt robot like devices to useful tasks. In the mid-1970s, General Motors financed a development program in which Massachusetts Institute of Technology researcher Victor Scheinman expanded upon a motor-driven "arm" he had invented to produce a so-called "Programmable Universal Manipulator for Assembly," or PUMA. The PUMAs that resulted mark the beginning of the age of robots in North America. In 1997, there were around 712,000 industrial robots in operation. As can be anticipated, approximately 413,000 were in Japan – one for every 36 workers. In Toyota's car assembly plant, one literally has to search to notice workers because their role has changed to checking and maintaining tuned conditions of robots.

Robotic systems have been used in space as early as the 1960's [1]. In the late 60's, unmanned Surveyor lunar mission used a rudimentary manipulator arm to dig and collect soil samples. The versatility of the space robots was demonstrated during the Surveyor 7 mission where the manipulator was employed to jab open an instrument that had failed to deploy automatically. In 1970, and again in 1973, the Soviet Lunakhod rovers surveyed large areas of the moon and used a deployable arm to lower an instrumentation package to the surface. The Viking landers, in 1976, used robotic manipulators to collect and process Martian soil samples.

The Canadian contribution to space robotics has been through the now famous Canadarm, introduced in 1981. It has played diverse, significant roles in almost all NASA's Space Shuttle missions: platform to support astronauts; position experiment modules; satellite launch and retrieval; loosened a jammed solar panel; even knocked-off a block of ice from a clogged waste water vent [2]. Perhaps its most dramatic success came in 1993 when it successfully retrieved the malfunctioning Habble Telescope, placed it in the cargo bay for repair and relaunched it. In December 1998, it assisted in the integration of the U.S. "Unity" module with the Russian control module called "Zarya" (Sunrise), launched a few weeks earlier, thus initiating construction of the International Space Station.

For the Space Station, which is scheduled to be operational in year 2004, the Canadian contribution is through an extension of the Canadarm in the form of Mobile Servicing System (MSS, Figure 1-1). It consist of the Space Station Remote Manipulator System (SSRMS) and Special Purpose Dexterous Manipulator (SPDM). The MSS will play an important role in the construction, operation, and maintenance of the space station [3-5]. It will also assist in the Space Shuttle docking maneuvers; handle cargo; as well as assemble, release, and retrieve satellites.

A number of other space robots have been proposed and some are under development. The American Extravehicular Activity Helper/Retriever (EVAHR) and Ranger Telerobotic Flight Experiment, as well as the Japanese ETS-VII, are examples of free-flying telerobotic systems which will be used for satellite inspection, servicing and retrieval [6,7]. Thus manipulators are serving as a useful tool in the space exploration. All indications suggest the trend to accentuate with future missions becoming more dependent on

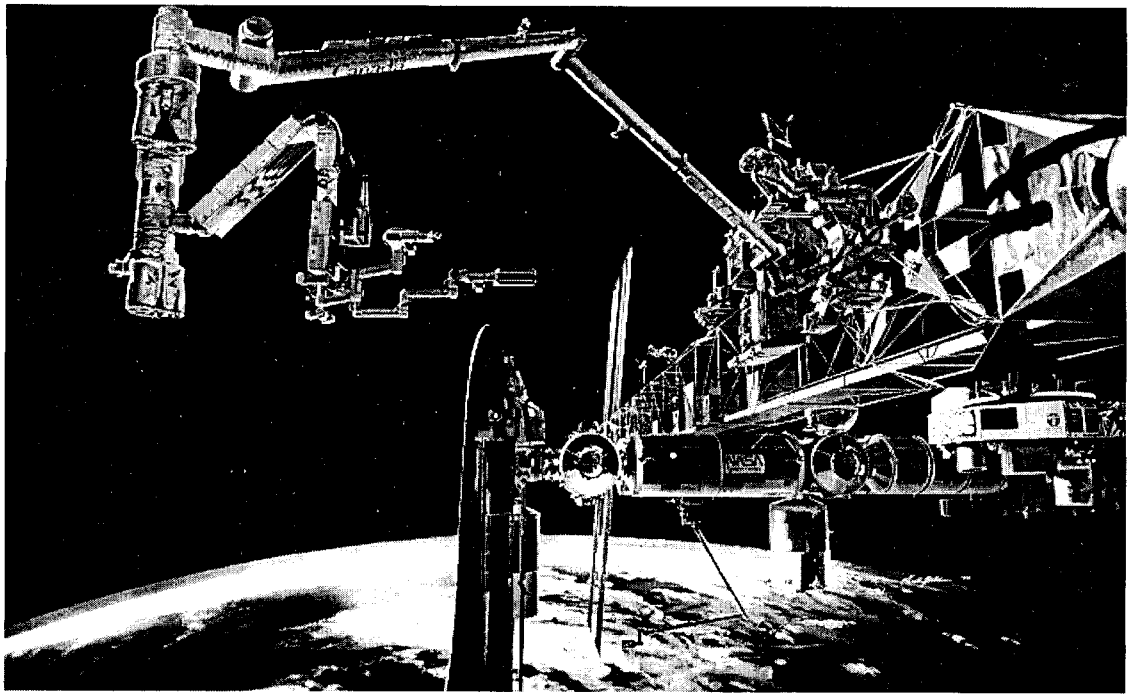

Figure 1-1 Artist view of the International Space Station with its Mobile Servicing System (MSS) as prepared by the Canadian Space Agency.

robotic systems. As the Space Station will operate in the harsh environment at an altitude of 400 km, it is desirable to minimize extravehicular activity by astronauts. Robotics is identified as one of the key technologies to reach that goal. It is important to point out that all the space-based robotic devices mentioned above use revolute joints, i.e. links are free to undergo slewing motion (Figure 1-2), as in the case of the Canadarm and MSS abode the International Space Station.

With this as background, the thesis undertakes a study aimed at a novel flexible multimodule manipulator capable of varying its geometry. Each module consists of two links (Figure 1-3a), one free to slew (revolute joint) while the other is permitted to deploy and retrieve (prismatic joint). A combination of such modules can lead to a snakelike variable geometry manipulator (Figure 1-3b) with several advantages [8]. It reduces coupling effects

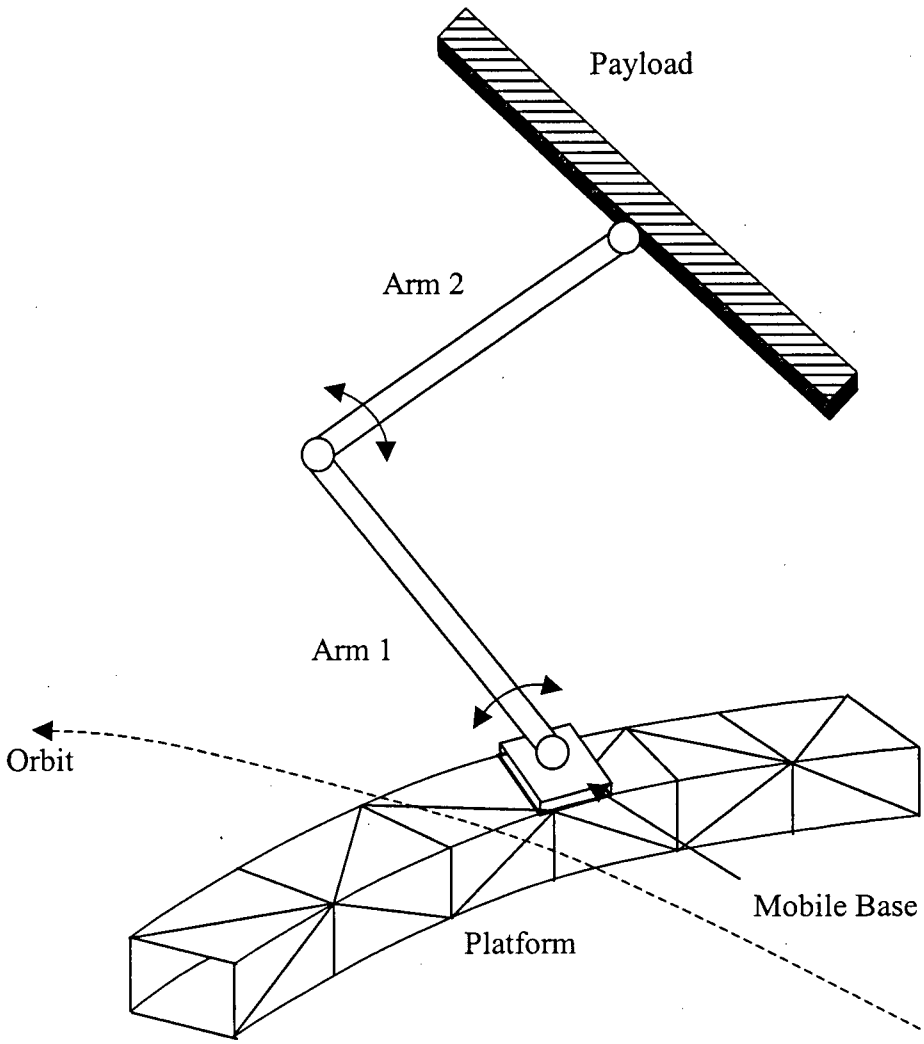

Figure 1-2 All the space-based manipulators have used, so far, revolute joints thus permitting only slewing motion of links.

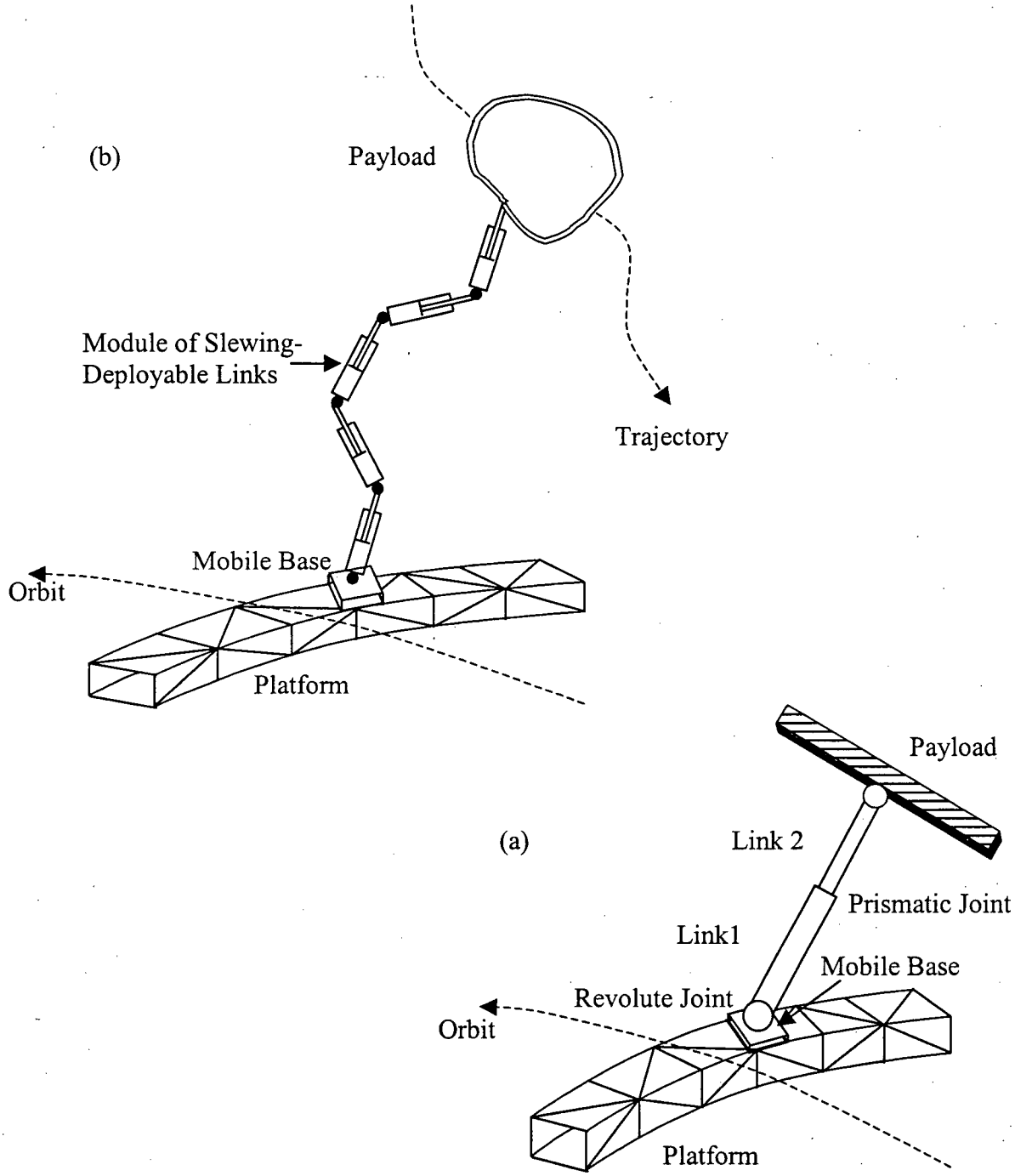

Figure 1-3 Variable geometry manipulator showing: (a) single module with a pair of slewing and deployable links; (b) several modules connected to form a snakelike geometry.

resulting in relatively simpler equations of motion and inverse kinematics, decreases the number of singularities, and facilitates obstacle avoidance (Figure 1-4). Dynamics and control of such Multi-module Deployable Manipulator System (MDMS), free to traverse an orbiting elastic platform and carrying a payload, represent a challenging task.

1.2 A Brief Review of the Relevant Literature

As can be expected, the amount of literature available on the subject of robotics is literally enormous. The objective here is to touch upon contributions directly relevant to the study in hand.

1.2.1 Characteristics of space-based manipulators

There are several significant differences between the orbiting space platform supported manipulators and their ground-based counterparts:

(a) Due to zero weight condition at the system center of mass and microgravity field elsewhere, the environmental torques due to gravity gradient, Earth's magnetic field and solar radiations can become significant in the study of space manipulators [9]. The large temperature variations encountered in space may significantly affect the system dynamics and control due to thermal deformations [10,11].

(b) As the manipulator rests on a flexible orbiting platform, their dynamics are coupled [12,13]. The manipulator maneuvers can affect attitude of the platform as well as excite it to vibrate [14]. Conversely, the librational motion of the platform would affect the manipulator's performance. Fortunately, manipulator maneuvers in space tend to be relatively slow permitting the end-effector to approach equilibrium [15].

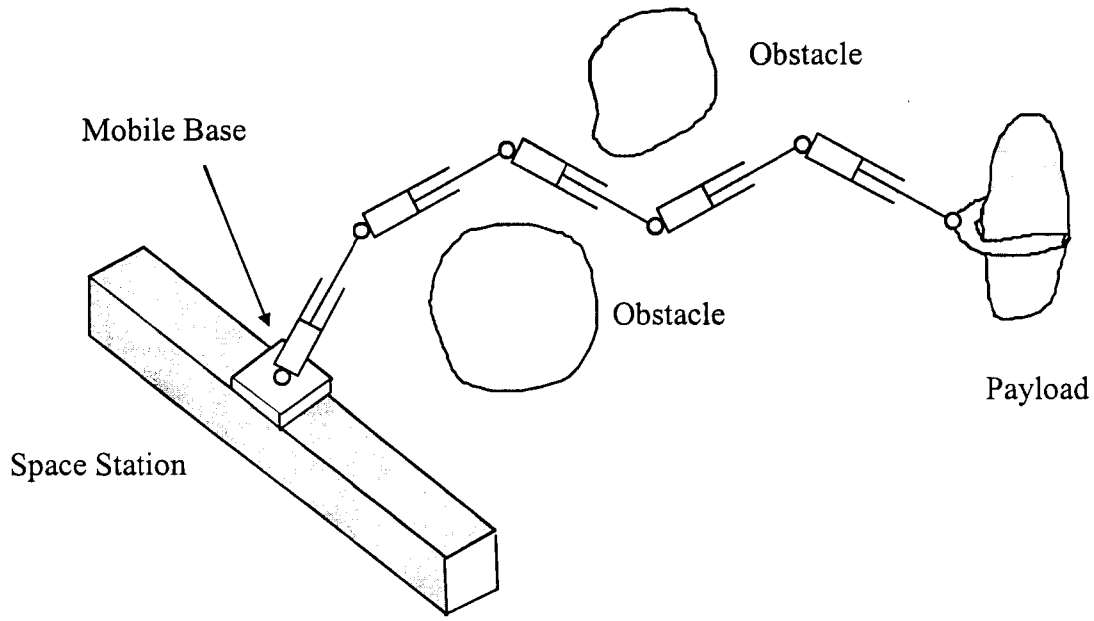

Figure 1-4 Variable geometry manipulator showing obstacle avoidance character.

(c) Space manipulators tend to be large in size, lighter and highly flexible. Obviously, this will make the study of system dynamics , and its control, a formidable task.

(d) The ratio of the payload to manipulator mass for a typical space-based system can be several orders of magnitude higher [16]. For example, in case of the Canadarm the ratio is 61.5. The corresponding ground based manipulator used in nuclear industry (supplied by the same manufacturer) has the payload to manipulator mass ratio of 0.167 !

(e) Obviously, space manipulators are not readily accessible for repair in case of, say, joint failure. This requires incorporation of a level of redundancy in their design [17]. Correspondingly, more degrees of freedom are involved than required for a given task.

(f) Remote operation of a space-based manipulator would involve time delay, an important factor in control of the system. For the ROTEX teleoperation experiment it reached seven seconds [18] !

These important differences emphasize the fact that one cannot entirely rely on the vast body of literature available for ground-based manipulators. We will have to explore and understand distinctive character of the space robotic systems. Dynamics and control of a large orbiting flexible platform (like the International Space Station), supporting a mobile elastic manipulator, carrying a compliant payload represent a class of problems never encountered before. Major challenges presented by such large-scale systems are summarized in Figure 1-5. It is only recently, some of the issues mentioned here have started to receive attention. Obviously, there is an enormous task facing space dynamicists and control engineers that will keep them occupied for years to come. The points which concern us are

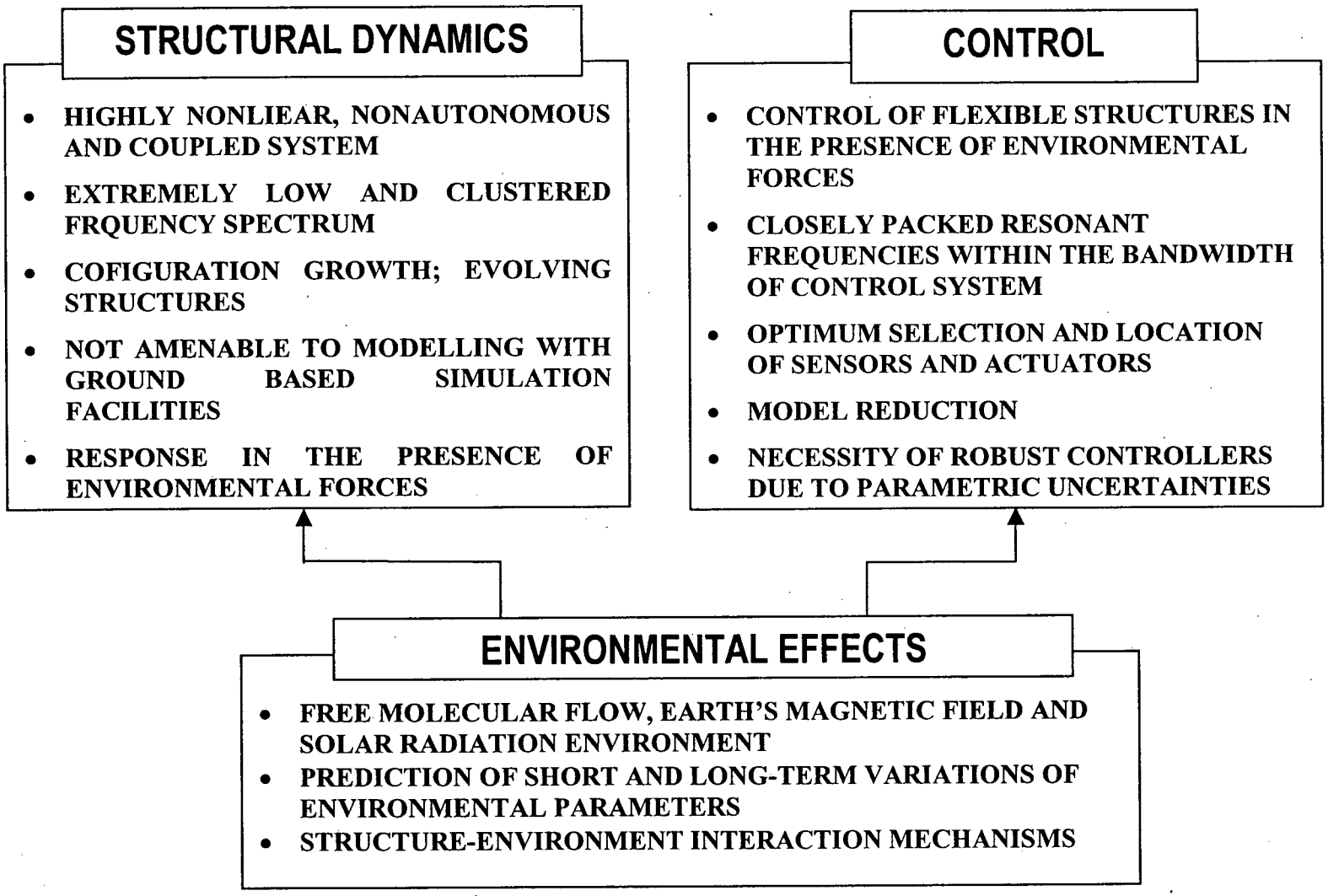

Figure 1-5 Challenges faced by studies aimed at dynamics and control of large, space-based systems

the nonlinear, nonautonomous and coupled character of the governing equations of motion, relatively low frequencies, and development of a controller, preferably robust.

1.2.2 Dynamics of space-based manipulators

From the observations made earlier, it is apparent that space manipulators, as well as large flexible space structures in general, have unveiled a new and challenging field of spacedynamics and control. Over the years, a large body of literature has evolved, which has been reviewed quite effectively by a number of authors including Meirovitch and Kwak [19], Roberson [20], Likins [21], as well as Modi *et al.* [22 - 26]. Dubowski and Papadopoulos have discussed the important problems associated with the dynamics and control of space robots and reviewed the advances made in this field [27,28]. They concluded that a thorough understanding of the fundamental dynamics of these systems would result in effective solutions to their control problems. For this purpose, they introduced the concept of "virtual manipulator" to describe the dynamics of space robots. Other authors have also emphasized the need for realistic dynamic modelling for the precise and accurate control of space robotic systems [29,30]. The desirability for accurate mathematical models is further emphasized by the prohibitive cost of conducting dynamic experiments in orbit and the virtual impossibility of simulating the space environment on the ground.

Development of relatively general computer codes for studying dynamics of multibody systems, like the space station and multilink manipulators, have also received some attention. Dynamic simulation codes such as DISCOS [31], *treetops* [32], and several others are publicly available. However, the inherent limitations of these software have prompted several researchers to develop their own computer codes.

Pascal developed a simplified model for a flexible space manipulator based on a servicing satellite [33]. She then used this model to study the dynamics and control of the robot while grasping another satellite. Chan investigated the planar dynamics of a two-link manipulator located on a base free to translate on a space platform [34]. Although flexibility effects were included in the manipulator links and joints, the platform was assumed to be rigid. Mah derived the equations of motion of a general flexible multibody system in chain topology [35]. He used this model to study the dynamics of a general manipulator based on an orbiting platform, both considered flexible. The studies mentioned so far focused on open-chain configurations. On the other hand, Lilly and Bonaventura developed a generalized formulation for the simulation of space robots in either open- or closed-chain geometry [36].

Xu and Shum investigated the coupling between the motion of the manipulator and supporting platform [13]. They proposed a coupling factor representing the degree of dynamic interactions between the two. It was suggested that the coupling factor might serve as a performance index for optimizing robot configuration and location to reduce base motion. Papadopoulos focused on large payload manipulation [37]. The effects of satellite capture, berthing, docking, and other types of impacts on the dynamics of the platform/manipulator system have also received some attention [38,39].

In the above-mentioned studies aimed at manipulators, only revolute joints were involved, i.e. links were permitted to undergo slewing motion. On the other hand, several space structures feature deployment capabilities. For instance, a large solar array was deployed from the Space Shuttle cargo-bay during the Solar Array Flight Experiment (SAFE), in September 1984. Cherchas [40], as well as Sellappan and Bainum [41], studied the deployment dynamics of extensible booms from spinning spacecraft. Modi and Ibrahim

developed the equations of motion for a system with multiple booms (beams) deploying from a central rigid body, with considerable emphasis on the proposed Waves In Space Plasma (WISP) experiment [42]. Subsequently, Modi and Shen [43] extended the study to permit the slewing degree of freedom to deploying appendages. About the same time, Marom proposed a two-link, deployable manipulator and investigated its planar dynamics and control [44]. Here, the manipulator links were taken to be rigid, however, the joint flexibility was accounted for. Hokamoto *et al.* extended this model by accounting for an arbitrary number of flexible links [45]. Recently, Caron *et al.* developed a relatively general model for studying planar dynamics of a space-based manipulator with slewing and deployable links. A parametric analysis of the system dynamics showed significant coupling between the rigid-body motion and structural vibration [46].

A subject of considerable importance is the effect of manipulator maneuvers on the dynamics of the supporting platform. Presence of redundancy is often desirable in order to cope with partial failure of joints. As pointed out by de Silva [47], redundancy can also be used, quite effectively, to isolate dynamic coupling between manipulator maneuvers and the supporting platform, or between links.

1.2.3 Formulation of multibody systems

Dynamical formulation of multibody systems can be approached in a variety of ways. Major among these are: application of d'Alembert principle, Newton-Euler method, Lagrangian approach, and Hamilton's principle. Of these, the Newton-Euler method and Lagrangian approach have been more popular. The former, involving freebody analysis, is attractive for relatively simple rigid systems having a small number of degrees of freedom.

However, for a flexible system with moving center of mass and a large number of degrees of freedom, its application, without approximations, presents a challenge. Under such situations, the Lagrangian approach is preferred. It has well-established energy-based methodology, does not suffer form any limitations, and satisfies both holonomic (implicitly) and nonholonomic constraints (through Lagrange multipliers). Furthermore, energy expressions can be used to validate the formulation and corresponding numerical code.

The equations governing dynamics of robotic systems may be expressed in the general form as

$$\mathbf{M}(\boldsymbol{q},t)\ddot{\boldsymbol{q}} + \boldsymbol{F}(\dot{\boldsymbol{q}},\boldsymbol{q},t) = \boldsymbol{Q}(\dot{\boldsymbol{q}},\boldsymbol{q},t) \ , \tag{1.1}$$

where: $\mathbf{M}(\boldsymbol{q},t)$ is the system mass matrix; $\boldsymbol{q}$, the vector of the generalized coordinates; $\boldsymbol{F}(\dot{\boldsymbol{q}},\boldsymbol{q},t)$ contains the nonlinear terms associated with the centrifugal, Coriolis, gravitational, elastic, and internal dissipative forces; and $\boldsymbol{Q}(\dot{\boldsymbol{q}},\boldsymbol{q},t)$ represents generalized forces, including control inputs. Equation (1.1) describes the inverse dynamics of the system. For simulations, forward dynamics of the system is required, i.e. Eq. (1.1) must be solved for $\ddot{\boldsymbol{q}}$,

$$\ddot{\boldsymbol{q}} = \mathbf{M}^{-1}(\boldsymbol{Q} - \boldsymbol{F}). \tag{1.2}$$

The solution of these equations of motion generally requires $O(N^3)$ arithmetic operations, where N represents the number of bodies considered in the study. In other words, the number of computations required by an $O(N^3)$ algorithm will vary with the cube of the number of bodies. Clearly, the computational cost can become prohibitive for a large N. This is particularly true with a manipulator system that has redundant degrees of freedom. Hence, development of an $O(N)$ algorithm, where the number of arithmetic operations increases

linearly with the number of bodies (or degrees of freedom) in the system, has been the focus of several studies in the field of multibody dynamics.

Hollerbach has proposed a recursive $O(N)$ Lagrangian formulation for the inverse dynamics of rigid multibody systems [48], which makes real-time applications possible. It should be noted that the forward dynamics of the same model is not of $O(N)$. Keat has used a velocity transformation approach to obtain an $O(N)$ algorithm describing the dynamics of flexible multibody systems [49]. Rosenthal has based his $O(N)$ formulation, which considers rigid bodies, on Kane's equations [50]. Suzuki and Kojima applied this approach to analyze the deployment of a spacecraft panel [51]. Banerjee extended Rosenthal's algorithm in order to consider deployment and retrieval of beams with large bending and rotation [52]. Jain and Rodriguez used the filtering and smoothing approach of optimal estimation, and introduced spatial operators to obtain a recursive $O(N)$ formulation for flexible multibody systems [53]. On the other hand, Bae and Haug adopted an approach based on the virtual work to the same end [54].

Most $O(N)$ formulations reported in the literature are recursive: they rely on a series of forward and backward passes along the chain of bodies in order to compute accelerations and forces in the system. The main advantage of a nonrecursive formulation is that the computations for each body can be executed independently making it suitable for parallel processing. Pradhan *et al.* [55] have introduced a nonrecursive formulation procedure for flexible multibody systems, which uses the Lagrangian approach, in conjunction with two velocity transformations. The velocity transforms decompose the system mass matrix into a product of matrices. The inversion of this new form of the mass matrix is computationally far

less intensive. As most arithmetic operations in Eq. (1.2) arise from the inversion of the mass matrix, the resulting algorithm is of $O(N)$ and hence considerably more efficient.

1.2.4 Control of space-based manipulators

In the recent past, experiments have been carried out in orbit to investigate the dynamics and control of robots, as well as large flexible structures. The goal of the Spacecraft COntrol Laboratory Experiment (SCOLE) was to control a reflector antenna supported by a beam, located in the Space Shuttle cargo bay, during slewing maneuvers [56]. Although tests were carried out on the ground, the experiment was not flown. The German ROTEX experiment took place during the Spacelab II mission: A robotic manipulator, located on the Shuttle Orbiter, was teleoperated from the ground to conduct various maneuvers, including the capture of floating objects [57].

Precise and efficient dynamical models are required for the control of space robotic systems. The attitude of the space platform, the motion of the manipulator links, the location of the manipulator base along the platform, as well as the vibration of the various structural components must be controlled to an acceptable level for successful completion of a given mission.

Relatively coarse control of the space platform's attitude can be achieved even by use of the environmental forces such as Earth's gravity gradient and magnetic fields [9]. For instance, the "long" axis (i.e. the axis of minimum moment of inertia) of the platform may be aligned with the local vertical direction. This stable equilibrium configuration can be used to advantage. However, normally thrusters and Control Momentum Gyros (CMGs) are used to regulate the attitude of the system [58,59]. Librational control of the platform by reorienting

the manipulator has also been suggested [60]. However, this method is limited to cases where the mass of the manipulator is significant compared to that of the platform.

As mentioned earlier, the orbiting platform and the manipulator links can be highly flexible. Moreover, the compliance of the actuator shafts and transmission drives may lead to significant flexibility of the joints. Undesirable vibrations can arise and the accuracy of the manipulator can be severely affected. Consequently, control of manipulators with flexible links, flexible joints, or both, have also received some attention [61-63]. Structural damping, as well as other passive dampers can reduce the amount of vibrations experienced. However, active vibration suppression is often desirable. Through adequate path planning of the manipulator joints, excessive elastic deformations as well as attitude disturbances can be avoided. As pointed out earlier, redundant degrees of freedom provided by manipulators can be used to advantage in isolating the base from disturbances arising from the manipulator motion [47,64]. In fact, Hanson and Tolson have shown that the base reaction could be decreased by as much as 90% with such schemes [65]. Vibration of the manipulator links and joints can also be reduced by applying compensating torques at the revolute joints [34]. The use of distributed piezoelectric films or lumped piezoelectric elements acting as collocated sensor/actuator systems has also been suggested for vibration control [66].

Several strategies are available for the control of space robotic systems. Often, simple proportional-derivative (PD) feedback control schemes are adequate [67]. The computed torque technique has been widely used for ground-based robots [68,69]. The Feedback Linearization Technique (FLT) has been proposed for the attitude control of the platform, as well as for the control of the rigid motion of the manipulator [70]. Optimal control has also received considerable attention. Here, position and velocity errors, actuator outputs,

structural vibration, as well as various other cost functions are minimized throughout the operation of the system. When all state variables are available, a Linear Quadratic Regulator (LQR) may be used for optimal control [71,72]. If these quantities are not directly available, but are observable, a Linear Quadratic Gaussian (LQG) controller has been proposed [73,74]. The field is wide open to other control procedures including adaptive, knowledge-based and fuzzy logic strategies, to mention a few.

1.3 Scope of the Investigation

In the present investigation, an efficient mathematical model is developed for studying the three-dimensional dynamics and control of a flexible, space-based manipulator (Figure 1-3b). The relatively general nature of the model considers a serial manipulator with an arbitrary number (N) of flexible modules. Each module is free to rotate, i.e. *slew,* and is capable of changing its length, thus is *deployable.*

The formulation provides for arbitrary variation of geometric, inertia, stiffness, and damping characteristics along the manipulator. The manipulator is mounted on a mobile base which is free to translate along an orbiting space platform. The coupling effects between the orbital, librational, slew, deployment, and vibrational degrees of freedom, associated with the platform and manipulator, are also taken into account. An essential feature of the model is the time-varying length of each unit, with prismatic joints providing the deployment degrees of freedom. As each of the manipulator units can be deployed and retrieved independently, there is a machanism for changing the librational and vibrational characteristics of the system. Note, the model considered here is rather general and is applicable to a large class of

systems. A number of existing space- and ground-based manipulators become particular cases of the general model developed here.

In Chapter 2, the governing equations of motion are derived, using the Lagrangian procedure and $O(N)$ approach, for spatial operation of the manipulator. It also includes an explanation of Lagrange multipliers to account for constraint forces.

Chapter 3 discusses development of a FORTRAN code for integration of the equations of motion. The structure of the program is presented and computational issues are discussed. Validity of the formulation and computer code is checked through the conservation of energy for a few test-cases.

A comprehensive parametric study is presented in Chapter 4. The effects of various sets of initial disturbances, parameter combinations, manipulator maneuvers, and manipulator configurations are assessed. It also evaluates, for a particular case, improvement in computational efficiency due to $O(N)$ character of the formulation. Results suggest that under some combinations of system parameters and disturbances the response may not confirm to the acceptable limit. This points to a need for active control.

The performance of a nonlinear control strategy, based on the Feedback Linearization Technique (FLT), is assessed in Chapter 5. It successfully regulates the attitude of the platform, as well as the rigid-body maneuvers of the single module manipulator.

Chapter 6 focuses on reduction of coupling between modules which, in turn, decreases transmission of force and moment to the platform during trajectory tracking. A two-module manipulator is considered and effects of module mass ratio as well as force/moment weighting function are investigated.

In Chapter 7, the general equations of motion developed in Chapter 2 are reduced for application to the ground-based, two-module manipulator constructed by Chu [8]. Effectiveness of the PID and FLT control procedures is assessed on the prototype performing several trajectory-tracking maneuvers and results are compared with the corresponding numerical simulation data.

Finally, Chapter 8 summarizes the important findings of this thesis, outlines its contributions, and suggests future avenues of investigation.

2. FORMULATION OF THE PROBLEM

2.1 Introductory Remarks

As pointed out before, the thesis aims at studying dynamics and control of a novel manipulator. The distinctive character of the manipulator lies in its module with slewing as well as deployable links (Figure 1-3). This combination of revolute and prismatic joints in a manipulator design for space application has received virtually no attention although, as mentioned earlier, it presents several important advantages. Significant features of the system under study may be summarized as below:

(a) The manipulator with an arbitrary number of modules, each with a slewing and a deployable link thus involving both revolute and prismatic joints, is supported by a mobile base free to traverse a platform. The platform is in an orbit around Earth.

(b) The supporting platform, manipulator modules and revolute joints are treated as flexible. Prismatic joints are considered as integral parts of modules.

(c) The module is permitted to have variable mass density, flexural rigidity and cross-sectional area along its length.

(d) The system is permitted to undergo three-dimensional librational as well as vibrational motions. The slewing maneuver at any joint can also be spatial.

(e) The damping is accounted for through Rayleigh's dissipation function.

(f) The governing equations account for gravity gradient effects, shift in center of mass and change in inertia due to maneuvers.

Note, the model considered is rather general and applicable to a large class of space as well as ground-based manipulator systems. The Canadarm and the MSS on board the International Space Station are particular cases of the model.

The Lagrangian approach adopted here for derivation of the governing equations is particularly well suited for the flexible multibody system, with a large number of degrees of freedom, under consideration. It automatically satisfies holonomic constraints while the nonholonomic constraints can be accounted for, quite readily, using Lagrange multipliers. The form of the equations of motion conveys a clear physical meaning in terms of contributing forces. Equally important is the fact that the equations are readily amenable to stability study and well suited for controller design.

As pointed out in Chapter 1, dynamics of a robotic system is governed by an equation of the form

$$\mathbf{M}(q,t)\ddot{q} + F(\dot{q},q,t) = Q(\dot{q},q,t)\ , \tag{2.1}$$

i.e.
$$\ddot{q} = \mathbf{M}^{-1}(Q - F). \tag{2.2}$$

where: $\mathbf{M}(q,t)$ is the system mass matrix; q is the vector of the generalized coordinates; $F(\dot{q},q,t)$ contains the nonlinear terms associated with the centrifugal, Coriolis, gravitational, elastic, and internal dissipative forces; and $Q(\dot{q},q,t)$ represents generalized forces, including control inputs. Computational demand associated with the evaluation of $\mathbf{M}^{-1}$ was indicated, and advantage of the order N formulation procedure was emphasized. Such algorithm would reduce the computational time and memory requirements considerably making the real-time applications possible.

This chapter focuses on the Order N, Lagragian formulation approach.

2.2 Kinematics of the System

2.2.1 Reference frames

The mobile manipulator with an arbitrary number of modules (bodies) is supported by a platform orbiting around Earth. To help appreciate notation for such a general system, let us consider a simple case of the manipulator with one module (Figure 2-1). Note, body 1 refers to the orbiting platform and body 2 represents module 1 of the manipulator, supported by the mobile base.

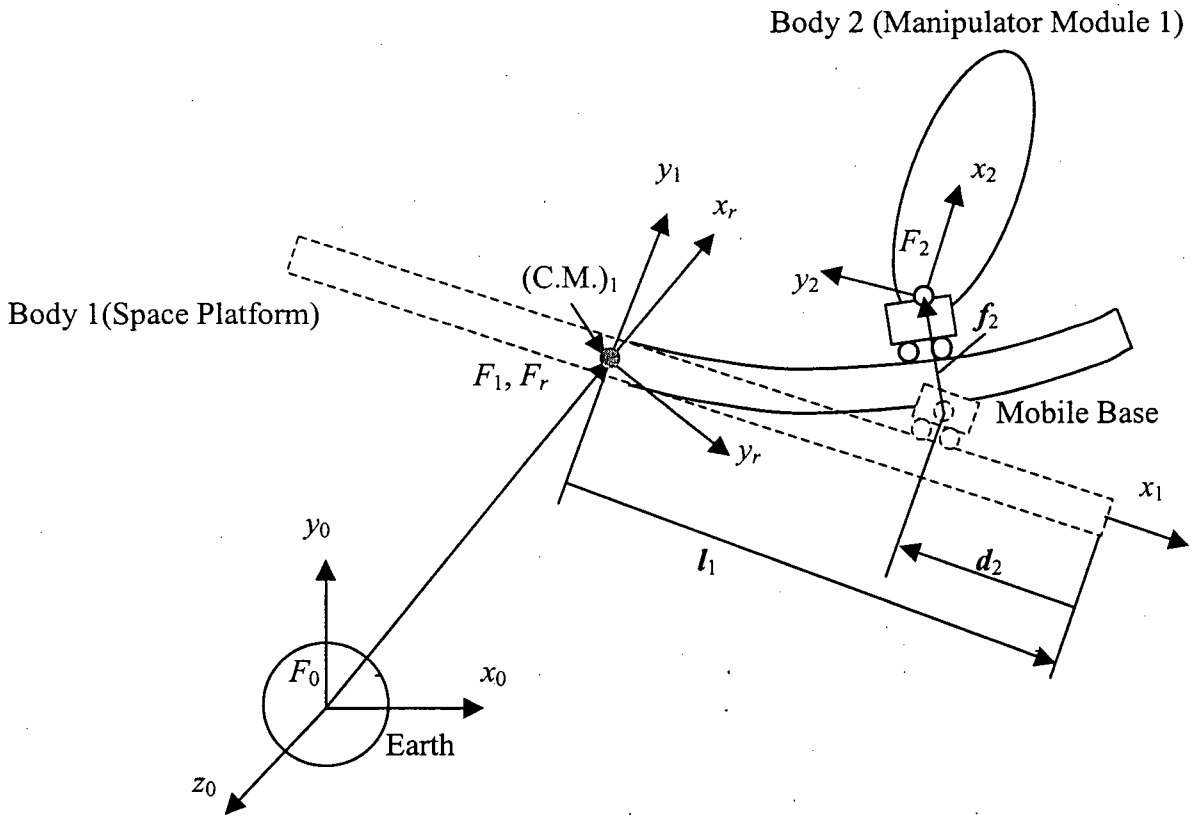

Figure 2-1 Simplified system showing a space platform supporting one-module manipulator.

The inertial frame F_0 is located at the center of Earth. The x_0, y_0-axes establish the orbital plane and z_0 represents the orbit normal. The position and attitude of each body are described by the body-fixed frames F_1 and F_2. The frame F_1 has its origin at the center of mass of the platform while F_2 is attached to body 2 at the joint with the mobile base. As the platform and manipulator modules are considered to be beam-type structures, the x_1 is taken along the beam axis, y_1 is perpendicular to x_1 in the orbital plane and z_1 completes the orthogonal triad according to the right hand rule. For a massive platform, as in the case of the International Space Station, the system center of mass will essentially coincide with the platform center of mass. However, the present formulation accounts for their distinct identity.

The orbital reference frame F_r has its origin at the center of mass $(\text{C.M.})_1$ of the platform. Here, x_r is along the local vertical, y_r is aligned with the local horizontal, and z_r is the orbit normal. Thus relative motion between the F_1 and F_r frames corresponds to the platform's librational motion (pitch, roll and yaw).

The base provides for the translational motion of body 2 (manipulator) on body 1 (platform). Such motion of the Mobile Servicing System (MSS) will be present on the International Space Station and hence must be accounted for in the formulation. So a word about the position of the base on the deflected configuration of the platform would be appropriate. This is specified by the three vectors: $\boldsymbol{l}_1$, $\boldsymbol{d}_2$, and $\boldsymbol{f}_2$. Here $\boldsymbol{l}_1$ represents distance from the $(\text{C.M.})_1$ to the tip of the platform; $\boldsymbol{d}_2$ is measured from the platform tip to the mobile base when the platform is undeformed; and $\boldsymbol{f}_2$ corresponds to deflection of the platform at the location of the base. Thus $\boldsymbol{l}_1 + \boldsymbol{d}_2 + \boldsymbol{f}_2$ gives position of the base (i.e. origin of the frame F_2) with respect to the center of mass of the platform. To keep the formulation general, such relative translational motion between adjacent bodies is permitted throughout the chain,

although normally it will be present only between bodies 1 and 2. The relative translational motion, when not present, can be eliminated quite readily by the introduction of constraints through Lagrange multipliers.

With these introductory comments, consider the chain-type manipulator with N bodies as shown in (Figure 2-2). As before, body 1 represents the platform, while the remaining bodies (2 to N) correspond to the manipulator modules. Thus, the second body represents the first module of the manipulator, while the body N corresponds to the ($N^{th} - 1$) module. Note, the lengths of bodies 2 to N can vary with time. Moreover, each body is free to rotate and translate with respect to its neighbors. As in the case of one module system (Figure 2-1), the x_i axis is along the length $\boldsymbol{l}_i$ of the body i; y_i is perpendicular to x_i in the orbital plane; while z_i completes the orthogonal triad. It may be emphasized that for both the platform and manipulator modules, the stiffness, damping and inertia properties can vary along x_i. $\boldsymbol{D}_i$ represents the position vector to the frame F_i, attached to the body i at the joint between bodies i-1 and i, with respect to the frame F_0. As explained earlier, $\boldsymbol{l}_{i-1} + \boldsymbol{d}_i + \boldsymbol{f}_i$ would represent position of the base, free to traverse body i-1, if it were present. If not, $\boldsymbol{d}_i$ will be eliminated through introduction of the Lagrange multipliers.

2.2.2 Position and velocity vectors of a mass element

The derivation of the equations of motion begins with the evaluation of the kinetic energy of an arbitrary body i of the multibody system. This would require velocity of a mass element dm_i in the body. The approach here is to evaluate the position vector $\boldsymbol{R}_{dm_i}$ defining location of the mass element with respect to the inertial frame F_0. Its time derivative will give the required velocity. Note, the i^{th} body of the system is free to translate and rotate in a three

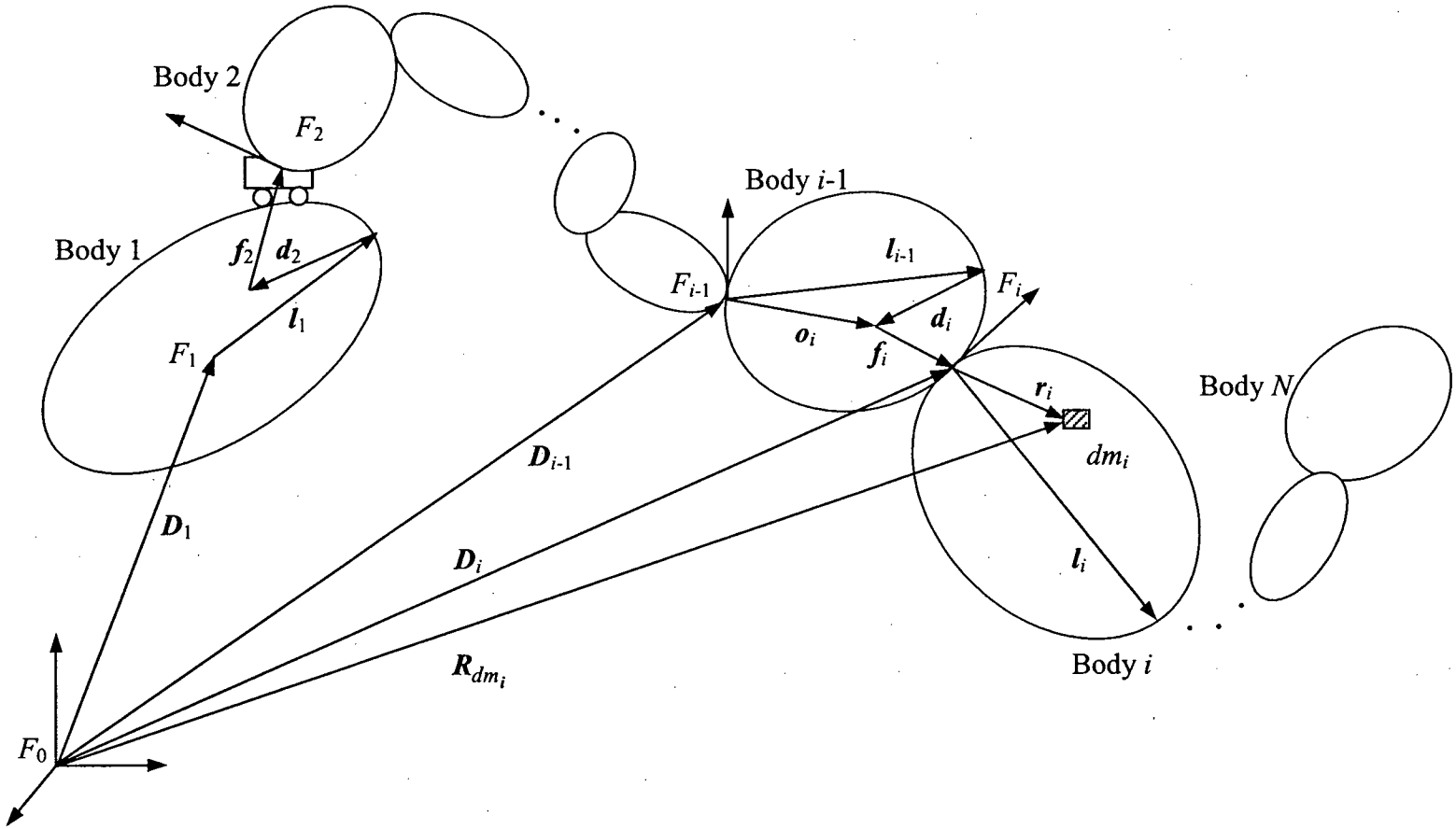

Figure 2-2 Schematic diagram of a multibody system in a chain topology showing coordinate frames and vectors used to define an elemental mass dm_i on body i.

dimensional space. From Figure 2-2, the vector $\boldsymbol{R}_{dm_i}$ to the mass element dm_i on the i^{th} body can be written as

$$\boldsymbol{R}_{dm_i} = \boldsymbol{D}_i + \mathbf{T}_i(\boldsymbol{r}_i + \Phi_i \delta_i), \tag{2.3}$$

where $\boldsymbol{D}_i$ refers to the inertial position of the frame F_i ; $\boldsymbol{r}_i = [x_i, y_i, z_i]^T$ is the position vector to dm_i with respect to the frame F_i (in absence of deformation of the body i) and $\boldsymbol{f}_i(\boldsymbol{r}_i) = \Phi_i \delta_i$ is the flexible deformation at $\boldsymbol{r}_i$. Here Φ_i are the admissible shape functions and δ_i represents generalized coordinates (Appendix A).

The matrix $\mathbf{T}_i$ in Eq. (2.3) denotes a rotational transformation from the body fixed frame F_i to the inertial frame F_0, i.e. $F_0 = \mathbf{T}_i F_i$. It is defined by the standard 3-2-1 sequence of the Eulerian rotations as

$$\mathbf{T}_i = \begin{bmatrix} C_{\psi i2} C_{\psi i1} & -C_{\psi i3} S_{\psi i1} + S_{\psi i3} S_{\psi i2} S_{\psi i1} & S_{\psi i3} S_{\psi i1} + C_{\psi i3} S_{\psi i2} S_{\psi i1} \\ C_{\psi i2} S_{\psi i1} & C_{\psi i3} C_{\psi i1} + S_{\psi i3} S_{\psi i2} S_{\psi i1} & -S_{\psi i3} C_{\psi i1} + C_{\psi i3} S_{\psi i2} S_{\psi i1} \\ -S_{\psi i2} & S_{\psi i3} C_{\psi i2} & C_{\psi i3} C_{\psi i2} \end{bmatrix}, \tag{2.4}$$

where ψ_{i1} , ψ_{i2} and ψ_{i3} are the Euler angles with C_x, S_x representing cos(x) and sin(x), respectively (Appendix B).

The rotation ζ_i of the frame F_i with respect to the frame F_{i-1} has three contributions. Figure 2-3(a) shows two components of rotation about the x_i-axis: rotation of the actuator rotor (α_i), which corresponds to the controlled motion of the revolute joint; and elastic deformation of the joint i (χ_{i1}). Figure 2-3 (b) presents rotation in the x_i, y_i-plane: elastic deformation of the (i^{th} - 1) body (ξ_{i2}); rotation of the actuator rotor (β_i), which corresponds

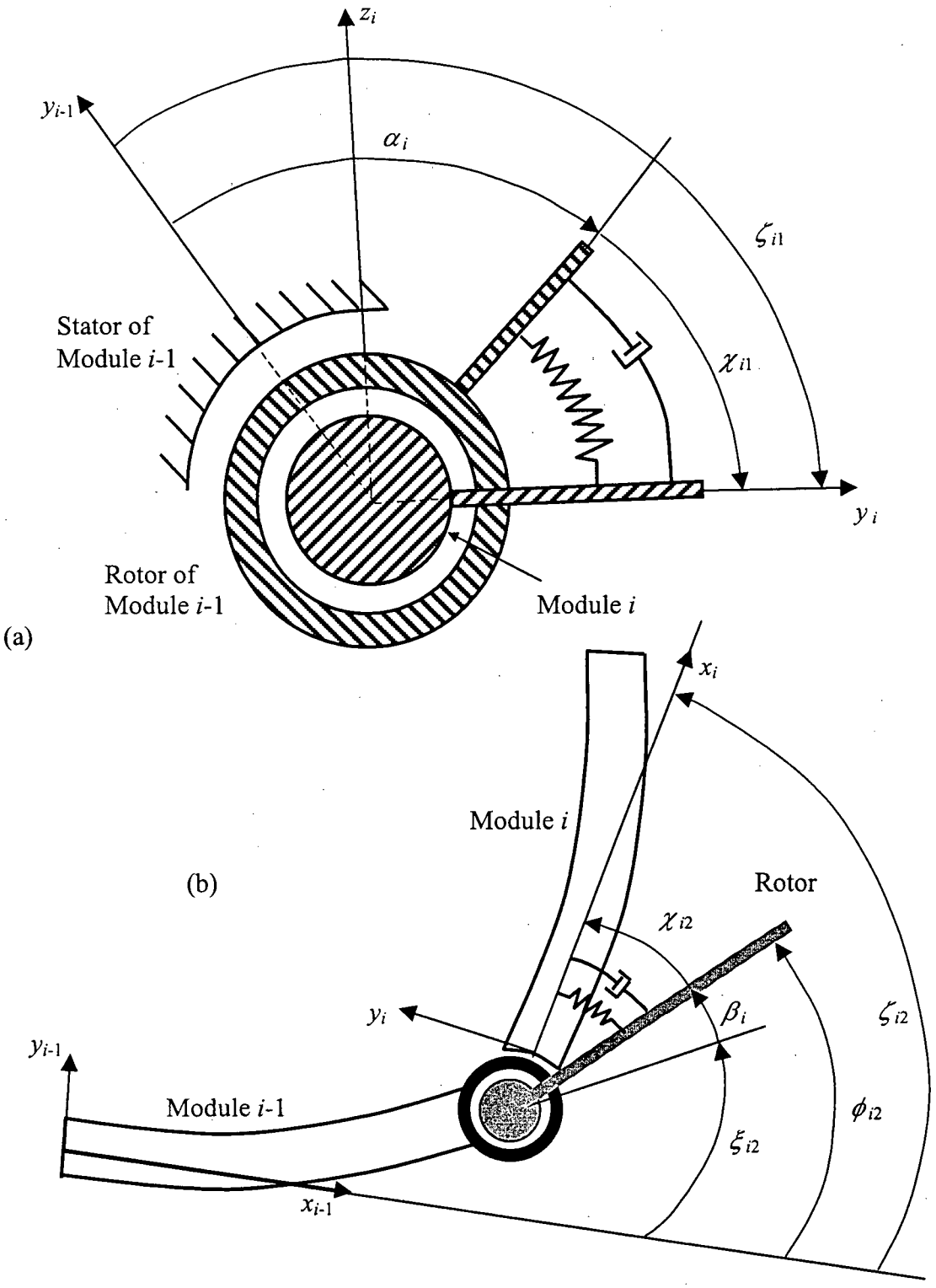

Figure 2-3 Description of the rotations of the body-fixed frame F_i relative to the preceding frame F_{i-1} : (a) rotation about x_i along the length of the module; (b) rotation about the axis z_i perpendicular to the length of the module.

to the controlled rotation of the revolute joint; and the elastic deformation of the joint i (χ_{i2}). Rotations in the z_i, x_i-plane can be described in the similar fashion. The three revolute joints, in reality, would be physically distinct. In the formulation, they are taken to be coincident at a point. Thus:

$$\zeta_{i1} = \chi_{i1} + \alpha_i \quad ; \tag{2.5a}$$

$$\zeta_{i2} = \xi_{i2} + \chi_{i2} + \beta_i \quad ; \tag{2.5b}$$

$$\zeta_{i3} = \xi_{i3} + \chi_{i3} + \gamma_i \quad . \tag{2.5c}$$

Let

$$\eta_i = \begin{pmatrix} \eta_{i1} \\ \eta_{i2} \\ \eta_{i3} \end{pmatrix} \tag{2-6}$$

be the vector of three Eulerian angles indicating the orientation of the rotor of joint i with respect to the inertial frame F_0. Considering three components representing joint flexibility $[\chi_{i1}, \chi_{i2}, \chi_{i3}]^T$, orientation of F_i relative to F_0 can be written as

$$\psi_i = \eta_i + \chi_i . \tag{2.7}$$

Note, ψ_i represents new locations of the axes for Eulerian rotations.

Let $\boldsymbol{g}_i = \boldsymbol{r}_i + \Phi_i \delta_i$. Differentiation of Eq. (2.3) with respect to time leads to

$$\dot{\boldsymbol{R}}_{dm\,i} = \dot{\boldsymbol{D}}_i + \mathbf{P}_i(\boldsymbol{g}_i)\dot{\psi}_i + \mathbf{T}_i \Phi_i \dot{\delta}_i + \mathbf{T}_i \boldsymbol{s}_i \dot{l}_i \ , \tag{2.8}$$

where: $\mathbf{P}_i(\boldsymbol{g}_i)\,\dot{\psi}_i = \dot{\mathbf{T}}_i \boldsymbol{g}_i$; $\psi_i = [\psi_{i1}, \psi_{i2}, \psi_{i3}]^T$; $\boldsymbol{s}_i = \boldsymbol{i}\dfrac{|\boldsymbol{r}_i|}{l_i} + \Phi \mathbf{L}_i \delta_i$; and l_i is the length of the i^{th} module. Details are presented in the Appendices B and C.

2.3 Kinematics of the System

2.3.1 Cylindrical orbital coordinates

The $\boldsymbol{D}_1$ term in Eq.(2.3) describes the orbital motion of the first body and is composed of three Cartesian coordinates $D_{x_1}, D_{y_1}, D_{z_1}$ (Figure 2-4). However, over the cycle of one orbit, D_{x_1}, D_{y_1} vary significantly, in the range of Earth's radius. This must be avoided since large variation in the coordinates can cause severe truncation error during their numerical integration. Hence, it is desirable to express the Cartesian components in terms of more stationary variables. This is readily accomplished by using cylindrical coordinates.

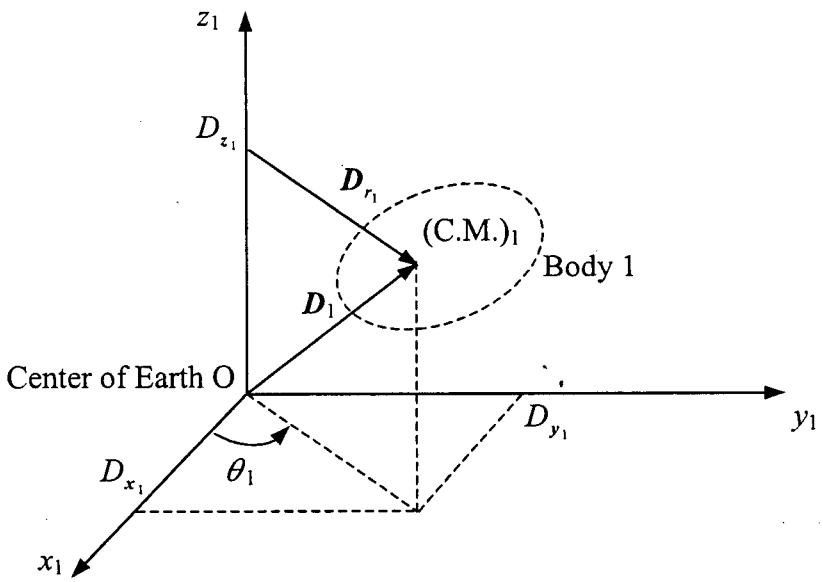

Figure 2-4 Vector components in cylindrical orbital coordinates.

Note, cylindrical coordinates are applied only to $\boldsymbol{D}_1$ as the center of mass of body 1 closely follows the orbital motion. From Figure 2-4, it is apparent that

$$\boldsymbol{D}_1 = \begin{Bmatrix} D_{x_1} \\ D_{y_1} \\ D_{z_1} \end{Bmatrix} = \begin{Bmatrix} D_{r_1} \cos\theta_1 \\ D_{r_1} \sin\theta_1 \\ D_{z_1} \end{Bmatrix},$$

$$= \underbrace{\begin{bmatrix} \cos\theta_1 & 0 & 0 \\ \sin\theta_1 & 0 & 0 \\ 0 & 0 & 1 \end{bmatrix}}_{\mathbf{D}_{T_1}} \underbrace{\begin{Bmatrix} \mathrm{D}_{r_1} \\ \theta_1 \\ \mathrm{D}_{z_1} \end{Bmatrix}}_{\boldsymbol{D}_{s_1}} = \mathbf{D}_{T_1} \boldsymbol{D}_{s_1}, \tag{2.9}$$

where D_{r_1} is the in-plane radial distance; θ_1, the true anomaly; and D_{z_1}, the out-of-plane perturbation normal to the orbital plane.

The total derivative of $\boldsymbol{D}_1$ with respect to time gives, in the column matrix form,

$$\dot{\boldsymbol{D}}_1 = \begin{bmatrix} \dfrac{\partial}{\partial D_{r_1}} \dot{\boldsymbol{D}}_{r_1} & \dfrac{\partial}{\partial \theta_1} \dot{\theta}_1 & \dfrac{\partial}{\partial D_{z_1}} \dot{\boldsymbol{D}}_{z_1} \end{bmatrix} = \boldsymbol{D}_{D_1} \dot{\boldsymbol{D}}_{s_1}, \tag{2.10}$$

where

$$\mathbf{D}_{\boldsymbol{D}_1} = \begin{bmatrix} \cos\theta_1 & -\mathrm{D}_{r_1} \sin\theta_1 & 0 \\ \sin\theta_1 & \mathrm{D}_{r_1} \cos\theta_1 & 0 \\ 0 & 0 & 1 \end{bmatrix}. \tag{2.11}$$

For all the remaining bodies,

$$\mathbf{D}_{T_i} = \mathbf{D}_{D_i} = \begin{bmatrix} 1 & 0 & 0 \\ 0 & 1 & 0 \\ 0 & 0 & 1 \end{bmatrix}, \qquad i = 2 \ldots N, \tag{2.12}$$

and

$$\boldsymbol{D}_{S_i} = \begin{Bmatrix} D_{x_i} \\ D_{y_i} \\ D_{z_{1i}} \end{Bmatrix}, \qquad i = 2 \ldots N. \tag{2.13}$$

2.3.2 Generalized coordinates

If the position and orientation of the body-fixed frames are known relative to the inertial frame, in addition to the length (l_i) and elastic deformation ($\boldsymbol{f}_i$) of each body, then the kinematic description of the system is complete. In Eq. (2.3), position of the frame F_i is specified directly relative to the inertial frame by $\boldsymbol{D}_i$ and its orientation by the Eulerian angles ψ_i.

The kinematics of the space platform is described by the generalized coordinates: $\boldsymbol{D}_{s_1}$, ψ_1 and δ_1. The coordinates $\boldsymbol{D}_{s_1}$ characterizes the orbital motion of the center of mass of the platform, as described in the last section. The set of generalized coordinates which specify the motion of the platform can be represented as

$$\tilde{\boldsymbol{q}}_1 = \begin{pmatrix} \boldsymbol{D}_{s_1} \\ \psi_1 \\ \delta_1 \end{pmatrix}. \tag{2.14}$$

The kinematics of the manipulator units is represented by the generalized coordinates $\boldsymbol{D}_i$, ψ_i η_i and δ_i. It should be noted that l_i is included as a generalized coordinate for each manipulator unit to account for deployment. Therefore, the set of generalized coordinates describing the kinematics of each manipulator module is given by

$$\tilde{q}_i = \begin{pmatrix} D_i \\ \eta_i \\ \psi_i \\ \delta_i \\ l_i \end{pmatrix}, \tag{2.15}$$

with $i = 2, \ldots, N$. The set of generalized coordinates required for the complete description of the system kinematics can thus be written as

$$\tilde{q} = \begin{pmatrix} \tilde{q}_1 \\ \tilde{q}_2 \\ \vdots \\ \tilde{q}_N \end{pmatrix}, \tag{2.16}$$

where N is the total number of bodies involved in the system.

2.4 Kinetic Energy

With the velocity representation of an arbitrary mass element dm_i in the i^{th} body in hand and considering the revolute joint actuator's mass and inertia ($\mathbf{m}_{ai}$, $\mathbf{J}_{ai}$, respectively), the kinetic energy T of the system can be readily obtained using Eq. (2.8) as

$$T = \sum_{i=1}^{N} \frac{1}{2} \int_{m_i} \dot{R}_{dm_i}^T \dot{R}_{dm_i} dm_i + \sum_{i=2}^{N} \frac{1}{2} (\dot{D}_i^T \mathbf{m}_{ai} \dot{D}_i + \dot{\eta}_i^T \mathbf{J}_{ai} \dot{\eta}_i), \tag{2.17}$$

where:

$$\mathbf{m}_{ai} = \begin{bmatrix} m_{ai1} & 0 & 0 \\ 0 & m_{ai2} & 0 \\ 0 & 0 & m_{ai3} \end{bmatrix}; \quad \mathbf{J}_{ai} = \begin{bmatrix} J_{ai1} & 0 & 0 \\ 0 & J_{ai2} & 0 \\ 0 & 0 & J_{ai3} \end{bmatrix}; \tag{2-18}$$

and $\dot{\eta}_i$ represents rotor angular velocity with respect to the inertia reference frame F_0.

Rewriting Eq.(2.8) in a matrix-vector form, gives the relation

$$\dot{R}_{dm_i} = [\mathbf{I}^3 \quad \mathbf{0} \quad \mathbf{P}_i(g_i) \quad \mathbf{T}_i\Phi_i \quad \mathbf{T}_i s_i]\dot{\tilde{q}}_i, \tag{2.19}$$

where $\mathbf{I}^3$ is the identity matrix and

$$\dot{\tilde{q}}_i = \begin{pmatrix} \dot{D}_i \\ \dot{\eta}_i \\ \dot{\psi}_i \\ \dot{\delta}_i \\ \dot{l}_i \end{pmatrix}.$$

Inserting from Eq. (2.19) into Eq. (2.17) and integrating, the kinetic energy for the system can be written as

$$\mathrm{T} = \sum_{\mathrm{i}=1}^{N} \frac{1}{2} \dot{\tilde{q}}_i^T \tilde{\mathbf{M}}_{i1} \dot{\tilde{q}}_{\mathrm{i}} + \sum_{i=2}^{N} \frac{1}{2} \dot{\tilde{q}}_i^T \begin{bmatrix} \mathbf{m}_{ai} & 0 & 0 \\ 0 & \mathbf{J}_{ai} & 0 \\ 0 & 0 & 0 \end{bmatrix} \dot{\tilde{q}}_{\mathrm{i}}, \tag{2.20}$$

where

$$\tilde{\mathbf{M}}_{i1} = \begin{bmatrix} m_i\mathbf{I}^3 & 0 & \mathbf{P}_{\mathrm{i}}(\int g_i dm_i) & \mathbf{T}_{\mathrm{i}} \int \Phi_i dm_i & \mathbf{T}_{\mathrm{i}} \int s_i\, dm_i \\ 0 & 0 & 0 & 0 & 0 \\ sym & 0 & \int \mathbf{P}_{\mathrm{i}}^{\mathrm{T}}(g_i)\mathbf{P}_i^T(g_i) dm_i & \int \mathbf{P}_{\mathrm{i}}^{\mathrm{T}}(g_i)\mathbf{T}_i\Phi_i dm_i & \int \mathbf{P}_i^T(g_i)\mathbf{T}_i\, s_i\, dm_i \\ sym & 0 & \int \Phi_i^T\Phi_i dm_i & \int \Phi_i^T\Phi_i dm_i & \int \Phi_i^T\, s_i\, dm_i \\ sym & 0 & sym & sym & \int s_i^T\, s_i\, dm_i \end{bmatrix}.$$

Denoting

$$\tilde{\mathbf{M}}_i = \begin{bmatrix} (m_i \mathbf{I}^3 + \mathbf{m}_{ai}) & 0 & \mathbf{P}_i(\int \boldsymbol{g}_i dm_i) & \mathbf{T}_i \int \Phi_i dm_i & \mathbf{T}_i \int \boldsymbol{s}_i dm_i \\ 0 & \mathbf{J}_{ai} & 0 & 0 & 0 \\ sym & 0 & \int \mathbf{P}_i^T(\boldsymbol{g}_i)\mathbf{P}_i^T(\boldsymbol{g}_i) dm_i & \int \mathbf{P}_i^T(\boldsymbol{g}_i)\mathbf{T}_i \Phi_i dm_i & \int \mathbf{P}_i^T(\boldsymbol{g}_i)\mathbf{T}_i \boldsymbol{s}_i dm_i \\ sym & 0 & \int \Phi_i^T \Phi_i dm_i & \int \Phi_i^T \Phi_i dm_i & \int \Phi_i^T \boldsymbol{s}_i dm_i \\ sym & 0 & sym & sym & \int \boldsymbol{s}_i^T \boldsymbol{s}_i dm_i \end{bmatrix}, \tag{2.21}$$

the kinetic energy for the entire system, i.e. with N bodies, can now be stated as

$$T = \frac{1}{2}\sum_{i=1}^{N} \dot{\tilde{\boldsymbol{q}}}_i^T \tilde{\mathbf{M}}_i \dot{\tilde{\boldsymbol{q}}}_i = \frac{1}{2} \dot{\tilde{\boldsymbol{q}}}^T \tilde{\mathbf{M}} \dot{\tilde{\boldsymbol{q}}} \ , \tag{2.22}$$

where $\dot{\tilde{\boldsymbol{q}}} = (\dot{\tilde{\boldsymbol{q}}}_1^T, \dot{\tilde{\boldsymbol{q}}}_2^T, ..., \dot{\tilde{\boldsymbol{q}}}_N^T)^T$ and $\tilde{\mathbf{M}}$ is a block diagonal matrix with $\tilde{\mathbf{M}}_i$ on its diagonal,

$$\tilde{\mathbf{M}} = \begin{bmatrix} \tilde{\mathbf{M}}_1 & 0 & 0 & \cdots & 0 \\ 0 & \tilde{\mathbf{M}}_2 & 0 & \cdots & 0 \\ 0 & 0 & \tilde{\mathbf{M}}_3 & \cdots & 0 \\ \vdots & \vdots & \ddots & \ddots & \vdots \\ 0 & 0 & \cdots & 0 & \tilde{\mathbf{M}}_N \end{bmatrix}. \tag{2.23}$$

Note, for rigid bodies, this symmetric mass matrix is considerably simpler and can be described in terms of the center of mass and inertia tensor of the bodies. Furthermore, the kinetic energy expression in Eq. (2.22) has the quadratic form, which can be easily manipulated during the Lagrangian formulation of the equations of motion. Finally, most integrals in Eq. (2.21) can be evaluated symbolically (using, e.g., MAPLE) and hence coded directly in the FORTRAN language.

2.5 Gravitational Potential Energy

The gravitational potential energy of the i^{th} body, in Earth's gravitational field, is given as

$$\dot{V}_{g_i} = -\mu \int_{m_i} \frac{dm_i}{\left|R_{dm_i}\right|}, \tag{2.24}$$

where μ is Earth's gravitational constant: Using the binomial expansion and retaining terms up to the third degree gives

$$V_{g_i} = \frac{-\mu m_i}{|\boldsymbol{D}_i|} + \frac{\mu}{2|\boldsymbol{D}_i|^3}\left[\int \boldsymbol{g}_i^T\, \boldsymbol{g}_i\, dm_i + 2\,\boldsymbol{D}_i^T\,\mathbf{T}_i \int \boldsymbol{g}_i\, dm_i - \frac{3}{|\boldsymbol{D}_i|^2}\boldsymbol{D}_i^T\,\mathbf{T}_i^T \int \boldsymbol{g}_i^T\, \boldsymbol{g}_i\, dm_i \mathbf{T}_i\, \boldsymbol{D}_i\right], \tag{2.25}$$

which is expressed in terms of symbolically evaluated integrals.

2.6 Strain Energy

The strain at a location x_i on the i^{th} body can be written as

$$\varepsilon_i = \frac{\partial u_i}{\partial x_i} + \frac{1}{2}\left[\left(\frac{\partial v_i}{\partial x_i}\right)^2 + \left(\frac{\partial w_i}{\partial x_i}\right)^2\right], \tag{2.26}$$

where u_i, v_i and w_i are deformations in the longitudinal (x_i) and transverse (y_i, z_i) directions, respectively (Appendix A, Eq. A.5). The strain energy of body i is given by

$$V_{ei} = \frac{1}{2} E_i A_i \int_0^{l_i} \varepsilon_i^2 dx_i, \tag{2.27}$$

where E_iA_i is the flexural stiffness. The strain energy due to flexible revolute joints can be written as

$$V_j = \frac{1}{2}\sum_{i=2}^{N} \chi_i^T K_i \chi_i , \tag{2-28}$$

where

$$K_i = \begin{bmatrix} k_{i1} & & 0 \\ & k_{i2} & \\ 0 & & k_{i3} \end{bmatrix}$$

is the stiffness matrix of the joint i. Thus total potential energy of the system has the form

$$P_e = \sum_{i=1}^{N} (V_{gi} + V_{ei}) + V_j . \tag{2.29}$$

2.7 Lagrange Equations of Motion

With the kinetic and potential energy expressions derived, the equations of motion can be obtained quite readily using the Lagrangian principle

$$\frac{d}{dt}\left(\frac{\partial T}{\partial \dot{q}_i}\right) - \frac{\partial (T - P_e)}{\partial q_i} = Q_{q_i} . \tag{2.30}$$

Substituting from Eqs.(2.22) and (2.29) into Eq. (2.30) leads to the familiar matrix form of the coupled equations of motion for the system,

$$\tilde{\mathbf{M}}(q,t)\ddot{q} + F(\dot{q},q,t) = Q(\dot{q},q,t), \tag{2.31}$$

where $\tilde{\mathbf{M}}$ is the nonlinear symmetric mass matrix; $\boldsymbol{F}$ contains the terms associated with the centrifugal, Coriolis, gravitational, elastic and internal dissipative forces; and $\boldsymbol{Q}_q$ is the vector of generalized external forces, including control inputs. Note, inversion of the mass matrix $\tilde{\mathbf{M}}$ is required to solve the equation. Normally, it leads to a large number of computational steps, of the order of N_q^3, where N_q is the total number of generalized coordinates in the system. However, in the present case, due to block diagonal character of the mass matrix $\tilde{\mathbf{M}}$, its inversion involves only O(N) operation where N is the number of bodies. Note, in deriving the energy expressions of the system, the focus was on the decoupled system; i.e., each body was considered independent of others. Thus we are still faced with the problem of constraints imposed by joints connecting the adjacent bodies. Although choice of decoupled generalized coordinates $\tilde{\boldsymbol{q}}_i$ simplified evaluation of the kinetic and potential energies, it is not suitable for specification of constraints. This is better achieved through specifying the body frame F_i with respect to the inertial frame F_0 recursively along the chain of bodies from one to $i-1$. A new set of generalized coordinates $\boldsymbol{q}_i$ accomplishes this,

$$\boldsymbol{q}_i = \begin{pmatrix} \boldsymbol{d}_i \\ \eta_i \\ \psi_i \\ \delta_i \\ l_i \end{pmatrix},$$

such that $\boldsymbol{q} = (\boldsymbol{q}_1^T, \boldsymbol{q}_2^T, ..., \boldsymbol{q}_N^T)^T$ gives the total generalized coordinate vector of the system. Thus the formulation involves two different sets of generalized coordinates: $\tilde{\boldsymbol{q}}_i$ to evaluate

energy of the system; and q_i to account for constraints imposed by interconnected bodies. The next logical step is to find relations between these two sets of generalized coordinates. This is achieved through position and velocity transformations.

2.8 Coordinate Transformations

The only difference between q_i and $\tilde{q}_i$ is the presence of d_i in place of D_i. Here, D_i is the inertial position of F_i from F_0, whereas d_i is defined as the offset position of F_i relative to the end of the body i-1 in absence of its elastic deformation (Figure 2-2).

2.8.1 Position transformation

From Figure 2-2, D_i can be defined as

$$D_i = \sum_{j=1}^{i} (\mathbf{T}_{j-1} d_j + \mathbf{T}_{j-1} f_j(o_j) + \mathbf{T}_{j-1} i\, l_{j-1}), \tag{2.32}$$

where $f_j(o_j) = \Phi_{j-1}[(l_{j-1} + d_{xj})]\delta_{j-1}$ is the translational motion caused by the deflection at the end point of the vector o_j on the j-1 body. Defining $\mathbf{KA}_{j-1} = \Phi_{j-1}[(l_{j-1} + d_{xj})]$ and recognizing that $l_0 = 0, \delta_0 = 0$ give

$$D_i = \sum_{j=1}^{i-1} (\mathbf{T}_{j-1} d_j + \mathbf{T}_j \mathbf{KA}_j \delta_j + \mathbf{T}_j i\, l_j) + \mathbf{T}_{i-1} d_i. \tag{2.33}$$

From Eq.(2-32)

$$\boldsymbol{D}_{i-1} = \sum_{j=1}^{i-1} (\mathbf{T}_{j-1}\boldsymbol{d}_j + \mathbf{T}_{j-1}\boldsymbol{f}_j(\boldsymbol{o}_j) + \mathbf{T}_{j-1}\boldsymbol{i}\,l_{j-1}), \tag{2-34}$$

therefore

$$\boldsymbol{D}_i = \boldsymbol{D}_{i-1} + \mathbf{T}_{i-1}\{l_{i-1}\,\boldsymbol{i} + \boldsymbol{d}_i\} + \mathbf{T}_{i-1}\Phi_{i-1}[(l_{i-1} + \boldsymbol{d}_{xi})]\delta_{i-1}. \tag{2.35}$$

In matrix form the relationship between $\tilde{\boldsymbol{q}}_i$ and $\boldsymbol{q}_i$ can now be written as

$$\begin{pmatrix} \boldsymbol{D}_i \\ \eta_i \\ \psi_i \\ \delta_i \\ l_i \end{pmatrix} = \sum_{j=1}^{i-1} \begin{bmatrix} \mathbf{T}_{j-1} & 0 & 0 & \mathbf{T}_j\mathbf{K}\mathbf{A}_j & \mathbf{T}_j\boldsymbol{i} \\ 0 & 0 & 0 & 0 & 0 \\ 0 & 0 & 0 & 0 & 0 \\ 0 & 0 & 0 & 0 & 0 \\ 0 & 0 & 0 & 0 & 0 \end{bmatrix} \begin{pmatrix} \boldsymbol{d}_j \\ \eta_j \\ \psi_j \\ \delta_j \\ l_j \end{pmatrix} + \begin{bmatrix} \mathbf{T}_{i-1} & 0 & 0 & 0 & 0 \\ 0 & \mathbf{I}^3 & 0 & 0 & 0 \\ 0 & 0 & \mathbf{I}^3 & 0 & 0 \\ 0 & 0 & 0 & \mathbf{I}^{n_{fi}} & 0 \\ 0 & 0 & 0 & 0 & 1 \end{bmatrix} \begin{pmatrix} \boldsymbol{d}_i \\ \eta_i \\ \psi_i \\ \delta_i \\ l_i \end{pmatrix}, \tag{2.36}$$

where n_{fi} is the number of modes considered for the i^{th} body.

Thus

$$\tilde{\boldsymbol{q}}_i = \sum_{j=1}^{i-1} (\boldsymbol{R}_j^p \boldsymbol{q}_j) + \boldsymbol{R}_i \boldsymbol{q}_i, \tag{2.37}$$

where:

$$\boldsymbol{R}_j^p = \begin{bmatrix} \mathbf{T}_{j-1} & 0 & 0 & \mathbf{T}_j\mathbf{K}\mathbf{A}_j & \mathbf{T}_j\boldsymbol{i} \\ 0 & 0 & 0 & 0 & 0 \\ 0 & 0 & 0 & 0 & 0 \\ 0 & 0 & 0 & 0 & 0 \\ 0 & 0 & 0 & 0 & 0 \end{bmatrix};$$

and

$$\boldsymbol{R}_i = \begin{bmatrix} \mathbf{T}_{i-1} & 0 & 0 & 0 & 0 \\ 0 & \mathbf{I}^3 & 0 & 0 & 0 \\ 0 & 0 & \mathbf{I}^3 & 0 & 0 \\ 0 & 0 & 0 & \mathbf{I}^{n_{fi}} & 0 \\ 0 & 0 & 0 & 0 & 1 \end{bmatrix}.$$

For the entire system,

$$\tilde{\boldsymbol{q}} = \boldsymbol{R}^p \boldsymbol{q}\,. \tag{2.38}$$

Here $\boldsymbol{R}^p$ is a lower block diagonal matrix relating $\tilde{\boldsymbol{q}}$ and $\boldsymbol{q}$,

$$\boldsymbol{R}^p = \begin{bmatrix} \boldsymbol{R}_1 & 0 & 0 & \cdots & 0 \\ \boldsymbol{R}_1^p & \boldsymbol{R}_2 & 0 & \cdots & 0 \\ \boldsymbol{R}_1^p & \boldsymbol{R}_2^p & \boldsymbol{R}_3 & \cdots & 0 \\ \vdots & \vdots & \ddots & \ddots & \vdots \\ \boldsymbol{R}_1^p & \boldsymbol{R}_2^p & \cdots & \boldsymbol{R}_{N-1}^p & \boldsymbol{R}_N \end{bmatrix}. \tag{2.39}$$

2.8.2 Velocity transformations

The velocities of the generalized coordinates $\tilde{\boldsymbol{q}}$ and $\boldsymbol{q}$ are related by the following two transformations. The first one is in the format of multiplication of several matrices. It will extend the benefit of the order-N format into the formulation with constraints. The second one relates the vectors $\dot{\tilde{\boldsymbol{q}}}$ and $\dot{\boldsymbol{q}}$ to make the formulation consistent with the $\boldsymbol{q}$ set of generalized coordinates.

First transformation

From Figure 2-2 as well as Eq. (2.33),

$$\boldsymbol{D}_i = \boldsymbol{D}_{i-1} + \mathbf{T}_{i-1}[\boldsymbol{i}\, l_{i-1} + \boldsymbol{d}_i + \mathbf{KA}_{i-1}\delta_{i-1}]. \tag{2.40}$$

Differentiating Eq. (2.40) with respect to time gives (Appendix C)

$$\begin{aligned}\dot{\boldsymbol{D}}_i = \dot{\boldsymbol{D}}_{i-1} &+ \mathbf{T}_{i-1}\{\mathbf{I}^3 + \mathbf{KAD}_{i-1}\delta_{i-1}\boldsymbol{i}^T\}\dot{\boldsymbol{d}}_i + \mathbf{P}_{i-1}(\boldsymbol{h}_{i-1})\dot{\psi}_{i-1} \\ &+ \mathbf{T}_{i-1}\mathbf{KA}_{i-1}\dot{\delta}_{i-1} + \mathbf{T}_{i-1}\{\boldsymbol{i} + \mathbf{KAL}_{i-1}\delta_{i-1}\}\,\dot{l}_{i-1},\end{aligned} \tag{2.41}$$

where: $\mathbf{KAD}_{i-1} = \dfrac{d\,\mathbf{KA}_{i-1}}{d\,\boldsymbol{d}_i}$; $\mathbf{KAL}_{i-1} = \dfrac{d\,\mathbf{KA}_{i-1}}{d\,l_{i-1}}$; and $\boldsymbol{h}_{i-1} = \boldsymbol{d}_i + \boldsymbol{i}\, l_{i-1} + \mathbf{KA}_{i-1}\delta_{i-1}$.

Following a procedure similar to the one used in the position transformation, Equation (2.41) can be rewritten as

$$\begin{pmatrix} \dot{\boldsymbol{D}}_i \\ \dot{\eta}_i \\ \dot{\psi}_i \\ \dot{\delta}_i \\ \dot{l}_i \end{pmatrix} = \begin{bmatrix} \mathbf{I}^3 & 0 & \mathbf{P}_{i-1}(\boldsymbol{h}_{i-1}) & \mathbf{T}_{i-1}\mathbf{KA}_{i-1} & \mathbf{T}_i\mathbf{KL}_{i-1} \\ 0 & 0 & 0 & 0 & 0 \\ 0 & 0 & 0 & 0 & 0 \\ 0 & 0 & 0 & 0 & 0 \\ 0 & 0 & 0 & 0 & 0 \end{bmatrix} \begin{pmatrix} \dot{\boldsymbol{D}}_{i-1} \\ \dot{\eta}_{i-1} \\ \dot{\psi}_{i-1} \\ \dot{\delta}_{i-1} \\ \dot{l}_{i-1} \end{pmatrix}$$

$$+ \begin{bmatrix} \mathbf{T}_{i-1}\mathbf{KD}_{i-1} & 0 & 0 & 0 & 0 \\ 0 & \mathbf{I}^3 & 0 & 0 & 0 \\ 0 & 0 & \mathbf{I}^3 & 0 & 0 \\ 0 & 0 & 0 & \mathbf{I}^{n_{fi}} & 0 \\ 0 & 0 & 0 & 0 & 1 \end{bmatrix} \begin{pmatrix} \dot{\boldsymbol{d}}_i \\ \dot{\eta}_i \\ \dot{\psi}_i \\ \dot{\delta}_i \\ \dot{l}_i \end{pmatrix}, \tag{2.42}$$

where: $\mathbf{KD}_{i-1} = \mathbf{I}^3 + \mathbf{KAD}_{i-1}\delta_{i-1}\boldsymbol{i}^T$; and $\mathbf{KL}_i = \boldsymbol{i} + \mathbf{KAL}_{i-1}\delta_{i-1}$.

The relation between $\dot{\tilde{\boldsymbol{q}}}_i$ and $\dot{\boldsymbol{q}}_i$ can now be obtained as

$$\dot{\tilde{\boldsymbol{q}}}_i = \mathbf{R}^n_{i-1}\dot{\tilde{\boldsymbol{q}}}_{i-1} + \mathbf{R}_i\dot{\boldsymbol{q}}_i, \tag{2.43}$$

with

$$\boldsymbol{R}_{i-1}^{n} = \begin{bmatrix} \mathbf{I}^3 & 0 & \mathbf{P}_{i-1}(h_{i-1}) & \mathbf{T}_{i-1}\mathbf{KA}_{i-1} & \mathbf{T}_i\mathbf{KL}_{i-1} \\ 0 & 0 & 0 & 0 & 0 \\ 0 & 0 & 0 & 0 & 0 \\ 0 & 0 & 0 & 0 & 0 \\ 0 & 0 & 0 & 0 & 0 \end{bmatrix}; \quad \boldsymbol{R}_i = \begin{bmatrix} \mathbf{T}_{i-1}\mathbf{KD}_{i-1} & 0 & 0 & 0 & 0 \\ 0 & \mathbf{I}^3 & 0 & 0 & 0 \\ 0 & 0 & \mathbf{I}^3 & 0 & 0 \\ 0 & 0 & 0 & \mathbf{I}^{n_f} & 0 \\ 0 & 0 & 0 & 0 & 1 \end{bmatrix}. \tag{2.44}$$

For the entire system,

$$\dot{\tilde{\boldsymbol{q}}} = \mathbf{R}^n\tilde{\boldsymbol{q}} + \mathbf{R}_i\dot{\boldsymbol{q}} \tag{2.45}$$

Here:

$$\boldsymbol{R}^n = \begin{bmatrix} 0 & 0 & 0 & \cdots & 0 \\ \boldsymbol{R}_1^n & 0 & 0 & \cdots & 0 \\ 0 & \boldsymbol{R}_2^n & 0 & \cdots & 0 \\ \vdots & \vdots & \ddots & \ddots & \vdots \\ 0 & 0 & \cdots & \boldsymbol{R}_{N-1}^n & 0 \end{bmatrix}; \tag{2.46}$$

and

$$\mathbf{R} = \begin{bmatrix} \mathbf{R}_1 & 0 & 0 & \cdots & 0 \\ 0 & \mathbf{R}_2 & 0 & \cdots & 0 \\ 0 & 0 & \mathbf{R}_3 & \cdots & 0 \\ \vdots & \vdots & \ddots & \ddots & \vdots \\ 0 & 0 & \cdots & 0 & \mathbf{R}_4 \end{bmatrix}. \tag{2.47}$$

Thus, in matrix form, for the entire system,

$$\dot{\tilde{\boldsymbol{q}}} = (\mathbf{I} - \mathbf{R}^n)^{-1}\mathbf{R}\dot{\boldsymbol{q}}. \tag{2.48}$$

Note the inverse character of the matrix $(\mathbf{I}-\mathbf{R}^n)^{-1}$. This is beneficial for the order N property.

Second transformation

Vector $\boldsymbol{D}_i$ in Eq.(2.40) can also be expressed in the recursive fashion as

$$\boldsymbol{D}_i = \sum_{j=1}^{i}(\mathbf{T}_{j-1}\boldsymbol{d}_j + \mathbf{T}_{j-1}\mathbf{KA}_{j-1}\delta_{j-1} + \mathbf{T}_{j-1}\boldsymbol{i}\,l_{j-1}). \tag{2.49}$$

As $l_0 = \psi_0 = \delta_0 = 0$,

$$\boldsymbol{D}_i = \sum_{j=1}^{i-1}(\mathbf{T}_{j-1}\boldsymbol{d}_j + \mathbf{T}_j\mathbf{KA}_j\delta_j + \mathbf{T}_j\boldsymbol{i}\,l_j) + \mathbf{T}_{i-1}\boldsymbol{d}_i. \tag{2.50}$$

Taking the time derivative of $\boldsymbol{D}_i$ as before and following the similar procedure,

$$\dot{\boldsymbol{D}}_i = \sum_{j=1}^{i-1}\{\mathbf{T}_{j-1}[\mathbf{I}^3 + \mathbf{KAD}_{j-1}\delta_{j-1}\boldsymbol{i}^T]\dot{\boldsymbol{d}}_j + \mathbf{P}_j(\boldsymbol{h}_j)\dot{\psi}_j + \mathbf{T}_j\mathbf{KA}_j\dot{\delta}_j + \mathbf{T}_j[\boldsymbol{i} + \mathbf{KAL}_j\delta_j]\dot{l}_j\}.$$

$$+ \mathbf{T}_{i-1}[\mathbf{I}^3 + \mathbf{KAD}_{i-1}\delta_{i-1}\hat{\boldsymbol{i}}^T]\dot{\boldsymbol{d}}_i \ . \tag{2.51}$$

In matrix form

$$\begin{pmatrix} \dot{\boldsymbol{D}}_i \\ \dot{\eta}_i \\ \dot{\psi}_i \\ \dot{\delta}_i \\ \dot{l}_i \end{pmatrix} = \sum_{j=1}^{i-1}\begin{bmatrix} \mathbf{T}_{j-1}\mathbf{KD}_{j-1} & 0 & \mathbf{P}_j(\boldsymbol{h}_j) & \mathbf{T}_j\mathbf{KA}_j & \mathbf{T}_j\mathbf{KL}_j \\ 0 & 0 & 0 & 0 & 0 \\ 0 & 0 & 0 & 0 & 0 \\ 0 & 0 & 0 & 0 & 0 \\ 0 & 0 & 0 & 0 & 0 \end{bmatrix}\begin{pmatrix} \dot{\boldsymbol{D}}_{j-1} \\ \dot{\eta}_{j-1} \\ \dot{\psi}_{j-1} \\ \dot{\delta}_{j-1} \\ \dot{l}_{j-1} \end{pmatrix}$$

$$+ \begin{bmatrix} \mathbf{T}_{i-1}\mathbf{KD}_{i-1} & 0 & 0 & 0 & 0 \\ 0 & \mathbf{I}^3 & 0 & 0 & 0 \\ 0 & 0 & \mathbf{I}^3 & 0 & 0 \\ 0 & 0 & 0 & \mathbf{I}^{n_{fi}} & 0 \\ 0 & 0 & 0 & 0 & 1 \end{bmatrix}\begin{pmatrix} \dot{\boldsymbol{d}}_i \\ \dot{\eta}_i \\ \dot{\psi}_i \\ \dot{\delta}_i \\ \dot{l}_i \end{pmatrix}, \tag{2.52}$$

or in short

$$\dot{\tilde{\boldsymbol{q}}}_i = \sum_{j=1}^{i-1} \mathbf{R}_i^d \dot{\tilde{\boldsymbol{q}}}_j + \mathbf{R}_i \dot{\boldsymbol{q}}_i , \tag{2.53}$$

where

$$\mathbf{R}_i^d = \begin{bmatrix} \mathbf{T}_{j-1}\mathbf{KD}_{j-1} & 0 & \mathbf{P}_j(\boldsymbol{h}_j) & \mathbf{T}_j\mathbf{KA}_j & \mathbf{T}_j\mathbf{KL}_j \\ 0 & 0 & 0 & 0 & 0 \\ 0 & 0 & 0 & 0 & 0 \\ 0 & 0 & 0 & 0 & 0 \end{bmatrix}. \tag{2.54}$$

For the entire system,

$$\dot{\tilde{\boldsymbol{q}}} = \mathbf{R}^v \dot{\boldsymbol{q}} , \tag{2.55}$$

with

$$\mathbf{R}^v = \begin{bmatrix} \mathbf{R}_1 & 0 & 0 & \cdots & 0 \\ \mathbf{R}_1^d & \mathbf{R}_2 & 0 & \cdots & 0 \\ \mathbf{R}_1^d & \mathbf{R}_2^d & \mathbf{R}_3 & \cdots & 0 \\ \vdots & \vdots & \ddots & \ddots & \vdots \\ \mathbf{R}_1^d & \mathbf{R}_2^d & \cdots & \mathbf{R}_{N-1}^d & \mathbf{R}_N \end{bmatrix}. \tag{2.56}$$

The second transformation relates the $\dot{\tilde{\boldsymbol{q}}}$ and $\dot{\boldsymbol{q}}$ through matrix $\mathbf{R}^v$. It is used for terms, such as $\boldsymbol{F}$ in (Eq. 2.2), which do not involve inverse operation in solving the equations of motion. As mentioned earlier, the details are given in Appendix C. It may be pointed out that such

velocity transformation for the three-dimensional variable geometry manipulators, with non-recursive formulation, have not be developed before.

2.9 Energy Dissipation

Dissipation of energy was included in the model. Accurate mathematical model for damping is an area of research in itself. Here, the objective is to capture its overall effect on the system response. To that end, a Rayleigh dissipation function is used [75]. It is defined as one-half of the instantaneous rate of change of mechanical energy occurring in the system,

$$R_d = \frac{1}{2}\sum_{i=2}^{N}\left(C_{i1}^{J}\chi_{i1}^{2} + C_{i2}^{J}\chi_{i2}^{2} + C_{i3}^{J}\chi_{i3}^{2}\right) + \sum_{i=1}^{N}\int_{l_i}\frac{1}{2}C_{u,i}^{L}I(x_i)\left(\frac{\partial \dot{u}_i}{\partial x_i}\right)^2 dx_i + \sum_{i=1}^{N}\frac{1}{2}\int_{l_i}C_{v,i}^{L}A(x_i)\left(\frac{\partial \dot{v}_i}{\partial x_i}\right)^2 dx_i + \sum_{i=1}^{N}\frac{1}{2}\int_{l_i}C_{w,i}^{L}A(x_i)\left(\frac{\partial \dot{w}_i}{\partial x_i}\right)^2 dx_i \quad , \tag{2.57}$$

where the first term accounts for the damping in the flexible joints; the second term corresponds to the structural damping in the longitudinal direction, while the third and the fourth terms represent the dissipation in the transverse y_i and z_i directions, respectively. I denotes the sectional mass moment of inertia while A corresponds to the moment of inertia of the cross-sectional area about its neutral axis. Note that C_{i1}^{J}, C_{i2}^{J}, and C_{i3}^{J} represent joint damping coefficients while $C_{u,i}^{L}$, $C_{v,i}^{L}$, and $C_{w,i}^{L}$ correspond to equivalent viscous damping coefficients for the longitudinal as well as the transverse modes of vibration of the bodies, respectively.

2.10 Equations of Motion

As seen before, there are velocity transformations from $\dot{\tilde{q}}$ to $\dot{q}$ (Eqs. 2.48, 2.55). Correspondingly, they lead to two kinetic energy expressions in terms of $\dot{q}$. Substituting from Eq. (2.55) into Eq. (2.22), the first of the two expressions for kinetic energy can be written as

$$T = \frac{1}{2}\dot{q}^T[(\mathbf{R}^v)^T \tilde{\mathbf{M}}\, \mathbf{R}^v]\dot{q}\,. \tag{2.58}$$

Similarly, substituting from Eq. (2.48) into Eq. (2.22) yields the second expression as

$$T = \frac{1}{2}\dot{q}^T[(\mathbf{I}-\mathbf{R}^n)^{-1}\mathbf{R}]^T \tilde{\mathbf{M}}[(\mathbf{I}-\mathbf{R}^n)^{-1}\mathbf{R}]\dot{q}\,. \tag{2.59}$$

Consequently, two factorized coupled mass matrices of the system can be represented as

$$\mathbf{M} = \mathbf{R}^{vT}\tilde{\mathbf{M}}\,\mathbf{R}^v \tag{2.60}$$

and

$$\mathbf{M} = [(\mathbf{I}-\mathbf{R}^n)^{-1}\mathbf{R}]^T \tilde{\mathbf{M}}[(\mathbf{I}-\mathbf{R}^n)^{-1}\mathbf{R}]\,. \tag{2.61}$$

Inverting Eq. (2.61) leads to

$$\mathbf{M}^{-1} = (\mathbf{R})^{-1}(\mathbf{I}-\mathbf{R}^n)\tilde{\mathbf{M}}^{-1}[(\mathbf{R})^{-1}(\mathbf{I}-\mathbf{R}^n)]^T\,. \tag{2.62}$$

Since both $\mathbf{R}$ and $\tilde{\mathbf{M}}$ are block diagonal matrices, their inverse is simply the inverse of each block on the diagonal. Also, each block is of the size $n_i \times n_i$, where n_i is the number of

generalized coordinates considered for the i^{th} body. Note, the order N character suggests that when the number of bodies increases by one, the cost of inverting $\mathbf{M}$ will rise only through the presence of one more block matrix. Thus inversion of $\mathbf{M}$ is the *O(N)* operation. Also, the form of $\mathbf{M}$ in Eq. (2.60) does not involve inverse operation and hence can be readily employed in evaluating the term $\frac{\partial(T-P_e)}{\partial \boldsymbol{q}_i}$ in Eq. (2.30).

The equations of motion with the damping effect, in the O(N) form, can now be obtained using the Lagrangian procedure

$$\frac{d}{dt}\left(\frac{\partial T}{\partial \dot{\boldsymbol{q}}_i}\right)-\frac{\partial(T-P_e)}{\partial \boldsymbol{q}_i}+\frac{\partial R_d}{\partial \dot{\boldsymbol{q}}_i}=\boldsymbol{Q}_{q_i}, \tag{2.63}$$

where $\boldsymbol{Q}_{q_i}$ corresponds to the nonconservative generalized forces. The governing equations can be written as

$$\ddot{\boldsymbol{q}}=\mathbf{M}^{-1}\boldsymbol{Q}-\mathbf{M}^{-1}\left(\dot{\mathbf{M}}\dot{\boldsymbol{q}}-\frac{1}{2}\frac{\partial(\dot{\boldsymbol{q}}^T\mathbf{M}\dot{\boldsymbol{q}})}{\partial \boldsymbol{q}}+\frac{\partial P_e}{\partial \boldsymbol{q}}+\frac{\partial R_d}{\partial \dot{\boldsymbol{q}}}\right), \tag{2.64}$$

where P_e and R_d are defined in Eqs. (2.29) and (2.57), respectively; and $\mathbf{M}^{-1}$ is given by Eq. (2.62). The terms $\dot{\mathbf{M}}$ and $\frac{\partial(\dot{\boldsymbol{q}}^T\mathbf{M}\dot{\boldsymbol{q}})}{\partial \boldsymbol{q}}$ are described in detail in Appendix D.

2.11 Generalized Forces

The generalized forces $\boldsymbol{Q}$ can represent nonconservative environmental effects, such as atmospheric drag, solar radiation pressure and thermal effects, interaction with Earth's magnetic field, etc. However, the present study considers only the generalized forces arising from the system's control actuators. They correspond to the torques applied by control momentum gyros on the platform, revolute joint actuators, as well as forces applied by linear actuators (at prismatic joints) responsible for link deployment.

The control inputs applied to the space-platform are the torques arising from the control momentum gyros which regulate its attitude in pitch, roll, yaw ($\boldsymbol{T}_1$) and its vibration ($\boldsymbol{T}_{e1}$). Motion of the mobile base would involve the force $\boldsymbol{F}_b$. The actuator located at the i^{th} joint of the manipulator provides the i^{th} body with a torque $\boldsymbol{T}_i$ which results in slewing motion of the unit. Furthermore, each module is equipped with a linear actuator responsible for its deployment and retrieval. This actuator provides a force F_i along the length of the i^{th} body. Therefore, the set of actuator forces can be written as

$$\boldsymbol{u} = [\boldsymbol{T}_1^T,\ \boldsymbol{T}_{e1}^T,\ \boldsymbol{F}_b^T,\ \boldsymbol{T}_2^T,\ F_2,\cdots,\ \boldsymbol{T}_i^T,\ F_i,\cdots,\boldsymbol{T}_N^T,\ F_N]^T, \tag{2.65}$$

Note, the total number of actuators involved is $n_a = 5 + 4(N-1)$.

The generalized forces $\boldsymbol{Q}$ can be evaluated through the principle of virtual work,

$$Q_i = \sum_{j=1}^{n_a} \boldsymbol{F}_{ej} \bullet \frac{\partial \boldsymbol{R}_j}{\partial q_i}, \tag{2.66}$$

where Q_i and q_i represent the i^{th} components of $\boldsymbol{Q}$ and $\boldsymbol{q}$, respectively; and $\boldsymbol{F}_{ej}$ symbolize the j^{th} external force applied at $\boldsymbol{R}_j$. Eq. (2.63) is used to derive the relationship between $\boldsymbol{Q}$ and $\boldsymbol{u}$,

$$\boldsymbol{Q} = \mathbf{Q}^d \boldsymbol{u}, \tag{2.67}$$

where:

$$\mathbf{Q}^d = \begin{bmatrix} \mathbf{Q}_1^d & 0 & 0 & \cdots & 0 \\ 0 & \mathbf{Q}_2^d & 0 & \cdots & 0 \\ 0 & 0 & \mathbf{Q}_3^d & \cdots & 0 \\ \vdots & \vdots & \ddots & \ddots & \vdots \\ 0 & 0 & \cdots & 0 & \mathbf{Q}_N^d \end{bmatrix} \in \mathrm{R}^{n_s \times n_a}; \tag{2.68}$$

with

$$\mathbf{Q}_1^d = \begin{bmatrix} 0 & 0 & 0 & 0 & 0 \\ 0 & 0 & 0 & 0 & 0 \\ 0 & 0 & 0 & 0 & 0 \\ 1 & 0 & 0 & 0 & 0 \\ 0 & 1 & 0 & 0 & 0 \\ 0 & 0 & 1 & 0 & 0 \\ 0 & 0 & 0 & 0 & 0 \\ 0 & 0 & 0 & 0 & 0 \\ 0 & 0 & 0 & 0 & 0 \\ 0 & & 0 & 0 & 0 \\ 0 & 0 & 0 & \phi_{1a} & 0 \\ 0 & 0 & 0 & 0 & \phi_{1b} \\ 0 & 0 & 0 & 0 & 0 \end{bmatrix} \quad ; \quad \mathbf{Q}_2^d = \begin{bmatrix} 1 & 0 & 0 & 0 & 0 & 0 & 0 \\ 0 & 1 & 0 & 0 & 0 & 0 & 0 \\ 0 & 0 & 1 & 0 & 0 & 0 & 0 \\ 0 & 0 & 0 & 1 & 0 & 0 & 0 \\ 0 & 0 & 0 & 0 & 1 & 0 & 0 \\ 0 & 0 & 0 & 0 & 0 & 1 & 0 \\ 0 & 0 & 0 & 0 & 0 & 0 & 0 \\ 0 & 0 & 0 & 0 & 0 & 0 & 0 \\ 0 & 0 & 0 & 0 & 0 & 0 & 0 \\ 0 & 0 & 0 & 0 & 0 & & 0 \\ 0 & 0 & 0 & 0 & 0 & 0 & 0 \\ 0 & 0 & 0 & 0 & 0 & 0 & 0 \\ 0 & 0 & 0 & 0 & 0 & 0 & 1 \end{bmatrix} \quad ;$$

$$\mathbf{Q}_i^d = \begin{bmatrix} 0 & 0 & 0 & 0 \\ 0 & 0 & 0 & 0 \\ 0 & 0 & 0 & 0 \\ 1 & 0 & 0 & 0 \\ 0 & 1 & 0 & 0 \\ 0 & 0 & 1 & 0 \\ 0 & 0 & 0 & 0 \\ 0 & 0 & 0 & 0 \\ 0 & 0 & 0 & 0 \\ 0 & 0 & 0 & 0 \\ 0 & 0 & 0 & 0 \\ 0 & 0 & 0 & 0 \\ 0 & 0 & 0 & 1 \end{bmatrix} \quad ; \qquad i = 3,.....,N.$$

It may be pointed out that ϕ_{1a} and ϕ_{1b} are evaluated at the locations of the momentum gyros.

Here n_s represents the number of generalized coordinates for the system:

Body One – three for orbital position of the C.M. , three for librational motion, three for vibration (considering one mode in each direction), and one for deployment, i.e. ten degrees of freedom for the platform.

Body Two – three for the mobile base, three for the revolute joint slew motion, three for the joint flexibility, three for vibration (one mode representation as in the case of body one), and one for deployment, i.e. thirteen degrees of freedom.

Bodies Three to N – same as body two except the base motion is eliminated through introduction of the Lagrange multipliers as explained in the following section, i.e. ten degrees of freedom.

2.12 Specified Equations of Motion

The equations of motion were derived with a time dependent offset of the joint attachment point, d_i, which was treated as a generalized coordinate. However, one may constrain it to a fixed or time-specified value. This is achieved through the introduction of Lagrange multipliers. One begins by assigning the multiplier to all the constrained equations. Thus letting $f = F - Q$ in Eq.(2.1) gives

$$\mathbf{M}\ddot{q} + f = \mathbf{P}^c \Lambda , \tag{2.69}$$

where Λ is the vector of Lagrange multipliers and $\mathbf{P}^c$ is the permutation matrix assigning the appropriate Λ_i to its corresponding constrained equations. Inverting $\mathbf{M}$ and pre-multiplying both sides by $\mathbf{P}^{c^T}$ gives

$$\mathbf{P}^{c^T}(\ddot{q} + \mathbf{M}^{-1} f) = [\mathbf{P}^{c^T}\mathbf{M}^{-1}\mathbf{P}^c]\Lambda . \tag{2.70}$$

i.e.

$$\ddot{q}_s + \mathbf{P}^{c^T}\mathbf{M}^{-1} f = [\mathbf{P}^{c^T}\mathbf{M}^{-1}\mathbf{P}^c]\Lambda , \tag{2.71}$$

where $\ddot{\boldsymbol{q}}_s$ is the desired offset acceleration vector. Note that, both $\ddot{\boldsymbol{q}}_s$ and $(\mathbf{P}^{c^T}\mathbf{M}^{-1}\boldsymbol{f})$ are known. Thus, the solution for Λ has the form

$$\Lambda = [\mathbf{P}^{c^T}\mathbf{M}^{-1}\mathbf{P}^c]^{-1}(\ddot{\boldsymbol{q}}_s + \mathbf{P}^{c^T}\mathbf{M}^{-1}\boldsymbol{f}). \tag{2.72}$$

Now, substituting Eq. (2.72) into Eq. (2.69) and rearranging the terms gives

$$\ddot{\boldsymbol{q}} = -\mathbf{M}^{-1}\boldsymbol{f} + \mathbf{M}^{-1}\mathbf{P}^c[\mathbf{P}^{c^T}\mathbf{M}^{-1}\mathbf{P}^c]^{-1}(\ddot{\boldsymbol{q}}_s + \mathbf{P}^{c^T}\mathbf{M}^{-1}\boldsymbol{f}), \tag{2.73}$$

which is the constrained vector equation of motion with specified coordinates $\ddot{\boldsymbol{q}}_s$ predetermined.

It may be pointed out that the equations of motion still retain their O(N) character, even in the presence of constraints, as the Lagrange multipliers can be obtained recursively [76]. Thus, in the case where the j^{th} variable is constrained to be constant at its initial value, $\ddot{\boldsymbol{q}}_{s_j} = 0$. In the case of prescribed maneuvers, $\ddot{\boldsymbol{q}}_{s_j}$ is simply defined as the desired acceleration profile. Later in the study, a sinusoidal acceleration profile is adopted for prescribed maneuvers. It assures zero velocity and acceleration at the beginning and end of the maneuver, thereby reducing the structural response of the system. The maneuver time history considered is as follows,

$$\boldsymbol{q}_{s_j} = \frac{\Delta \boldsymbol{q}_{s_j}}{\Delta \tau}\left\{\tau - \frac{\Delta \tau}{2\pi} sin\left(\frac{2\pi}{\Delta \tau}\tau\right)\right\}, \tag{2.74}$$

where $\boldsymbol{q}_{s_j}$ is the constrained coordinate; $\Delta \boldsymbol{q}_{s_j}$ is its desired variation; τ is the time; and $\Delta\tau$ is the time required for the maneuver. The time history for $\boldsymbol{q}_{s_j}$, $\dot{\boldsymbol{q}}_{s_j}$, and $\ddot{\boldsymbol{q}}_{s_j}$ are plotted, for the

case $\Delta q_{s_j} = 1$ and $\Delta \tau = 1$, in Figure 2-5. In case other profile is needed, one can always change the format of Eq. (2.74) to specify the motion.

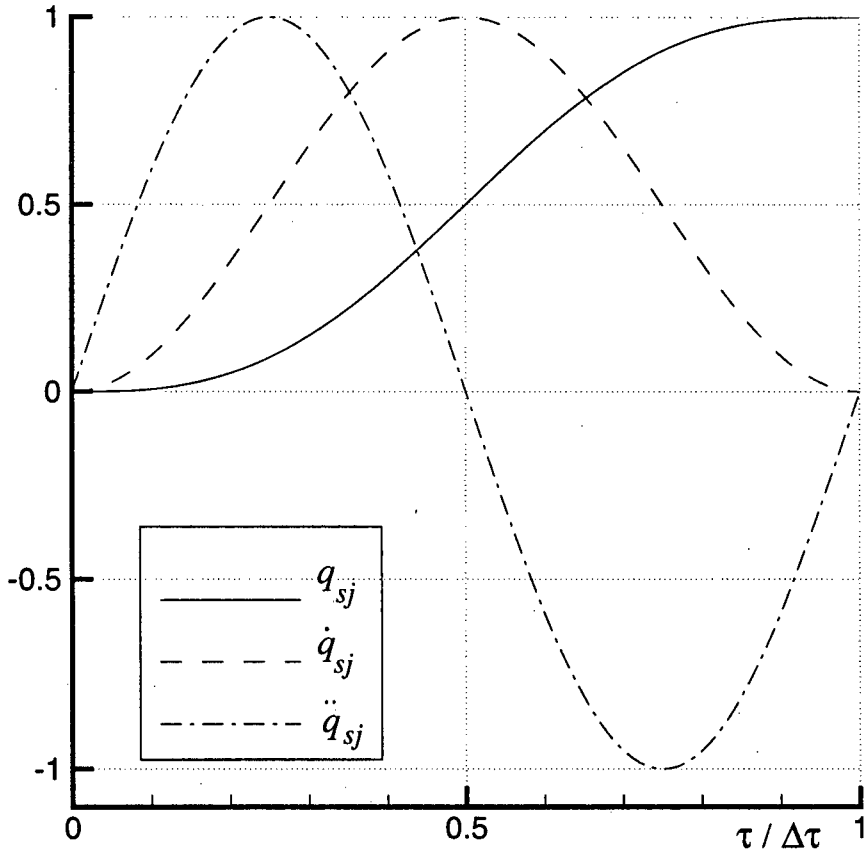

Figure 2-5 Normalized time histories of the sinusoidal maneuvering profile showing displacement, velocity, and acceleration.

3. COMPUTER IMPLEMENTATION

3.1 Introduction

The equations of motion governing general three-dimensional dynamics of an *N*-body space-based manipulator system were derived in Chapter 2. As can be expected, the equations are extremely lengthy even in the matrix notation. Furthermore, they are highly nonlinear, nonautonomous and coupled. As pointed out before, they can be cast into a form

$$\mathbf{M}(q,t)\ddot{q} + F(\dot{q},q,t) = Q(\dot{q},q,t) \ , \tag{3.1}$$

which is suitable for studying inverse dynamics of the system. In the present study, the interest is in the forward dynamics as given by

$$\ddot{q} = \mathbf{M}^{-1}(Q - F). \tag{3.2}$$

As a closed-form solution of this formidable set of equations is virtually impossible (except for some particular, trivial cases), one is forced to turn to a numerical approach.

At the outset it was recognized that this would represent an enormous commitment of time. The main objective of the thesis is to lay a sound foundation for approaching this class of novel manipulators free to undergo three-dimensional dynamics. There lies the challenge and innovation (Chapter 2). Development of the corresponding computer code, though important, was not considered the primary objective and contribution of the thesis.

It was recognized that three-dimensional character of the formulation significantly added to the complexity of the governing equations, and hence would demand commensurate time for the code development. What is important is to give physical appreciation of the system dynamics (interactions between various degrees of freedom) and control behaviour. Therefore, it was decided to develop a program for the planar case.

The planar dynamics refers to the situation where the system is free to vibrate in the orbital plane. Thus the platform is free to undergo pitch motion, and its vibration is confined to the plane of the orbit (x_0,y_0 –plane). The same is true with the manipulator maneuvers and the module vibrations. This closely resembles important dynamics of the International Space Station with the Mobile Servicing System.

Furthermore, as pointed out in Chapter 1, one of the objectives of the investigation is to compare numerical simulation results, during controlled operation, with those obtained using the ground-based prototype manipulator, already constructed by Chu [8]. This is discussed in Chapter 7. As the prototype is free to operate in the horizontal plane, the governing equations in Chapter 2 will have to be reduced to correspond to the ground-based planar condition. This not only strengthened the case for development of a code for planar study, but also brought to light that such reduction of the formulation for space-based system to earthbound manipulators has not been reported. Such versatility is indeed desirable and would constitute an important contribution.

The acceleration vector $\ddot{\boldsymbol{q}}$ must be integrated twice over time to obtain the displacement response $\boldsymbol{q}(t)$ of the various degrees of freedom. Although, conceptually it appears simple, in reality it is a formidable task due to the character of the set of equations. The problem is further complicated by the fact that the equations of motion form a stiff set of differential equations; i.e. the bandwidth involved shows large differences. For instance, the librational period of the system has the order of the orbital period, while the structural vibrations of the various components have frequencies in the range of a few Hz. Any algorithm developed must take this into account; otherwise numerical error may result.

As pointed out before, the variable geometry manipulator system is highly redundant. That means, it has more degrees of freedom than are minimally required to perform a task. Presence of kinematic redundancy in robot manipulators is often desirable in order to cope with failure of some of the joints, or navigate around obstacles in a specified task path. The redundancy can also be used, quite effectively, in isolating the dynamic coupling between the manipulator supporting structure (platform) and links, or between links, from the disturbances induced by manipulator maneuvers [51]. Furthermore, it can serve as an effective tool to optimize the task trajectory according to a suitable performance criterion (e.g., minimum dynamic interactions; minimum base reaction; minimum actuator effort; etc.).

This chapter discusses the computer program written for the dynamical simulation of the manipulator and its supporting platform. The aim has been to develop an efficient code that is capable of dealing with a wide range of conditions likely to be encountered in practice. First, the structure of the computer code is introduced. Then, the procedure followed to validate both the formulation and the computer code is presented. Some sample test cases are provided to illustrate the validation procedure and to confirm the accuracy of the numerical model.

3.2 Numerical Algorithm

3.2.1 Structure of the computer code

The simulation of the system's dynamics requires solution of Eq.(3-2). Therefore, the main task of the program consists essentially in finding $\mathbf{M}^{-1}$, $\boldsymbol{F}$, $\boldsymbol{Q}$, and thus $\ddot{\boldsymbol{q}}$ for each time-step. The system dynamics is represented in the first order form as

$$\dot{\boldsymbol{x}} = \begin{bmatrix} \dot{\boldsymbol{q}} \\ \ddot{\boldsymbol{q}} \end{bmatrix} = \begin{bmatrix} \dot{\boldsymbol{q}} \\ \mathbf{M}^{-1}(\boldsymbol{Q} - \boldsymbol{F}) \end{bmatrix}, \tag{3-3}$$

where $\boldsymbol{x} = [\boldsymbol{q}^T \ \dot{\boldsymbol{q}}^T]^T$. The state rate vector $\dot{\boldsymbol{x}}$ is integrated at each desired point in time using Gear's method, which is essentially a backward differentiation formula for stiff equations, employing an implicit linear multi-step approach of the predictor-corrector type [52].

The architecture of the program, which performs these tasks, is shown in Figure 3-1. The program was designed in a highly modular fashion to provide the necessary flexibility and to facilitate modifications. The number of manipulator units and the number of vibrational modes per body are specified in the file "number.dat". It should be pointed out that every time this file is modified, the entire program must be re-compiled in order to adjust the size of the matrices accordingly.

Initially, the program asks the user if the platform and the manipulator links are rigid or flexible. In the rigid case, the appropriate flexibility generalized coordinates are "disabled". This is computationally more efficient than modeling rigid bodies by using extremely large stiffness. After the appropriate choice is made for a rigid or flexible model for the platform and the manipulator units, the code reads assigned values of parameters from input files. These are:

- initial conditions for all degrees of freedom, i.e. $\boldsymbol{x}(0) = [\boldsymbol{q}(0)^T \ \dot{\boldsymbol{q}}(0)^T]^T$
- system's inertia, stiffness, and damping parameters;
- payload mass and inertia;
- starting time, duration, and amplitude of joint slewing, deployment, and mobile base translation;
- relative error tolerance, initial integration step-size, and number of time-steps for the simulation.

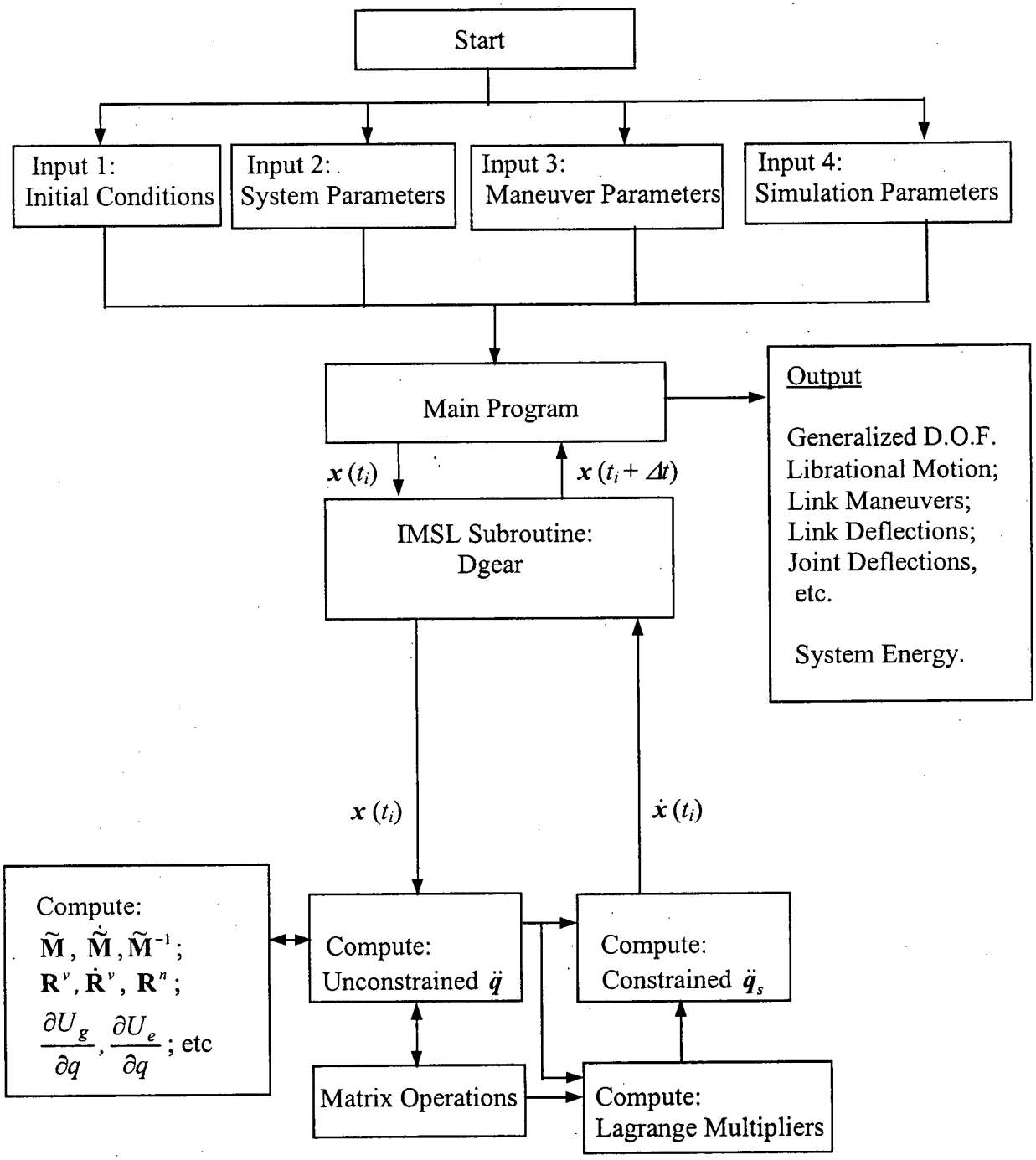

Figure 3-1 Flow diagram showing the architecture of the computer program.

Except for the initial conditions and integration parameters, all input quantities are made available to the other subroutines through common statements. The initial conditions define the state $\boldsymbol{x}(0)$, which is saved in an output file.

After the input parameters have been specified, the *IMSL* DGEAR subroutine is called in. It features a version of Gear's method where the selection of the integration step-size is automatic and based on the user-specified relative error-bound. The subroutine reads in the initial state $\boldsymbol{x}(0)$, the error tolerance, and the initial step-size. It then calls the "equation" subroutine, which calculates $\dot{\boldsymbol{x}}$. The "equation" subroutine is called as many times as the number of iterations required by Gear's method to converge to the solution $\boldsymbol{x}(t_i)$, within the specified error-bound. It automatically avoids presence of any numerical instability. The final solution $\boldsymbol{x}(t_i)$ is recorded in an output file and becomes the new initial state for the next time-step. This procedure is repeated in the subsequent time-steps, up to the final simulation time-step, t_f. All the solution states $\mathbf{x}(t_0), \boldsymbol{x}(t_1), \boldsymbol{x}(t_2), \ldots, \boldsymbol{x}(t_f)$ are recorded in output files. It may be pointed out that the vectors $\boldsymbol{x}(t_i)$ can be modified into more suitable forms using various output subroutines.

The "equation" subroutine constitutes major part of the program. For each iteration that is required by the DGEAR subroutine, it defines the $\tilde{\mathbf{M}}$, $\dot{\tilde{\mathbf{M}}}$, $\tilde{\mathbf{M}}^{-1}$, $\mathbf{R}^{-1}(\mathbf{I}-\mathbf{R}^n)$, $\mathbf{R}^v$, $\dot{\mathbf{R}}^v$, $\partial\{\dot{\boldsymbol{q}}^T\mathbf{M}\dot{\boldsymbol{q}}\}/\partial\boldsymbol{q}$, $\partial U_g/\partial\boldsymbol{q}$, $\partial U_e/\partial\boldsymbol{q}$, $\partial\mathbf{R}^p/\partial\dot{\boldsymbol{q}}$, and $\boldsymbol{Q}$ matrices. This allows computation of the term $\mathbf{M}^{-1}(\boldsymbol{Q}-\boldsymbol{F})$. The "equation" subroutine then calls the "constraint" subroutine, which computes the Lagrange multipliers Λ and the matrix $\mathbf{P}^c$. The constrained acceleration vector $\ddot{\boldsymbol{q}}$ is obtained and converted into the first order derivative form $\dot{\boldsymbol{x}}$. It should be noted that most cases do involve specified coordinates. The specified components of the $\dot{\boldsymbol{x}}$ vector are not integrated, since their respective time histories are already known.

The computations leading to the acceleration vector $\ddot{q}$ require a significant number of matrix multiplications and additions. Several of the matrices involved have a number of constituent block submatrices as zero. Efficient subroutines were designed specifically for each matrix product. An effort was made not to multiply the zero elements, thereby reducing considerably the number of computations.

Finally, it should be noted that the shape functions used and their derivatives must be integrated over each body. These integrations can become quite involved for time-varying shape functions. In the past, many researchers have coped with those integrals using numerical integration routines. However, the integrals must be evaluated in every iteration cycle of the solution. Therefore, numerical integration can reduce significantly the speed of the simulation. This emphasized a need for symbolic expressions for the integrals. The symbolic manipulator *MAPLE V* was used in order to evaluate analytically the shape function integrals. It offered the additional advantage of converting the expressions to *FORTRAN* code directly.

3.2.2 Verification of the computer code

The validity of the computer code was established through several checks. The size of the governing equations of motion, in addition to the number of operations required to derive them, can easily lead to formulation and programming errors (the computer code contains over 10,000 lines!). To some extent, these errors can be minimized through careful, systematic derivation and programming. Furthermore, discrepancies may reveal themselves when the computer code is compiled and its constituting parts are linked, thereby resulting in "compiling" and "linking" errors. However, some errors may be quite elusive and require precise checks.

Ideally, the results obtained with the code should be compared with data collected from an actual spacecraft supporting a flexible manipulator. Unfortunately, dedicated well-planned dynamics and control experiments in space are rare. Furthermore, frequently such information is not made available in the open literature. Obviously, for the novel system proposed here, no such data are available. Hence, the lack of relevant information does not permit comparison of the simulation results with those for an actual space-based manipulator. A more convenient avenue is to check the conservation of energy for undamped systems. Similarly, the conservation of angular momentum can also be verified. Another alternative is to match simulation results for particular cases studied by other researchers. In the thesis, the conservation of energy check is used to ensure the validity of the computer code and formulation.

3.3 Conservation of Energy

In the absence of damping and external, nonconservative, generalized forces, the total energy of the system must remain constant. Thus, variation of the total energy for a conservative system would indicate an error in the program or/and in the derivation of the equations of motion.

A thorough check of the conservation of energy was performed on several cases, involving a variety of system parameters, initial conditions, number of bodies, and manipulator configurations. A check was considered successful if and only if the variation of energy was found to correspond to the numerical noise. It was observed that even small truncation errors led to significant variations in the total energy of the system. Hence, even errors which might be considered negligible were found to have noticeable effects on the conservation of energy. Since the orbital motion of the platform accounts for most of the

system's total energy, its effects were removed in test-cases. In other words, the gravitational parameter μ, as well as the orbital velocity and acceleration, were all set to zero, resulting in a free-floating system. This allowed errors associated with structural vibrations to become more apparent. This phase of the program verification was considered complete when the selected cases led to constant total energy. The following two test-cases serve as examples. They illustrate the methodology adopted and validity of the computer code for widely differing situations.

The first case considers a five-body system. The first body, representing the rigid platform, has a length of 120 m and a mass of 120000 kg. Each of the remaining rigid bodies (manipulator with four modules) is 10 m long with a mass of 400 kg. The bodies are all connected with flexible joints of a torsional stiffness $K = 10^4$ Nm/rad. The chain is initially straight, aligned with the platform, which is in equilibrium along the local vertical. The system is nominally in a circular orbit at an altitude of 400 km with an angular velocity of $\dot{\theta} = 0.0648°/s$. It is now subjected to an initial disturbance of 30° in pitch ($\psi = 30°$) and a small change in $\dot{\theta}$. Figure 3-2 shows evolution of the system dynamics over one orbit. The change in the motion of the system's center of mass is shown ($\Delta \boldsymbol{D}_1$) as well as the attitude motion of each individual body. Note, the altitude after half the orbit period has diminished by 120 m ($\Delta \boldsymbol{D}_1$) resulting in a slightly elliptic orbit of eccentricity 0.0066. The flexible revolute joints cause the manipulator modules to vibrate with a maximum amplitude that is less than one degree (χ_2), while the system is undergoing undamped librational motion of $\approx 30°$. Thus there is transfer of energy between orbital, librational and joint vibrational degrees of freedom. Even in this complex situation, the total energy is conserved with an error (e) of less than 10^{-12} %, which essentially represents computational noise having no

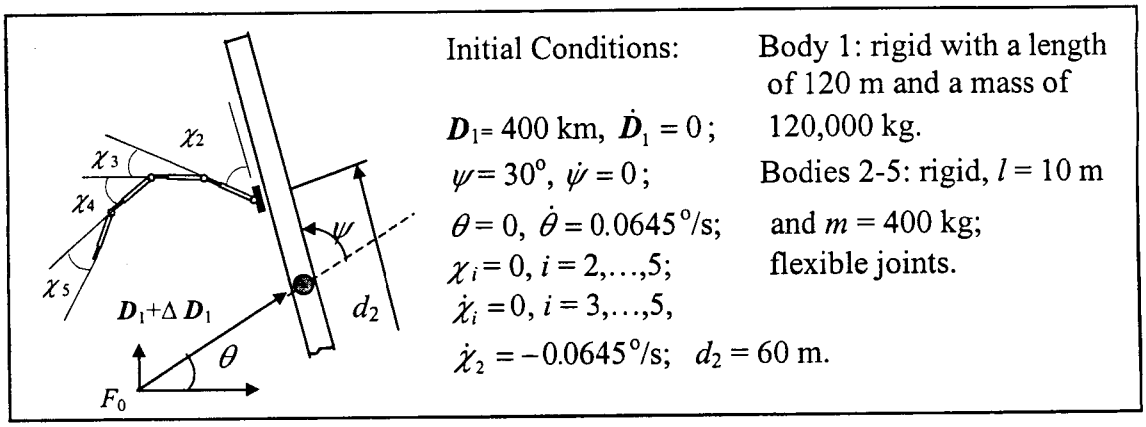

Initial Conditions:

$\boldsymbol{D}_1 = 400$ km, $\dot{\boldsymbol{D}}_1 = 0$;

$\psi = 30°$, $\dot{\psi} = 0$;

$\theta = 0$, $\dot{\theta} = 0.0645°/s$;

$\chi_i = 0$, $i = 2,\ldots,5$;

$\dot{\chi}_i = 0$, $i = 3,\ldots,5$,

$\dot{\chi}_2 = -0.0645°/s$; $d_2 = 60$ m.

Body 1: rigid with a length of 120 m and a mass of 120,000 kg.

Bodies 2-5: rigid, $l = 10$ m and $m = 400$ kg; flexible joints.

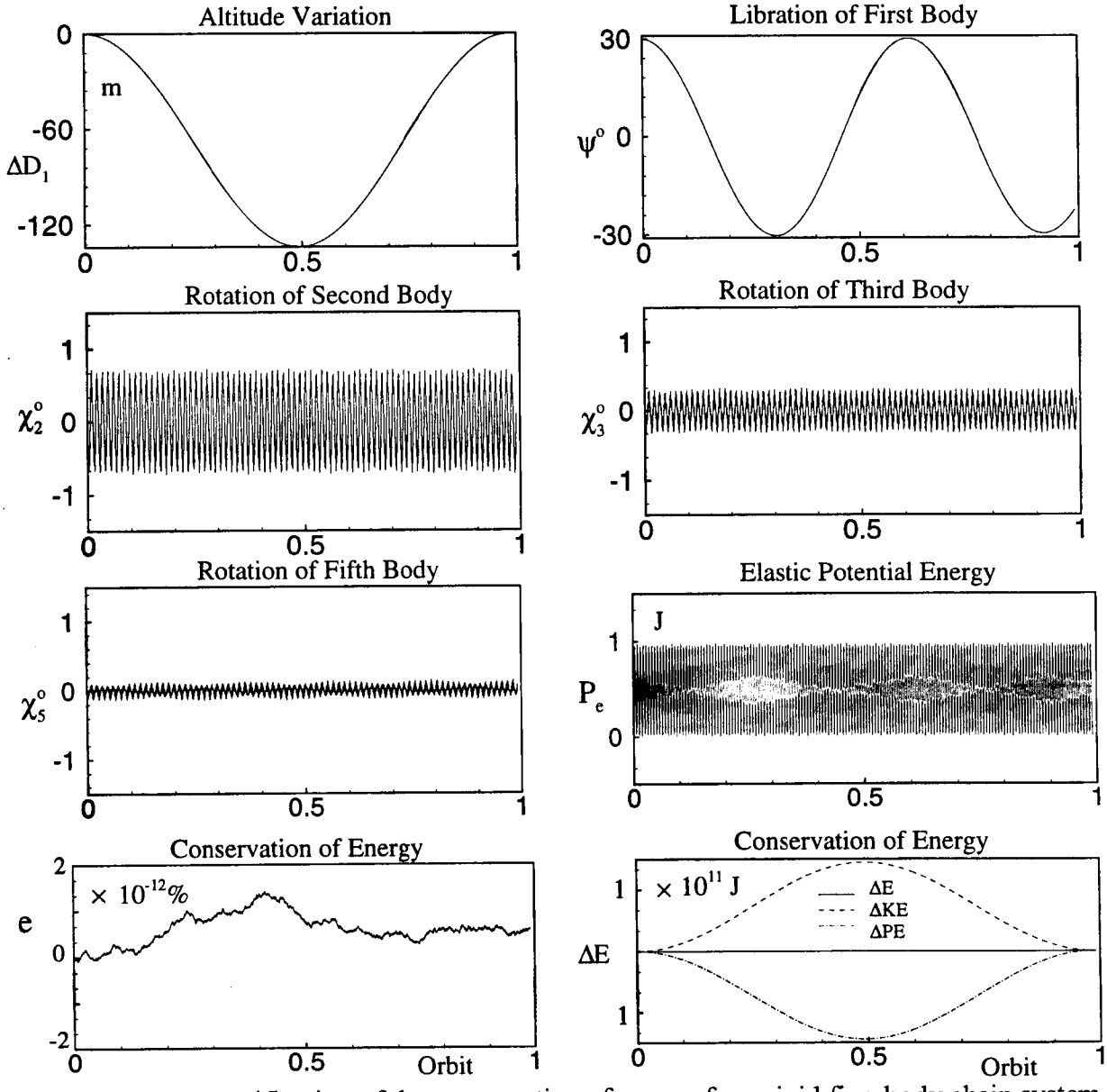

Figure 3-2 Verification of the conservation of energy for a rigid five-body chain system with flexible joints (E, total energy; PE, potential energy; KE, kinetic energy).

discernable features. Note, the change in energy (ΔE) is virtually zero. The program is indeed quite sensitive and is able to track time variation of the strain energy (P_e) as small as 1 J.

The second case examines the effect of link flexibility on the position of the manipulator's end-effector with the system in a circular orbit at a height of 400 km (92.5 minutes period, Figure 3-3). A five-unit manipulator (i.e. 10 links, five free to slew while the other five deployable), shown in the inset, is located at the center of the platform with its base held fixed. The individual joints are locked in position as stated in the legend for the diagram (specified coordinates), and so are the deployable links. The platform is subjected to an initial tip deflection of 2 m in the first mode together with a pitch disturbance of 30°. To assess the effects of link flexibility, the response of a rigid manipulator (with flexible joints) system is also included for comparison. The joint rotations due to tip deflections of the flexible links, about the specified β_i positions, are represented by ϕ_2, ϕ_3,..., ϕ_6 (Figure 3-3a). Note, the manipulator modules two to six exhibit oscillations with insignificant amplitude (ϕ_3 to ϕ_6, amplitude less than 0.01°), while the first module (ϕ_2) displays around ± 9° oscillations about the specified $\beta_2 = 50°$ orientation. As expected, the response is at the forcing frequency corresponding to the platform vibration. Note the modulations of the pitch response (ψ) due to joint (solid line) as well as platform flexibility. The platform tip oscillations progress undamped (Figure 3-3b). x_e represents the manipulator-tip motion parallel to the undeformed platform, while y_e gives the displacement in the transverse direction, both with respect to the reference coordinate frame F_1. The results clearly show significant influence of the system flexibility on the position of the end-effector. Obviously, this has implication on the path planning. Furthermore, although there is a considerable transfer of energy between various

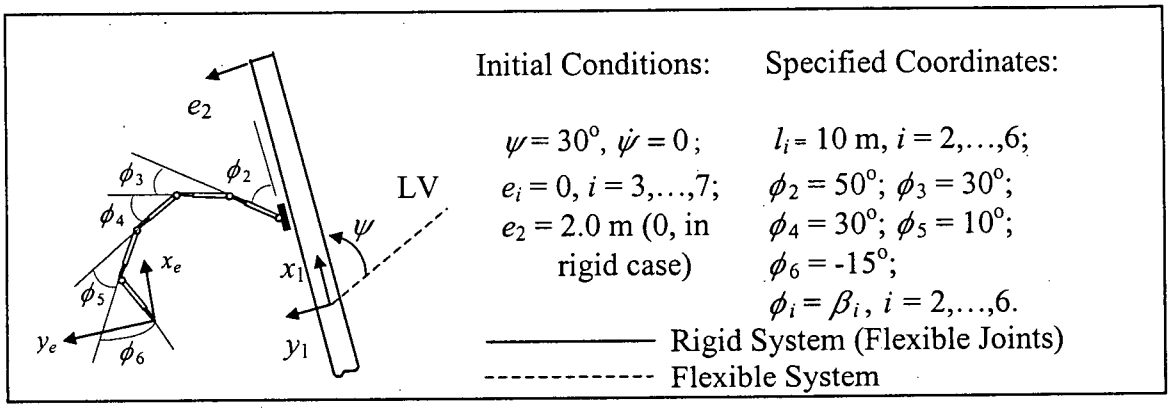

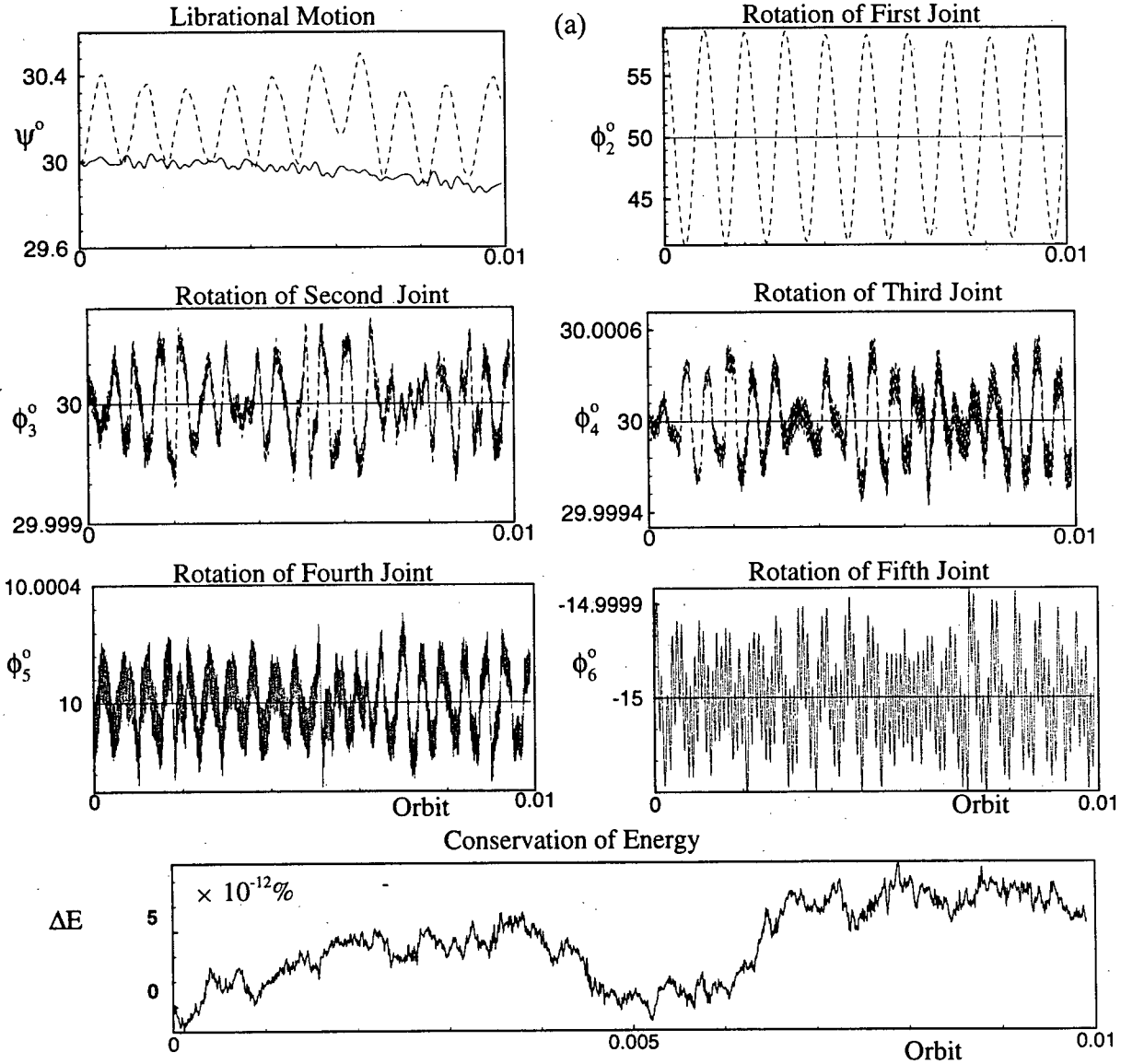

Figure 3-3 Effect of flexibility of the platform and manipulator on the system dynamics with a platform tip displacement of 2 m and librational disturbance of 30°. The system comprises of a five-unit manipulator supported by an orbiting platform: (a) platform libration, rotations of links and energy conservation; (b) platform and manipulator tip dynamics.

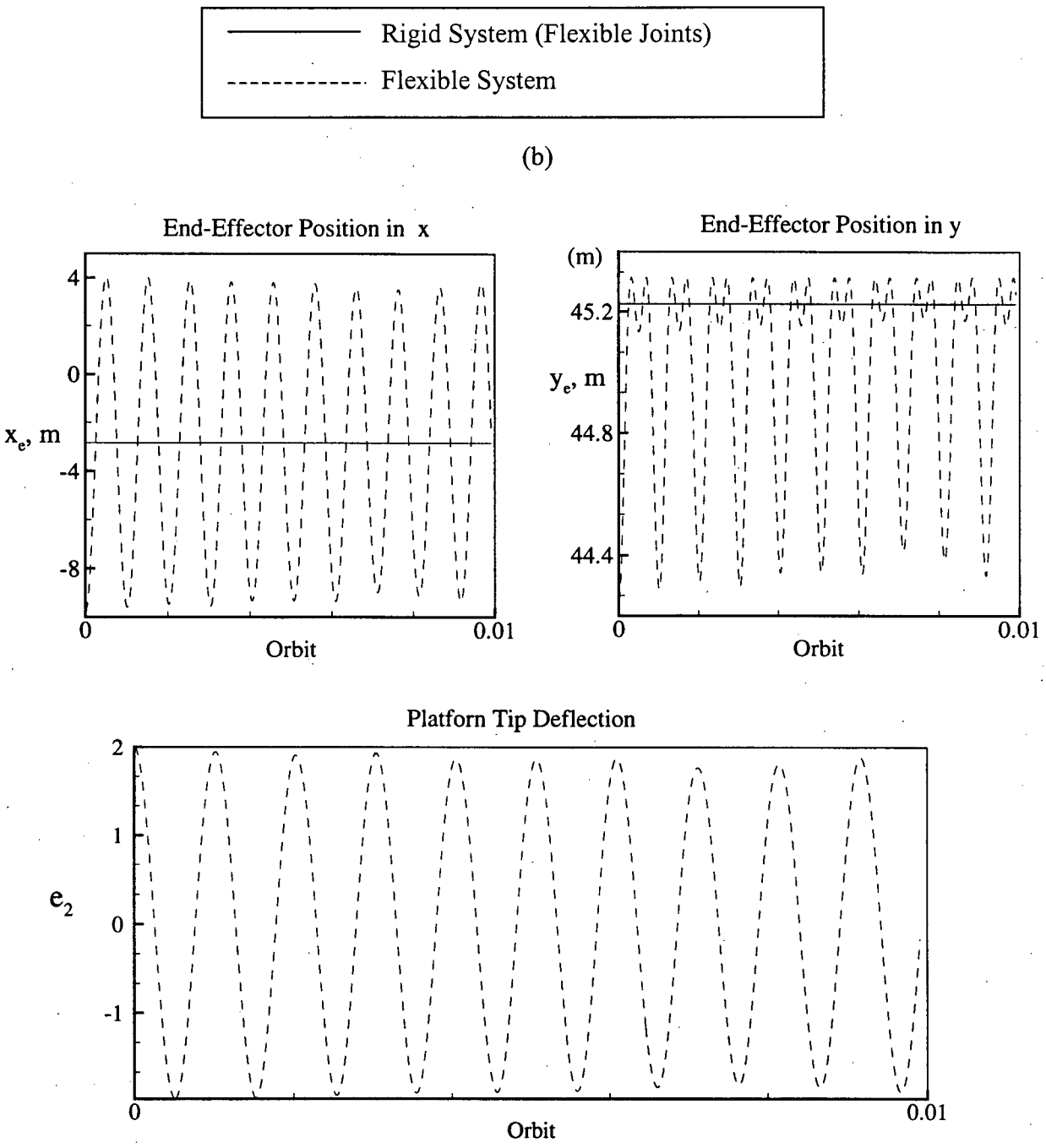

Figure 3-3 Effect of flexibility of the platform and manipulator on the system dynamics with a platform tip displacement of 2 m and librational disturbance of 30°. The system comprises of a five-unit manipulator supported by an orbiting platform: (a) platform libration, rotations of links and energy conservation; (b) platform and manipulator tip dynamics.

degrees of freedom, the total energy is conserved. As before, variation in the total energy, of the order of 10^{-12} %, is attributed to the computational noise.

A wide variety of such studies gave confidence as to the validity of the formulation and computer code.

4. DYNAMICAL STUDY OF THE SYSTEM

The previous chapter described an approach to the development of a computer code to simulate dynamics of a serial manipulator with an arbitrary number of slewing, deployable modules. The next logical step is to gain physical insight into the dynamics of this class of space manipulators through parametric analysis. Several factors are of importance: configuration of the system; variation of system parameters; number of manipulator units; initial disturbance; and specifications of manipulator maneuvers. The parametric study provided, literally, enormous amount of information. For conciseness, only a few representative cases, illustrating typical dynamical behavior, are reported here.

To begin with, the case of an orbiting platform, supporting a one-unit manipulator, is investigated. This relatively simple system exhibits important dynamical characteristics inherent to more complex configurations, and hence helps in the physical understanding of the response. This is followed by the study of more elaborate manipulator systems consisting of two, three, and five modules connected in series by revolute joints (Figure 4-1). Finally, dynamics of the system, having two modules of different scales, is explored with application aimed at gross and fine manipulations.

4.1 Numerical Data

Unless otherwise specified, the following numerical data were used in simulations:

Orbit

- Circular orbit at an altitude of 400 km; Period = 92.5 min.

Platform

- Cylindrical geometry with axial to transverse inertia ratio of 0.005;
- Mass, m_p = 120,000 kg;

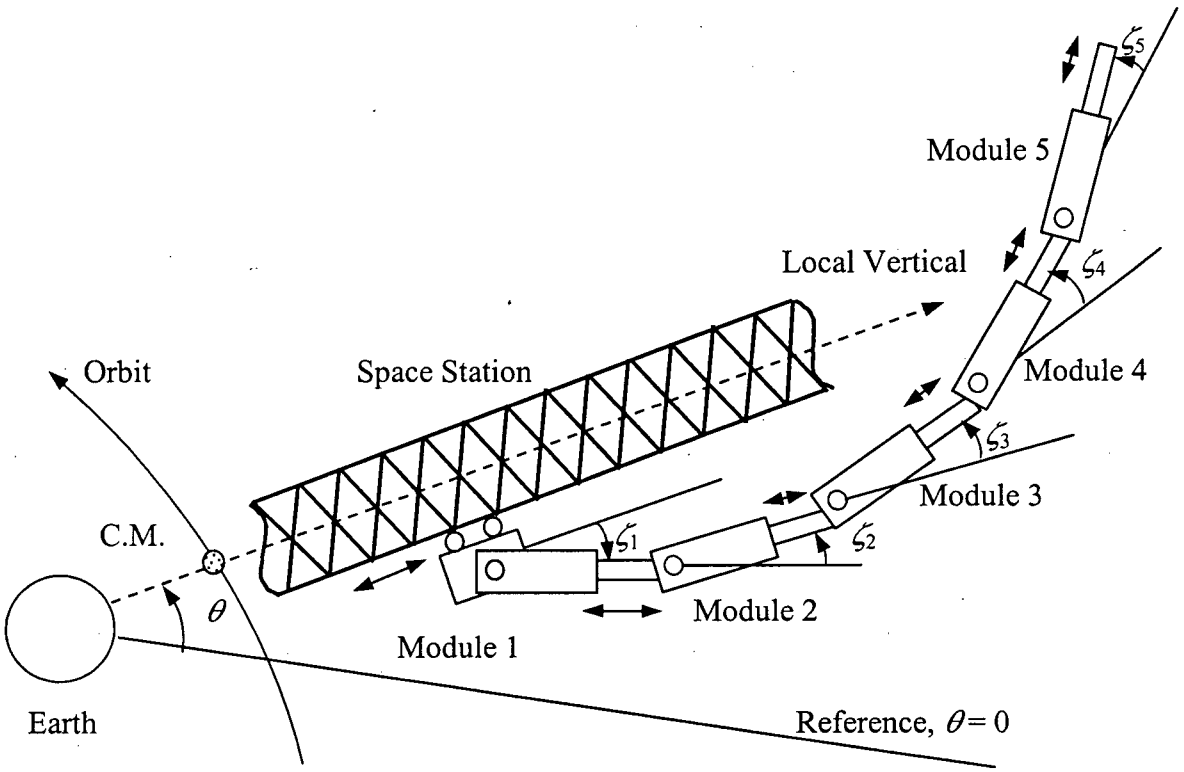

Figure 4-1 A schematic diagram of the multiunit manipulator system, based on an orbiting space platform, used for parametric study.

- Length, $l_p = 120$ m;
- Flexural Rigidity, $EI_p = 5.5 \times 10^8$ Nm^2.

Manipulator Joints

- Type: Revolute Joints;
- Mass, $m_j = 20$ kg;
- Moment of Inertia = 10 kg m^2 ;
- Stiffness (K) = 10^4 Nm/rad.

Manipulator Links (Slewing and Deployable)

- Cylindrical geometry with axial to transverse inertia ratio of 0.005;
- Mass; m_s, $m_d = 200$ kg;
- Length; l_s, $l_d = 7.5$ m;
- Flexural Rigidity; EI_s, $EI_d = 5.5 \times 10^5$ Nm^2.

Recall that a manipulator module consists of two telescopic links: one is free to slew and supports the other, which is deployable.

In the following simulations, longitudinal deformations being negligible are not reported, as well as the dynamics of the mobile base. Normally, the base will be locked in position during manipulator maneuvers. In general, only the first mode of transverse vibration is considered for the deformation of each body. Furthermore, the manipulator supports a point payload at the extremity of the last link. The ratio between the payload mass and the mass of a single module, referred to as the payload ratio, is used to specify the mass of the payload. For most cases, a payload ratio of 1 is considered, i.e. a payload of 400 kg. Cases involving different values of the payload ratio are clearly identified. It should also be noted that, for

most cases in this dynamical parametric study, energy dissipation is purposely not included in order to obtain a conservative estimate of the system response.

In the simulations, the following degrees of freedom are specified:

d_{2x}, d_{2y} offsets of the mobile base from the center of mass of the platform;

d_{ix}, d_{iy} base offsets of the (i^{th}-1) manipulator unit from the tip of the (i^{th}-2) unit;

β_i commanded rotation of the joint i, i.e rigid body rotation of the body i relative to the body (i-1);

l_i length of the (i^{th}-1) manipulator unit.

Here:

$$d_{2y} = 1.5 \text{ m},$$

$$d_{ix} = d_{iy} = 0.$$

d_{2x}, the offset of the manipulator system along the platform, β_i and l_i are either fixed at their respective initial values or vary as specific functions of time, as defined by Eq. (2-71). Once the manipulator maneuver and time taken are specified, Equation (2-71) can be used to compute the time-history of that variable. Note that, unless mentioned otherwise, the mobile base is taken to be located 60 m from the center of the platform, i.e. at the tip, to impart a severe disturbance.

At times, it is convenient to represent response of the system using variables other than the generalized coordinates for better understanding of the system dynamics. Hence, the following response variables are used:

ψ 'pitch' angle between the platform's long axis and the local vertical (LV), $\psi = \psi_1 - \theta$,

e_2 elastic displacement of the platform's tip relative to its undeformed position,

$$e_2 = \Phi_1\Big|_{\frac{l_1}{2}} \delta_1;$$

χ_i elastic angular deformation of the i^{th} joint, $\chi_i = \psi_i - \beta_i - \xi_i - \psi_{i-1}$;

e_i tip deflection of the (i^{th}-1) module relative to its undeformed position,

$$e_i = \Phi_{i-1}\big|_{l_{i-1}} \delta_{i-1}$$

In general, the platform is initially oriented along the local vertical, i.e. $\psi(0) = 0$, and

$$\chi_i(0) = 0, \qquad i = 2, \ldots, N;$$

$$e_i(0) = 0, \qquad i = 2, \ldots, N;$$

Important response variables are indicated in Figure 4-2.

4.2 System Response

This section briefly summarizes principal findings of a comprehensive dynamical response study.

4.2.1 Effect of manipulator location and orientation

Before proceeding to assess the influence of complex manipulator maneuvers on the system response, it would be of interest to explore the effect of unbalance caused just by its location and orientation, in absence of any maneuvers. The nominal stable equilibrium position of the platform is close to the local vertical with the base located at the center of the platform and the manipulator modules aligned with the longitudinal axis x_1 of the platform. Each of the manipulator modules has a length of 7.5 m and orientation as specified by the β_i initial conditions mentioned before.

Figure 4-3 shows the effect of base location for a two-module manipulator. Note, with $\beta_1 = \beta_2 = 0$ the platform would essentially remain aligned with the local vertical, except for a small offset of the module attachment point at the base (Figure 4-1) which is taken as 1.5 m.

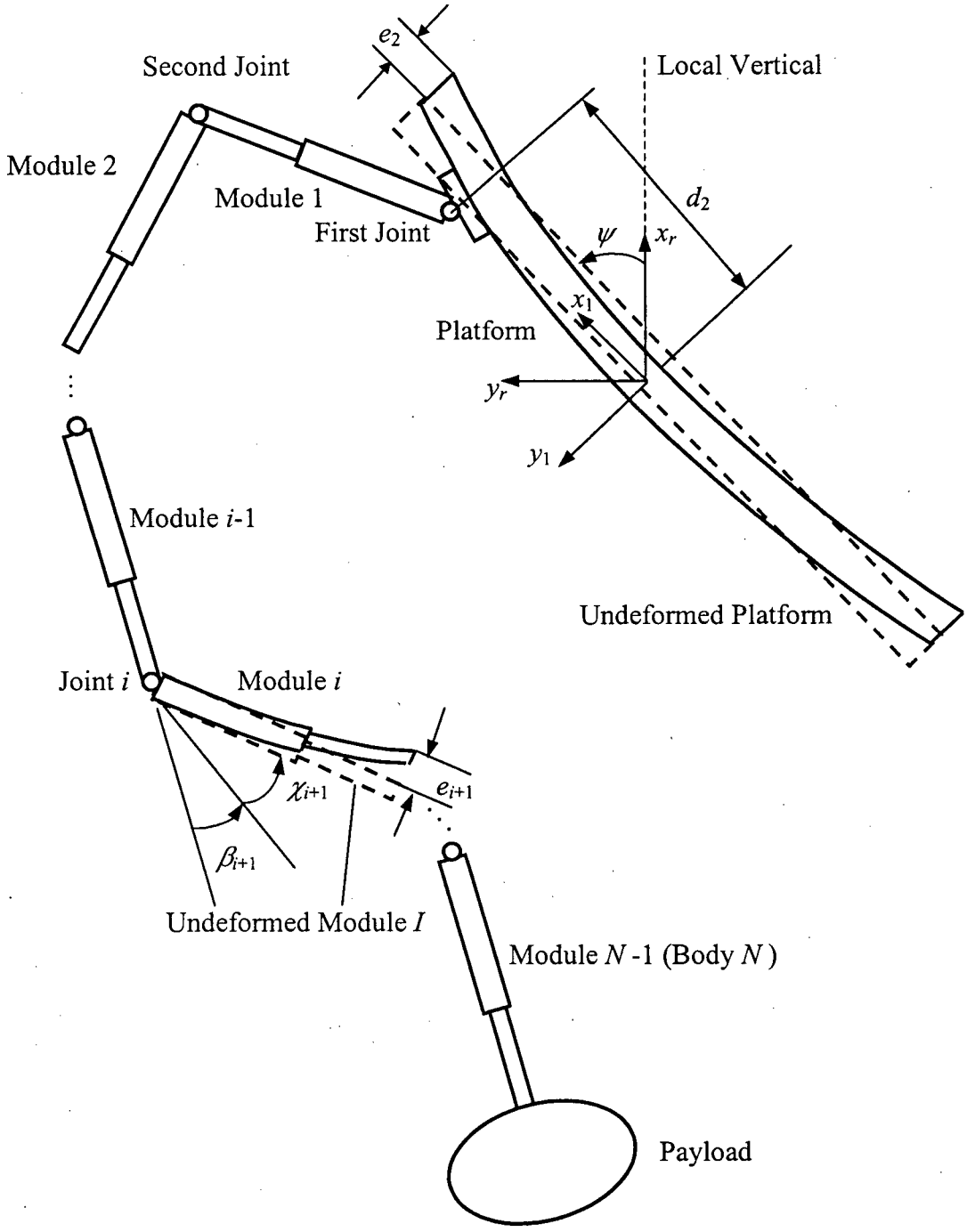

Figure 4-2 Schematic diagram of the manipulator system showing the coordinates considered for the dynamical study. x_r, y_r represent the orbital coordinates with origin at the system center of mass; x_1, y_1 correspond to the platform-based body coordinates.

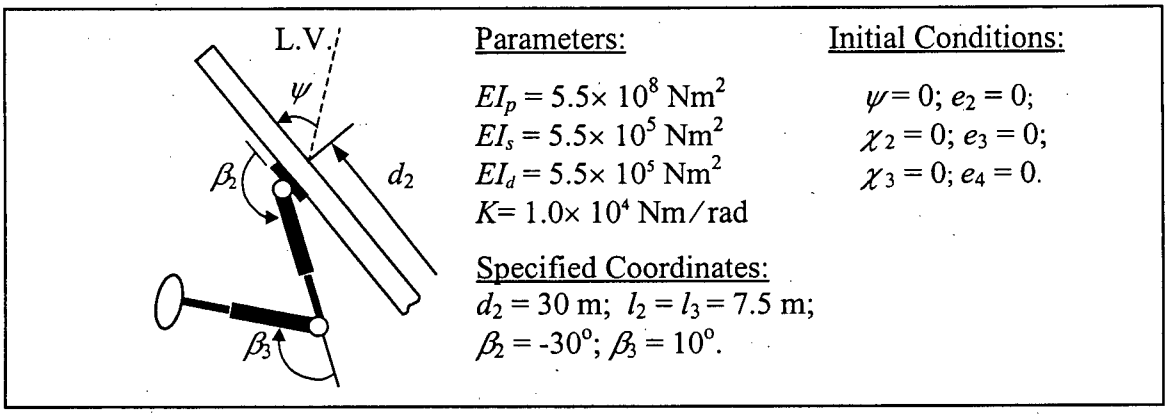

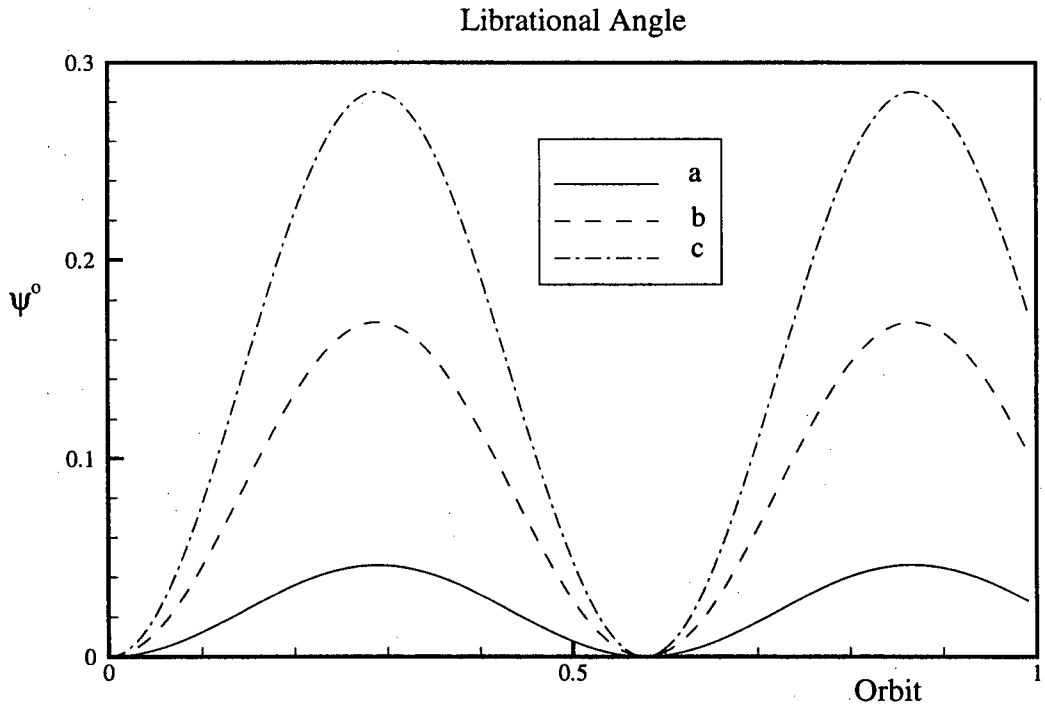

Figure 4-3 System response with a two-module manipulator located at different positions on the platform: (a) at the center; (b) 30 m from the center; (c) 60 m from the center.

With $\beta_1 = -30^\circ$ and $\beta_2 = 10^\circ$, movement of the manipulator center of mass results in a moment which increases as the base moves towards the platform tip. This leads to the librational motion with an amplitude of around 0.28°. It may appear small, however, depending on the mission, the permissible deviation may be as small as 0.1°.

Figure 4-4 presents the libration response as affected by the number of modules with the manipulator located at the platform tip ($d_{2x} = d_2 = 60$ m) with $\beta_1 = -30^\circ$, and β_2 to β_6 equal to 10°. As can be expected, the unbalance moment increases with the number of modules (each module weighs 400 kg) resulting in large amplitude vibrations.

In the above two cases, the platform was initially in the local vertical stable equilibrium position. Figure 4-5 considers the situation where the platform is initially in the unstable local horizontal configuration. The one-module manipulator is located at the tip as in the case of Figure 4-4. Note the unbalance leads to large amplitude librations about the local vertical. The flexible joint as well as manipulator and platform tip show rather minute oscillations, with modulations, which the formulation and the associated numerical code are able to capture quite effectively. The peak response corresponds to the instant when the platform crosses the local vertical and has the maximum velocity. Similarity between the joint and manipulator responses is due to their closely coupled character (joint motion excites the manipulator tip). The high frequency component corresponds to the manipulator's fundamental frequency (3.1Hz) with a payload of 400 kg.

4.2.2 One unit manipulator

The first case examines the response of the one-unit manipulator to the vibration of the supporting platform (Figure 4-6). The manipulator configuration, important parameters, and initial conditions are indicated in the legend. The slew and deployment joints are both locked

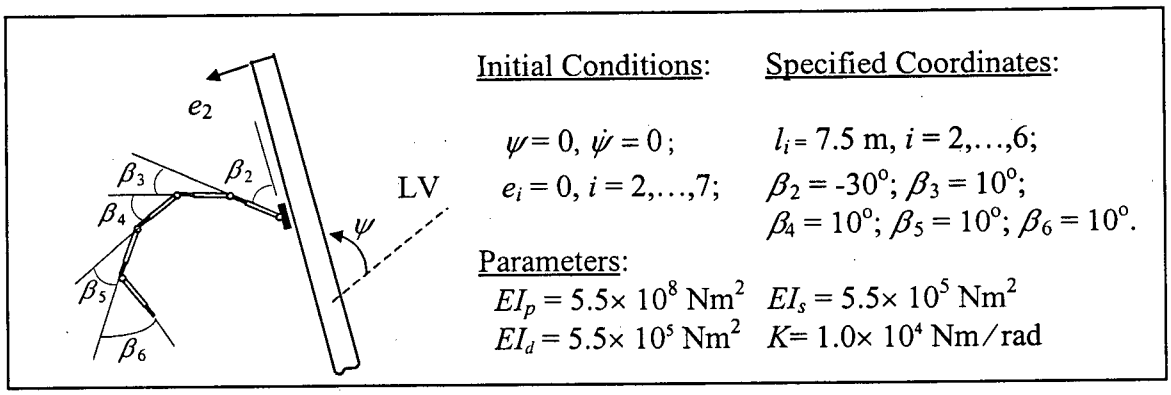

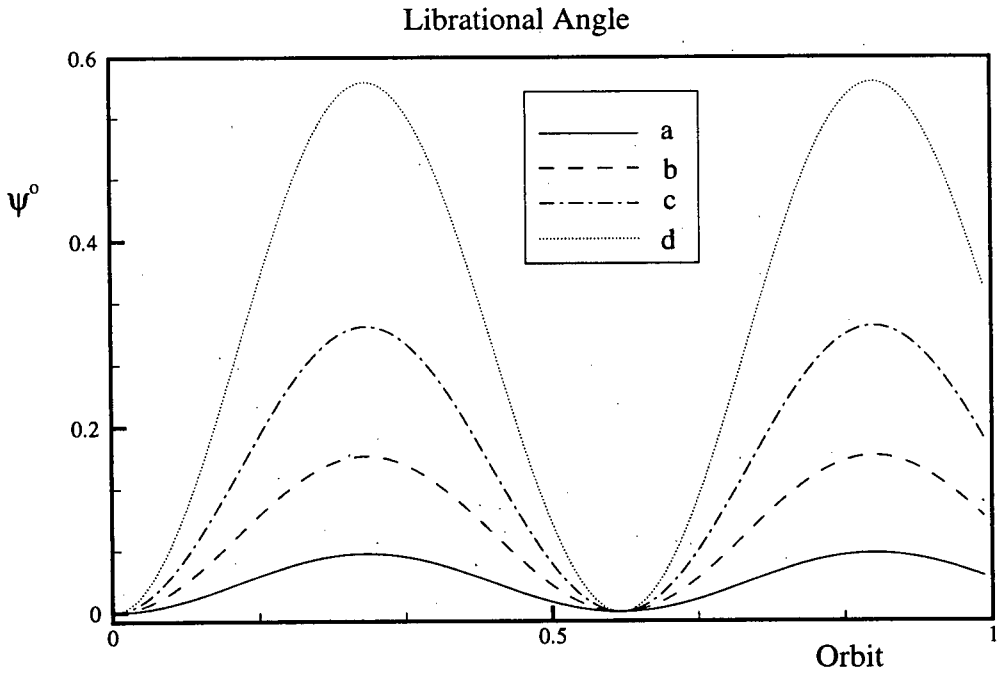

Figure 4-4 System response with different number of modules in the manipulator system: (a) one-unit; (b) two-units; (c) three-units; (d) five-units.

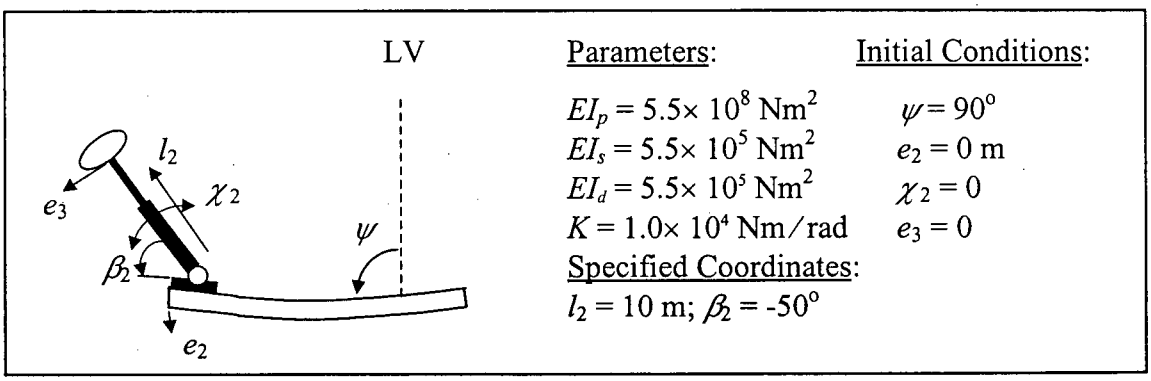

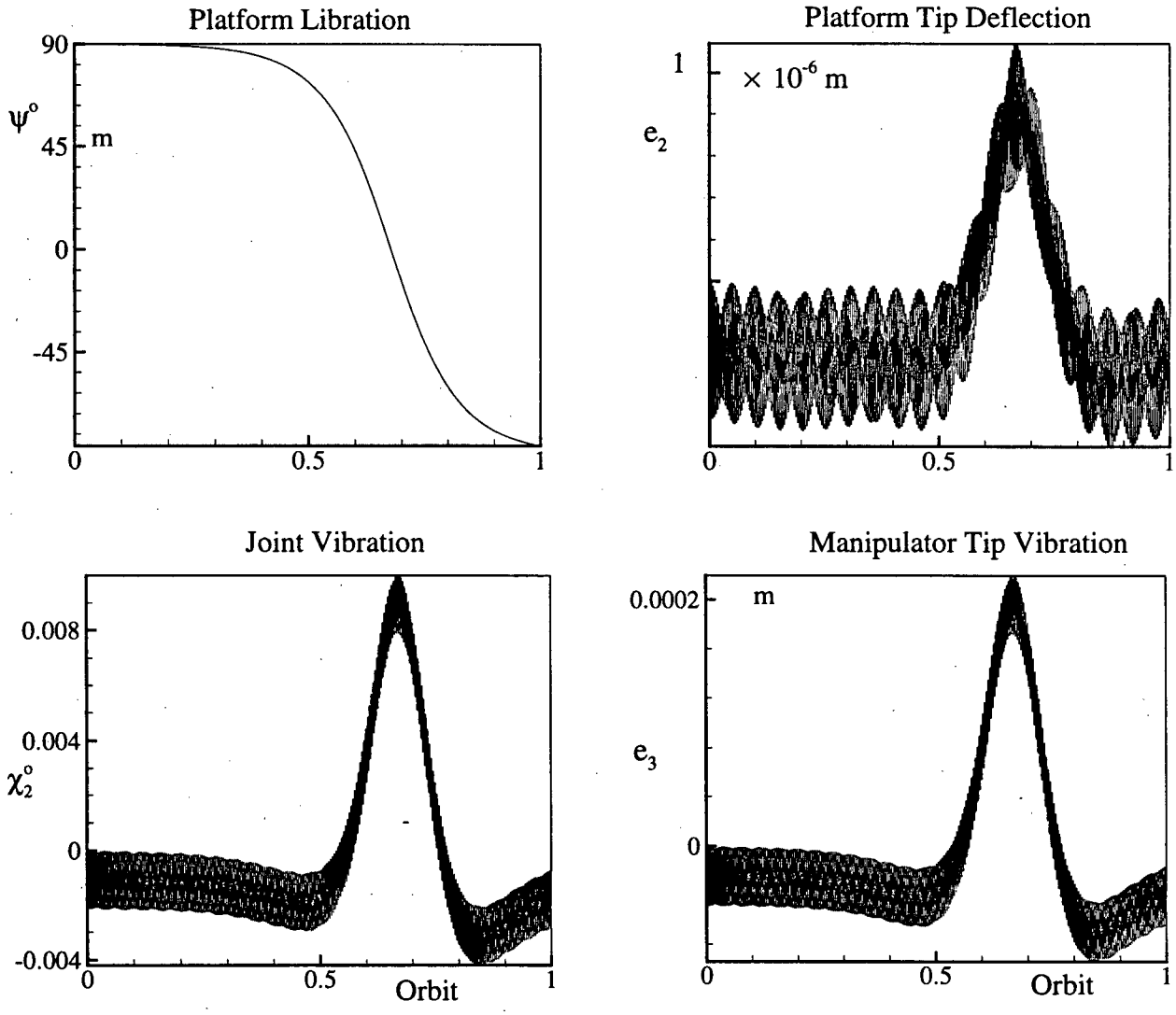

Figure 4-5 System response for unstable platform configuration ($\psi = 90^\circ$) with one-module manipulator.

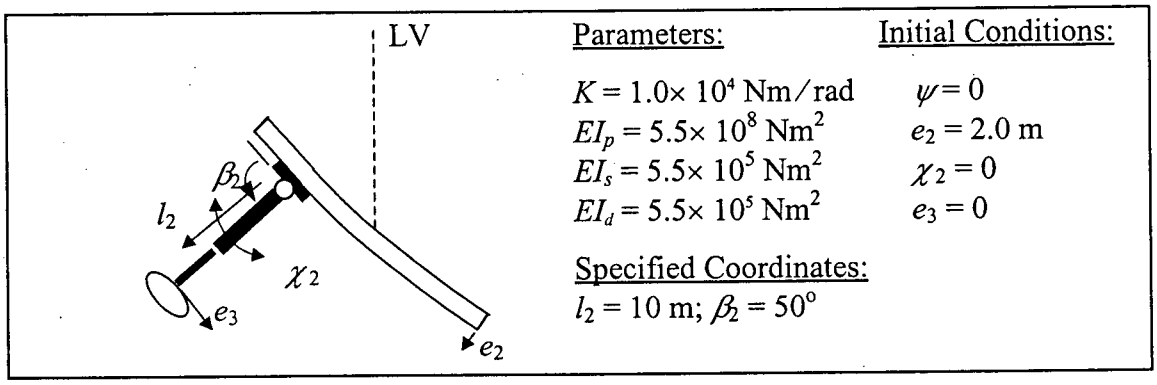

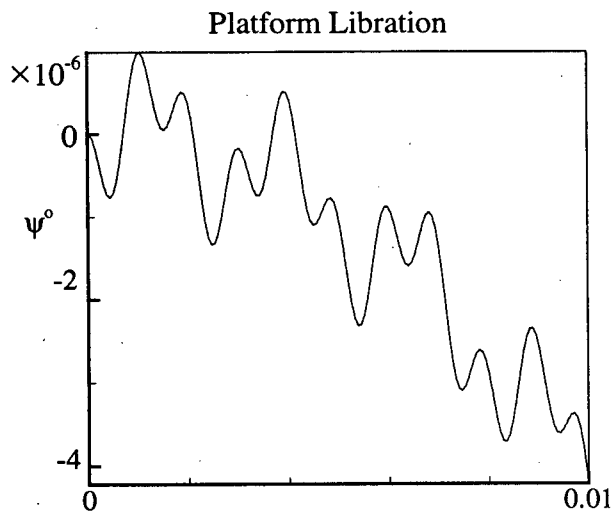

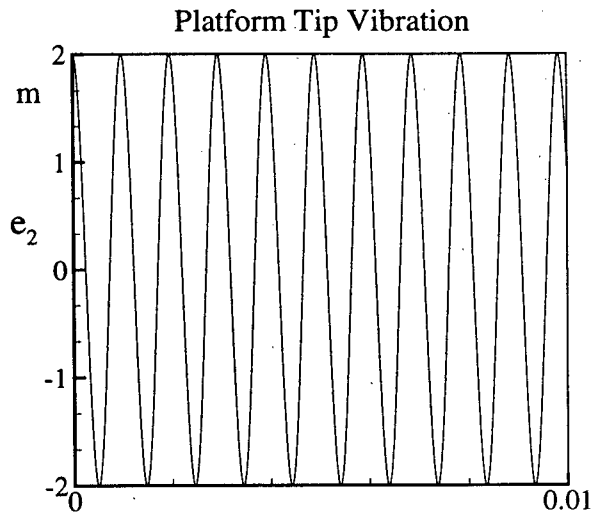

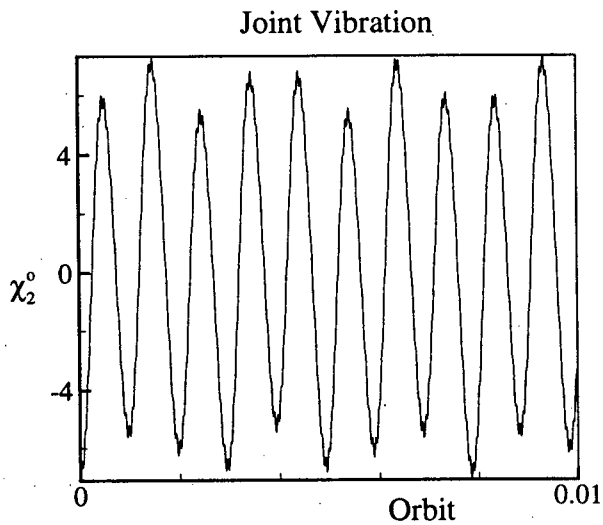

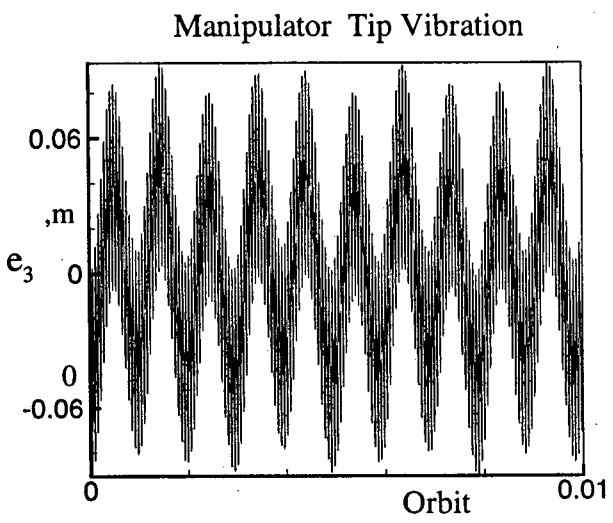

Figure 4-6 Response of the one-module manipulator to the vibration of the supporting platform.

in positions (l_2 = 10 m, $\beta_2 = 50^\circ$). The platform is given an initial tip deflection e_2 = 2 m. The figure describes the system response to this disturbance.

Energy is transferred from the platform's vibration to other degrees of freedom. Clearly, the joint, link, and platform vibrations, as well as the system pitch librational motion, are coupled. It should be noted that, because of the manipulator's position and orientation, the platform's equilibrium pitch angle changes from $\psi = 0$ to $\psi = 0.082^\circ$. Therefore, the system oscillates about this new equilibrium orientation. Since the librational period is approximately 0.58 orbit, this motion is not observable in the figure. Note, the librational motion is imperceptibly small, yet clearly shows modulations at the vibrational frequency of the platform. This reflects favorably on the formulation as well as the computer code. They are able to capture such minute features associated with coupling effects.

The vibration of the platform progresses, essentially, unaffected by the motion of the manipulator. This is understandable as the mass of the platform is 150 times greater than that of the manipulator/Payload combination. Therefore, the motion of the manipulator has almost negligible effects on the platform's response. On the other hand, it is apparent that the platform dynamics has a significant influence on the manipulator response, which now goes through slewing oscillations with an amplitude of $\chi_2 \approx 8^\circ$, around the specified orientation of $\beta_2 = 50^\circ$. The joint response clearly shows the platform's forcing frequency (0.18 Hz), modulated by the joint frequency (0.07 Hz). The joint motion, in turn, would excite the module to vibrate at its own natural frequency (3.1 Hz). One can also discern these minute high frequency modulations at the peaks of the χ_2 response. Of particular interests are the manipulator tip oscillations, e_3. They clearly show modulations in the presence of three vibrational frequencies, which correspond to the natural frequencies of the platform, joint and link.

Figure 4-7 examines effects of the payload mass on the system response. The mobile base is located at the edge of the platform for maximum effect. The manipulator undergoes a 180° slewing maneuver in 0.005 of the orbit. Payload ratios of 1, 2 and 5 are considered. EI_p, EI_s and EI_d correspond to flexural rigidities of the platform, slewing and deployable links, respectively. K refers to torsional stiffness of the revolute joint. Note, the maximum amplitudes are reached near the end of the maneuver. It is apparent that an increase in the mass of the payload increases the amplitude of the responses. Furthermore, a higher payload also increases the inertia of the system while the system's stiffness parameters remain unchanged. As a result, the vibrational frequencies for the joint deformation and manipulator tip deflection become lower.

As explained before, the manipulator dynamics has virtually no effect on the platform's librational response due to its large inertia in pitch. As the manipulator is located at the platform's tip and the maneuver is rather fast (normally, in practice, such maneuver will be completed in 0.1 orbit, i.e. approximately nine minutes), the platform's tip motion (e_2) reaches a modest value of 6 cm for the case of the largest payload of 2,000 kg. The rate of maneuver particularly affects the manipulator dynamics. For the case where the payload ratio is 5, the vibrational amplitudes reach 90° and 15 cm, for the manipulator joint and payload, respectively. Thus in presence of a large payload and a fast maneuver, active control of the manipulator will have to be implemented.

The next four test cases also consider one-module manipulator system. The response of the system to a 0.1 m initial deflection of the manipulator's tip is first investigated (Figure 4-8). The manipulator's vibration results in almost negligible response of the platform. However, it leads to significant vibration of the joint about its equilibrium position. In turn,

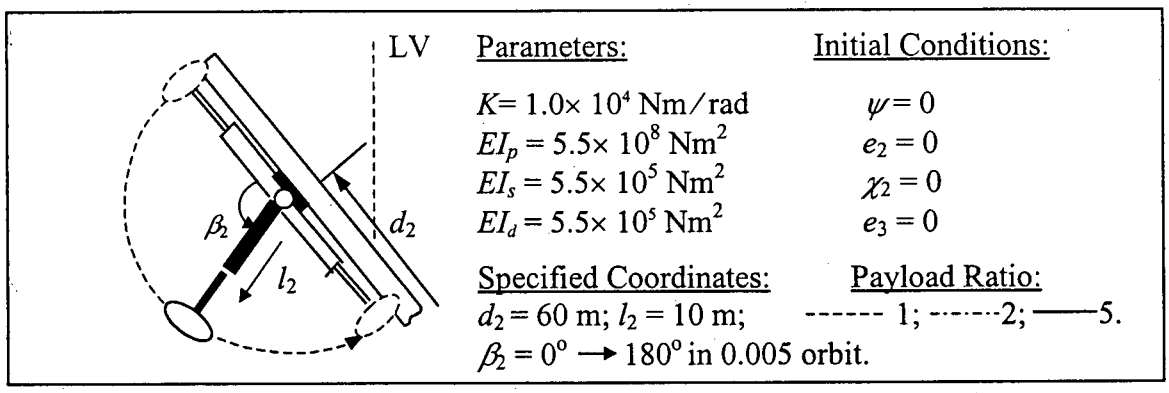

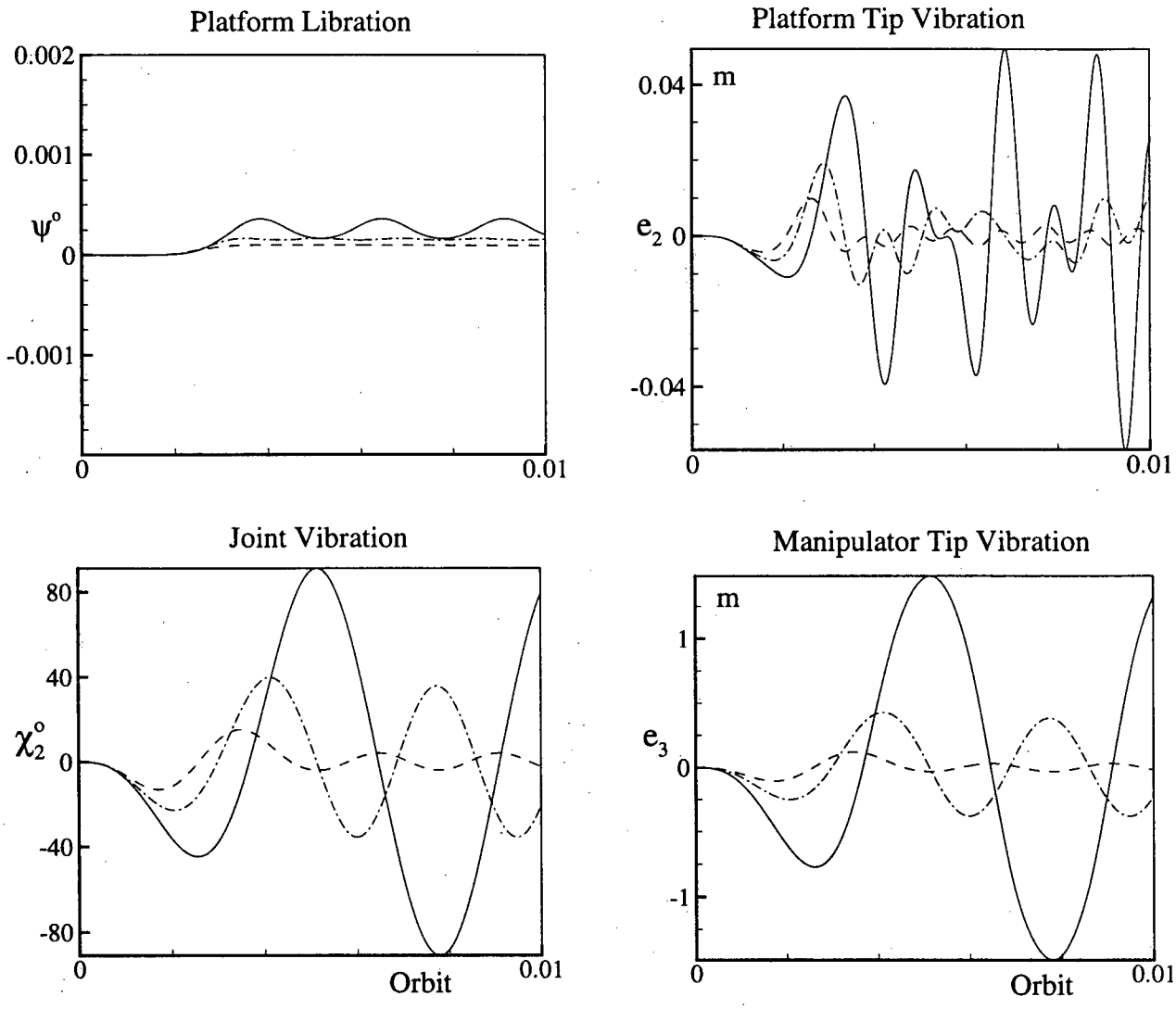

Figure 4-7 Effect of the payload mass on the system response to the slewing maneuver through 180°.

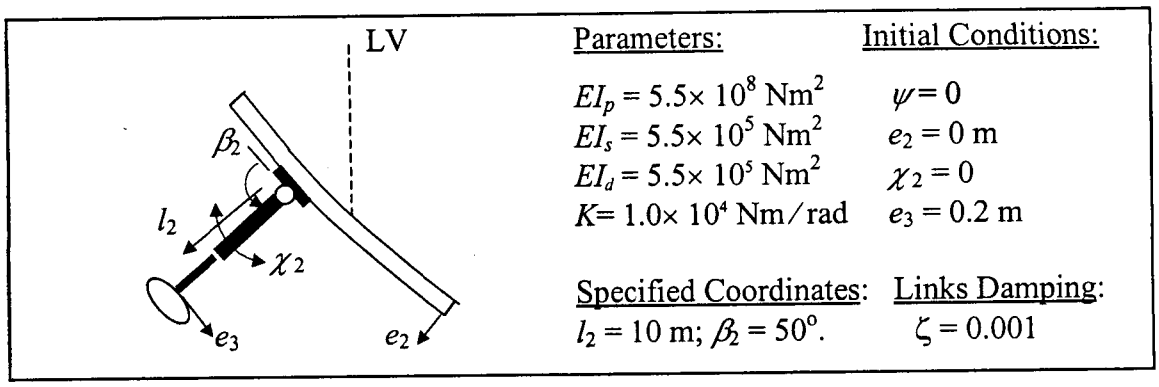

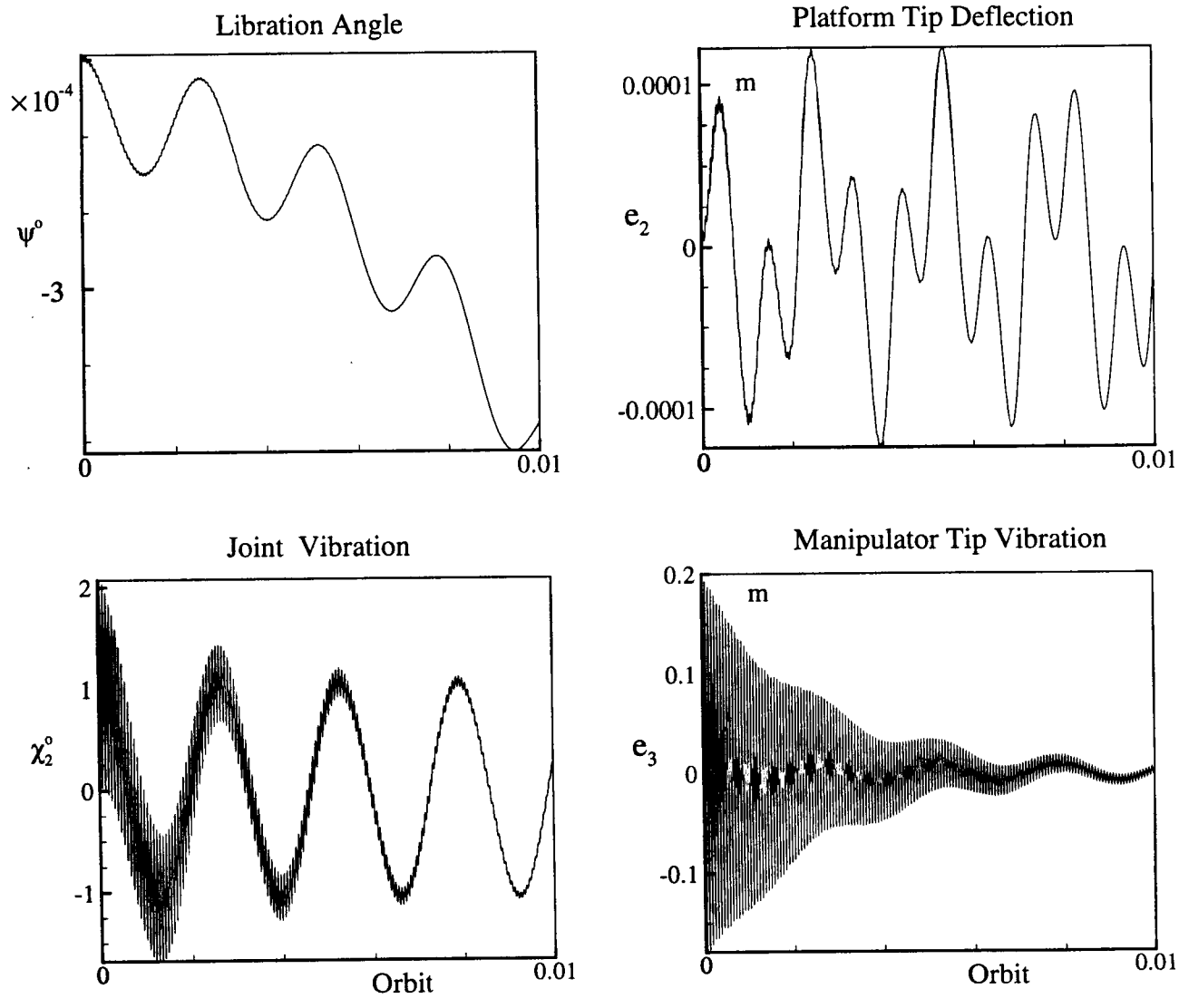

Figure 4-8 Effect of structural damping on the dynamical response of the manipulator to a 0.1 m displacement applied at its tip. A damping ratio corresponding to 0.1 % of the critical damping is assumed for the manipulator.

the vibration of the joint slightly modulates the link response. The vibrational motion of the platform is also modulated by the joint and link responses. The platform's response clearly exhibits all three vibrational frequencies (platform, joint, and manipulator links).

It should be noted that structural damping was included in the manipulator links for this case. A damping ratio corresponding to 0.1% of the critical damping was assumed. Figure 4-8 shows that even this minute amount of damping has a significant effect on the system response. As expected, the vibration of the manipulator module decreases in an underdamped fashion. It is interesting to note that the slewing oscillations of the joint also decrease with time; not only the modulation due to the vibration of the links, but also the oscillations at the joint's natural frequency. This can be attributed to the strong coupling between the joint and link dynamics.

Thus, inclusion of a small amount of structural damping in the manipulator links appears to modify the system response significantly. However, the effect consists mainly in attenuation of the free response. With the exception of the damped oscillations, the qualitative nature of the response remains relatively unchanged. For cases involving maneuvers, damping was observed to have little effect. Therefore, in the remaining cases, the damping is purposely neglected in order to obtain conservative estimates for the system response.

Next, the system response to slewing maneuvers is investigated. Figure 4-9 describes system's motion with the manipulator executing a 180° slewing maneuver from $t = 0$ to $t =$ 0.005 orbit. The unit is carrying a 400 kg payload. The response is shown for three locations of the mobile base: $d_2 = 0$ (i.e., center of the platform), $d_2 = 30$ m, and $d_2 = 60$ m (i.e., tip of the platform).

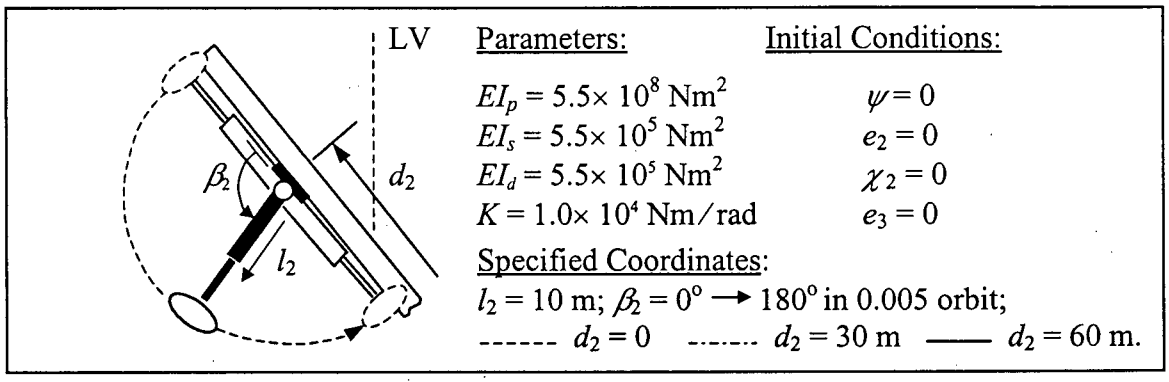

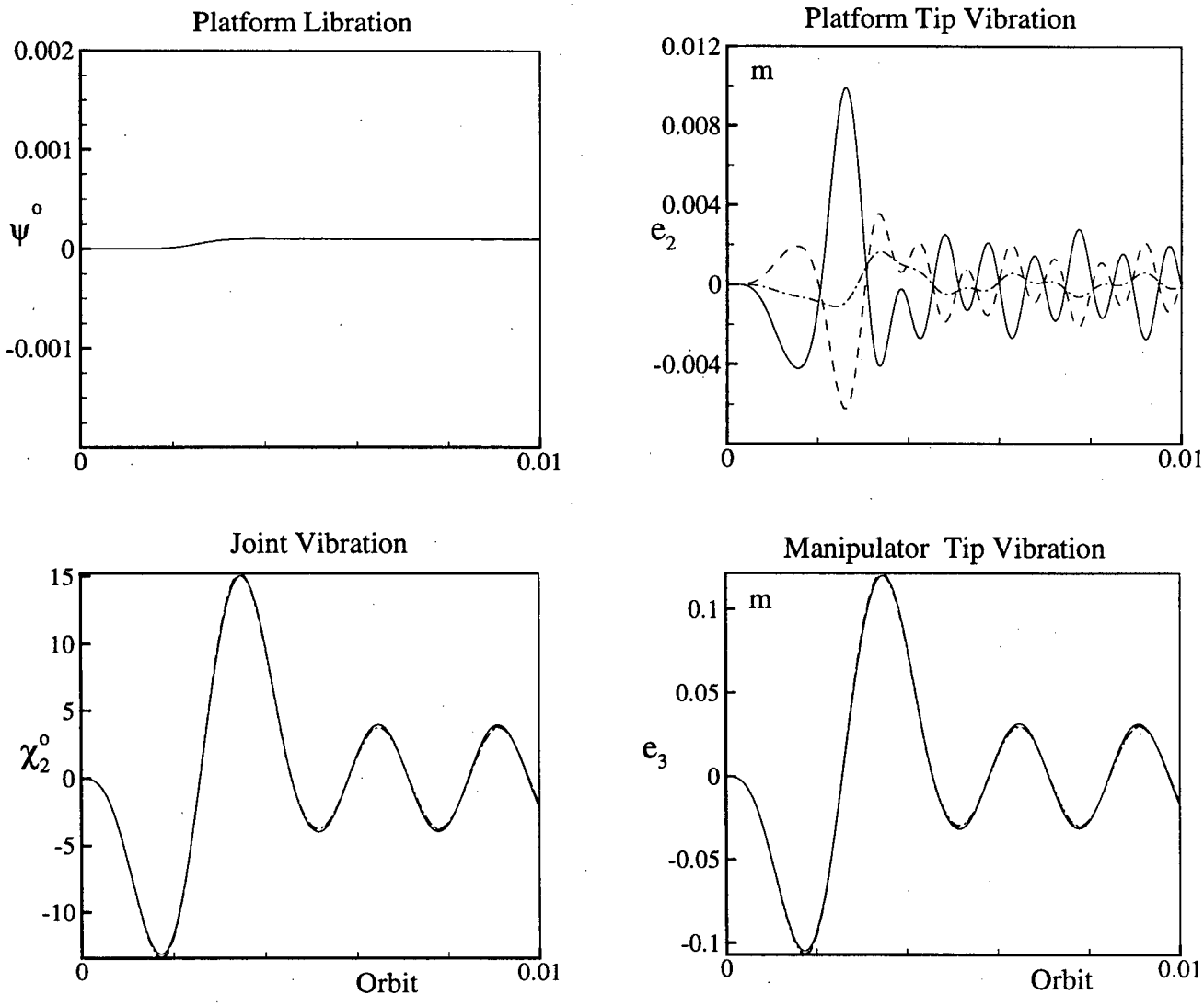

Figure 4-9 System response to a 180° slewing maneuver of the manipulator for various locations of the mobile base.

The maneuver slightly modifies the system's equilibrium orientation, due to transient change in inertia, resulting in rigid body oscillations of the platform. Librational motion is also induced by the inertia forces of the manipulator transmitted to the platform through the base. However, as before, the response is negligible. The slewing maneuver also induces vibration of the platform. The largest elastic deformation is obtained when the base is located near the platform's tip, with tip deflections reaching 1 cm during the maneuver. After the end of the maneuver, some residual vibrations persist in all three cases, but they are of the order of 10^{-4} m. It is interesting to note that the smallest platform vibrations correspond to the case where d_2= 30 m. Here, mobile base is located close to one of the nodes of the shape function, which is at x_1 = 33.1 m. Therefore, it is difficult for the exciting force to deform the platform at this location.

One would expect the influence of the maneuver on the manipulator's own dynamics to be essentially independent of its location on the platform. This is substantiated by the χ_2 and e_3 responses. Note, as the platform motion is negligible, the form of the manipulator joint and tip vibrations is quite similar. As before, the peak responses are reduced during the maneuver, with a maximum joint deformation of 15° and a peak tip deflection approaching 12 cm. After the end of the maneuver (i.e., t > 0.005 orbit), residual vibrations continue, with an amplitude of 4.0° for the manipulator joint and 3 cm for its tip deflection.

Figure 4-10 (a) shows the effect of higher order modes on the system response for the case investigated in Figure 4-9, but with a payload of 2000 kg, and with the manipulator located at the very edge of the platform. Only the time histories of the platform and manipulator tip deflections are shown, as higher modes had no noticeable effects on the platform libration and joint vibration. From the figure, it can be seen that the second mode

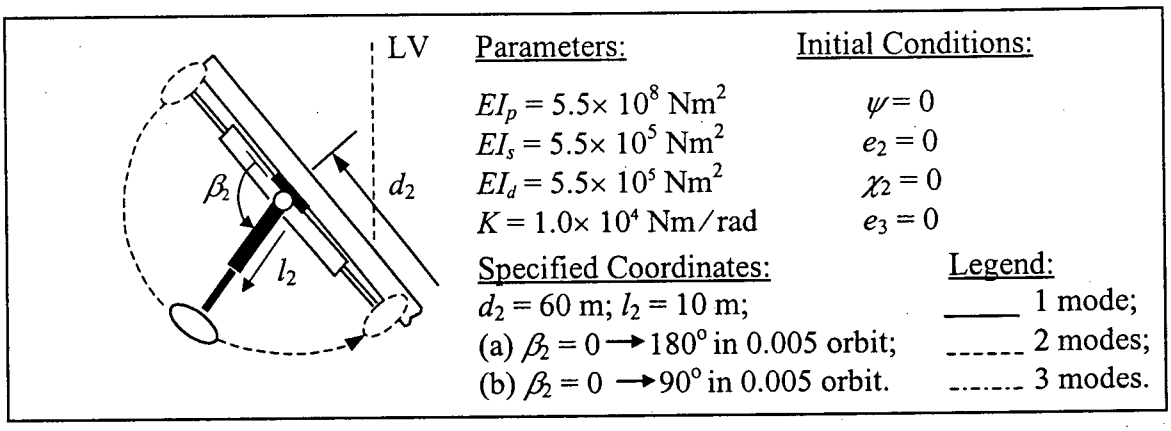

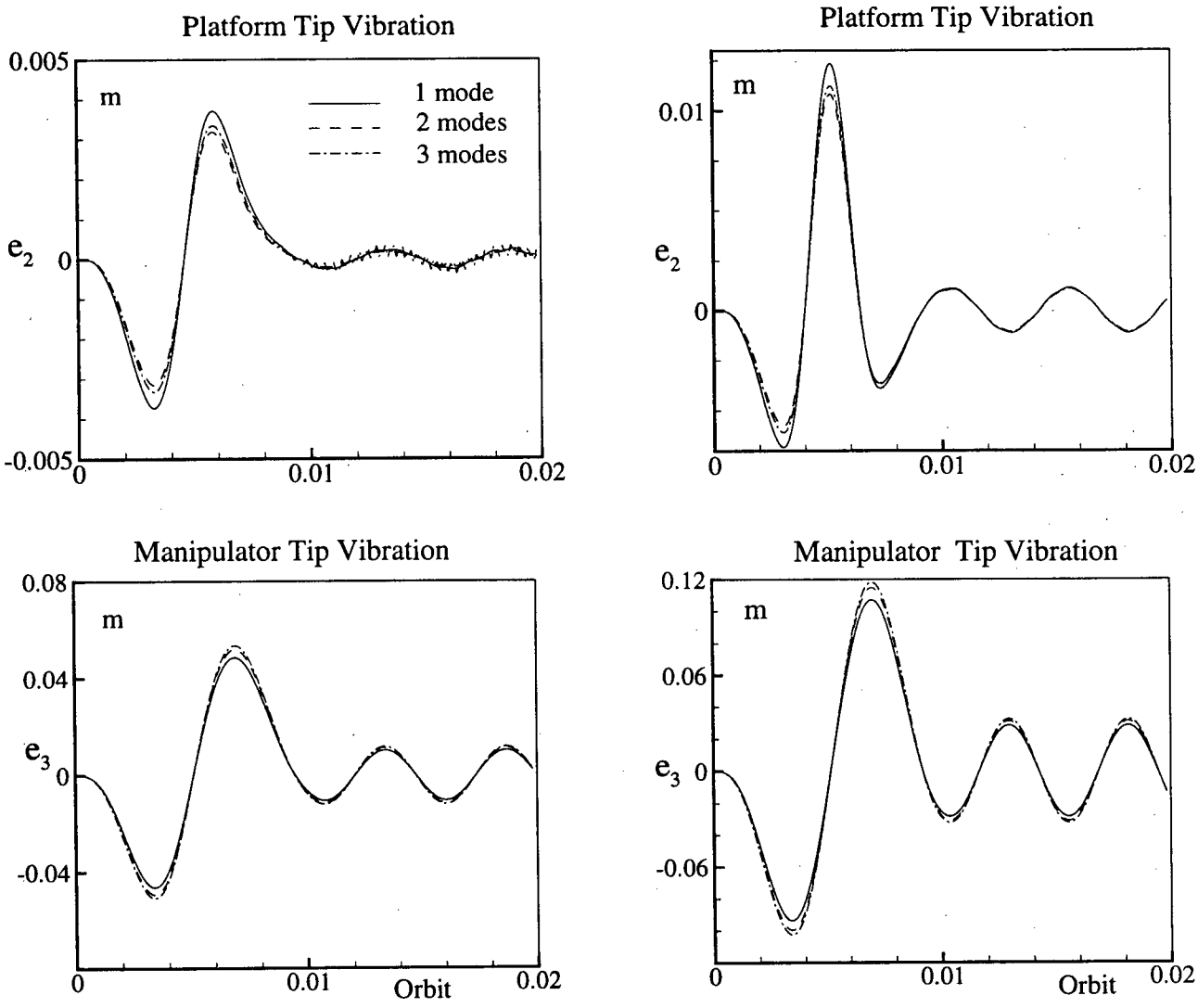

Figure 4-10 Effect of higher modes on the system's structural vibration. The manipulator is supporting a 2000 kg payload and is located at $d_2 = 60$ m: (a) 180° maneuver; (b) 90° maneuver.

introduces only minor correction to the response. Thus, the use of only one mode provides a sufficiently accurate result for the design purpose, with a significant saving in computational time. The third and higher modes have negligible effect on the system response.

Figure 4-10 (b) considers the same case, but with a faster maneuver through 90°. As can be expected, being a relatively severe disturbance, the e_2, e_3 responses are larger. Contributions of the second and higher order modes still remain negligible. The first mode continues to be sufficient to describe the vibration of the manipulator unit, even in demanding situations.

Thus it can be concluded that, in general, the fundamental mode is adequate to model the system dynamics. However, a word of caution is appropriate, particularly at extremely high maneuvering speeds, which may excite higher modes. On the other hand, it is a common practice in robotic control to limit the motion frequency to no more than half of the fundamental frequency of the structural components [48]. Thus the use of the fundamental mode appears to be sufficient to describe the system structural response.

The effect of manipulator deployment is now assessed. The manipulator is taken to be located near the edge of the platform (d_2 = 60 m) and is oriented perpendicular to the platform's longitudinal axis ($\beta_2 = 90^\circ$). Initially, the deployable link is fully retracted, i.e. l_2 = 7.5 m, and the vibration of the manipulator links is excited with an initial tip deflection of 10 cm. Softer links are considered in this case ($EI_s = EI_d = 5.5 \times 10^4$ Nm^2) to accentuate the response and capture coupling effects, if any. From $t = 0$ to $t = 0.005$ orbit, the manipulator length remains unchanged at $l_2 = 7.5$ m. From $t = 0.005$ to $t = 0.01$ orbit, the manipulator is extended to its maximum length of 15 m. It remains fully deployed until the end of the simulation.

The system response is shown in Figure 4-11. The initial tip deflection results in vibrations of the manipulator joint and links, as well as the platform. The deployment of the manipulator unit changes the inertia tensor of the system and modifies its attitude, as shown in the figure. Note, the program is sensitive enough to pick up minute platform librations and tip vibration. The peak platform tip deflections are experienced during the deployment. It should be noted that deployment makes the module structurally softer and lowers its natural frequency. Retrieval has the opposite effect and results in a higher natural frequency. This becomes obvious when the time history of the manipulator's tip deflection (e_3) is considered: when the module is fully extended, the vibrational amplitude of the links is larger and its frequency is lower. This strongly affects the joint vibration as well through coupling.

4.2.3 Manipulator with two units

The next case studies the response of the system when it is subjected to slewing maneuvers from two units (Figure 4-12). The manipulator is initially "folded over" (β_2 = 180°, β_3 = -180°), with both units parallel to the platform, and its base and tip are located exactly at the center of the platform. From t = 0.00 to t = 0.05 orbit, the joints rotate until the links are aligned along the direction perpendicular to the platform. Throughout the maneuver, the length of each unit remains constant ($l_2 = l_3$ = 15 m). The figure shows the vibrational response of the manipulator units and joints, as well as the platform's elastic character. The system's librational response is also presented. The maneuver is illustrated in the inset. The slewing maneuvers result in tip deflections of around 0.5 m to 1.3 m for two modules as well as joint deformations of, approximately, 12°-35°. The maneuver also excites a vibrational response of the platform resulting in a rather small tip deflection of around 3 mm. Note, the coupling between the various degrees of freedom is evident through modulations.

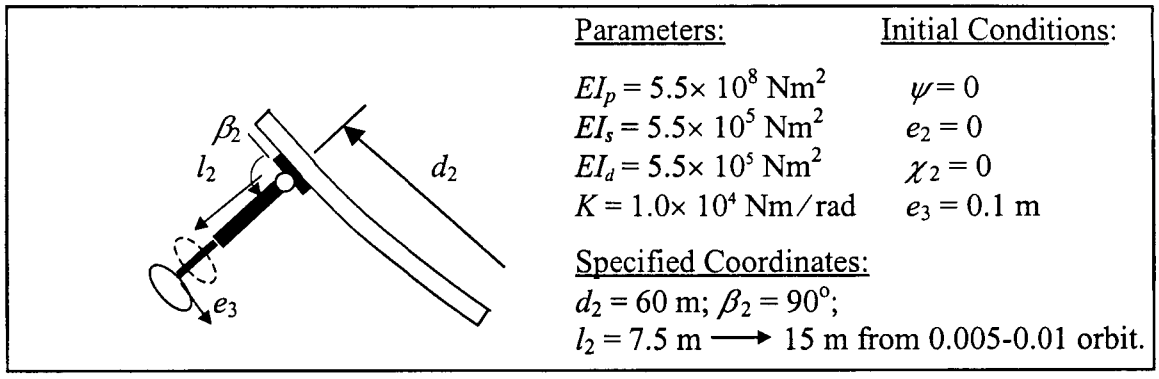

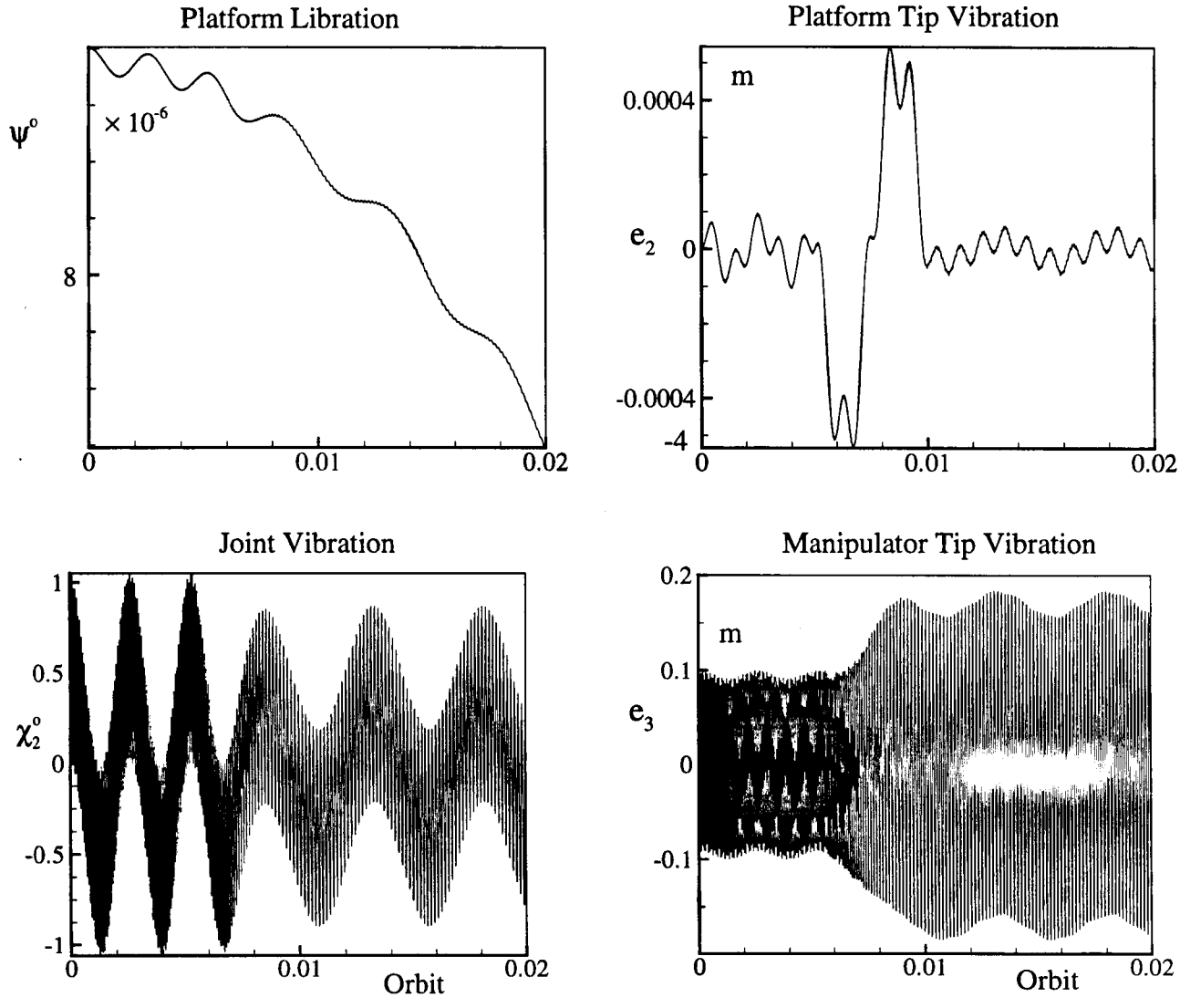

Figure 4-11 Effect of the manipulator's deployment maneuver on the system response in the presence of a 0.1 m disturbance of the manipulator tip.

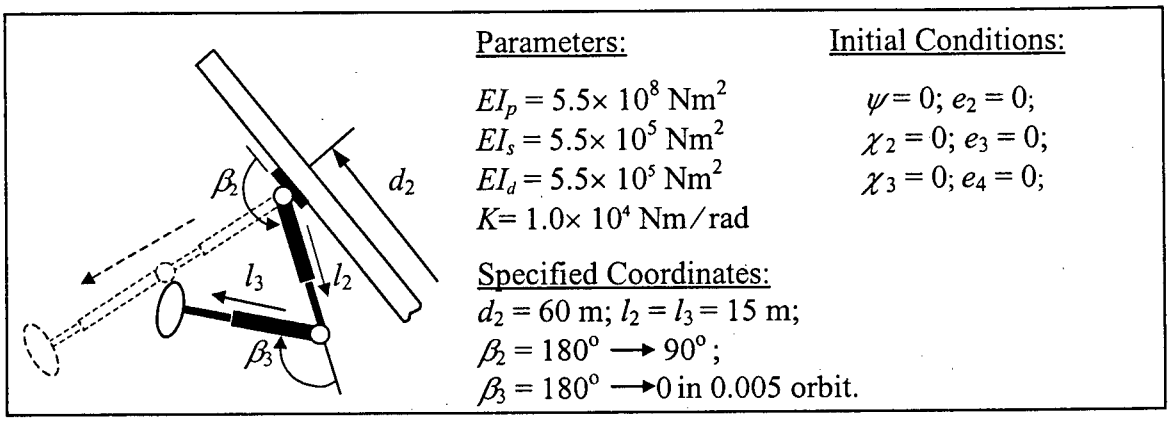

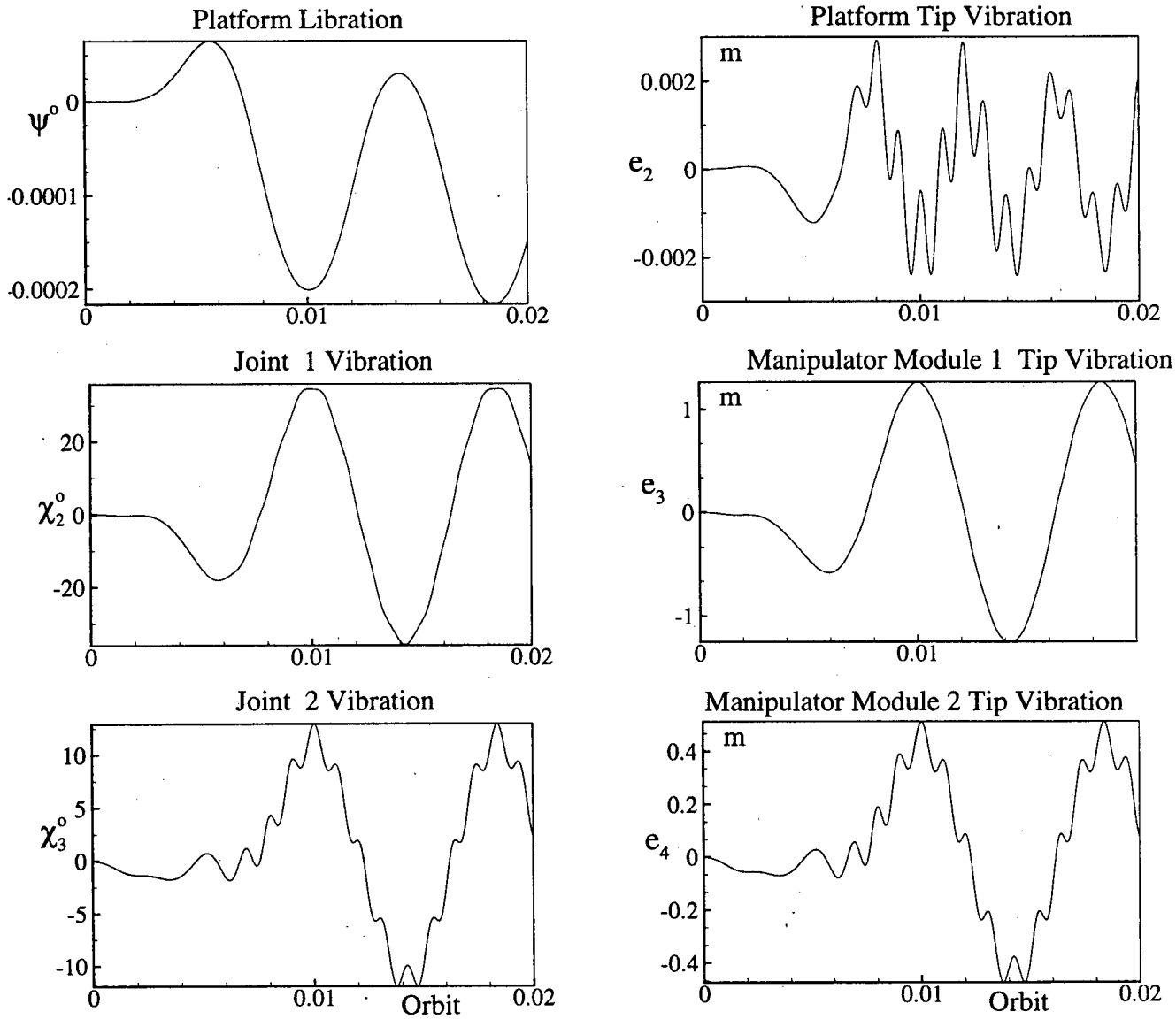

Figure 4-12 System dynamics due to simultaneous slew maneuvers involving two manipulator modules.

4.2.4 Three unit manipulator system

In practical situations, a service area to be covered by the manipulator would remain the same. Hence, with a large number of units, it would be logical to reduce the link lengths, which, in turn, would affect its mass and flexural rigidity. Of course, the joint conditions may also change. The revised parameters used for manipulators with three and larger number of units are as follows:

Manipulator Joints:

Type: revolute joints; Mass = 5 kg;

Moment of Inertia (I_{zz}) = 2.5 kg m^2;

Stiffness (K) = 1×10^3 Nm/rad.

Manipulator Links (Slewing and Deployable):

Geometry: cylindrical, with axial to transverse inertia ratio of 0.005;

Mass (m_s, m_d) = 50 kg:

Length (l_s, l_d) = 2.5 m;

Flexural Rigidity (EI_s,. EI_d) = 1×10^4 Nm^2.

Thus, each module has a maximum length of 5.0 m. All other parameters remain the same as before.

Figure 4-13 presents the response of a three-unit manipulator to a simultaneous rotation of its three revolute joints and deployment of the three units. The manipulator base is located at the extremity of the platform and the manipulator is initially in a folded configuration ($\beta_2 = -\beta_3 = \beta_4 = 180^\circ$), with all the three manipulator units parallel to the platform (inset). In 0.01 orbit, the joints rotate in order to align all the units in the direction perpendicular to the platform's long axis. At the same time, each unit deploys from a length of

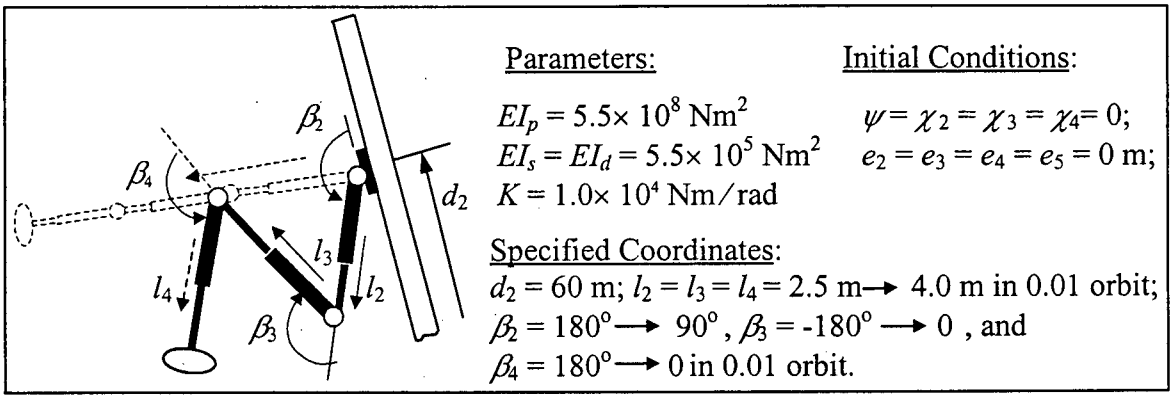

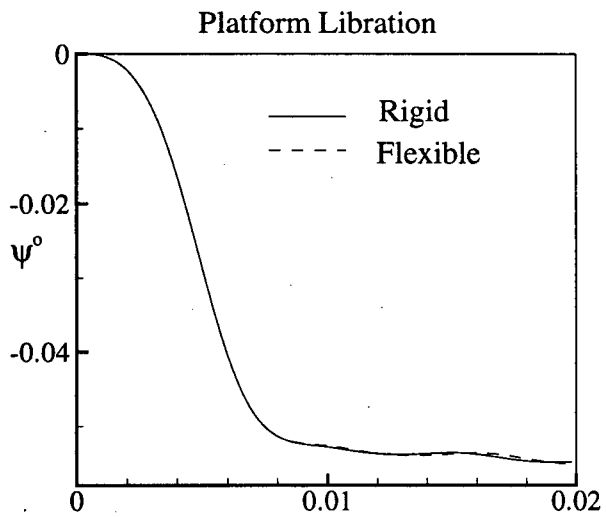

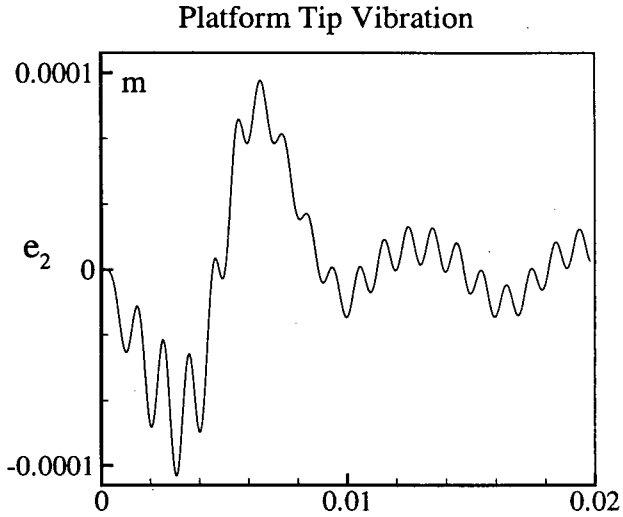

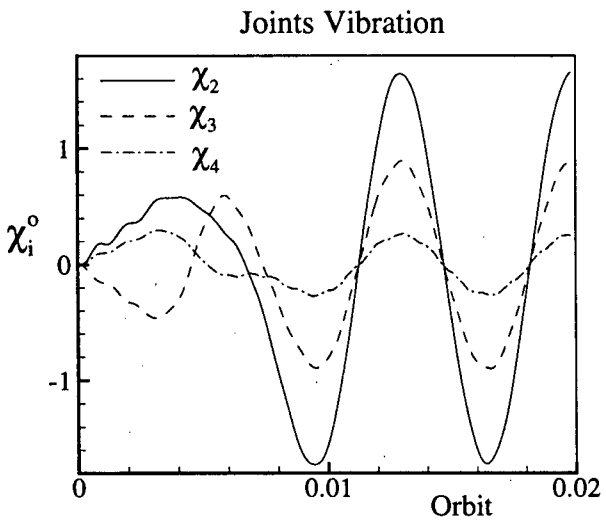

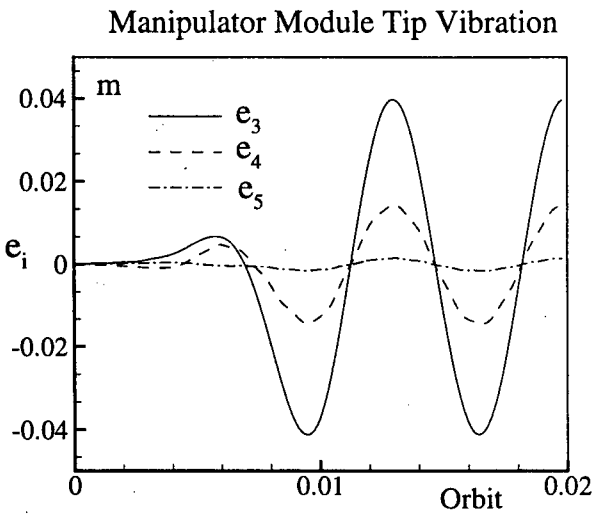

Figure 4-13 Simultaneous slew and deployment maneuvers of a three-module manipulator.

2.5 m to 4.0 m. Hence, the maneuver takes the tip of the manipulator from its initial location on the surface of the platform, 2.5 m from the platform's tip, to a point located 12 m from the surface of the platform.

The results show that while the vibrational motion induced in the platform remains small, the platform pitch response is relatively large. This can be attributed to the large effect that manipulator maneuvers have on the system's inertia tensor when the base is fixed near the tip. The joint and unit vibrations are also shown. One notes that the amplitude of vibration of both joints and links are greater for modules close to the platform. Joints and links located near the end of the manipulator exhibit vibrational modulations at the natural frequency of the links. Moreover, after the maneuver, all joint and link deformations seem to pass through zero at the same instant. These trends are also observed for manipulators with a greater number of units. This suggests that all flexible components reach their maximum and minimum elastic energies at the same time. Furthermore, these extrema should remain the same once the maneuver is completed as the total energy of the manipulator system remains constant.

4.2.5 Manipulator with four units

Here the base of the manipulator is locked at the center of the platform. Each module is deployed to a length of 4.0 m. The first three modules are aligned in the direction perpendicular to the platform, while the last unit undergoes a 180° slewing maneuver during 0.01 orbit. Figure 4-14 illustrates the maneuver, as well as the vibrational response of the platform, joints and manipulator units, in addition to the librational dynamics of the system. One notes that the amplitudes of joint and link vibrations are larger for components (i.e. joints, links) which are closer to the platform (i.e. away from the tip). In addition, the vibrational

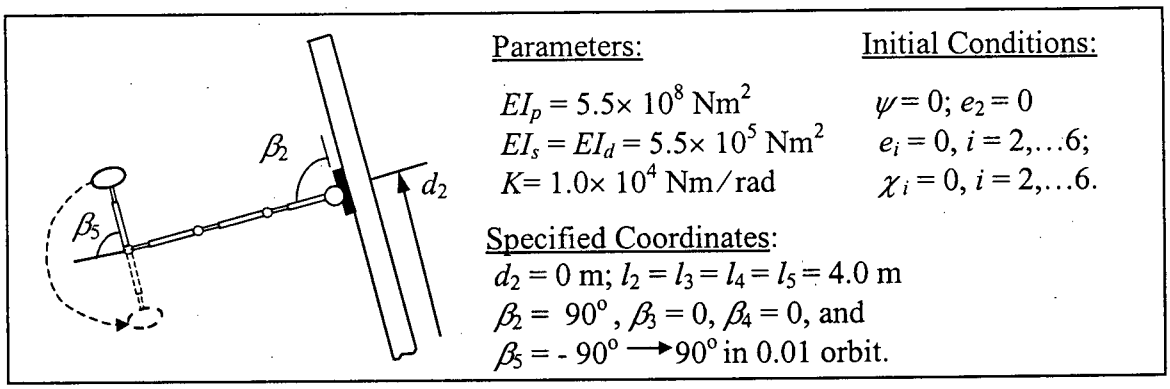

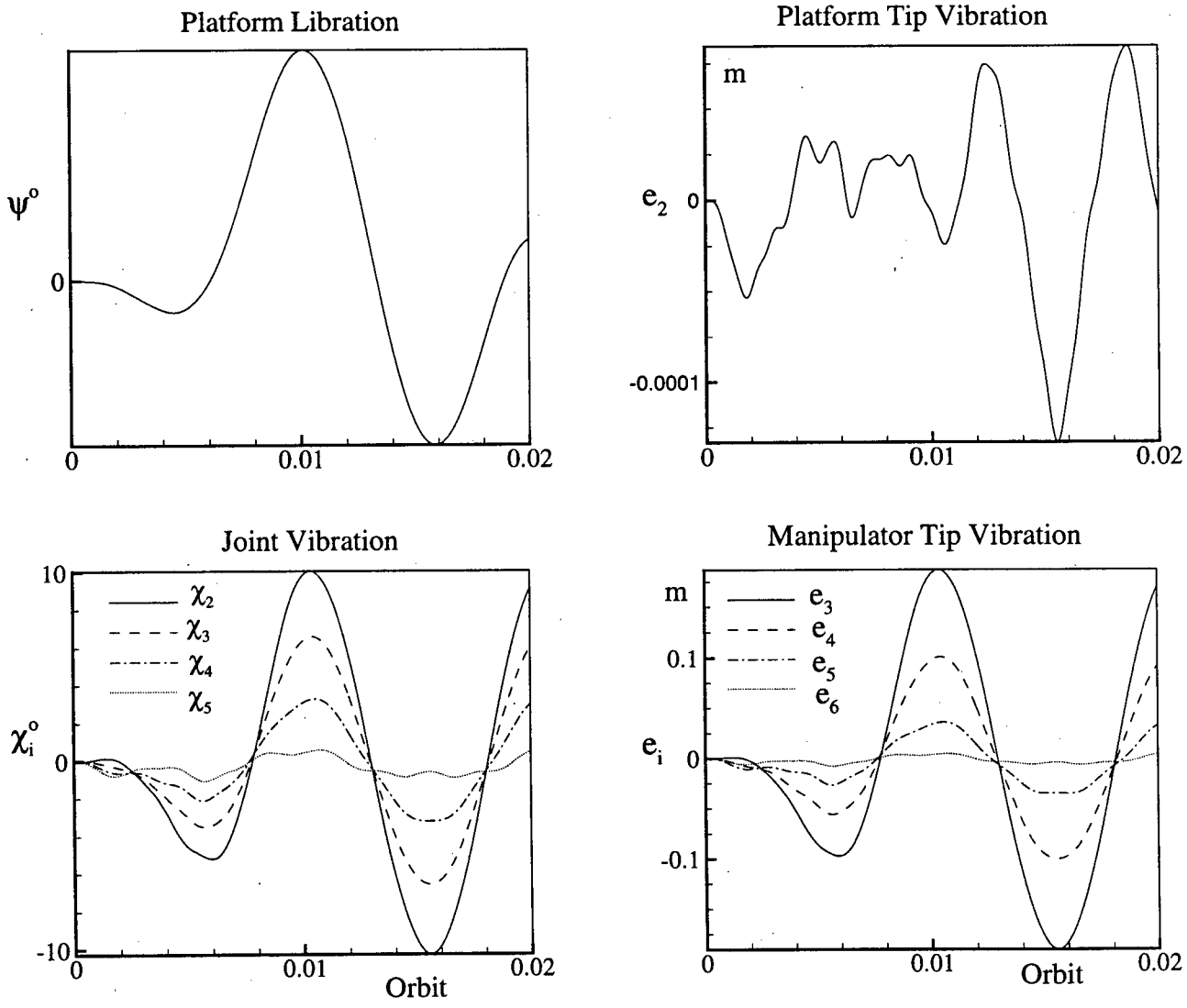

Figure 4-14 System response of a four-module manipulator to a 180° slewing maneuver from the fourth module.

frequencies are higher for components closer to the tip of the manipulator. Both observations seem to indicate that each unit acts as a tip mass for the previous unit and thus effectively reduces its natural frequency. Coupling effects are also apparent from the joint vibrations and tip deflections of the manipulator units. Again, the joint and link deformations pass through zero at the same instant near the end of the maneuver and after it is completed.

4.2.6 Five-unit manipulator system

The final case studies the system response of the five-unit manipulator to a translation maneuver along the platform. The manipulator base is initially located at $d_2 = 30$ m, i.e. 30 m away from the platform's centerline. All manipulator modules are fully retracted to their minimum length of 2.5 m and are aligned in the direction perpendicular to the platform. The base is now commanded to translate through 30 m in 0.01 orbit. Figure 4-15(a) shows the platform and manipulator tip responses. x_e represents the motion of the manipulator tip parallel to the undeformed platform, while y_e gives the displacement in the transverse direction, both with respect to the reference coordinate frame F_1, located at the center of the platform. To assess the effects of link and joint flexibility, the response of a rigid manipulator system is also included for comparison. The results clearly show significant influence of the system flexibility, on the position of the end-effector. Obviously, this has considerable implication on the path planning. The joint deformations result in large oscillations, mostly in the x_e direction, about the desired position. The joint and link vibrations are shown in Figure 4-15(b) for all components. As before, the vibrational amplitudes are larger for components located close to the platform because of the inertia effects. Again, the elastic joint deformations and tip deflections of the manipulator units pass through zero at the same instant, i.e. the deformation time-histories are in phase. Thus all flexible components continue to reach their

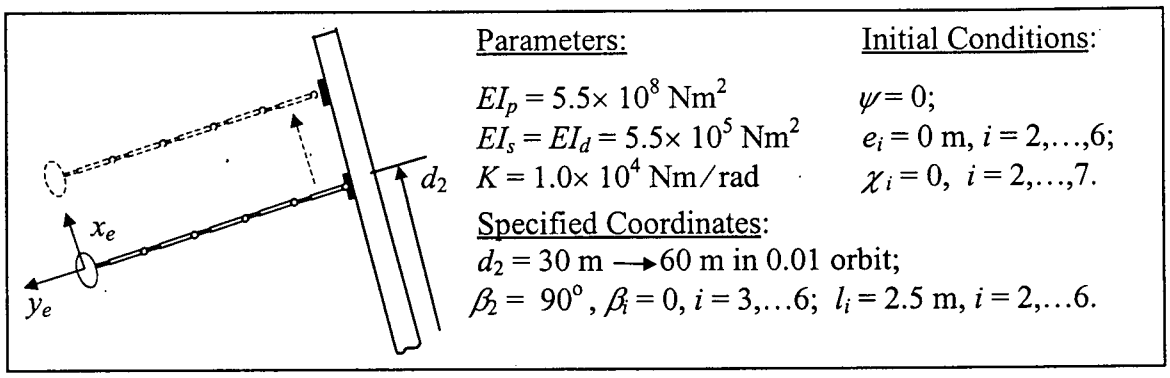

(a)

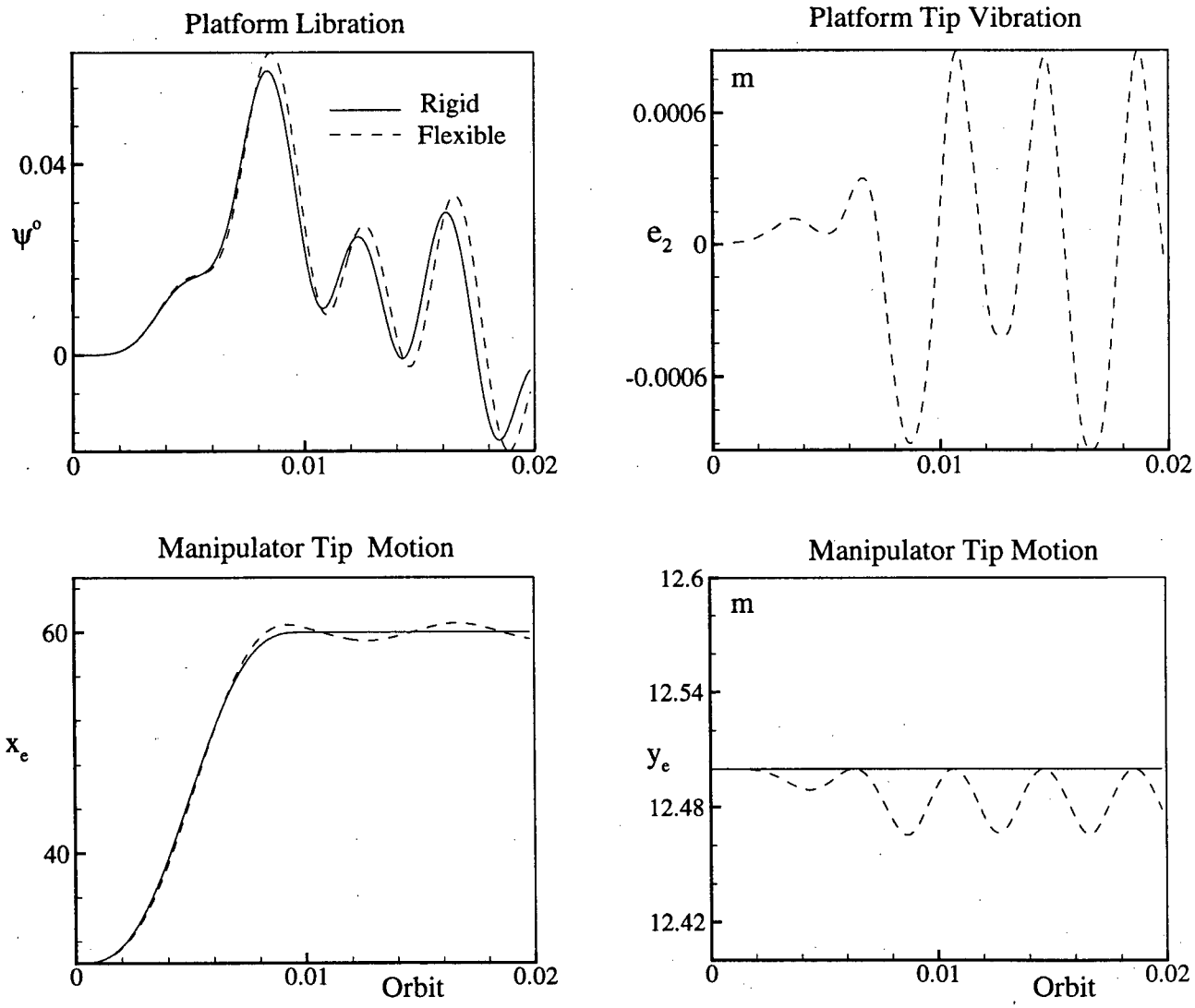

Figure 4-15 System dynamics during and after a 30 m translational maneuver along the platform: (a) platform response and trajectory of the end-effector; (b) joint and manipulator modules' response.

(b)

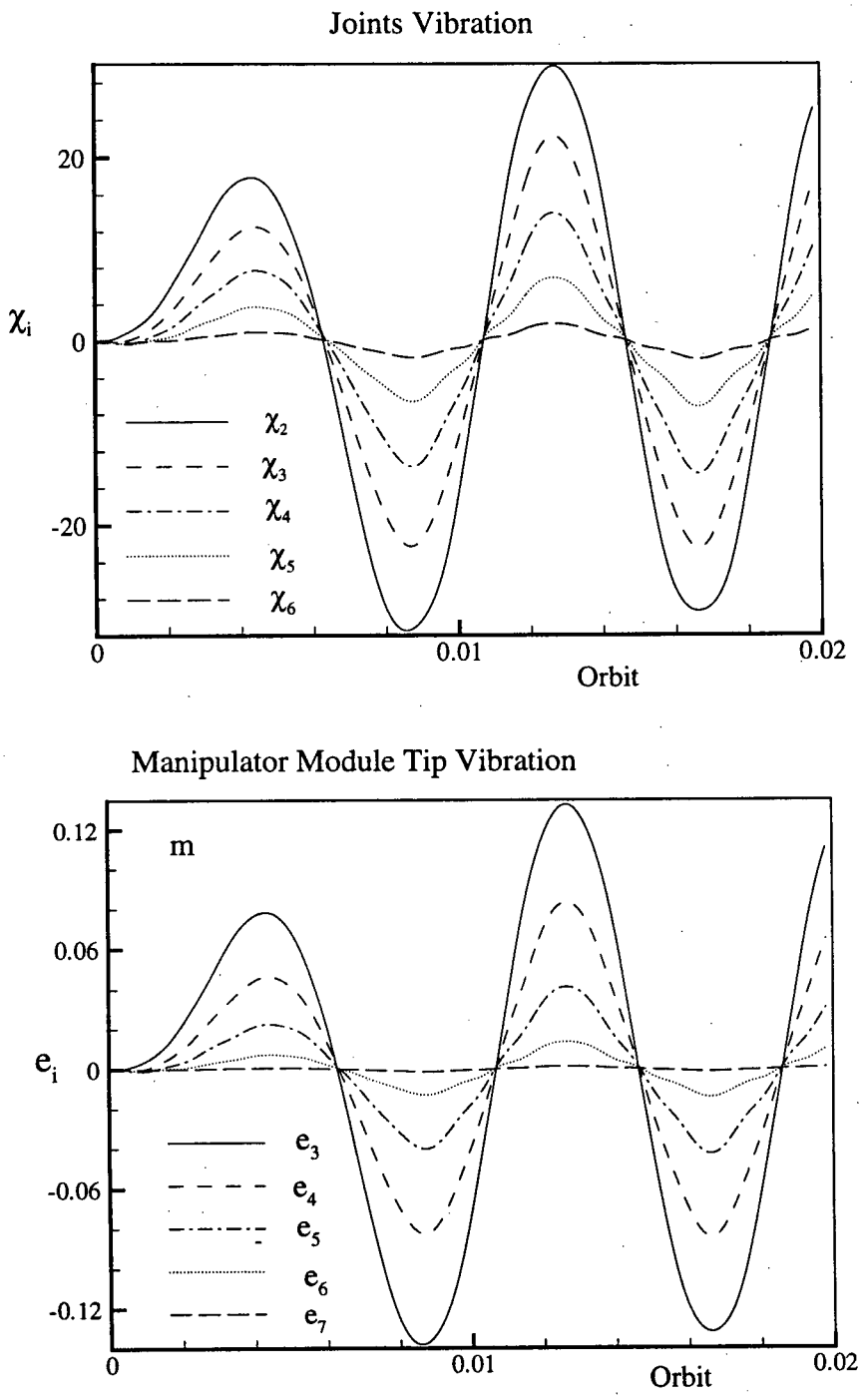

Figure 4-15 System dynamics during and after a 30 m translational maneuver along the platform: (a) platform response and trajectory of the end-effector; (b) joint and manipulator modules' response.

maximum and minimum elastic potential energies at the same time.

4.3 Computational Efficiency of the *O(N)* Formulation

As mentioned before, the formulation of the governing equations of motion, presented in Chapter 2, has the property of O(N). Thus, ideally, the computational cost should increase linearly with the number of bodies involved in the system. To assess validity of this property, the case of the platform along the local vertical was considered with the base located at $d_2 = 30$ m. The platform, manipulator modules and joints were taken to be flexible. Four cases were studied with the number of modules, N, increasing from 1 to 5. Note, no manipulator maneuvers are involved as in Section 4.2.1. The computer used was Compaq 5177 Presario with Pentium II 350Hz processor and 128 MB RAM. The results are shown in Figure 4-16. Essentially linear behavior is apparent. Note, doubling the number of bodies from three to six increases the time by 53 minutes, instead of 424 minutes for the conventional procedure.

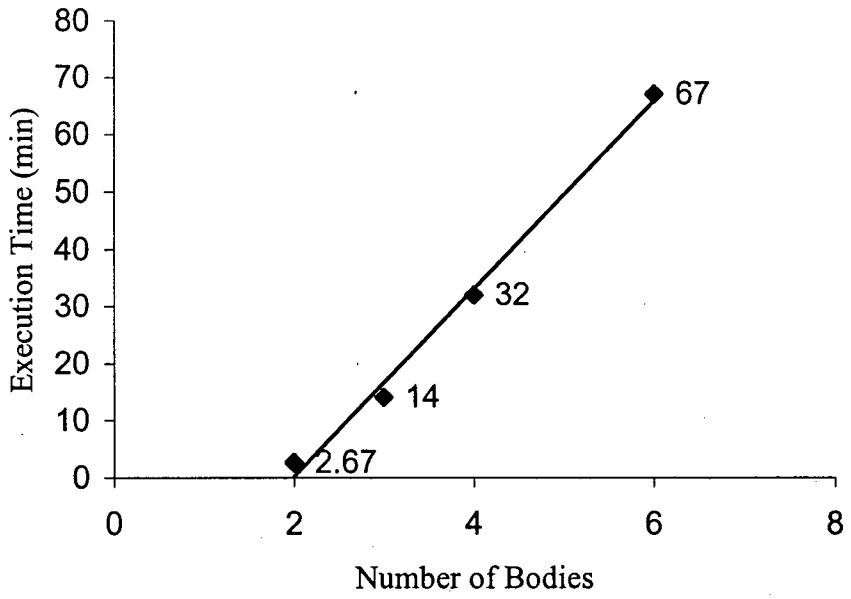

Figure 4-16 Execution time vs. number of bodies with O(N) formulation.

4.4 Gross and Fine Manipulations

4.4.1 Preliminary remarks

In this section, the idea of gross and fine manipulations is introduced for a robotic system with redundant degrees of freedom. If the manipulator is expected to perform a precise task, and at the same time has a large working space, a long arm carrying small and precise robotic unit may be able to effectively accomplish the job. The larger manipulator as a delivery tool, will move in a gross fashion to position the small robot close to the target. Now the latter will be able to perform the required fine, precise tasks on the work-piece. These two types of operations may be termed gross and fine manipulations of the robotic system [78]. A manipulator having redundant degrees of freedom will assist in implementing this concept in accurate and efficient manner. This emphasizes versatility of the formulation, which makes a variety of applications possible.

4.4.2 Dynamics of gross and fine manipulations

A two-module manipulator, i.e. with four links, two capable of slewing while the other two deployable, was considered (Figure 4-17). The manipulator, supported by the mobile base was free to translate over a flexible platform (free-free beam). To help appreciate complex interactions, the deployable links were locked in positions. The model accounts for the joint flexibility, however the links are purposely taken to be rigid to facilitate isolation of coupling effects. The base was also held fixed. The numerical data used in the simulation are summarized below:

length of the space platform $l_p = 120$ m;

mass of the space platform m_p=120,000 kg;

length of module 1	$l_1 = 7.5$ m;
mass of module 1	$m_1 = 250$ kg;
$R = m_2 / m_1 = l_2 / l_1$	$= 1, 0.5, 0.1$;
joint flexibility	$= 10^4$ Nm /rad.

Here m_2 and l_2 are mass and length of module 2, respectively.

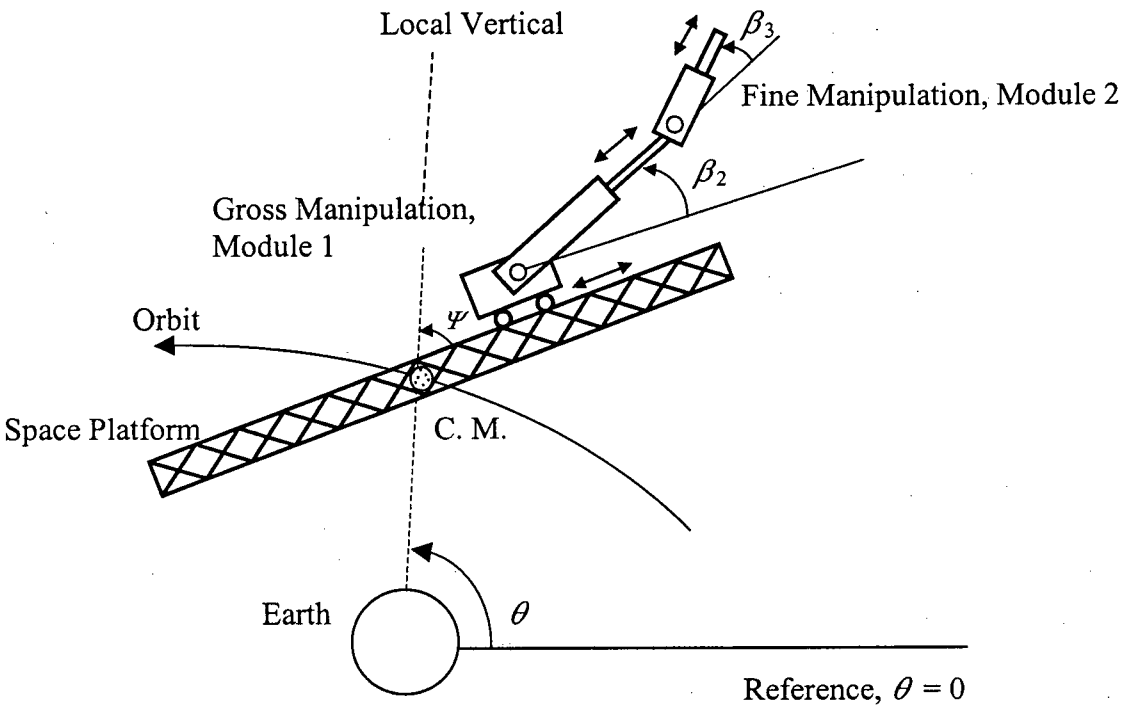

Figure 4-17 Planer two-module space manipulator system for gross and fine operations.

To begin with, the long duration behavior of the system was studied when subject to an initial disturbance of $\dot{\beta}_2 = \dot{\beta}_3 = 30^\circ$ /min, with the revolute joints kept free and $R = 1$ (Figure 4-18). As can be expected, in absence of any dissipation, module 1 exhibits rotary motion with module 2 oscillating about the longitudinal axis of module 1. Essentially the system response is similar to that of a double pendulum in a horizontal plane with the normal component F_{3n} of

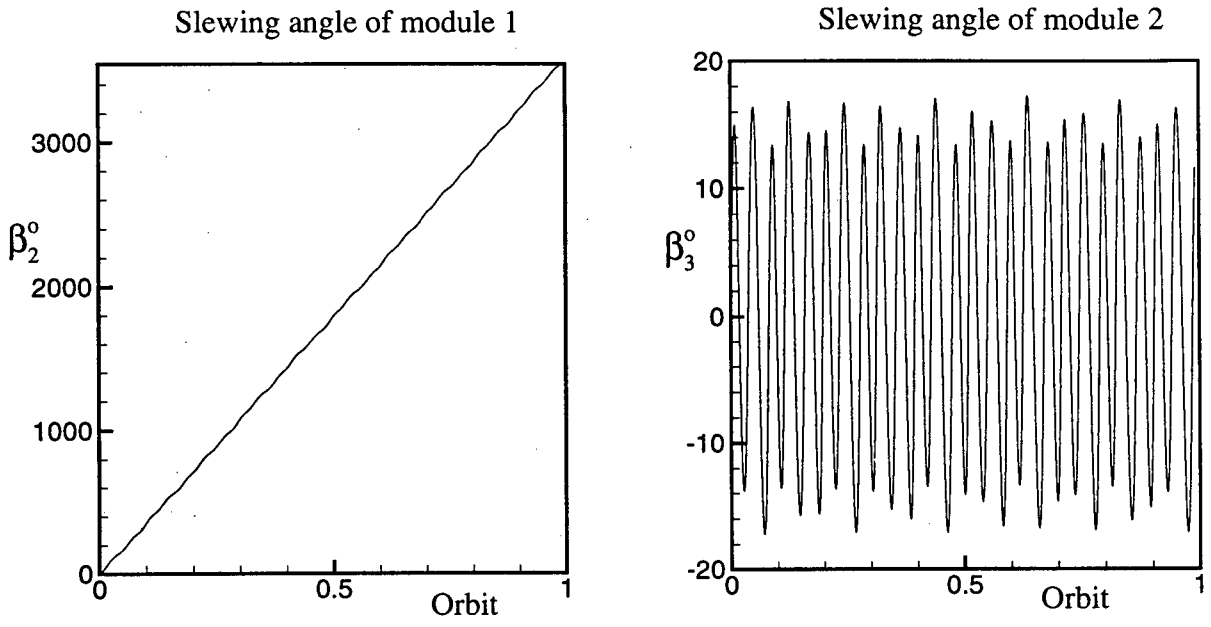

Figure 4-18 System response to an initial impulsive disturbance of $\dot{\beta}_2 = \dot{\beta}_3 = 30^\circ$ /min.

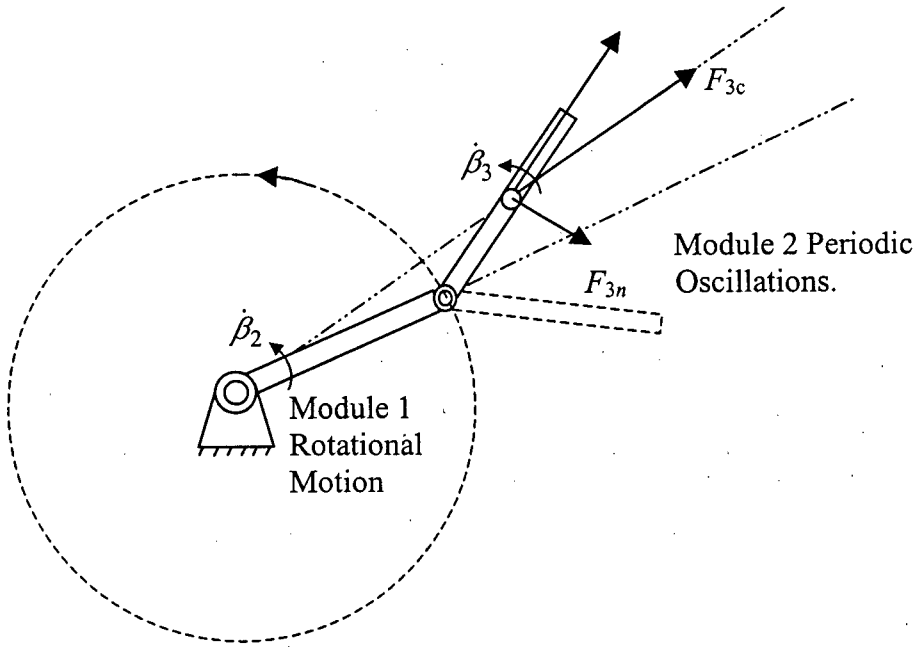

Figure 4-19 Schematic diagram showing coupled free oscillation of a two-module manipulator.

the centrifugal force F_{3c} providing the restoring moment (Figure 4-19). The transient period extended to around 50 s.

Next, the free response of the system was assessed under a variety of initial disturbances and three different values of the mass ratio: R = 1, 0.5, 0.1. Figure 4-20 shows response of the system with both the modules subjected to an initial disturbance of 30°/ min. In absence of any coupling, the modules should show a rotation of 60° in two minutes. However, due to interaction dynamics, angular velocities of the modules are affected. For m_2 / m_1 = 1, $\dot{\beta}_2$ is slightly increased giving the β_2 = 78° at t = 120 s. This is directly attributed to the moment on module 1 created by the reaction force at joint 2. The effect of decrease in m_2 / m_1 is to decrease the $\dot{\beta}_2$ by a small amount giving the $\beta_2 \approx 60°$ at t = 120 s for m_2 / m_1 = 0.1. On the other hand, the coupling effect on module 2 is to reduce $\dot{\beta}_3$. The reduction is rather large, particularly for large m_2 / m_1. Note, for m_2 / m_1 = 0.5 and 1, module 2 slows down so much in the opposite sense (i.e. clockwise direction) as to have a negative β_3. For example, at t = 120s, $\beta_3 \approx$-5°.

The effect of initial impulsive disturbance of $\dot{\beta}_3$ = 30°/min, applied to module 2, on system dynamics is presented in Figure 4-21. Note the small motion of module 1 ($\approx$9.5° in 2 min) due to the moment created by the reaction force at joint 2 as pointed out earlier. The effect of a reduction in m_2 / m_1 is as expected. Also larger the $\dot{\beta}_2$, greater it contributes to the reduction in $\dot{\beta}_3$. This is quite apparent from the trend observed in Figure 4-21.

Finally, Figure 4-22 shows response of the manipulator when module 1 executes a prescribed slewing maneuver from β_2 = 0 to β_2 =90° in 1 min. The maneuver follows a sine on ramp profile giving zero initial as well as terminal velocity and acceleration.

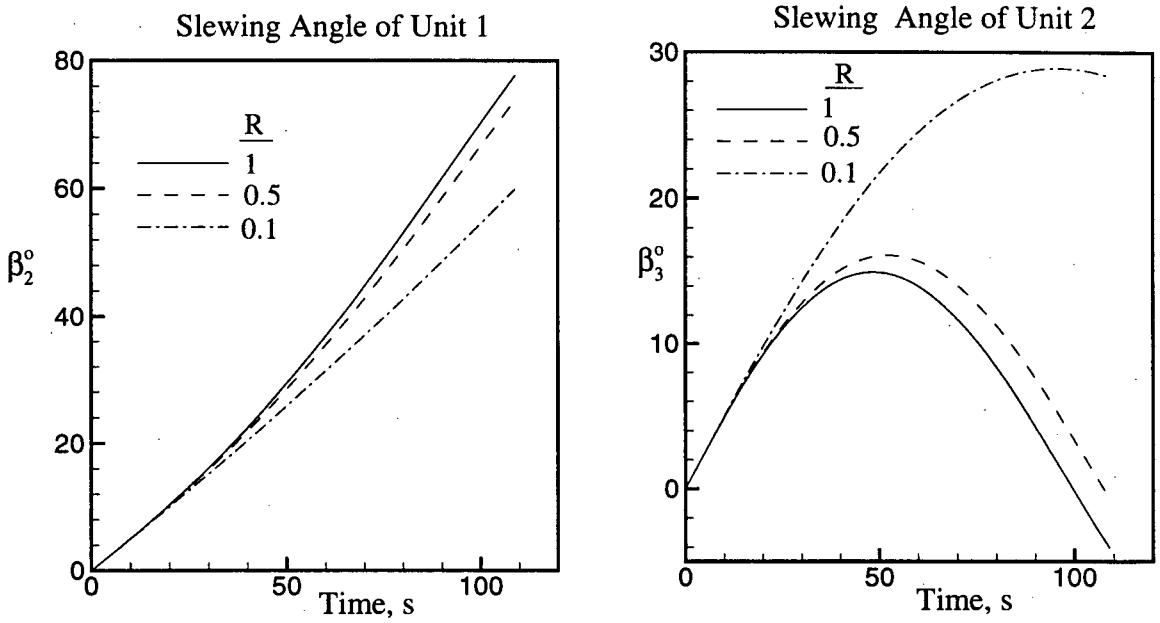

Figure 4-20 System response to an initial impulsive disturbance of $\dot{\beta}_2 = \dot{\beta}_3 = 30^o$ /min for three values of the mass ratio R. Note, the transient dynamics is computed over 120 s.

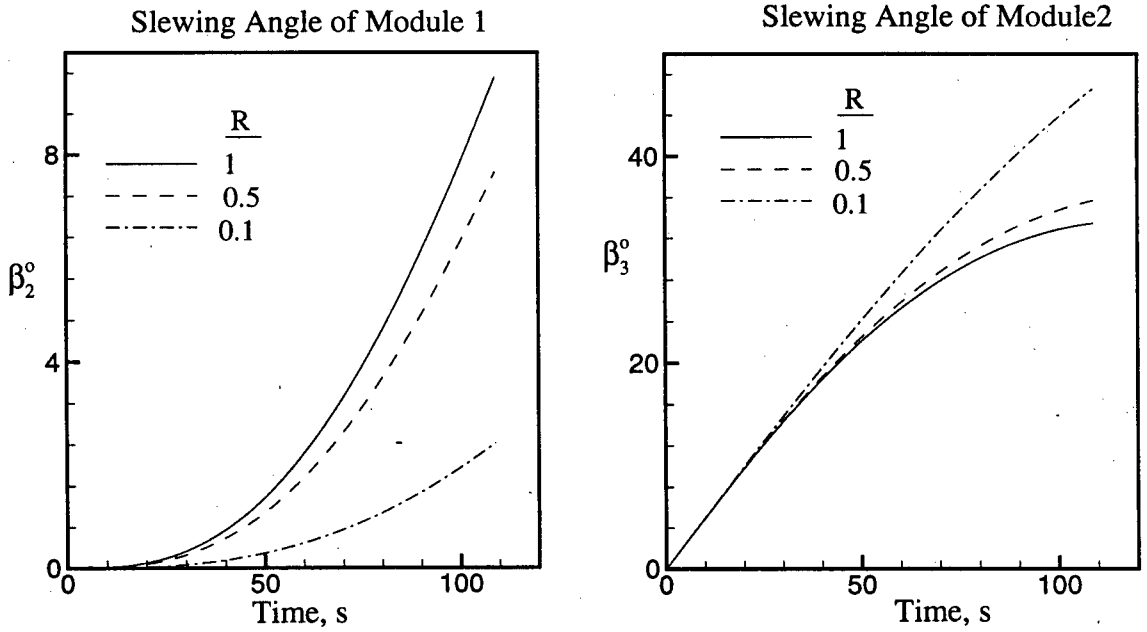

Figure 4-21 Effect of an initial impulsive disturbance of $\dot{\beta}_3 = 30^o$ /min (i.e. applied to module 2) on the system dynamics.

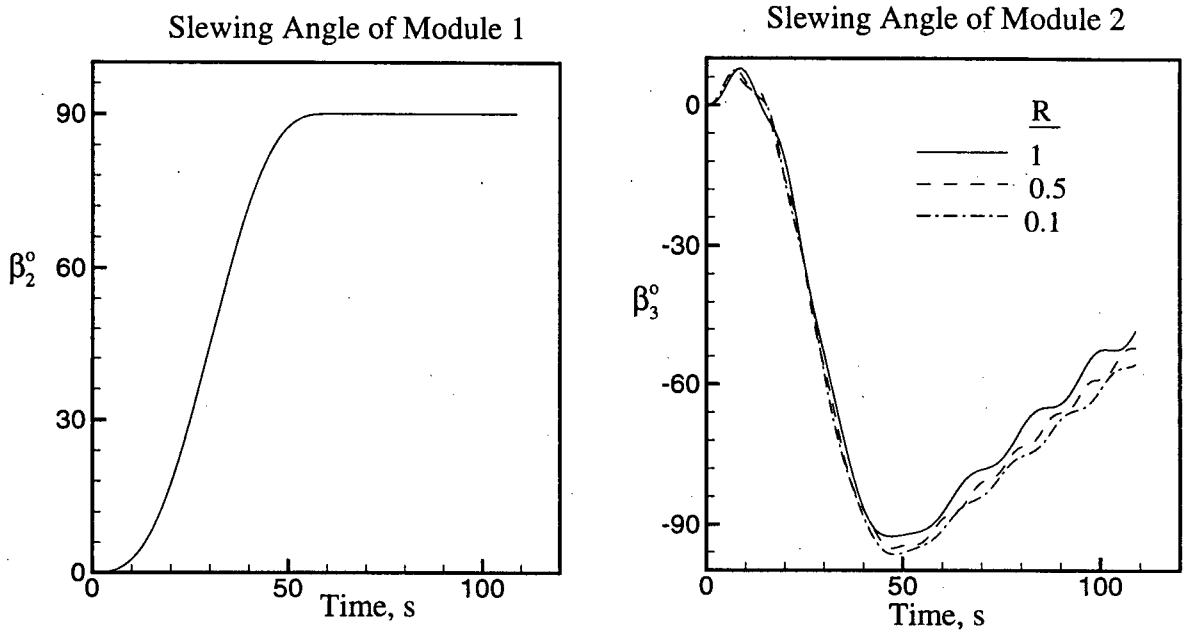

Figure 4-22 Influence of a prescribed 90° slewing maneuver in one minute of module 1 on the module 2 dynamics.

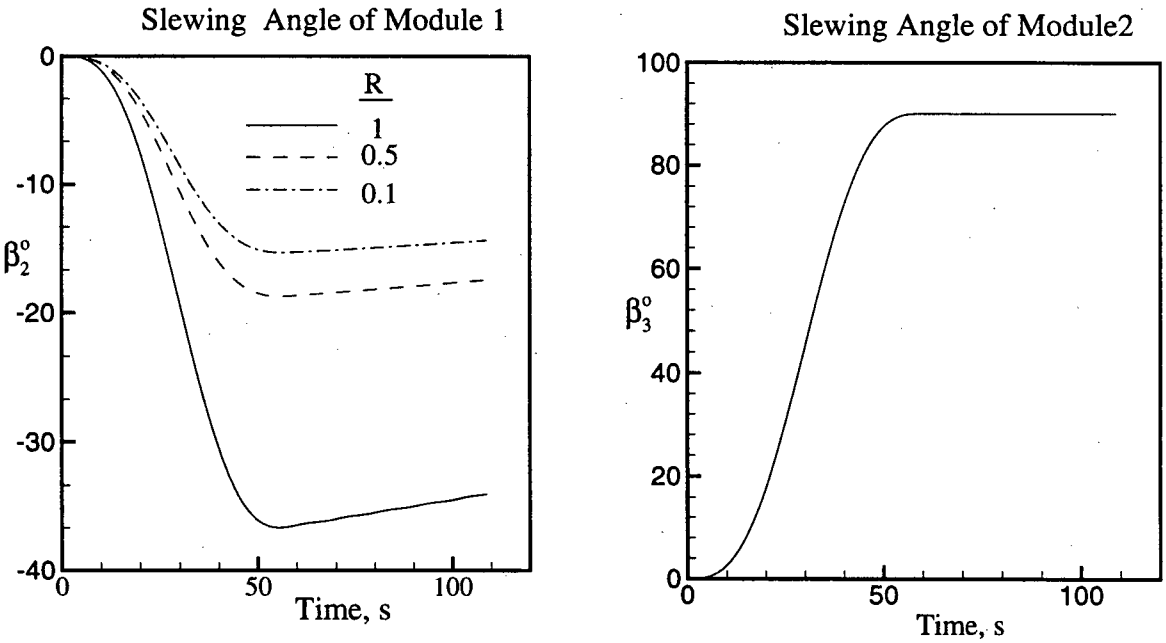

Figure 4-23 Interaction dynamics showing the effect of the prescribed maneuver of 90° slewing maneuver in one minute of module 2 on the module 1 response.

As anticipated, the second module attains approximately -90° position by the end of the maneuver. A small positive overshoot near the beginning of the maneuver and negative overshoot near the terminal phase may be attributed to the acceleration and deceleration of module 1 and associated inertia. The high frequency modulations of the β_3 response are due to the flexibility of the joint. Response of the system to a similar maneuver by module 2 is presented in Figure 4-23. Note, now the mass ratio has significant effect on the module 1 response. Of particular interest is the negative value of β_2 (as against positive β_2 in Figure 4-21) suggesting the response to depend on the acceleration time history. To summarize:

(i) Dynamics of the outer module has relatively less effect on the inner module response. On the other hand, the inner module dynamics affects the outer module response quite significantly. This is true during both an initially applied disturbance as well as a prescribed maneuver.

(ii) An initial slewing disturbance applied to the outer module induces angular velocity causing the inner module to move in the same sense as that of the disturbance. The induced motion accentuates with an increase in the mass ratio. On the other hand, an initial disturbance to the inner module leads to an induced velocity of the outer module in the opposite sense. Also, a higher mass ratio increases this effect as before.

(iii) Effect of a slewing maneuver by the outer module is to induce the inner module's motion. The effect of reducing the mass ratio is to decrease this coupling effect. The direction of the induced motion depends on the time history of the slewing maneuver. On the other hand, slewing motion of the inner module causes motion of the outer

module in the opposite sense. The module mass ratio has virtually no effect on this induced motion of module 2.

The results suggest that one can increase the length of the inner module and reduce the length of the outer module, i.e. reduce R, to minimize dynamical coupling without affecting the amount of work-space. This would help separation of gross and fine manipulations without seriously affecting the system performance.

5. NONLINEAR CONTROL

5.1 Preliminary Remarks

Versatility of the general formulation in studying dynamics of a variety of space-based manipulator configurations was demonstrated in Chapter 4. Results suggest that there are situations where the system response may not be acceptable. Hence, the next logical step is to develop a control algorithm suitable for the governing equations of motion which are nonlinear, non-autonomous and coupled. Furthermore, they are quite lengthy, even in matrix notation, as pointed out earlier.

Nonlinear control has received considerable attention in the robotics research. Although linear control procedures have served us well for a variety of relatively simple situations, with highly flexible nonlinear space-based systems they have often proved to be inadequate. Furthermore, for extremely lengthy as well as nonlinear equations of motion, as in the present case, linearization process itself becomes a demanding task. One possible solution was put forward by Freund [79]. The idea is to use the state feedback to decouple the nonlinear system in such a way that an arbitrary placement of poles is possible. The technique, however, was found to be difficult to apply to systems with more than three degrees of freedom. Freund [80] subsequently showed that by careful partitioning of the equations of motion, the procedure can be extended to systems with more than three degrees of freedom. However, the approach did involve simplification of the equations of motion.

Slotine and Sastry [81] applied the sliding mode theory to the control of robot manipulators. Consider a differential equation with the right-hand side discontinuous around a hyper-surface. If the trajectory of the solution points toward the discontinuity, it is plausible that the trajectory eventually slides along the hyper-surface. By a suitable choice of sliding

surfaces, control laws can be formulated to force the manipulator to travel along a specified trajectory defined by the surfaces. However, unmodeled dynamics usually results in high frequency oscillations of the manipulator as it slides along the surface. Slotine [82,83] improved the performance by using a filtering process with a high bandwidth for the sliding variable. Slotine and Li [84] also incorporated the sliding mode control in an adaptive PD feedback approach. The idea is to utilise the PD controller to give zero velocity error. The nonzero position errors are then eliminated through the sliding mode controller.

Inverse control, based on the Feedback Linearization Technique (FLT), was first investigated by Beijczy [85] and used by Singh and Schy [86] for rigid arm control. Spong and Vidyasagar [87,88] also used the FLT to formulate a robust control procedure for rigid manipulators. Using the FLT and given the dynamics model of the manipulator, the controller first utilizes the feedback to linearize the system followed by a linear compensator to achieve the desired system output. At times, the method is also referred to as the Computed Torque Technique which is, to be precise, is a particular case of the FLT. Spong [89] later extended the method to the control of robots with elastic joints. Advantages of this approach are twofold: (i) the control algorithm based on the FLT is simple; and (ii) the compensator design, based on a feedback linearized model, is straightforward. Recently, Modi et al. [70, 90] extended the technique to include structural flexibility for models of an orbiting manipulator system. The technique is found to provide adequate control for both rigid as well as flexible degrees of freedom.

The study in this chapter is based on the FLT as applied to the variable geometry manipulator system. The chapter begins with an introduction to the FLT. The method is

utilised to control the rigid degrees of freedom. This is followed by the application of the FLT to control the flexible manipulator system subjected to a variety of disturbances.

5.2 Feedback Linearization Technique

The governing equations of motion, Eq. (2.1), can be represented as

$$\begin{bmatrix} \mathbf{M}_{rr} & \vdots & \mathbf{M}_{rf} \\ \cdots & \cdots & \cdots \\ \mathbf{M}_{fr} & \vdots & \mathbf{M}_{ff} \end{bmatrix} \begin{Bmatrix} \ddot{\boldsymbol{q}}_r \\ \cdots \\ \ddot{\boldsymbol{q}}_f \end{Bmatrix} + \begin{Bmatrix} \boldsymbol{F}_r \\ \cdots \\ \boldsymbol{F}_f \end{Bmatrix} = \begin{Bmatrix} \boldsymbol{Q}_r \\ \cdots \\ \boldsymbol{Q}_f \end{Bmatrix} , \tag{5.1}$$

where subscripts r and f refer to the variables associated with rigid and flexible degrees of freedom, respectively. Assuming only the rigid degrees of freedom to be regulated, the control force Q_f is not applicable and hence set to zero giving:

$$\begin{aligned} &\mathbf{M}_{rr}\ddot{\boldsymbol{q}}_r + \mathbf{M}_{rf}\ddot{\boldsymbol{q}}_f + \boldsymbol{F}_r = \boldsymbol{Q}_r; \\ &\mathbf{M}_{fr}\ddot{\boldsymbol{q}}_r + \mathbf{M}_{ff}\ddot{\boldsymbol{q}}_f + \boldsymbol{F}_f = 0. \end{aligned} \tag{5.2}$$

Objective is to select $\boldsymbol{Q}_r$ in such a way that the system becomes linear and uncoupled in rigid degrees of freedom. A suitable choice for $\boldsymbol{Q}_r$ would be

$$\boldsymbol{Q}_r = \mathbf{M}\boldsymbol{v} + \boldsymbol{F} , \tag{5.3}$$

where $\boldsymbol{v} = (\ddot{\boldsymbol{q}}_r)_d + \boldsymbol{K}_v\{(\dot{\boldsymbol{q}}_r)_d - \dot{\boldsymbol{q}}_r\} + \boldsymbol{K}_p\{(\boldsymbol{q}_r)_d - \boldsymbol{q}_r\}$; $\mathbf{M} = \mathbf{M}_{rr} - \mathbf{M}_{rf}\mathbf{M}_{ff}^{-1}\mathbf{M}_{fr}$;

$\boldsymbol{F} = \boldsymbol{F}_r - \mathbf{M}_{rf}\mathbf{M}_{ff}^{-1}\boldsymbol{F}_f$. Subscript 'd' refers to the desired value of the coordinate. Now the controlled equations of motion become:

$$\begin{aligned} &\ddot{\boldsymbol{q}}_r = \boldsymbol{v}; \\ &\ddot{\boldsymbol{q}}_f = -\mathbf{M}_{ff}^{-1}\mathbf{M}_{fr}\boldsymbol{v} - \mathbf{M}_{ff}^{-1}\boldsymbol{F}_f. \end{aligned} \tag{5.4}$$

The error relation in Eq.(5.4) can now be written as

$$\ddot{\boldsymbol{e}} + \mathbf{K}_v\dot{\boldsymbol{e}} + \mathbf{K}_p\boldsymbol{e} = 0 , \tag{5.5}$$

with $\boldsymbol{e} = (\boldsymbol{q}_r)_d - \boldsymbol{q}_r$.

The function of K_p and K_v is now obvious; they are position and velocity gains to ensure asymptotic behaviour of the closed-loop system. A suitable candidate for K_p and K_v would be diagonal matrices of the form leading to a globally decoupled system with each generalized coordinate behaving as a critically damped oscillator with frequency ω_i:

$$\mathbf{K}_p = \begin{bmatrix} \omega_1^2 & & \\ & \ddots & \\ & & \omega_n^2 \end{bmatrix} ; \qquad \mathbf{K}_v = \begin{bmatrix} 2\omega_1 & & \\ & \ddots & \\ & & 2\omega_n \end{bmatrix} .$$

In attitude control of a rigid spacecraft, $\mathbf{K}_p$ and $\mathbf{K}_v$ are 3 × 3 matrices for pitch, roll, and yaw degrees of freedom. In general, a larger value of ω_i gives rise to a faster response of the i-th generalized coordinate.

Figure 5-1 shows a block diagram for the FLT. There are two loops in the system. The inner loop linearizes and decouples the system while the outer loop accomplishes the control. Since the system is linear and decoupled, any controller suitable for a linear system can be used. In this chapter only the PD control is employed to this end.

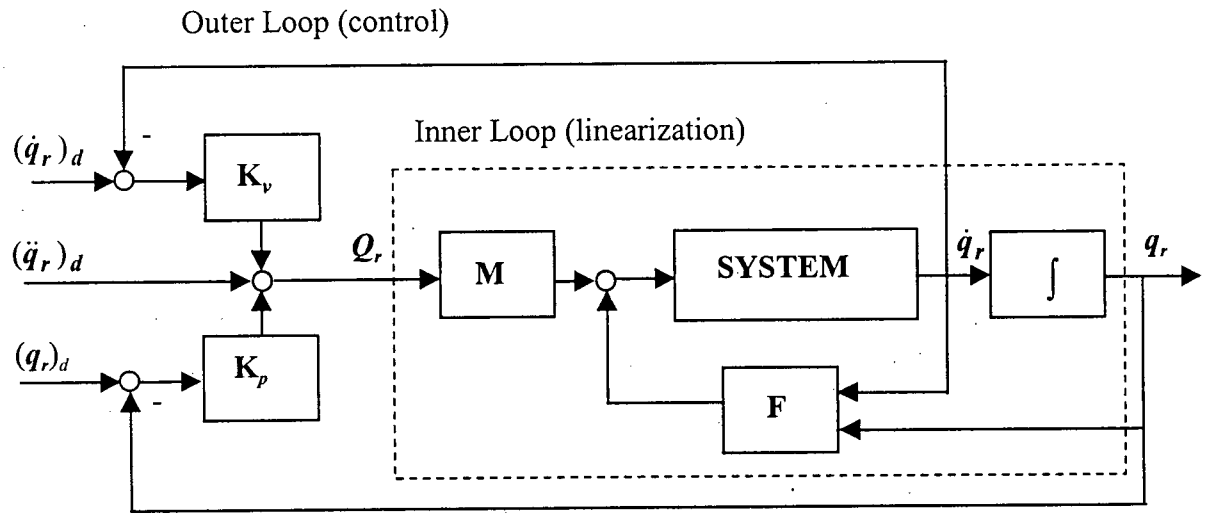

Figure 5-1 Block diagram for the Feedback Linearization Technique (FLT).

5.3 Controlled Behaviour of the System

The FLT is now applied to the space platform based one-module manipulator system as shown in Figure 5-2. The numerical values used in this study are the same as those given earlier (Chapter 4, p.68). When different, they are pointed out during the discussion of results or in the legend of the associated figure. Initial conditions, system configurations, manipulator maneuver speeds and system properties were varied to assess effectiveness as well as robustness of the controller.

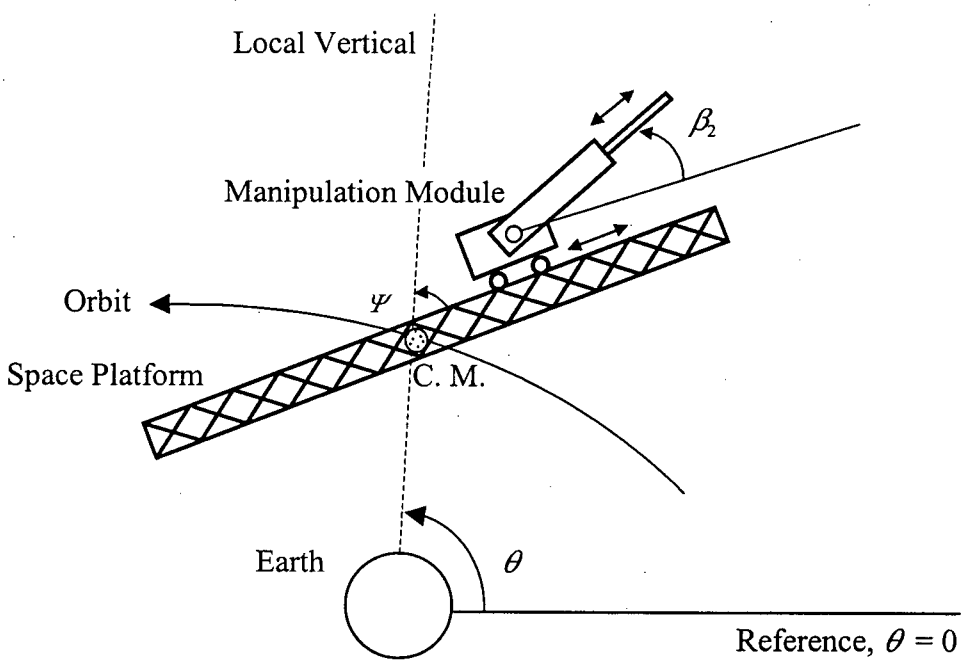

Figure 5-2 One-module space manipulator system for control study.

The first case considers the FLT control during a slew maneuver. The maneuver is through -90 °, from -30 ° to -120 °. The module length is held fixed at 10 m. The initial conditions are summarized below as well as indicated in the legend (Figure 5-3):

$d_2 = 30$ m, base fixed 30 m from the platform centerline;

$\psi = 0$, platform aligned with the local vertical;

$\beta_2 = -30°$;

$l_2 = 10$ m.

The K_v and K_p values were selected around the critically damped response estimate to account for changing manipulator geometry in an approximate manner:

- Platform libration $K_p = 1.5\times10^{-1}$, $K_v = 4$;
- module slew $K_p = 8.2943\times10^{-2}$, $K_v = 5.76$;
- module deployment $K_p = 8.2943\times10^{-2}$, $K_v = 5.76$.

The First row of Figure 5-3 shows the controlled librational motion and the corresponding torque time-history. Since the platform is a large structure, 120 m long and weighing 120 T, even with a small oscillation, 3×10^{-4} degree, a large amount of control torque is needed (700 Nm). However, the FLT controller very effectively brings the platform back to its desired orientation in less than 0.07 orbit (6 minutes). The second row shows the controlled joint motion of the module (β_2) and corresponding torque (T_2). It is apparent that controlled system reaches the desired position without overshoot. Although the flexible degrees of freedom are not under control, the coupling effect between rigid degrees of freedom and elastic generalized coordinates still exists. Note, both joint and tip vibrations of the module are thus indirectly controlled and stability is retained.

Next, the manipulator is moved to the tip of the platform (i.e. $d_2 = 60$ m). All the

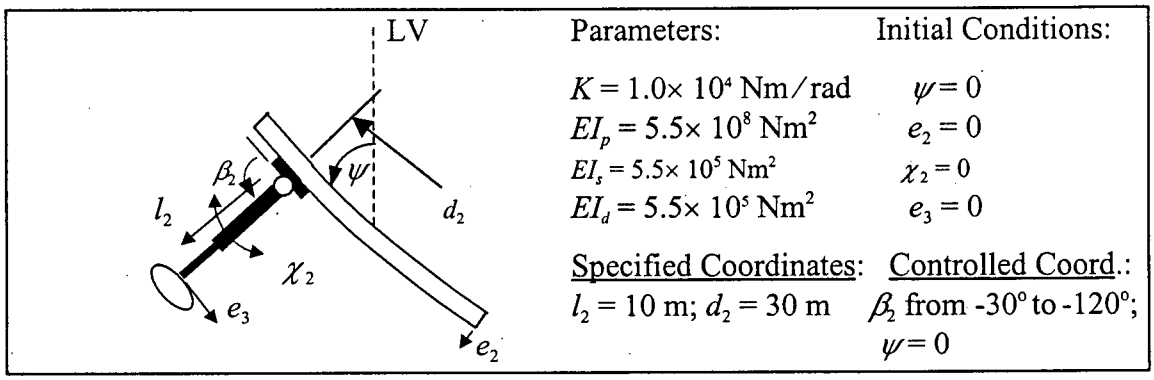

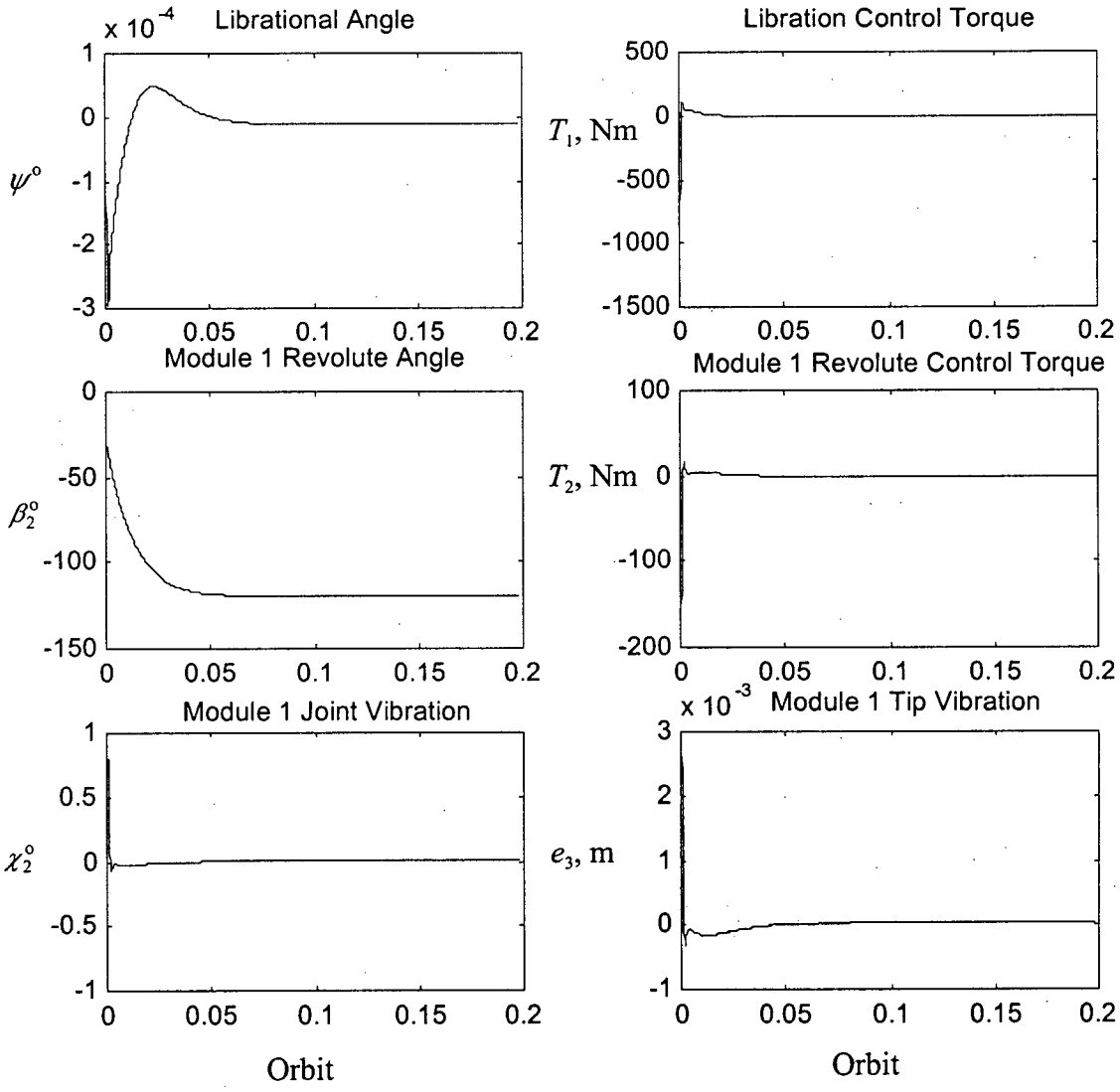

Figure 5-3 FLT control of the one-module manipulator system, executing a 90° maneuver, when located 30 m from the center of the platform.

other conditions are kept the same as before to facilitate comparison (Figure 5-4). Due to longer moment arm, the disturbance is relatively more severe. This is reflected in the librational response and the peak value of the control torque which now reaches around 2000 Nm. The manipulator reaches the commanded value of –120 ° rather quickly as before, and the flexible degrees of freedom (χ_2, e_3) are still controlled even in presence of such a large disturbance, through coupling.

In Chapter 4, Figure 4-5, an unstable system configuration ($\psi = 90°$) was investigated. Without control, platform experienced a large librational motion and attempted to settle at the stable equilibrium of $\psi = 0$. Figure 5-5 shows the system behaviour under the FLT control. Note, the manipulator is commanded to a position inclined to the platform ($\beta_2 = -50°$). This being not an equilibrium position, it acts as a small disturbance, inducing the platform to move towards the local vertical. However, the FLT control is quite successful in keeping the platform in the unstable local horizontal position. The demand on the controller is rather small (T_1 = 1.3 Nm, T_2 = 0.15 Nm). The elastic degrees of freedom remain virtually unexcited.

The extreme maneuver case studied in the Chapter 4 (Fig. 4-7) is now re-examined with the FLT control (Figure 5-6). All the conditions are kept the same as before with the payload to manipulator mass ratio taken to be 5, i.e. a 400 Kg manipulator is carrying a 2000 kg payload. The system is well under control with a small librational angle (0.005°). Manipulator reaches the desired angle in about 0.0195 orbit. Comparing with the uncontrolled case (Figure 4-7), vibration of the revolute joint reduces from around ± 90° to ± 18°. The manipulator tip vibration amplitude also shows a significant decrease, from 1.25 m (uncontrolled) to around 0.4 m (controlled). Note, the flexible degrees of freedom are

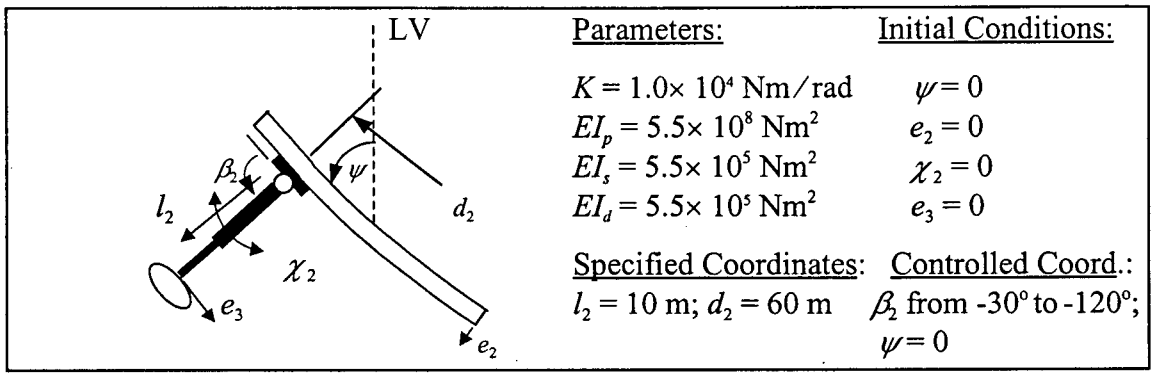

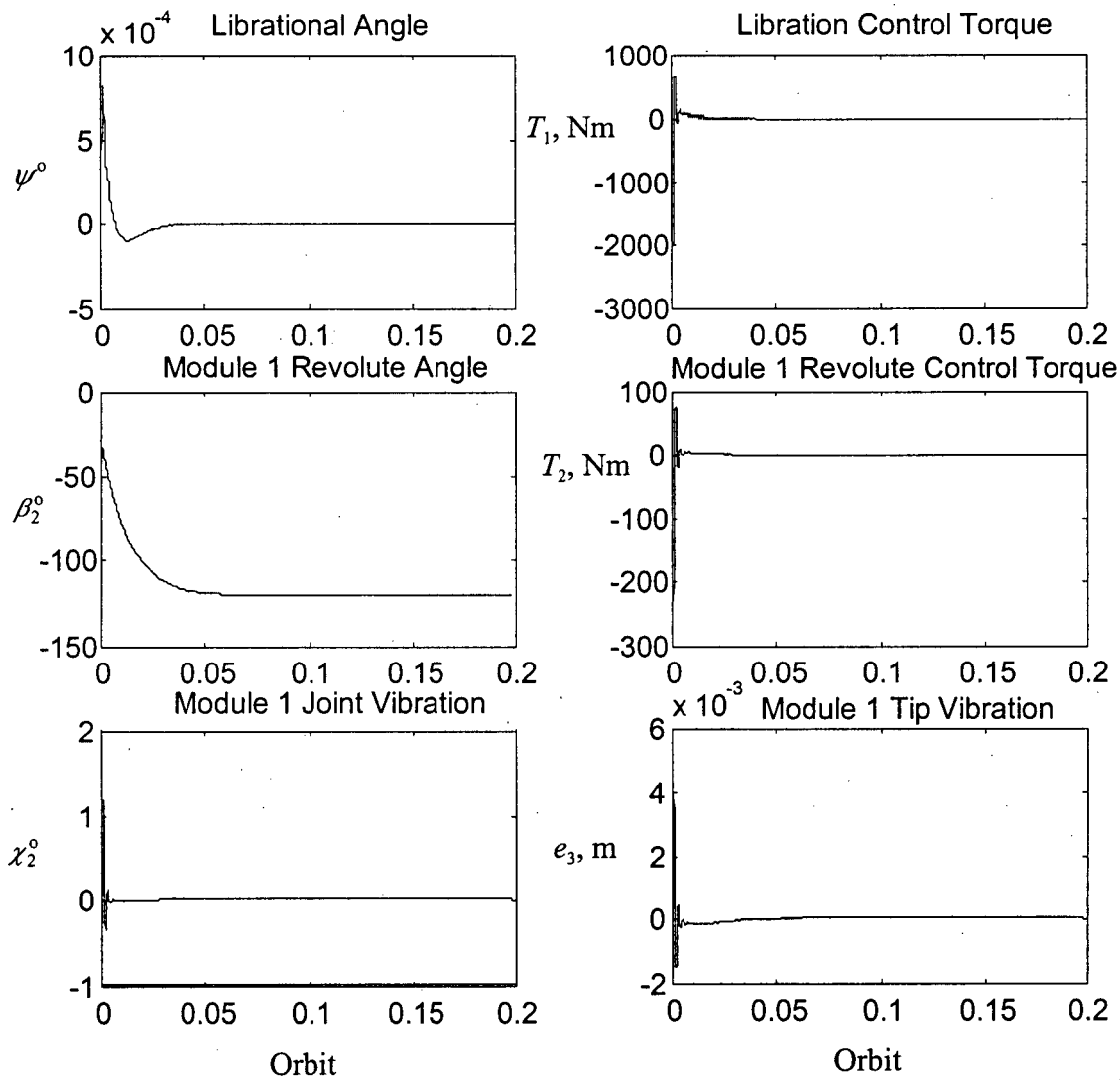

Figure 5-4 FLT control of the one-module manipulator system undergoing a 90° maneuver. The manipulator is located at the tip of the platform.

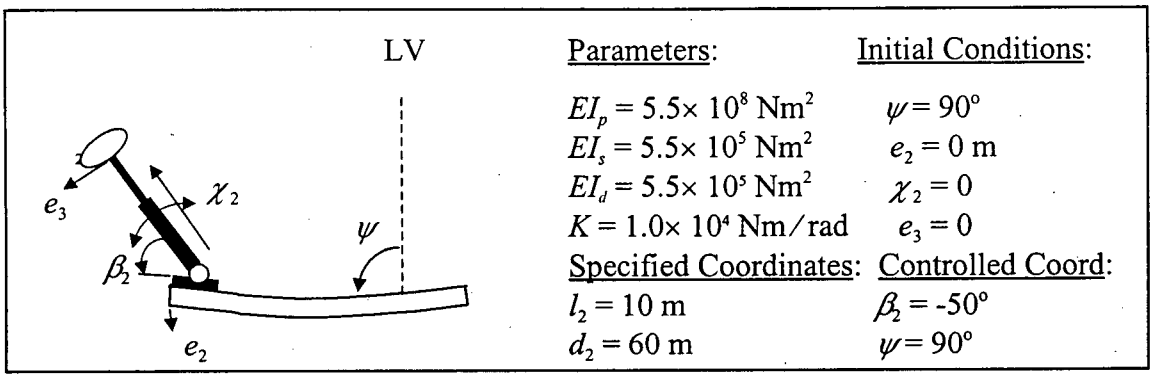

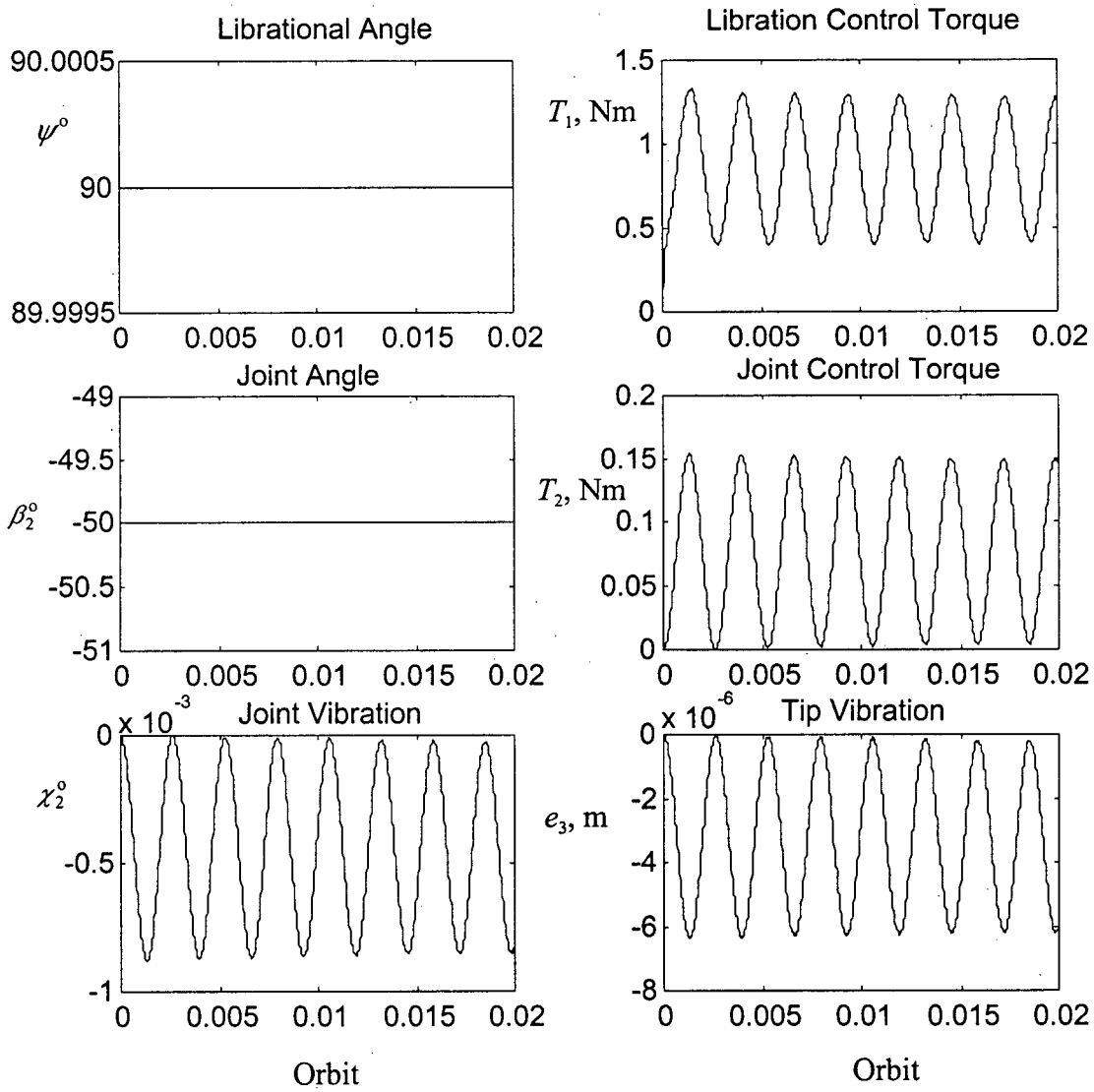

Figure 5-5 System response with the FLT control for unstable platform configuration (ψ= 90°). The one-module manipulator is located at the platform tip.

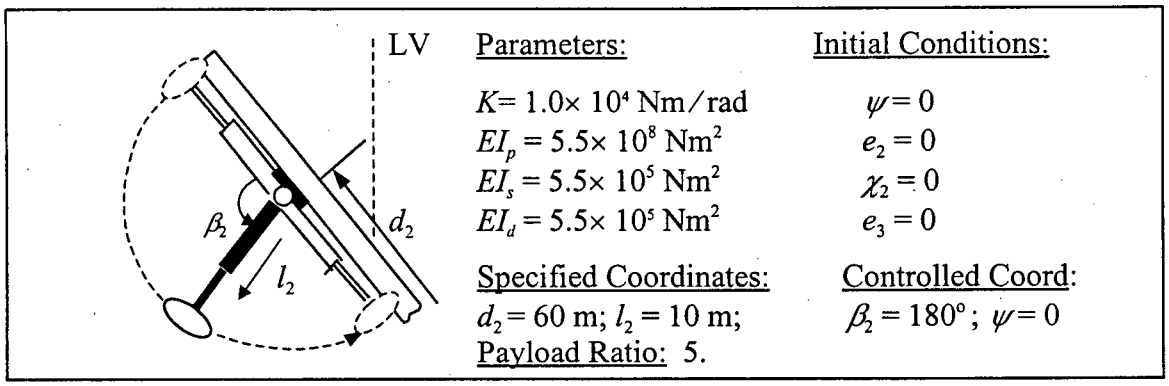

Parameters:

$K = 1.0\times 10^4$ Nm/rad
$EI_p = 5.5\times 10^8$ Nm^2
$EI_s = 5.5\times 10^5$ Nm^2
$EI_d = 5.5\times 10^5$ Nm^2

Specified Coordinates:

$d_2 = 60$ m; $l_2 = 10$ m;
Payload Ratio: 5.

Initial Conditions:

$\psi = 0$
$e_2 = 0$
$\chi_2 = 0$
$e_3 = 0$

Controlled Coord:

$\beta_2 = 180°$; $\psi = 0$

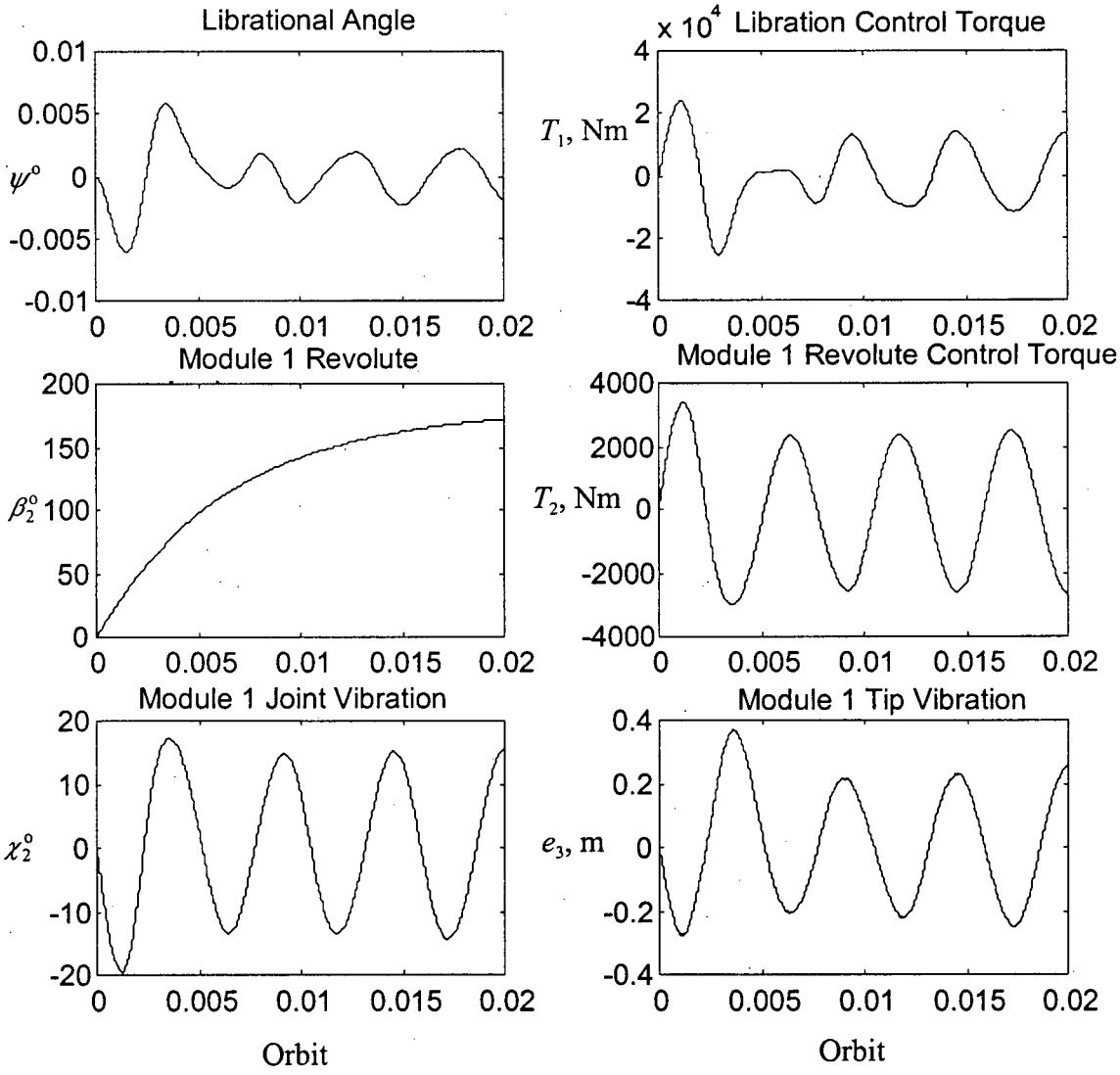

Figure 5-6 FLT controlled system response with a heavy payload (payload to manipulator mass ratio is five).

regulated indirectly, only through coupling. Even for this extreme maneuver, the control effort demand is rather modest. For platform, the peak control torque needed is about 2.4×10^4 Nm, while at the revolute joint actuator 3200 Nm of torque is required. Of course, with a limited power supply, one would normally avoid fast maneuvers with a heavy payload.

To assess effect of the manipulator flexibility, its flexural rigidity was changed systematically. Three values were considered: $EI_{d,s} = 2.75 \times10^5$ Nm^2 ; $EI_{d,s} = 5.5 \times10^5$ Nm^2; and $EI_{d,s} = 1.1 \times10^6$ Nm^2. They correspond to soft, medium and hard cases, respectively (Figure 5-7). The manipulator is located at $d_2 = 30$ m and carries a payload of 400 kg. It is commanded to reorient from $\beta_2 = 30°$ to $\beta_2 = 120°$. Note, it is able to do so in around 130 s, irrespective of the manipulator's flexural rigidity. The same is true for the platform response. Even the flexible joint behavior remains virtually unaffected by the variation in the link flexibility. Of course, as can be expected, the main effect is on the manipulator tip response, which diminishes as the system becomes hard.

The effect of deployment maneuver on the FLT control is studied with the same conditions as in Fig.4-11 of Chapter 4. The manipulator is commanded to deploy from 7.5 m to 15 m. The results are shown in Fig. 5-8. The libration angle continues to remain small and the vibration components are negligible due to the coupling effect. Of course, they can be suppressed completely by introducing a small amount of damping as seen earlier in Chapter 4 (Figure 4-8).

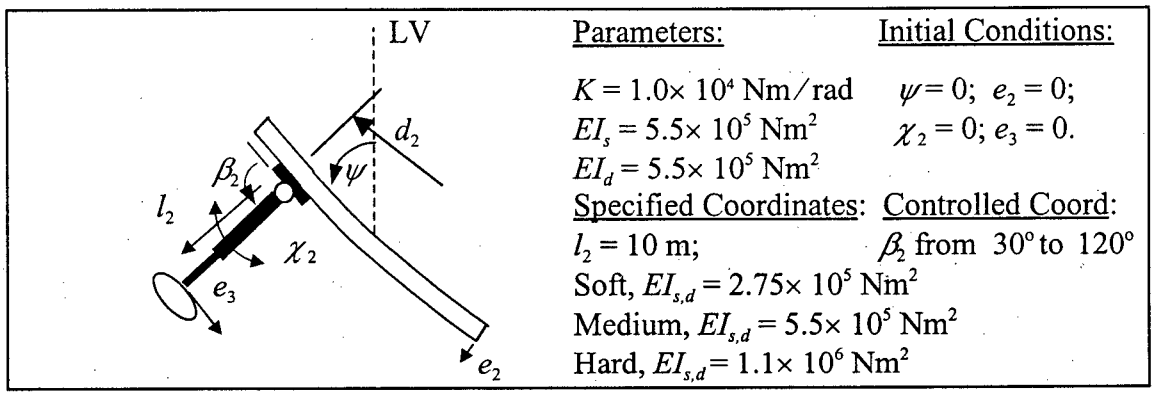

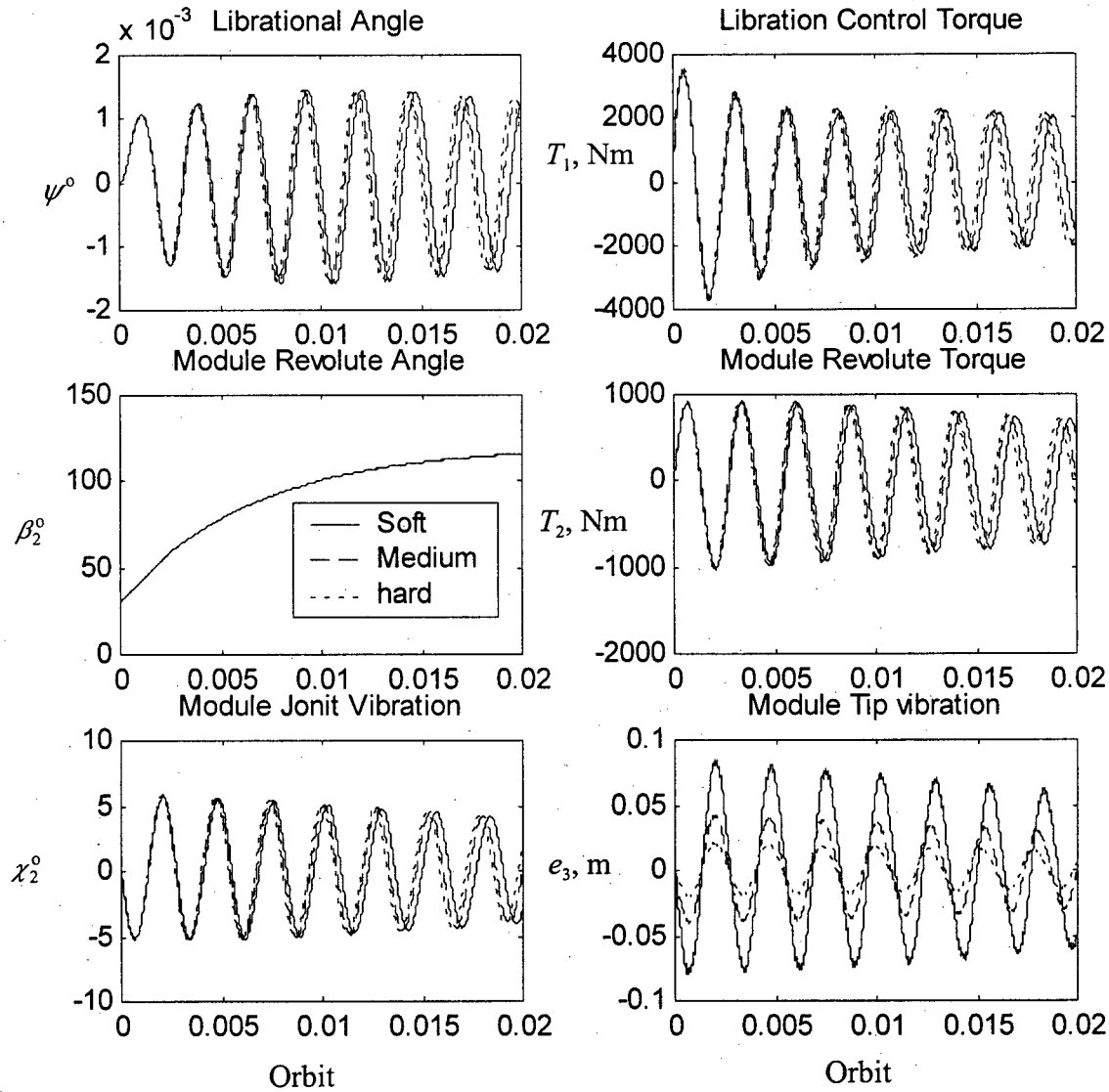

Figure 5-7 Effect of the manipulator link stiffness on the FLT control of the system.

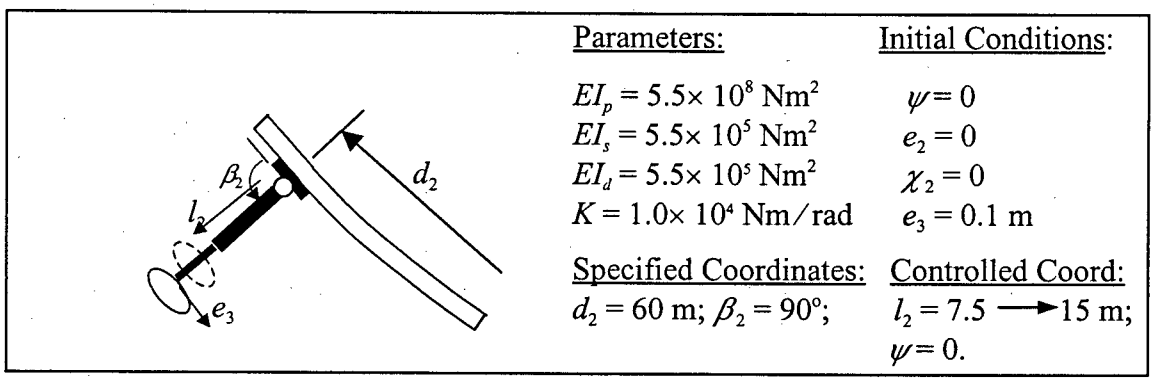

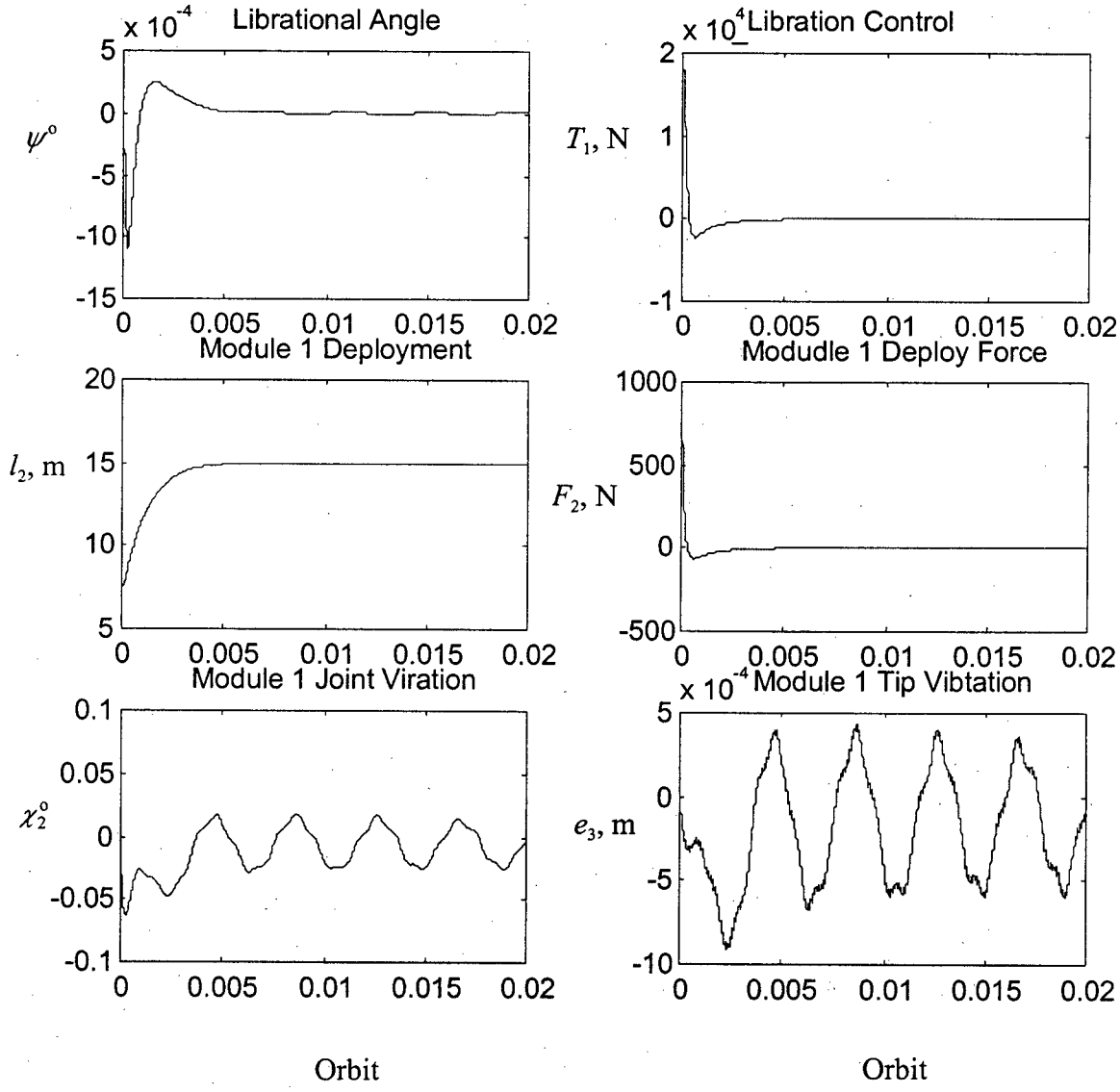

Figure 5-8 Effect of the manipulator's deployment maneuver on the FLT controlled system response.

The results show that the FLT controller is quite effective and robust. It performs remarkably well under a wide variety of system conditions, using the same set of controller gains. Active control of elastic degrees of freedom can further improve the performance if necessary.

6. OPTIMIZATION CONSIDERATIONS

As mentioned before, the presence of redundant degrees of freedom can be used to advantage. It may enable the manipulator to track a desired trajectory even when one or more joints are not functional. Furthermore, it may provide means to satisfy criteria for optimization: minimum control effort; minimum time to complete a task; minimum transmission of reaction forces and moments to the platform; and others. Here the focus is on the reduction of forces and moments at the base supporting the manipulator, i.e. at the platform. This is important for maintaining desired attitude of the platform and minimizing its vibratory response. Of course, the approach developed here can be applied to satisfy any other criterion.

6.1 Sequential Conjugate Gradient-Restoration Algorithm

There are several different methods for optimization. Here the suitable candidate is considered to be simple, reliable and able to provide global optimization. Here the sequential conjugate gradient-restoration algorithm, introduced by Miele [91] in 1979, is used to serve this purpose.

6.1.1 Problem definition

Consider the problem of minimizing the functional

$$I = \int_0^1 f(\boldsymbol{x}, \boldsymbol{u}, \boldsymbol{\pi}, t)dt + [g(\boldsymbol{x}, \boldsymbol{\pi}, t)]_1 \tag{6.1}$$

with respect to the state $\boldsymbol{x}(t)$, the control $\boldsymbol{u}(t)$, and the parameter $\boldsymbol{\pi}$ which satisfy the differential constraint

$$\dot{\boldsymbol{x}} = \boldsymbol{F}(\boldsymbol{x}, \boldsymbol{u}, \boldsymbol{\pi}, t), \qquad 0 \le t \le 1; \tag{6.2}$$

the non-differential constraint

$$\boldsymbol{S}(\boldsymbol{x},\boldsymbol{u},\pi,t)=0, \qquad 0\le \boldsymbol{t}\le 1; \tag{6.3}$$

and the boundary conditions

$$[\boldsymbol{x}]_0 = \text{given}, \tag{6.4a}$$

$$[\psi(\boldsymbol{x},\pi,t)]_1 = 0, \tag{6.4b}$$

where symbol $[f]_x$ denotes value of f at point x. Thus Eqs. (6.2) – (6.4) define the system under consideration.

6.1.2 Augmented functional

From the calculus of variation, the problem posed in Eqs.(6.1) to (6.4) is one of the Bolza type, i.e. it can be recast as that minimizing the augmented functional

$$\boldsymbol{J} = \int_0^1 [f + \lambda^{\mathrm{T}}(\dot{\boldsymbol{x}} - \boldsymbol{F}) + \rho^{\mathrm{T}}\boldsymbol{S}]dt + [g + \mu^T\psi]_1$$

$$= [\lambda^T\boldsymbol{x}]_0^1 + \int_0^1 (f - \lambda^T\boldsymbol{F} + \rho^T\boldsymbol{S} - \lambda^T\boldsymbol{x})dt + [g + \mu^T\psi]_1 \tag{6.5}$$

with respect to the state $\boldsymbol{x}(t)$, the control $\boldsymbol{u}(t)$, and the parameter π which satisfy Eqs.(6.1) to (6.4). Here $\lambda(t)$, $\rho(t)$ and constant μ are the Lagrange multipliers.

6.1.3 Optimality conditions

The optimal solution must satisfy not only the system Eqs.(6.2) to (6.4), but also the first-order optimality conditions:

$$\dot{\lambda} - f_x + F_x\lambda - S_x\rho = 0, \qquad 0\le t\le 1; \tag{6.6}$$

$$f_u - F_u\lambda + S_u\rho = 0, \qquad 0\le t\le 1; \tag{6.7}$$

$$\int_0^1 (f_\pi - F_\pi\lambda + S_\pi\rho)dt + (g_\pi\psi_\pi\mu)_1 = 0 \quad ; \tag{6.8}$$

$$[\lambda + g_x + \psi_x\mu]_1 = 0. \tag{6.9}$$

Summarizing, the solution is seeking functions $\boldsymbol{x}(t)$, $\boldsymbol{u}(t)$, π and Lagrange multipliers $\lambda(t)$, $\rho(t)$, μ which satisfy the constraints in Eqs.(6.2) to (6.4) and optimality conditions given by Eqs.(6.6) to (6.9).

6.1.4 Approximate approach

Since the differential constraints represented by Eqs.(6.2) to (6.4) and optimality conditions given by Eqs.(6.6) to (6.9) are generally nonlinear, iterative techniques are used in their solution. For this purpose, scalar functionals P and Q are defined:

$$P = \int_0^1 N(\dot{\boldsymbol{x}} - \boldsymbol{F})dt + \int_0^1 N(\boldsymbol{S})dt + N[(\psi)]_1 \quad ; \tag{6.10}$$

$$\begin{aligned} Q = &\int_0^1 N(\dot{\lambda} - \boldsymbol{f}_x + \boldsymbol{F}_x\lambda - \boldsymbol{S}_x\rho)dt + \int_0^1 N(\boldsymbol{f}_u - \boldsymbol{F}_u\lambda + \boldsymbol{S}_u\rho)dt + \\ &N\left[\int_0^1 (\boldsymbol{f}_\pi - \boldsymbol{F}_\pi\lambda + \boldsymbol{S}_\pi\rho)dt + [\boldsymbol{g}_\pi + \psi_\pi\mu]_1\right] + N[\lambda + \boldsymbol{g}_x + \psi_x\mu]_1; \end{aligned} \tag{6.11}$$

where P denotes the constraint error, Q represents the error in the optimality conditions, and $N(\boldsymbol{v})$ is an operator acting on vector $\boldsymbol{v}$ as

$$N(\boldsymbol{v}) = \boldsymbol{v}^T\boldsymbol{v}.$$

Note that, for the optimal solution, $P = 0$ and $Q = 0$. For an approximation to the optimal solution, let:

$$P \le \varepsilon_1; \tag{6.12a}$$

$$Q \le \varepsilon_2; \tag{6.12b}$$

where ε_1 and ε_2 are small, pre-selected numbers.

6.1.5 Construction of the sequential conjugate gradient-restoration algorithm

The sequential conjugate gradient-restoration algorithm is an iterative technique that includes a sequence of cycles having the following properties.

Property 1

The functions $\boldsymbol{x}(t)$, $\boldsymbol{u}(t)$, and π, available both at the beginning and end of each cycle, must be feasible; that is, they must be consistent with constraints in Eqs. (6.2) to (6.4) within the pre-selected accuracy stated in Eq. (6.12a).

Property 2

The functions $\boldsymbol{x}(t)$, $\boldsymbol{u}(t)$, and π obtained at the end of each cycle must be characterized by a value of the functional Q (Eq. 6.11) which is smaller than that associated with the functions available at the beginning of the cycle until Eq. (6.12b) is satisfied.

Property 3

The functions $\boldsymbol{x}(t)$, $\boldsymbol{u}(t)$, and π obtained at the end of each cycle must be characterized by a value of the augmented functional J (Eq. 6.5) which is smaller than that associated with the functions available at the beginning of the cycle.

Note that *Property* 3 is a consequence of *Properties* 1 and 2. Conversely, *Property* 2 is an outcome of *Properties* 1 and 3. To achieve the above properties, each cycle is made of two phases, a conjugate gradient phase and restoration phase.

6.1.6 Conjugate gradient phase

This phase is started only when the constraint error P satisfies the inequality in Eq. (6.12a). It involves iteration designed to decrease the value of the functional I or the augmented functional J, through minimization of the functional Q (Eq.6.12b), while

satisfying the constraints to the first order (i.e. the linearized system Eqs. 6.2 – 6.4). During this iteration, the first order variation of the functional Q is minimized, subject to the linearized constraints. This corresponds to the conjugate gradient phase loop in the flow-chart (Figure 6-1).

6.1.7 Restoration phase

This iteration phase is started only when the constraint error P violates the condition in Eq.(6.12a). In each of the restoration iterations, the objective is to reduce the error P, while the constraints are satisfied to the first order (Eq.6.6), and the norm of the variations of the control (Eq.6.7) and the parameter π (Eq.6.8) are minimized. The restoration phase is terminated when Eq. (6.12a) is satisfied. Figure 6-1 also shows the restoration phase.

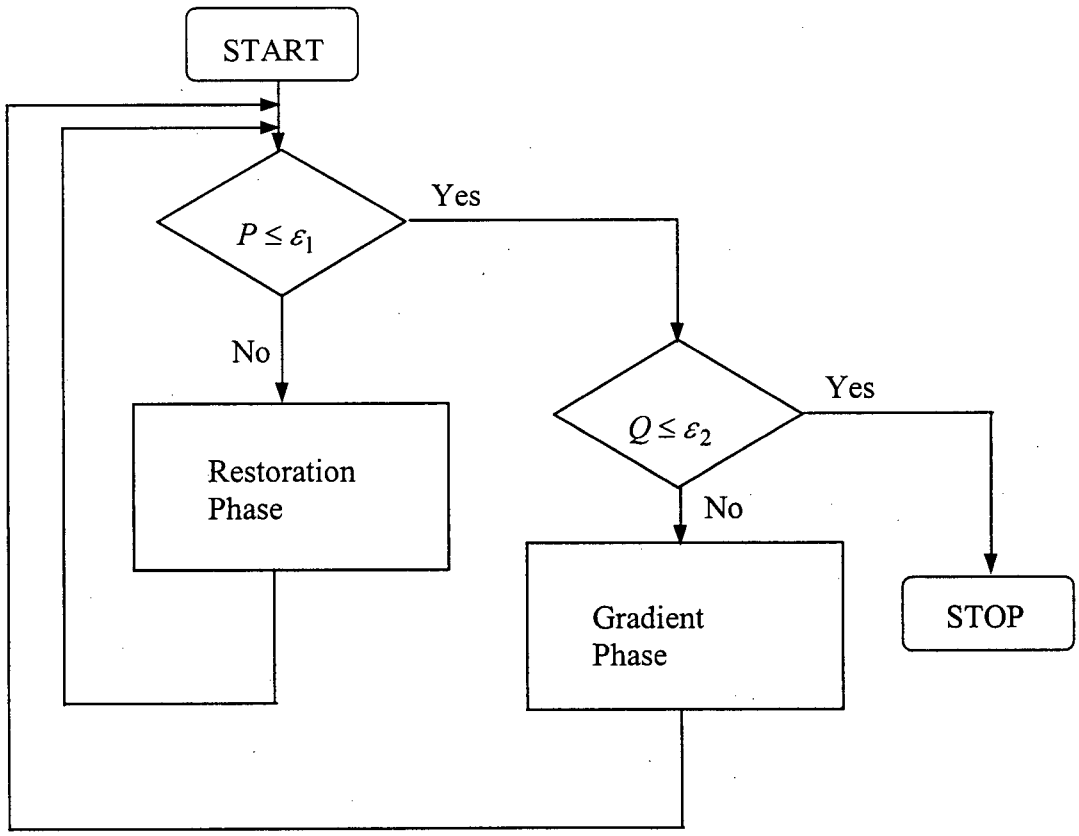

Figure 6-1 Flow-chart of the sequential conjugate gradient-restoration algorithm.

6.2 Optimal Trajectory Design

The optimal trajectory design was undertaken for a two-module manipulator as shown in Figure 6-2. To illustrate the approach, a simple ground-based system, operating in a horizontal plane, is purposely considered for clarity. It used the method by Miele [91] summarized in Section 6.1 and the corresponding algorithm developed as indicated in Figure 6-1. Note, in the planer case, the manipulator has four degrees of freedom (β_1, l_1, β_2, l_2) but only two generalized coordinates are required to identify the position of the manipulator tip. Thus there are two redundant degrees of freedom which are used to minimize transmission of force $\boldsymbol{F}_1 = [F_{1x}, F_{1y}]^T$ and moment $\boldsymbol{T}_1$ to the platform.

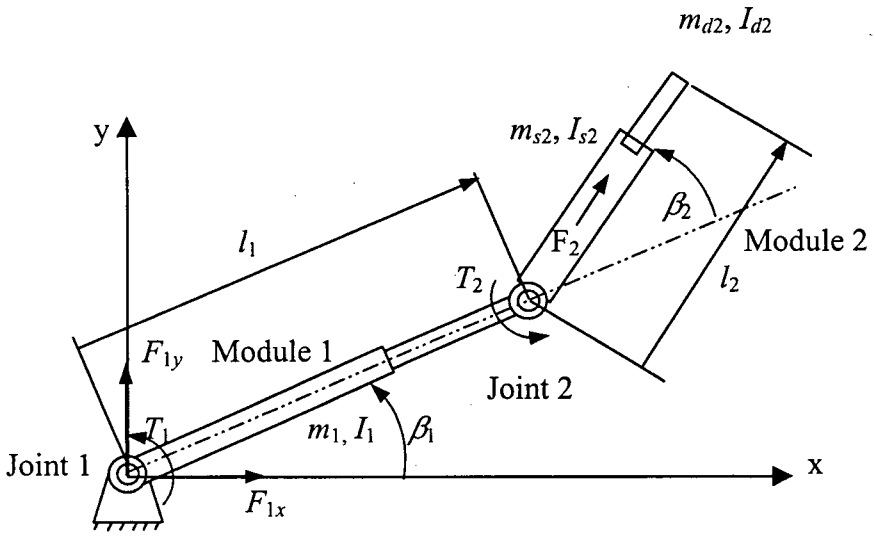

Figure 6-2 Two-module manipulator system used to study optimal trajectories for minimum transmission of force and moment.

Various symbols appearing in Figure 6-1 are defined below:

m_1 = mass of module 1, $m_{s1} + m_{d1}$;

m_{s1}, m_{d1} = mass of slewing and deployable links of module 1, respectively;

m_2 = mass of module 2, $m_{s2} + m_{d2}$;

m_2 = mass of module 2, $m_{s2} + m_{d2}$;

m_{s2}, m_{d2} = mass of slewing and deployable links of module 2, respectively;

m_2 / m_1 = mass ratio, R;

I_1 = mass moment of inertia of module 1 about its center;

I_{s1}, I_{d1} = mass moment of inertia of slewing and deployable links of module 1 respectively;

l_1, l_2 = lengths of module 1 and 2, respectively;

l_{s2}, l_{d2} = lengths of slewing and deployable links of module 2, respectively;

F_1, T_1; F_2, T_2 = forces and moments at joint 1and 2, respectively;

β_1, β_2 = slew angles at joints 1 and 2, respectively.

For this investigation, prismatic joint of module 1 is locked in position with l_1 = 7.5 m. The corresponding equations of motion can be written as:

$$\left\{I_1 + I_{S2} + I_{d3} + m_1\left(\frac{l_1}{2}\right)^2 + m_{S2}[l_1^2 + \left(\frac{l_{S2}}{2}\right)^2 + 2l_1\left(\frac{l_{d2}}{2}\right)\cos\beta_2] + m_{d2}\left[l_1^2 + \left(l_2 + \frac{l_{d2}}{2}\right)^2 + 2l_1\left(l_2 + \frac{l_{d2}}{2}\right)\cos\theta_2\right]\right\}\ddot{\beta}_1$$

$$+\left\{I_{S2} + I_{d2} + m_{S2}\left(\frac{l_{S2}}{2}\right)\left[\left(\frac{l_{S2}}{2}\right) + l_1\cos\beta_2\right] + m_{d2}\left[\left(l_2 + \frac{l_{d2}}{2}\right)^2 + l_1\left(l_2 + \frac{l_{d2}}{2}\right)\cos\beta_2\right]\right\}\ddot{\beta}_2$$

$$+\left(m_{d2}l_1\sin\beta_2\right)\ddot{l}_2 + \left\{-2l_1\left[m_{S2}\left(\frac{l_1}{2}\right) + m_{d2}\left(l_2 + \frac{l_{d2}}{2}\right)\right]\sin\beta_2\right\}\dot{\beta}_1\dot{\beta}_2$$

$$+\left\{2m_{d2}\left[\left(l_2 + \frac{l_{d2}}{2}\right) + l_1\cos\beta_2\right]\right\}\dot{l}_2\dot{\beta}_1 + \left\{-l_1\left[m_{S2}\left(\frac{l_{S2}}{2}\right) + m_{d2}\left(l_2 + \frac{l_{d2}}{2}\right)\right]\sin\beta_2\right\}(\dot{\beta}_2)^2$$

$$+\left\{2m_{d2}\left[\left(l_2 + \frac{l_{d2}}{2}\right) + l_1\cos\beta_2\right]\right\}\dot{l}_2\dot{\beta}_2 - T_1 = 0 \quad ; \tag{6.13}$$

$$\left\{I_{S2}+I_{d2}+m_{S2}\left(\frac{l_{S2}}{2}\right)^2+l_1\left(\frac{l_{S2}}{2}\right)\cos\beta_2)+m_{d2}\left[\left(l_2+\frac{l_{d2}}{2}\right)^2+l_1\left(l_2+\frac{l_{d2}}{2}\right)\right]\cos\beta_2\right\}\ddot{\beta}_1$$
$$+\left[I_{S2}+I_{d2}+m_{S2}\left(\frac{l_{S2}}{2}\right)^2+m_{d2}\left(l_2+\frac{l_{d2}}{2}\right)^2\right]\ddot{\beta}_2+\left\{l_1\left[m_{S2}\left(\frac{l_{S2}}{2}\right)+m_{d2}\left(l_2+\frac{l_{d2}}{2}\right)\right]\sin\beta_2\right\}(\dot{\beta}_2)^2$$
$$+\left[2m_{d2}\left(l_2+\frac{l_{d2}}{2}\right)\right]\dot{l}_2\dot{\beta}_1+\left[2m_{d2}\left(l_2+\frac{l_{d2}}{2}\right)\right]\dot{l}_2\dot{\beta}_2-T_2=0 \quad ; \tag{6.14}$$

$$[m_{d2}l_1\sin\beta_2]\ddot{\beta}_1+[m_{d2}]\ddot{l}_2+\left[-m_{d2}\left(l_2+\frac{l_{d2}}{2}\right)+l_1\cos\beta_2\right](\dot{\beta}_1)^2$$
$$+\left[-2m_{d2}\left(l_2+\frac{l_{d2}}{2}\right)\right]\dot{\beta}_1\dot{\beta}_2+\left[-m_{d2}\left(l_2+\frac{l_{d2}}{2}\right)\right](\dot{\beta}_2)^2-F_2=0 \tag{6.15}$$

The objective is to minimize the coupling effect acting on the joint between the manipulator and platform (joint 1) due to the motion of module 2. The cost function was taken in the quadratic form as

$$J=\int_0^{t_f}(w_1T_1^2+F_1^T\begin{bmatrix}w_2 & 0\\ 0 & w_2\end{bmatrix}F_1)\,dt\ , \tag{6.16}$$

where: T_1 = base reaction torque ;

w_1 = weight factor for T_1;

$F_1 = [F_{1x}, F_{1y}]^T$, reaction force at joint 1 between the manipulator and platform;

w_2 = weight factor for F_1.

The task is to move the tip of the manipulator from point A (0, 15 m) to point B (12.61 m, 5.12 m) using module 2 keeping the force and moment at joint 1 minimum. The sequential conjugate gradient-restoration algorithm discussed earlier is used to this end. The

differential constraints are the equations of motion (Eqs.6.13 to 6.15) and the boundary conditions are the starting point and the final position configurations. The following cases are considered to determine the optimal trajectory of the manipulator tip, the effect of weight ratio w_1/w_2 and the mass ratio of module 2 to module 1.

Case 1(mass ration R = 1)

- Module 1 (free to slew): mass = 250 kg, uniformly distributed; length (l_1) = 7.5 m, i.e. the link is fully deployed and remains locked.
- Module 2 (free to slew and deploy): mass m_{S2}, m_{d2} = 125 kg, uniformly distributed; length l_{S2}, l_{d2} = 3.75 m.
- Initial Conditions: β_1, = β_2 = 0; l_2 = 7.5 m, i.e. the deployable link of module 2 is fully extended.
- Initial tip position A: $x = 0$, $y = 15$ m. Final tip position B: $x = 12.61$ m, $y = 5.12$ m.
- Maneuver time: 1 minute.

From the dynamic point of view, if a heavier penalty is put on the torque (w_1:w_2 = 10:1), the optimal tip trajectory would tend to reduce the length of the module (thus diminishing its inertia) in order to decrease the torque required to rotate it. On the other hand, if reduction in the reaction force is more important, the optimal solution would emphasize slewing the module and then utilize the advantage of less coupling effect for the prismatic joint to retrieve the tip. This approach is open to a variety of optimization considerations. One can easily modify the cost function or change it completely to serve the desired objective.

The optimized tip trajectories for several different values of weight ratio are shown in Fig. 6-3(a) for $m_2 / m_1 = 1$. It is apparent that with an increase in w_1: w_2, the optimization

procedure tends to emphasize the reduction in the length of module 2 to reduce the moment of inertia. Thus, the torque required for the slew motion is globally minimized. From Fig. 6-3(b), it is clear that the length of module 2 reduces with an increase in the ratio w_1/w_2. In Figures 6-4(a) and 6-4(b), time histories of the rotation angles, deployable length and their associated torques and force are plotted. Note, with the increase in weight ratio from 1:1 to 10:1 the torque excursion diminishes from ≈ 25.42 Nm (≈ +11.00 to −14.42) to 21.25 Nm (≈ +9.57 Nm to −11.68 Nm). Due to heavier penalty on torque (w_1: w_2 = 10:1), the procedure provides configuration time history that will lead to reduced demand on moment. On the other hand, the force excursions increase from 1.48 N (1:1) to 2.74 N (10:1).

The same optimization procedure is now applied to the cases where the mass ratio between the two modules changes to assess the characteristic of the gross-fine manipulations.

Case 2 (mass ration R = 0.33)

- Module 1 (free to slew): mass = 375 kg, uniformly distributed; length (l_1) = 11.25 m, i.e. the link is fully deployed and remains locked.
- Module 2 (free to slew and deploy): mass m_{S2}, m_{d2} = 62.5 kg, uniformly distributed; length l_{S2}, l_{d2} = 1.875 m.
- Initial Conditions: β_1, = β_2 = 0; l_2 = 3.75 m, i.e. the deployable link of module 2 is fully extended.
- Initial tip position A: x = 0, y = 15 m. Final tip position B: x = 12.61 m, y = 5.12 m.
- Maneuver time: 1 minute.

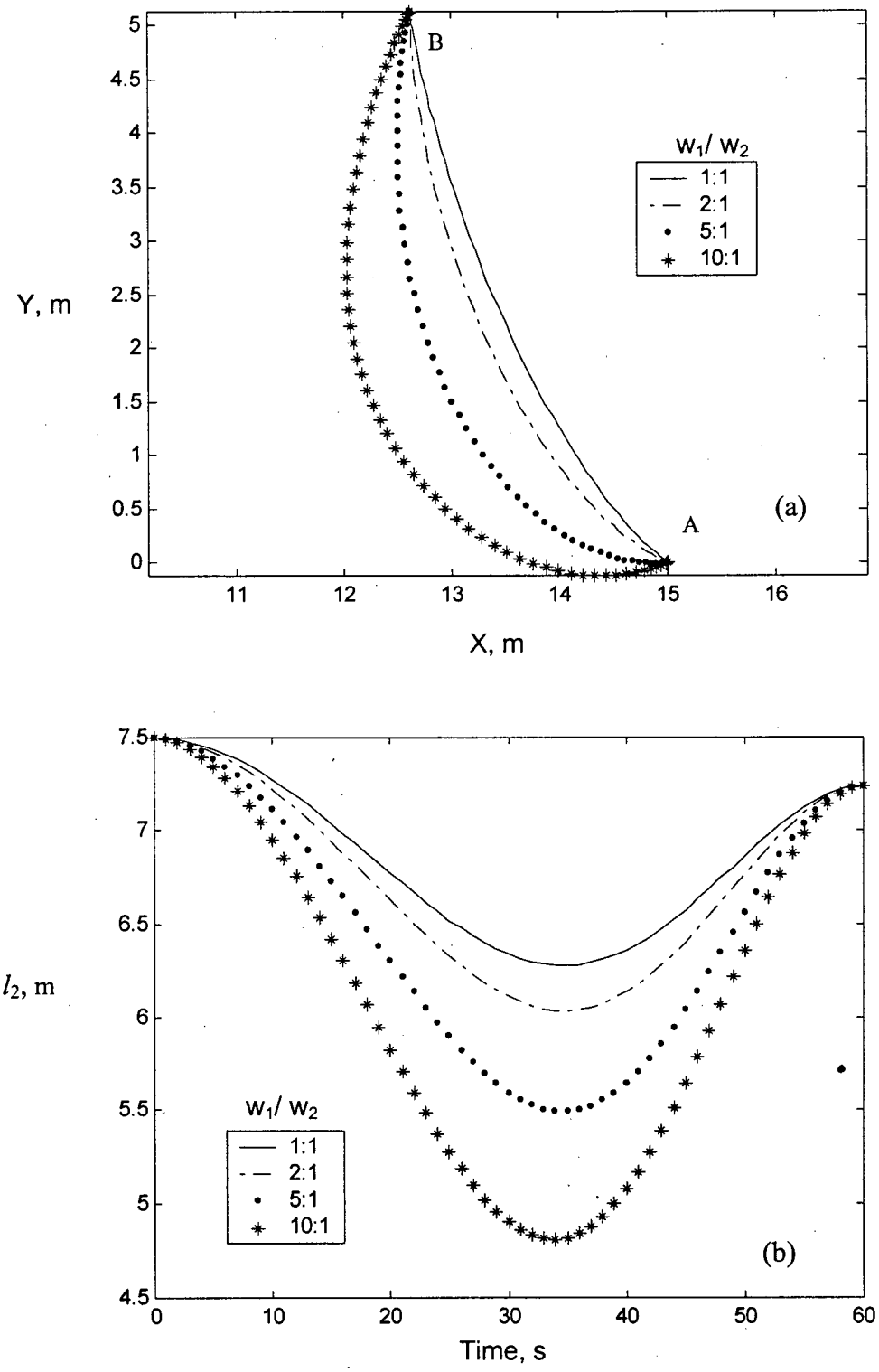

Figure 6-3 Effect of weight ratio, during optimization, on: (a) tip trajectory; (b) length of module 2.

(a)

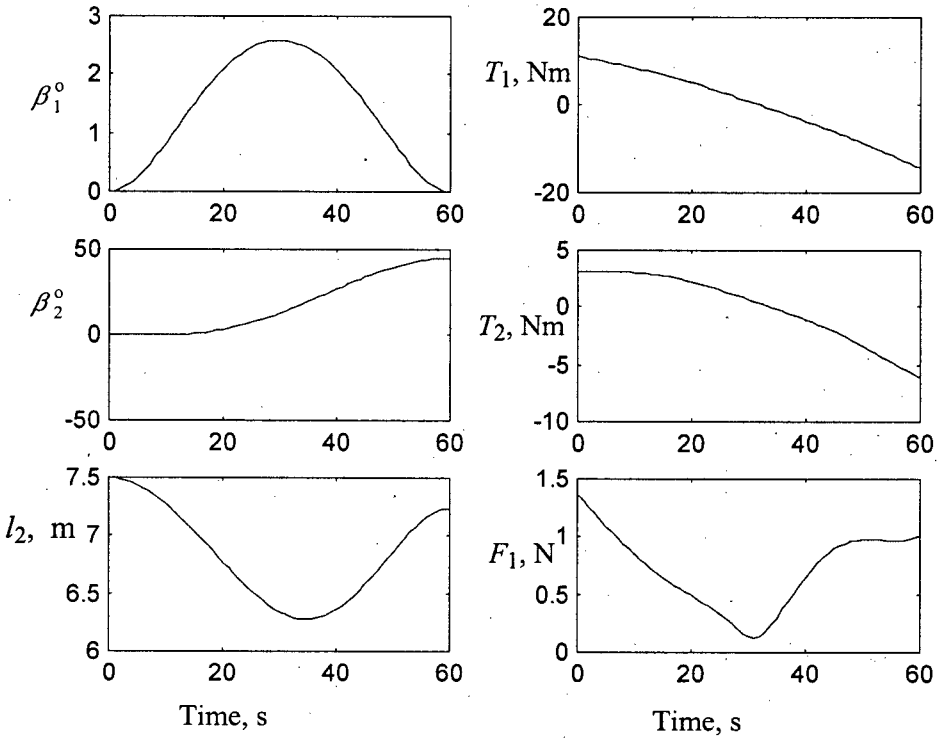

(b)

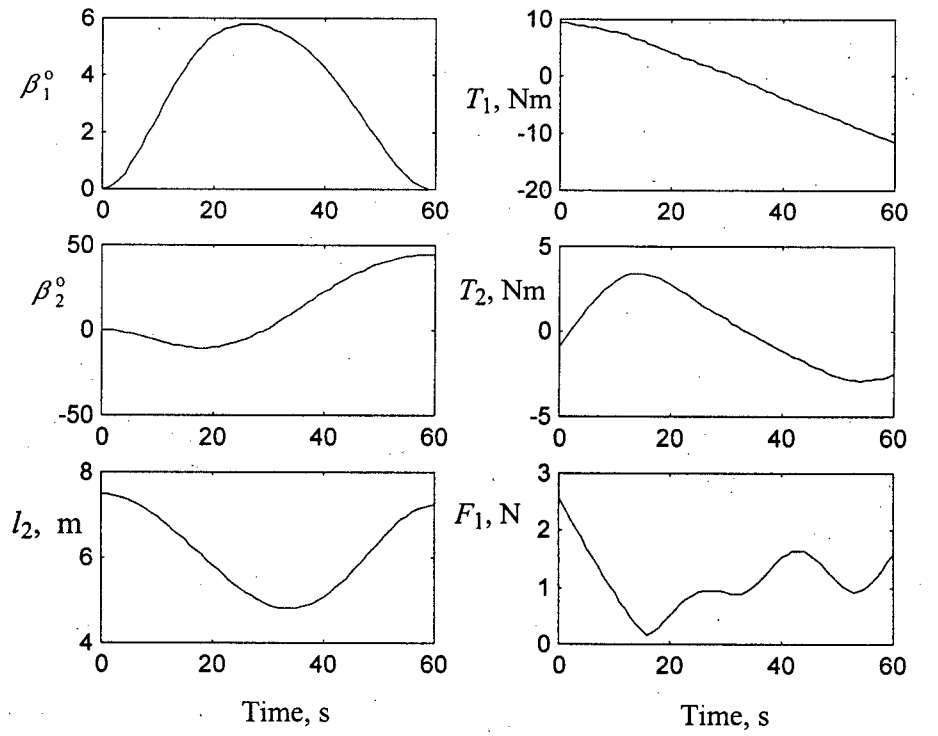

Figure 6-4 System behavior with optimization: (a) w_1/w_2 =1:1; (b) w_1/w_2 =10:1.

Case 3 (mass ration R = 0.2)

- Module 1 (free to slew): mass = 416.67 kg, uniformly distributed; length (l_1) = 12.5 m, i.e. the link is fully deployed and remains locked.
- Module 2 (free to slew and deploy): mass m_{S2}, m_{d2} = 41.67 kg, uniformly distributed; length l_{S2}, l_{d2} = 1.25 m.
- Initial Conditions: β_1, = β_2 = 0; l_2 = 2.5 m, i.e. the deployable link of module 2 is fully extended.
- Initial tip position A: $x = 0$, $y = 15$ m. Final tip position B: $x = 12.61$ m, $y = 5.12$ m.
- Maneuver time: 1 minute.

Figure 6-5 shows optimal tip trajectories of the manipulator as affected by the weight ratio. It follows the same trends as in the case of mass ratio of 1 except for a reduction in the retrieval distance for module 2. Note, decrease in the mass ratio also leads to a reduction in the coupling effect. However variations in the optimized trajectories with R are relatively less compared to those in Figure 6-3. This is particularly evident in Figure 6-6. Thus, with a properly designed manipulator system for a certain task, i.e. with a small m_2/ m_1, fine manipulations can be considered independent of the weight ratio. This simplifies optimization procedure significantly, particularly for a complex system.

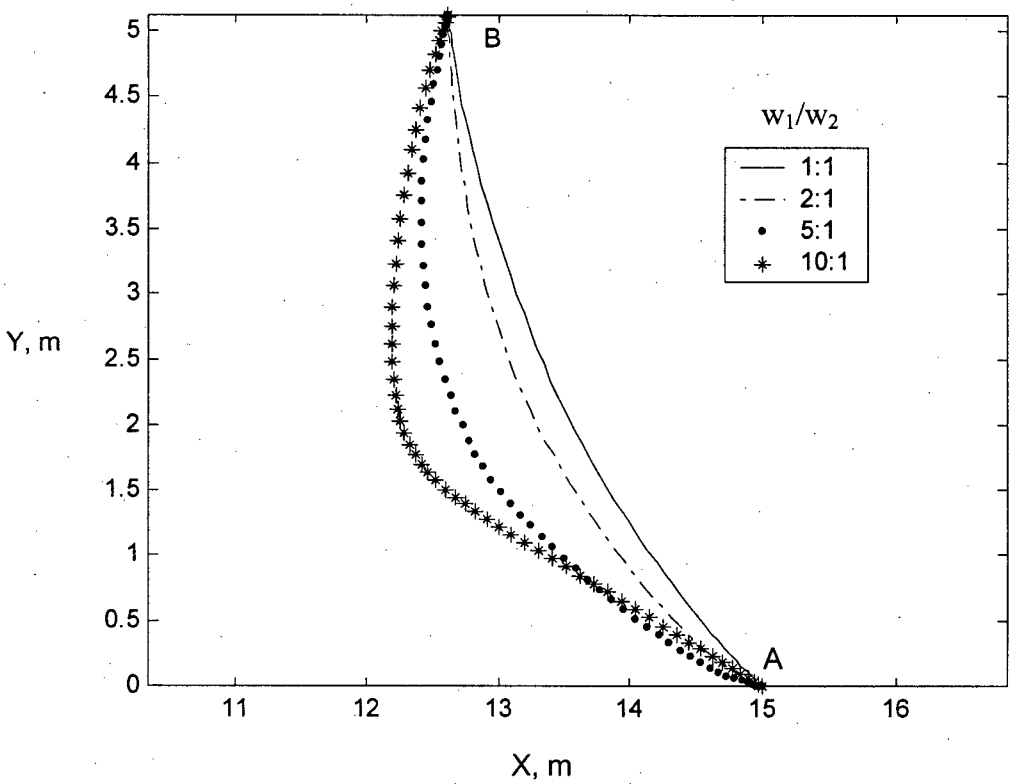

Figure 6-5 Effect of weight function on the tip trajectory for Case 2: $m_2/m_1 = 0.33$.

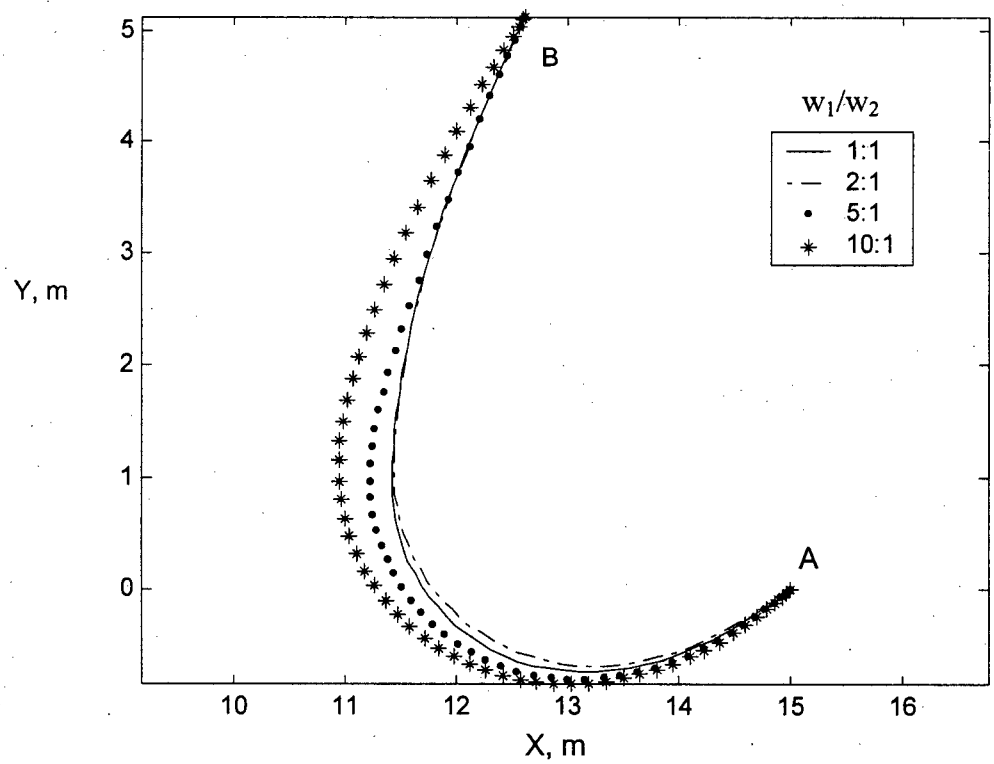

Figure 6-6 Effect of weight function on the tip trajectory for Case 3: $m_2/m_1 = 0.2$.

7. GROUND-BASED EXPERIMENTS

Experiments in space are very costly and time consuming. They can become prohibitive and infeasible in many cases. That is one of the main reasons for the necessity of lengthy mathematical modelling and investigation through computer simulation. As an alternative to space-based experimentation, one often turns to prototypes located on Earth. Of course, for practical reasons, no ground-based setup can simulate the space environment exactly. However, a carefully designed ground-based facility can be used to advantage in assessing the performance trends. Furthermore, once the ground-based computer simulations are verified through prototype experiments, it is possible to justify, by induction, their validity in space where the forces are significantly small. In fact, since the beginning of the space-age in 1957, around 20,000 spacecraft have been launched. Every one of them was primarily designed through extensive numerical simulations, complemented by a few simplified ground-based experiments. The objective here is to evaluate real-time controlled performance of the variable geometry manipulator using the ground-based prototype facility designed by Chu [8].

7.1 System Description

Figure 7-1 shows the manipulator system that has been developed and located in the IRIS Spacecraft Control Laboratory of the Department of Mechanical Engineering, University of British Columbia. The prototype manipulator, employed in the experimental study, consists of a fixed base that supports two modules of the robot connected in series. Each module has two links: one able to slew, and the other free to deploy and retract. The manipulator workspace has the shape of a human heart, extending 2 m from top to bottom and 2.5 m across. Rotational motion is made possible through the use of revolute joints

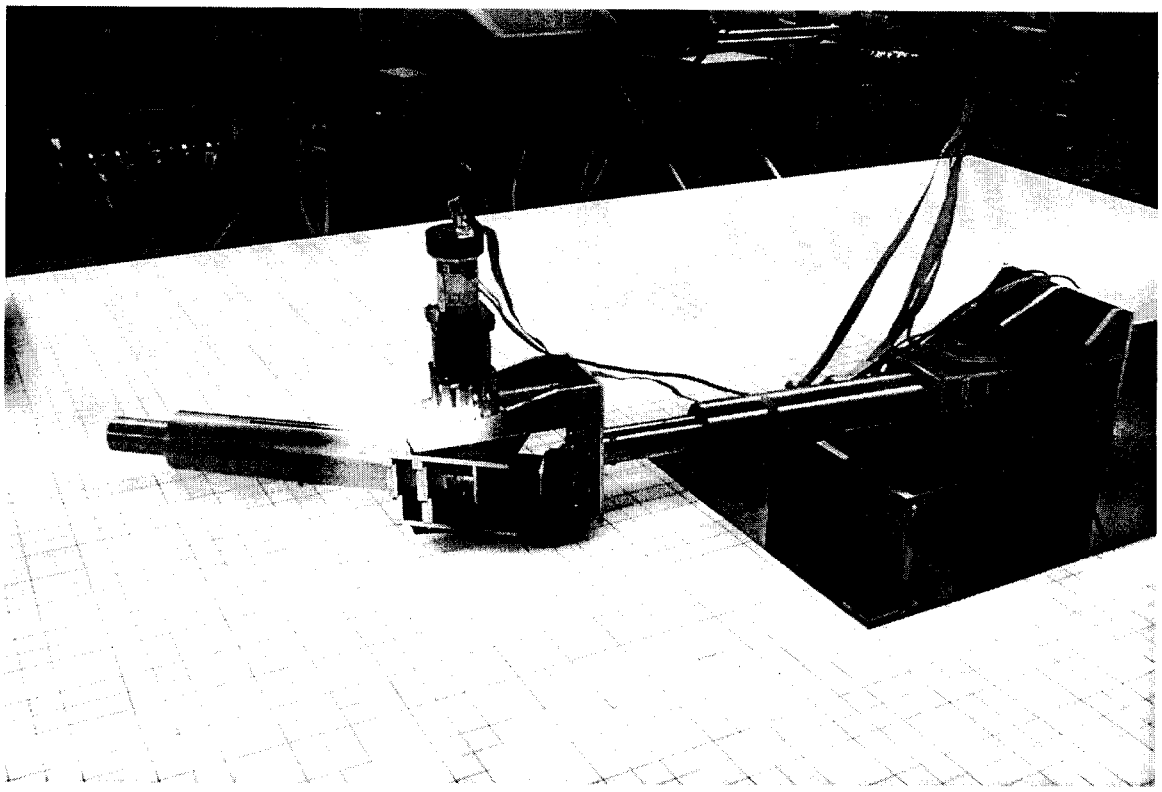

Figure 7-1 The prototype manipulator system.

actuated by DC servo-motors. The deployment and retraction are carried out with prismatic joints consisting of lead-screw and roller-nut assemblies, each of which transforms the rotational motion of a servo-motor into the translational motion of a deployable link (Figure 7-2). Actuator motors integrated with optical-encoder motion sensors are interfaced with a Pentium 200 MHz MMX PC through a three-axis multi-function input/output motion control card.

7.1.1 Manipulator base

The base supports the manipulator system. The first robot module is attached to the pivot plate, which is threaded to the pivot shaft. An 80 mm thrust bearing located between the pivot plate and the top plate of the base carries the weight of the manipulator.

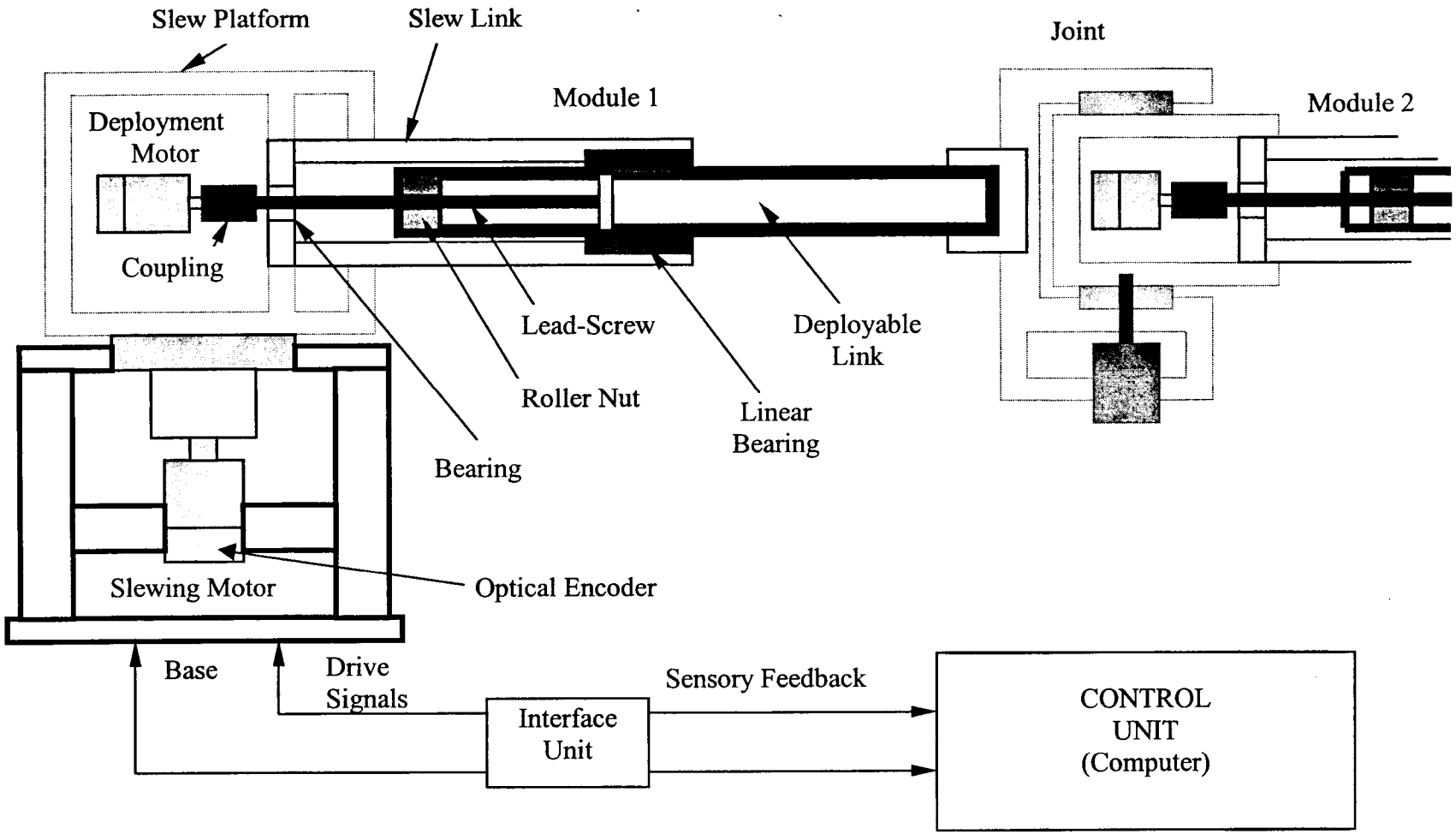

Figure 7-2 **Main components** of the **two-module** manipulator **system.**

This bearing also provides the slewing freedom about the rotational axis. A second bearing is located under the top plate of the base and is held in place with a lock nut. A flexible coupling connects the pivot shaft to a gear head with a transmission ratio of 20:1, which reduces the speed and amplifies the torque delivered by the DC servo-motor. The rotational motion of the base motor is transmitted in series, through the gear box, the flexible coupling, the pivot shaft, and finally to the pivot plate that holds the slew unit of the first module of the manipulator system (Figure 7-3).

7.1.2 Manipulator modules

Both modules of the prototype manipulator system are nearly identical in construction, each having one revolute joint and one prismatic joint. The first revolute joint is located at the base, while the second one is at the end of the first module; i.e. at the elbow joint. The deployment is realized with the transformation of the rotational motion of the motor that drives the lead screw into the translational motion of a roller nut that is fixed to the deployable link (Figure 7-4). The pitch of the lead screw of the first module is 2.5 mm (i.e., the deployable link moves 2.5 mm per revolution) while it is 1 mm for the second module.

7.1.3 Elbow joint

The elbow joint connects the deployable end of module 1 to the slewing link of module 2. The structural connection consists of two pivot plates bolted onto the deployable end of module 1. These plates support the slewing motor and the gear head. The elbow joint is supported on a flat structure within the workspace, through a spherical joint. The mechanism that provides the rotational motion at the elbow joint is identical to the one located at the base (Figure 7-5).

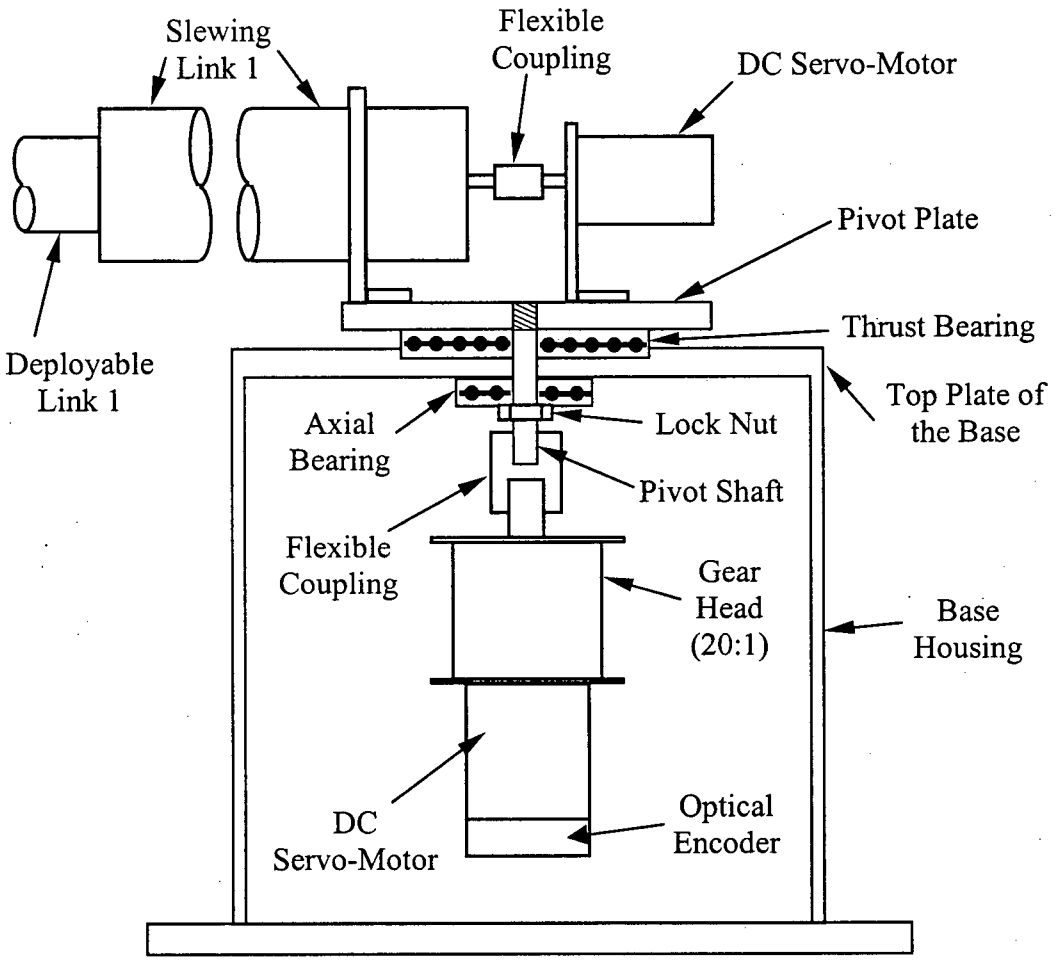

Figure 7-3 Main components of the manipulator base assembly (Module 1).

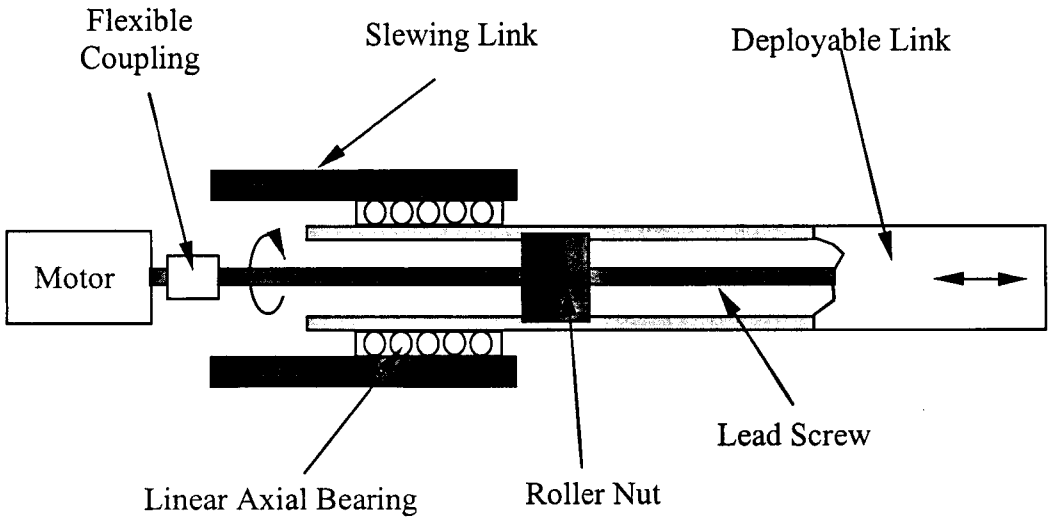

Figure 7-4 Prismatic joint mechanism which provides the deployment and retrieval capability.

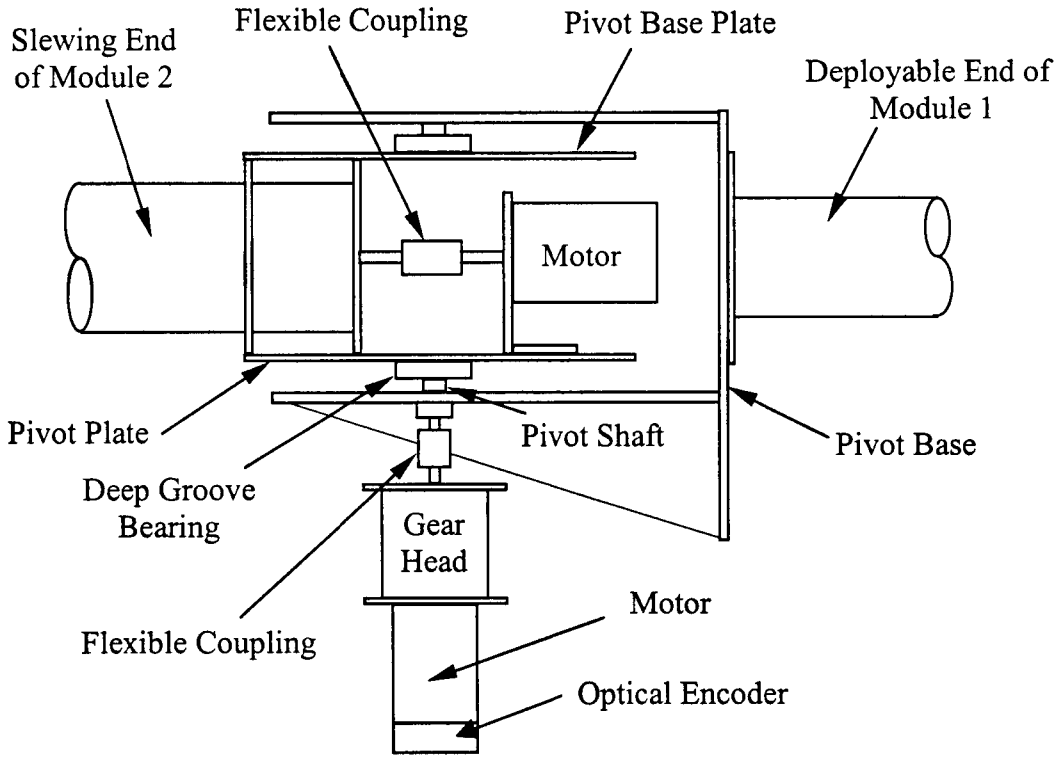

Figure 7-5 Main components of the elbow joint assembly.

7.2 Hardware and Software Control Interface

The hardware of a closed control loop of the prototype manipulator mainly consists of an IBM compatible host computer, an MFIO 3A motion control interface, a linear power amplifier, and a DC servo-motor with a built-in optical encoder (Figure 7-6). The control structure for all the degrees of freedom is identical.

Computer System

The computer used for control purposes is a Pentium 200 MHz MMX IBM compatible machine, with QNX as the operating system. Real-time application of a digital control system depends on an operating system that is capable of handling multiple events in a coordinated manner, within specified time constraints. The more responsive the operating system, the more freedom a real-time application has to meet its deadline. The QNX operating system provides multi-tasking, priority-driven preemptive scheduling, with fast context switching; and is particularly suitable for real-time control. Implementation time for the control loop was 2 ms.

Motion Control Interface Card

An MFIO-3A high-speed interface card for PCs is used for multi-axis, coordinated motion control. It has three-channel 16-bit digital-to-analog converter (D/A); three quadrature encoder inputs; 24 bits of programmable digital I/O, synchronized data reading and writing; a programmable interval timer; and a watchdog timer. The card has a SYNC signal, which allows for synchronization of data acquisition and analog outputs. The data from the D/A converters are latched into registers through the SYNC signal. The D/A channels have a 16-bit resolution. The encoder inputs are digitally filtered for noise suppression. The programmable interval timer can generate timed intervals from 0.25 μs to 515 seconds. The feedback controller runs as a task in the QNX operating system.

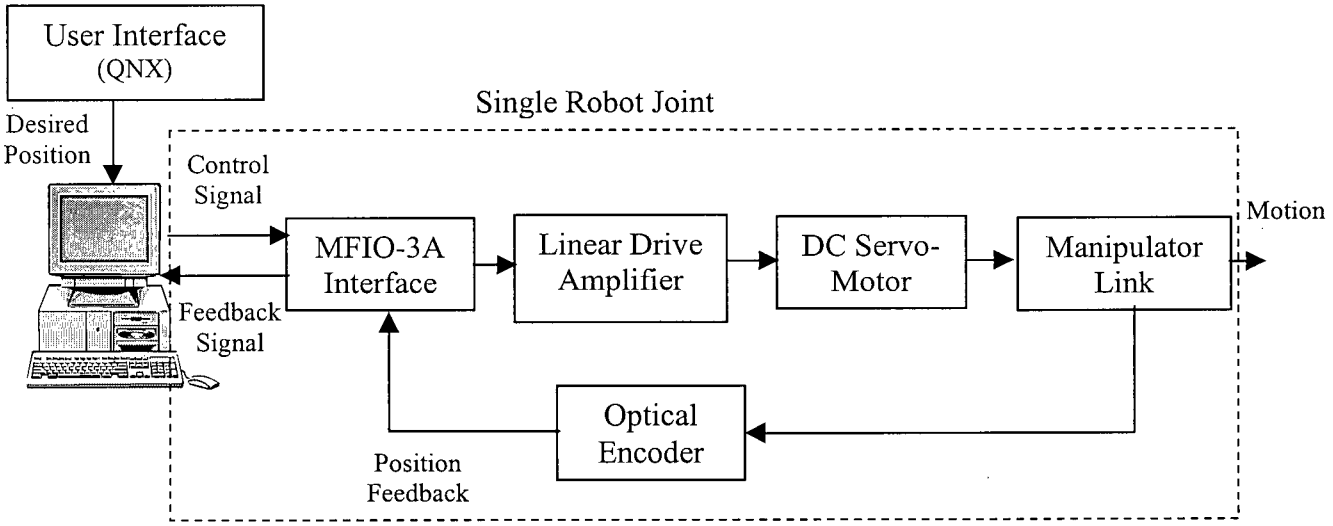

Figure 7-6 Open architecture of the manipulator control system for a single joint.

The card may be programmed either by accessing the hardware at the register level in C or through the use of Precision MicroDynamics' C-subroutine libraries. The source code is compiled with the Watcom-C compiler for QNX. A C-program library provides access to the MFIO-3A hardware with routines to initialize the board; set up the Programmable Interval Timer (PIT), watchdog timer, and SYNC signal; start the PIT and watchdog timer; set up the interrupts; read and write the digital I/O; read and write the encoders; and write the digital-to-analog converters.

Linear Power Amplifier

Linear amplifiers are used with the joint motors of the prototype manipulator. Their function is to transform the voltage signal in the range +/- 10 V from the controller, into a proportional current to drive the joint motors. The amplifier gain is set so that a 10V command generates the maximum drive current.

DC Servo-Motors

Slewing motors of the manipulator are Pittman 14202 (109 oz-in peak torque) and 9413 (16 oz-in peak torque) for modules 1 and 2, respectively. A NEMA 23-20 reduction gear head of transmission ratio 20:1 is used. The gear head reduces the speed while increasing the output torque of the motor nearly by a factor of twenty, depending on the efficiency. The deployment motors are Pittman 9414 (24 oz-in peak torque). The motors operate through the DC current supplied by the power amplifier, in response to a controller signal.

Optical Encoders

The position of each motor is sensed through the use of an optical encoder attached to the motor shaft. The encoders have the offset track configuration (two tracks with their windows having an offset of 1/4 pitch with respect to each other). An encoder disk has two identical tracks, each having 1000 windows. A third track with a lone window generates a reference pulse for every revolution. The physical resolution of the encoders is 0.09^{o}. The pulse count gives the joint position, while the pulse frequency provides the joint speed. The signal from the encoder is monitored at every sampling interval by the controller whose objective is to correct any deviation of the actual joint position from the desired one.

7.3 Dynamical Formulation for the Prototype Manipulator

A ground-based model can be obtained by eliminating the orbital motion of the space-based model. For testing control algorithms on the rigid degrees of freedom, the ground-based model is purposely chosen to be rigid.

Design parameters of the manipulator system are:

Slewing arm length	0.3 m;
Maximum extension of the deployable arm	0.2 m;
Slewing arm sweep range	-135 to 135 deg;
Maximum rotational speed	60 deg/s;
Maximum deployment speed	0.04 m/s.

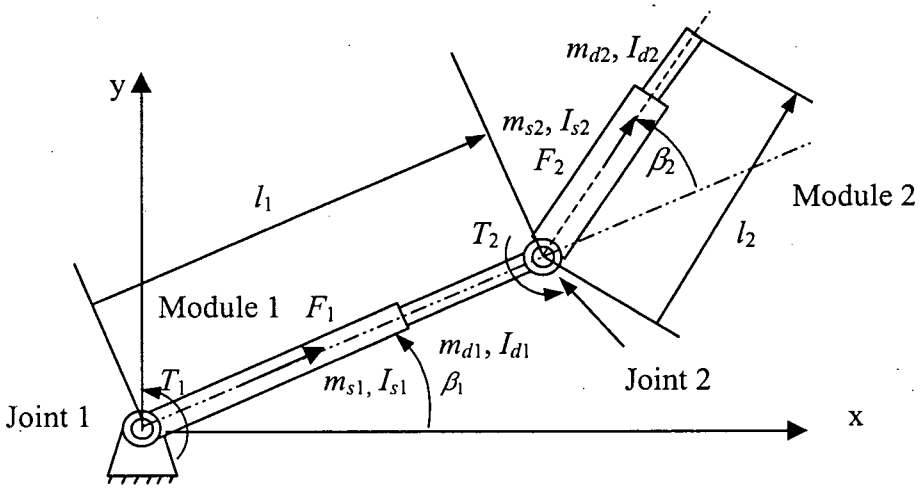

Figure 7-7 Two-module ground based manipulator system.

Various symbols shown in Figure 7-7 are defined below:

m_1 = mass of module 1, $m_{s1} + m_{d1}$;

m_{s1}, m_{d1} = mass of slewing and deployable links of module 1, respectively;

m_2 = mass of module 2, $m_{s2} + m_{d2}$;

m_{s2}, m_{d2} = mass of slewing and deployable links of module 2, respectively;

I_1 = mass moment of inertia of module 1 about its centroid;

I_{s1}, I_{d1} = mass moments of inertia of slewing and deployable links of module 1 about their centroids, respectively;

I_{s2}, I_{d2} = mass moments of inertia of slewing and deployable links of module 2 about their centroids, respectively;

l_1, l_2 = lengths of modules 1 and 2, respectively;

l_{s1}, l_{d1} = lengths of slewing and deployable links, respectively, of module 1;

l_{s2}, l_{d2} = lengths of slewing and deployable links, respectively, of module 2;

F_1, T_1; F_2, T_2 = forces and moments at joints 1and 2, respectively;

β_1, β_2 = slew angles at joints 1 and 2, respectively.

With $[\beta_1\ l_1\ \beta_2\ l_2]^T$ as the vector composed of generalized coordinates, the equations of motion can be derived by eliminating the orbital motion, gravity gradient, and the flexible degrees of freedom from the general space-based formulation described in Chapter 2. The resulting equation may be expressed as:

$$
\begin{aligned}
&\left\{ I_{S1} + I_{d1} + I_{S2} + I_{d2} + m_{S1}\left(\frac{l_{S1}}{2}\right)^2 + m_{d1}\left(l_1 - \frac{l_{d1}}{2}\right)^2 + m_{S2}\left[l_1^2 + \left(\frac{l_{S2}}{2}\right)^2 + \left(\frac{L_{d1}L_{S2}}{2}\right)\cos\beta_2 \right.\right. \\
&\left. + \left(l_1 - \frac{l_{d1}}{2}\right) l_{S2}\cos\beta_2 \right] + m_{d2}\left[l_1^2 + \left(l_2 - \frac{l_{d2}}{2}\right)^2 + 2\left(l_1 - \frac{l_{d1}}{2}\right)^2 \left(l_2 - \frac{l_{d2}}{2}\right)\cos\beta_2 \right. \\
&\left.\left. + L_2\left(l_2 - \frac{l_{d2}}{2}\right)\cos\beta_2 \right] \right\} \ddot{\beta}_1 \\
&+ \left\{ I_{S2} + I_{d2} + m_{S2}\left[\frac{l_{d1}l_{S2}}{4}\cos\beta_2 + \left(l_1 - \frac{l_{d1}}{2}\right)\left(\frac{l_{S2}}{2}\right)\cos\beta_2 + \left(\frac{l_{S2}}{2}\right)^2 \right] \right. \\
&\left. + m_{d2}\left[\left(l_2 - \frac{l_{d2}}{2}\right)^2 + \left(l_1 - \frac{l_{d1}}{2}\right)\left(l_2 - \frac{l_{d2}}{2}\right)\cos\beta_2 + \left(\frac{l_{d1}}{2}\right)\left(l_2 - \frac{l_{d2}}{2}\right)\cos\beta) \right] \right\} \ddot{\beta}_2 \\
&+ \left[-m_{d2}\left(l_2 - \frac{l_{d2}}{2}\right)\sin\beta_2 - m_{S2}\left(\frac{l_{S2}}{2}\right)\sin\beta_2 \right] \ddot{l}_1 + \left[m_{d2}\left(l_1 - \frac{l_{d1}}{2}\right)\sin\beta_2 + m_{d2}\left(\frac{l_{d1}}{2}\right)\sin\beta_2 \right] \ddot{l}_2 \\
&+ \left\{ -m_{S2}\left[\left(l_1 - \frac{l_{d1}}{2}\right)\left(\frac{l_{S2}}{2}\right) + \left(\frac{l_{d1}}{2}\right)\left(\frac{l_{S2}}{2}\right) \right] \sin\beta_2 \right. \\
&\left. - m_{d2}\left[\left(\frac{l_{d1}}{2}\right)\left(l_2 - \frac{l_{d2}}{2}\right) + \left(l_1 - \frac{l_{d1}}{2}\right)\left(l_2 - \frac{l_{d2}}{2}\right) \right] \sin\beta_2 \right\} (\dot{\beta}_2)^2
\end{aligned}
$$

$$
\begin{aligned}
&+\left\{-2m_{S2}\left[\left(l_1+\frac{l_{d1}}{2}\right)\frac{l_{S2}}{2}+\frac{l_{d1}}{2}\frac{l_{S2}}{2}\right]\sin\beta\right.\\
&\left.-2m_{d2}\left[\frac{l_{d1}}{2}\left(l_2+\frac{l_{d2}}{2}\right)+\left(l_1+\frac{l_{d1}}{2}\right)\left(l_2+\frac{l_{d2}}{2}\right)\right]\sin\beta_2\right\}\dot{\beta}_1\dot{\beta}_2\\
&+\left\{2\left[m_{S2}\frac{l_{S2}}{2}+m_{d2}\left(l_2+\frac{l_{d2}}{2}\right)\right]\cos\beta_2+2m_{d1}\left(l_2+\frac{l_{d2}}{2}\right)+2m_{S2}l_1+2m_{d2}l_1\right\}\dot{l}_1\dot{\theta}_1\\
&+\left\{2m_{d2}\left[\frac{l_{d1}}{2}\cos\beta_2+\left(l_1+\frac{l_{d1}}{2}\right)\cos\beta_2+\left(l_2+\frac{L_4}{2}\right)\right]\right\}\dot{l}_2\dot{\beta}_1\\
&+\left\{2m_{d2}\left[\frac{l_{d1}}{2}\cos\beta_2+\left(l_1+\frac{l_{d1}}{2}\right)\cos\beta_2+\left(l_2+\frac{l_{d2}}{2}\right)\right]\right\}\dot{l}_2\dot{\beta}_2-T_1=0
\end{aligned}
\tag{7.1}
$$

$$
\begin{aligned}
&\left\{-\left[m_{S2}\frac{l_{S1}}{2}+m_{d2}\left(l_2-\frac{l_{d2}}{2}\right)\right]\sin\beta_2\right\}\ddot{\beta}_1+\left\{-\left[m_{S2}\frac{l_{S2}}{2}+m_{d2}\left(l_2-\frac{l_{d2}}{2}\right)\right]\sin\beta_2\right\}\ddot{\beta}_2\\
&+[m_{d1}+m_{S2}+m_{d2}]\ddot{l}_1+[m_{d2}\cos\beta_2]\ddot{l}_2\\
&+\left\{-\left(l_1-\frac{l_{d2}}{2}\right)(m_{d1}+m_{S2}+m_{d2})-\left[m_{S2}\frac{l_{S2}}{2}+m_{d2}\left(l_2-\frac{l_{d2}}{2}\right)\right]\cos\beta_2-(m_{S2}+m_{d2})\frac{l_{d1}}{2}\right\}(\dot{\beta}_1)^2\\
&+\left[m_{S2}\frac{l_{d2}}{2}+m_{d2}\left(l_2-\frac{l_{d2}}{2}\right)\right]\cos\beta_2(\dot{\beta}_2)^2\\
&+\left\{-2\left[m_{S2}\frac{l_{S2}}{2}+m_{d2}\left(l_2-\frac{l_{d2}}{2}\right)\right]\cos\beta_2\right\}\dot{\beta}_1\dot{\beta}_2+[-2m_{d2}\sin\beta_2]\dot{\beta}_1\dot{l}_2\\
&+[-2m_{d2}\sin\beta_2]\dot{\beta}_2\dot{l}_1-F_1=0
\end{aligned}
\tag{7.2}
$$

$$\left[I_{S2}+I_{d2}+m_{S2}\left(\frac{l_{d2}}{2}\right)^2+m_{d2}\left(l_2-\frac{l_{d2}}{2}\right)^2+m_{S2}\frac{l_{d2}}{2}\cos\beta_2 l_1+m_{d2}\left(l_2-\frac{l_{d2}}{2}\right)\cos\beta_2 l_1\right]\ddot{\beta}_1$$
$$+\left[I_{S2}+I_{d2}+m_{S2}\left(\frac{l_{s2}}{2}\right)^2+m_{d2}\left(l_2-\frac{l_{d2}}{2}\right)^2\right]\ddot{\beta}_2$$
$$+\left[-m_{d2}\left(l_2-\frac{l_{d2}}{2}\right)\sin\beta_2-m_{S2}\left(\frac{l_{d2}}{2}\right)\sin\beta_2\right]\ddot{l}_1$$
$$+\left[m_{S2}\left(\frac{l_{d2}}{2}\right)l_1\sin\beta_2+m_4\left(l_2-\frac{l_{d2}}{2}\right)l_1\sin\beta_2\right](\dot{\beta}_1)^2$$
$$+\left\{2\left[m_{S2}\left(\frac{l_{d2}}{2}\right)+m_{d2}\left(l_2-\frac{l_{d2}}{2}\right)\right]\cos\beta_2\right\}\dot{l}_1\dot{\beta}_1$$
$$+\left[2m_{d2}\left(l_2-\frac{l_{d2}}{2}\right)\right]\dot{l}_2\dot{\beta}_1+\left[2m_{d2}\left(l_2-\frac{l_{d2}}{2}\right)\right]\dot{l}_2\dot{\beta}_2-T_2=0 \tag{7.3}$$

$$[m_{d2}l_1\sin\beta_2]\ddot{\beta}_1+\left\{-m_{S2}\left[\frac{l_{d2}}{2}+m_{d2}\left(l_2-\frac{l_{d2}}{2}\right)\right]\sin\beta_2\right\}\ddot{\beta}_2$$
$$+[m_{d2}\cos\beta_2]\ddot{l}_1+[m_{d2}]\ddot{l}_2$$
$$+\left[-m_{d2}l_1\cos\beta_2-m_{d2}\left(l_2-\frac{l_{d2}}{2}\right)\right](\dot{\beta}_1)^2$$
$$+\left[-m_{d2}\left(l_2-\frac{l_{d2}}{2}\right)\right](\dot{\beta}_2)^2$$
$$+\left[-2m_{d2}\left(l_2-\frac{l_{d2}}{2}\right)\cos\beta_2\right]\dot{\beta}_1\dot{\beta}_2+[-2m_{d2}\sin\beta_2]\dot{\beta}_1\dot{l}_1-F_2=0 \tag{7.4}$$

Note, even a simple ground-based manipulator with rigid links leads to governing equations of motion which are highly nonlinear, coupled and lengthy. A ground-based model is essential in the development of model-based control algorithms such as the FLT and LQR. For model-based controller, due to computational constraints, significant pre-processing is required to manage the task.

7.4 Validation of the Ground-Based Model

The ground-based model is first validated through energy conservation and comparison with known results. The system parameters used for this purpose are:

Module 1

- slewing link mass $m_{s1} = 0.69$ kg
- slewing link length $l_{s1} = 0.69$ m
- deployable link mass $m_{d1} = 0.69$ kg
- deployable link length $l_{d1} = 0.69$ m
- slewing link moment of inertia $I_{s1} = 0.0274$ kg m^2
- deployable link moment of inertia $I_{d1} = 0.0274$ kg m^2

Module 2

- slewing link mass $m_{S2} = 0.69$ kg
- slewing link length $l_{S2} = 0.69$ m
- deployable link mass $m_{d2} = 0.69$ kg
- deployable link length $l_{d2} = 0.69$ m
- slewing link moment of inertia $I_{S2} = 0.0274$ kg m^2
- deployable link moment of inertia $I_{d2} = 0.0274$ kg m^2

These parameters are identical to the ones reported by Chu [8].

For the validation test, the manipulator was treated as a double pendulum free to oscillate in a vertical plane. The lengths of both modules were held fixed at 1.38 m. The initial conditions were: $\beta_1 = 80^o; \beta_2 = \dot{\beta}_1 = \dot{\beta}_2 = 0$. The results are shown in Figure 7-8. It is seen that the total energy is conserved with a remarkable degree of accuracy. Note, ΔE

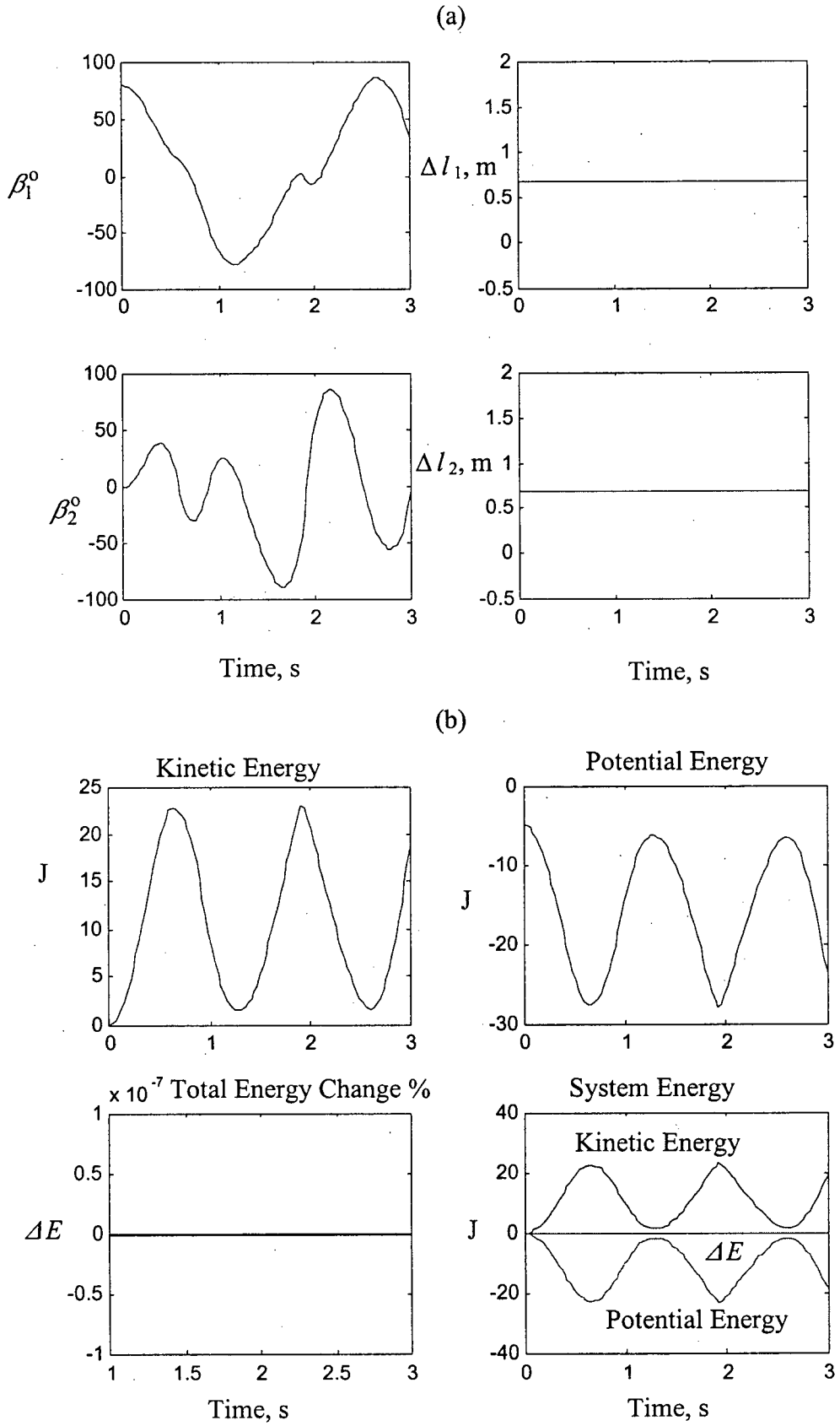

Figure 7-8 Double pendulum test results: (a) joint motion; (b) energy variations.

representing deviation of the total energy from its initial value divided by the initial value is less than 10^{-7} % !

Furthermore, it is well-known that for $\beta_1(0)/[\beta_1(0)+\beta_2(0)]=\pm 0.707$, the double pendulum executes simple harmonic motion with frequencies given by $\omega^2=(g/l)(2\pm\sqrt{2})$. Taking the case as shown in Figure 7-9(a) with $\beta_1(0)/[\beta_1(0)+\beta_2(0)]=-0.707$, i.e. $\omega^2=(g/l)(2-\sqrt{2})$, the oscillation frequencies of modules would be 4.926 rad /s, or the period of 1.275 seconds (l = 1.38 m). This matches rather well (Figure 7-9b). The total energy is also conserved with a fine measure of accuracy.

7.5 Control of the Ground-Based Model

From the equations of motion and Figure 7-2, it follows that the manipulator, as a control plant, is nonlinear, non-autonomous and coupled. That makes the Feedback Linearization Technique (FLT) a reasonable choice as a control procedure for this manipulator. As shown in Figure 5-1, the FLT, sometimes called the computed torque method, when applied in a feedforward fashion in robotics, consists of an innerloop which linearizes the nonlinear system and an outerloop with the proportional plus derivative action that controls the linearized system. A typical Proportional-Integral-Derivative (PID) controller is also implemented for the purpose of comparison with the FLT.

7.5.1 Control system parameters

The FLT has been discussed in Chapter 4. This control technique has several desirable properties as pointed out before. However, in order to implement the FLT, the system model and associated parameters must be known precisely. To that end, values of the moments of inertia I_{s1}, I_{d1}, I_{s2}, and I_{d2} were obtained experimentally through swing tests

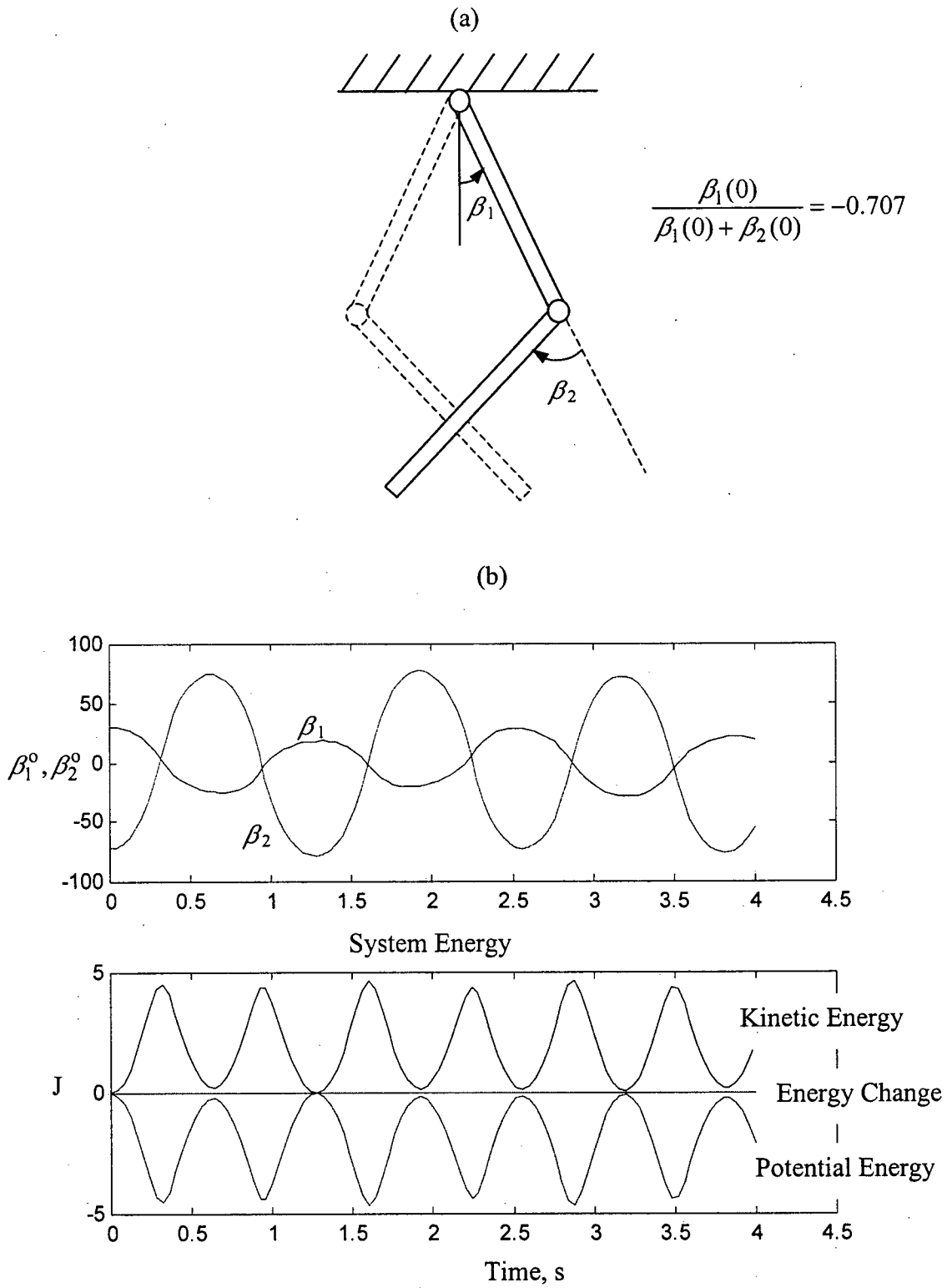

Figure 7-9 Double pendulum test for periodic motion: (a) schematic diagram of the test arrangement; (b) system response.

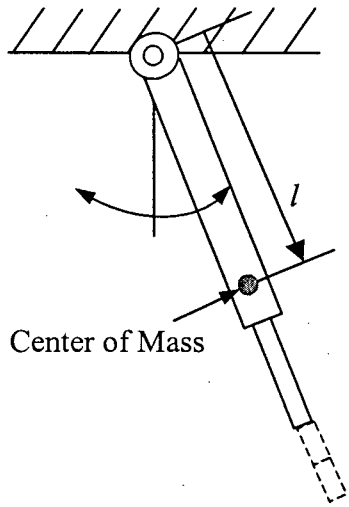

Figure 7-10 Schematic diagram of the swing test to determine the moments of inertia of the prototype modules with various lengths of the deployable link.

as shown in Figure 7-10. A typical test involved application of a small displacement from the vertical and counting the number of cycles over a known period of time. The moment of inertia about the swing axis is given by

$$I = \frac{mgl}{\omega^2} = \frac{mglT^2}{4\pi^2}, \tag{7.5}$$

where T = period of oscillation. The parameter values determined in this fashion are shown in Table 7-1. The moments of inertia were measured for the whole module with three different positions of the deployable link. For the FLT control, a single-module manipulator (module 2) was used, hence only the parameters for this module are relevant in the experiments.

Table 7-1 Swing test results for the ground-based robot.

	Mass (kg)	l (m)	T (s)	I (kg m^2)	Position
Module 1	4.5	0.276	1.343	0.557	fully retracted
		0.322	1.444	0.750	middle
		0.373	1.560	1.015	fully deployed
Module 2	2.4	0.106	1.021	0.066	fully retracted
		0.119	1.063	0.080	middle
		0.129	1.109	0.094	fully deployed

The parameters for the manipulator are:

Module 1

- slewing link mass m_{s1} = 4.30 kg;
- slewing link length l_{s1} = 0.33 m;
- deployable link mass m_{d1} = 0.20 kg;
- deployable link length l_{d1} = 0.31 m;

Module 2

- slewing link mass m_{s2} = 2.20 kg;
- slewing link length l_{s2} = 0.33 m;
- deployable link mass m_{d2} = 0.20 kg;
- deployable link length l_{d2} = 0.31 m;

Based on system parameters, the time constant varied in the range of 0.23 s to 0.28 s.

7.4.1 Controller design

Design of the PID controller is based on the experimental approach to selection of gains as proposed by Ziegler and Nichols [94]. In this context a linear and time-invariant system is assumed. The parameters obtained from the Ziegler-Nichols method give an initial set of values for the PID gains. Due to the nonlinear and non-autonomous nature of the system, these parameters need to be further refined and tuned for improved performance of the system.

As the FLT control is a model based method, it is rather computationally intensive. In the present set of experiments, it is applied only to the outer module of the system, with relatively simpler governing equations, in order to make the computational process manageable. Equations (7.3) and (7.4) with module 1 fixed reduced to:

$$m_{d2}\ddot{l}_2 - m_{d2}(l_2 - \frac{l_{d2}}{2})(\dot{\beta}_2)^2 = F_2 \quad ;$$

$$\underbrace{\left[I_{S2} + I_{d2} + m_{s2}\left(\frac{l_{s2}}{2}\right)^2 + m_{d2}\left(l_2 - \frac{l_{d2}}{2}\right)^2\right]}_{\hat{I}}\ddot{\beta}_2 + 2m_{d2}(l_2 - \frac{l_{d2}}{2})\dot{l}_2\dot{\beta}_2 = T_2 \quad ; \tag{7.6}$$

where $\hat{I}$ is the moment of inertia of module 2 about the swing axis. with linear representation of the results from the swing test (Table 7-1), we have:

$$\hat{I} = 4.206\times10^{-8}n + 0.066\,, \tag{7.7}$$

where n (4000 counts/mm) is the encoder reading from the actuator of the prismatic joint. The FLT algorithm can be expressed as

$$\tau = \mathbf{M}(\ddot{q}_d - u) + F\,, \tag{7.8}$$

where: $\mathbf{M} = \begin{bmatrix} m_{d2} & 0 \\ 0 & \hat{I} \end{bmatrix}$; $\boldsymbol{F} = \begin{bmatrix} -m_{d2}(l_2 - \frac{l_{d2}}{2})(\dot{\beta}_2)^2 \\ 2m_2(l_2 - \frac{l_{d2}}{2})\dot{l}_2\dot{\beta}_2 \end{bmatrix}$; $\boldsymbol{q} = \begin{bmatrix} l_2 \\ \beta_2 \end{bmatrix}$; $\tau = \begin{bmatrix} F_2 \\ T_2 \end{bmatrix}$; and

$\boldsymbol{u} = -\boldsymbol{K}_p\boldsymbol{e} - \boldsymbol{K}_d\dot{\boldsymbol{e}}$ with $\boldsymbol{e} = \boldsymbol{q}_d - \boldsymbol{q}$. The FLT involves compensation for change in the mass matrix **M** as the system moves and also for the dynamical coupling term $\boldsymbol{F}$. As a result, it should provide better performance compared to the fixed gain PID controller.

7.6 Trajectory Tracking

Once the controllers are designed, a series of trajectories tracking tests were performed using both the FLT and PID algorithms. These tests fall into two main categories: a) straight line tracking; b) circle tracking. The PID and FLT gains are shown in Tables 7-2 through 7-4.

Table 7-2 Controller gains for the prismatic joint of module 2.

Module 2 (Prismatic)	K_p	K_d	K_i
PID	0.5	0.001	0.0001
FLT	0.5	0.001	_

Table 7-3 Controller gains for the revolute joint of module 2.

Module 2 (Revolute)	K_p	K_d	K_i
PID	3	0.001	0.001
FLT	0.5	0.001	_

Table 7-4 Controller gains for the revolute joint of module 1.

Module 1 (Revolute)	K_p	K_d	K_i
PID	4	0.001	0.001

These gains were used throughout the experiments. For the FLT, a PD controller is used in the outer loop, for the errors and the derivatives of the errors, as mentioned in Chapter 5. Any other suitable controller may be used for the outer-loop control after linearization. Possible choices would be the Linear Quadratic Gaussian (LQG) and H_∞ procedures. Important symbols involved in the trajectory tracking are defined below:

$e_{l_2}, e_{\beta_1}, e_{\beta_2}$ tracking errors at prismatic, revolute joint 1 and revolute joint 2, respectively;

$I_{l_2}, I_{\beta_1}, I_{\beta_2}$ driving currents at prismatic and revolute joints, respectively;

β_1, β_2 rotation angles at revolute joints 1 and 2, respectively;

Δl_2 change in length of the deployable link of module 2.

7.6.1 Straight line trajectory

The first tracking test involves making the tip of the manipulator to follow a straight line by using one-revolute joint and one prismatic joint of the outer module (module 2) while the inner module is kept locked. First, the PID controller is used to perform the test. The line is located 41.5 cm from the base of module 2 and its length is 20 cm along the y direction. Figure 7-11(a) shows the location of the tracked line and the configuration of the manipulator. The specified tracking time is 4 seconds, and the tip trajectory has a prescribed ramp-on-sine profile as given in Eq. (2.74). The results of the tracking experiment are shown in Figure 7-12. It is seen that the manipulator tip follows the straight line with reasonable

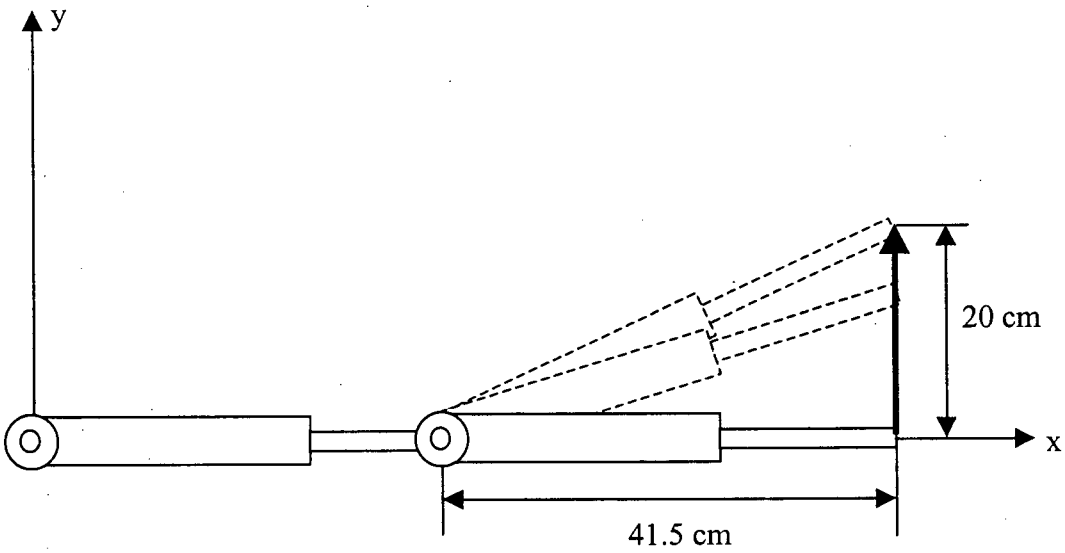

(a)

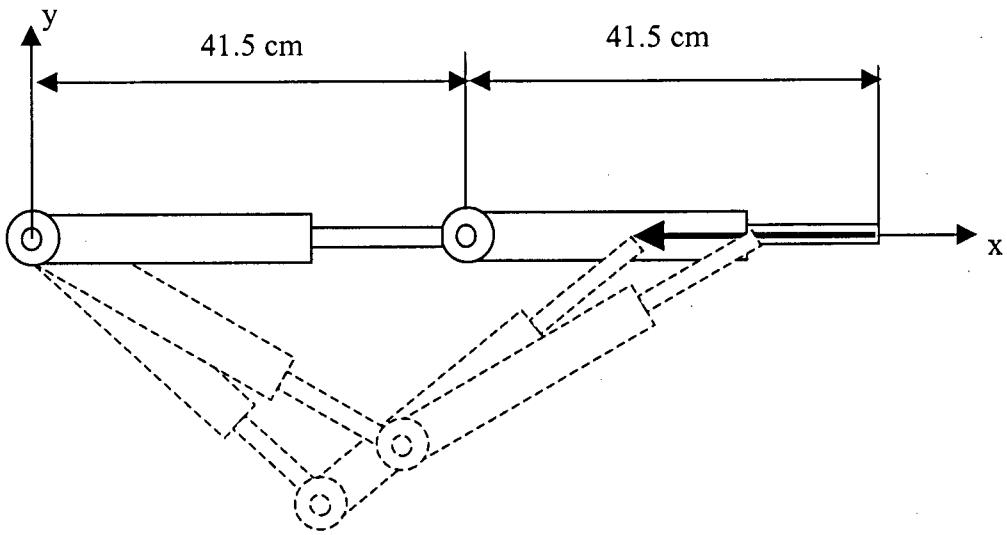

(b)

Figure 7-11 Schematic diagrams for straight line tracking using: (a) one revolute joint and one prismatic joint; (b) two revolute joints.

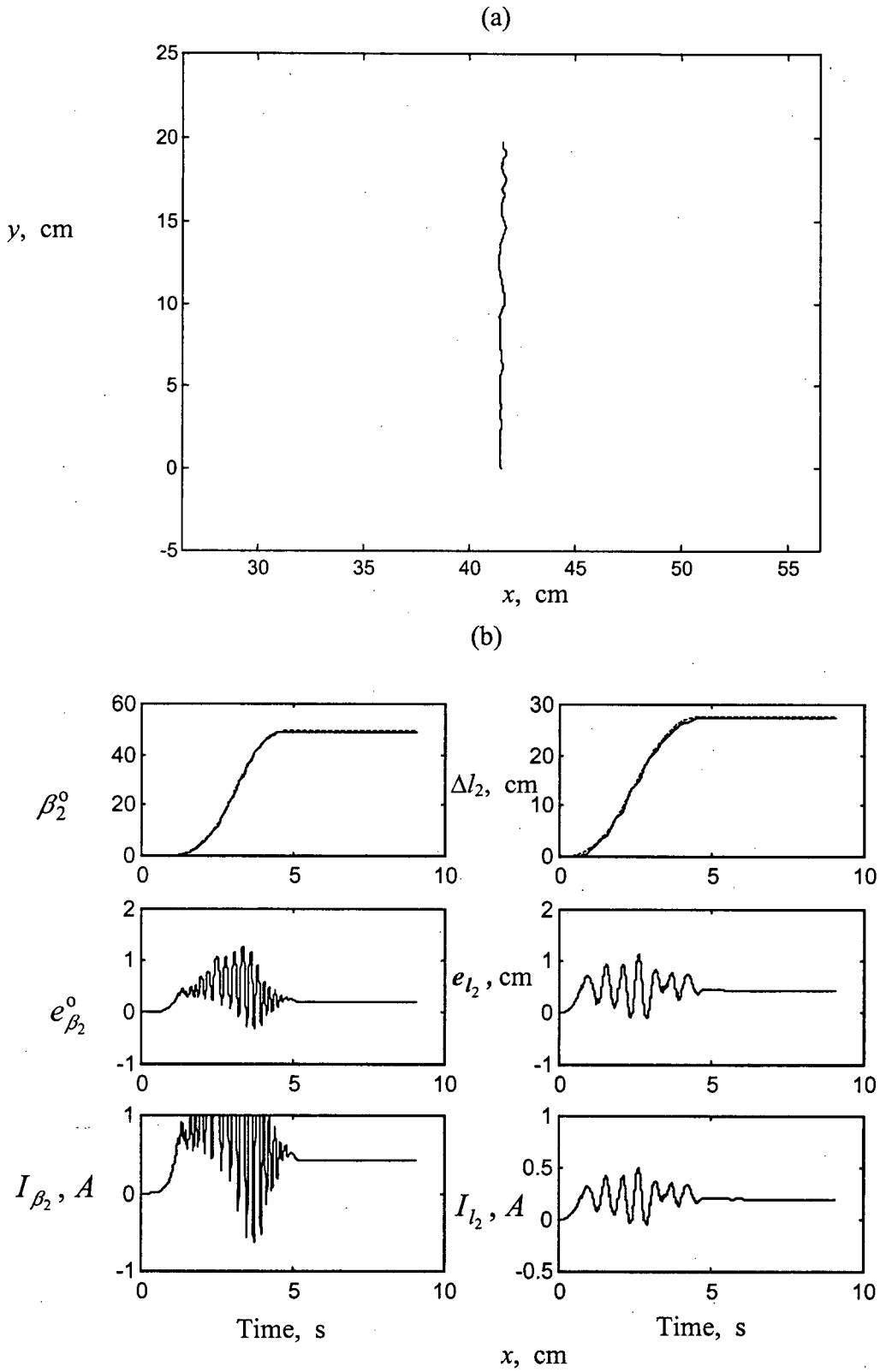

Figure 7-12 Straight line tracking using one revolute and one prismatic joint under the PID control: (a) tip trajectory; (b) joint motion and the corresponding control signals.

reasonable accuracy. The saturation in I_{β_2} is caused by the safety limit of the current that is transmitted to the motor, which is constrained to 1 A.

Figure 7-11 (b) shows another manipulator configuration for straight-line tracking. Now a distance of 20 cm is tracked along the x direction using two revolute joints, in 8 seconds. Note, the prismatic joints are locked with each module length fixed at 41.5 cm. As pointed out in previous chapters, a prismatic joint has the advantage that it does not possess dynamic coupling with the revolute joint of the same module, since the reaction force passes through the center of the joint. When two revolute joints are used, the reaction torque due to the rotational dynamics of the second module will try to rotate the first module in the counter-clockwise direction resulting in over-rotation of the first module. Thus the tracking error is biased in the negative direction of the y-axis, as is evident from the experimental results shown in Figure 7-13 (a). From the plot of e_{β_1} in Figure 7-13 (b), it is clear that error is in the negative side, as a result of the dynamical coupling. In a robotic system that has kinematic redundancy, it will be possible even to maneuver the first module to an appropriate position and then use only the prismatic joint for the line tracking. This will cause virtually no error in the tracking.

Next, the FLT controller is used to carry out the same task as that shown in Figures 7-12 for the PID control. Again, the execution time is set at 4 seconds and the length of the line is 20 cm. The results are shown in Figures 7-14. By comparing the behaviors of the PID and FLT controllers the following observations can be made: (i) The FLT has an adaptive capability with respect to the variation of the mass matrix. It also has a compensation capability for dynamical coupling. Thus, FLT produces more active control signals (high frequency I_{β_2} and I_{l_2}). (ii) The PID controller is simpler, requires less computational

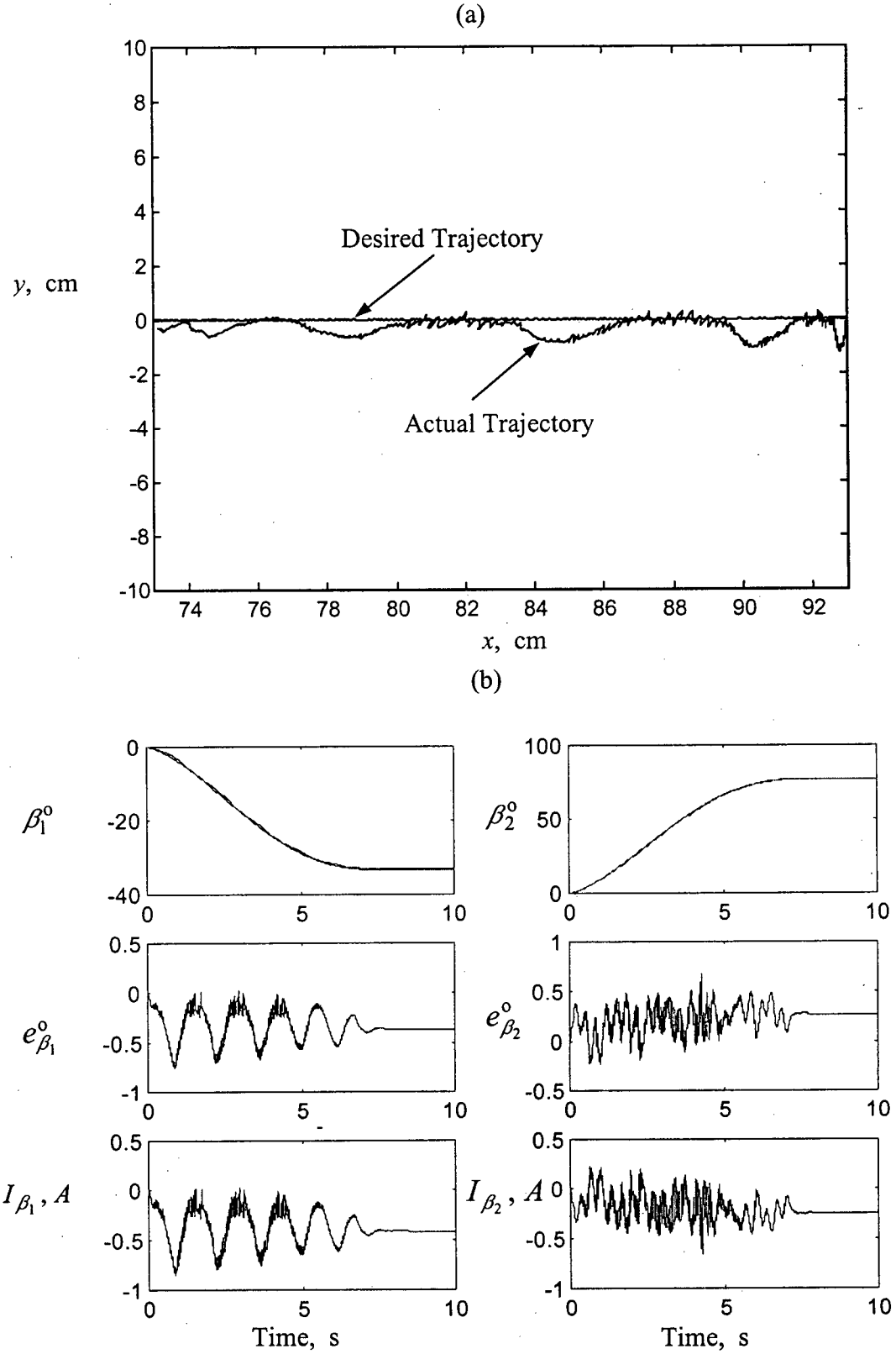

Figure 7-13 Straight line tracking using two revolute joints under the PID control: (a) tip trajectories; (b) joint motion and corresponding control signals.

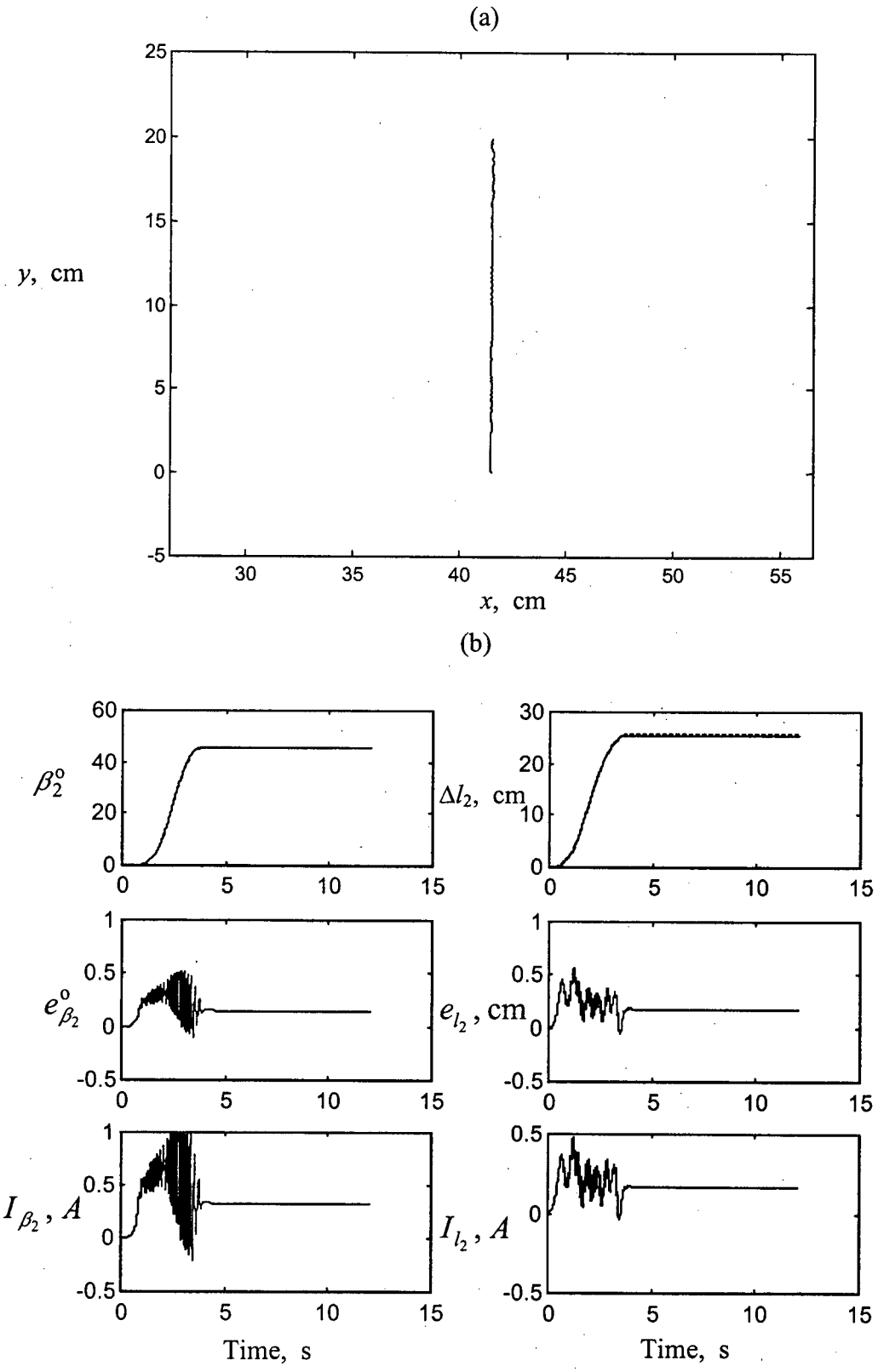

Figure 7-14 Straight line tracking using one revolute and one prismatic joint with the FLT: (a) tip trajectory; (b) joint motion and the corresponding control signals.

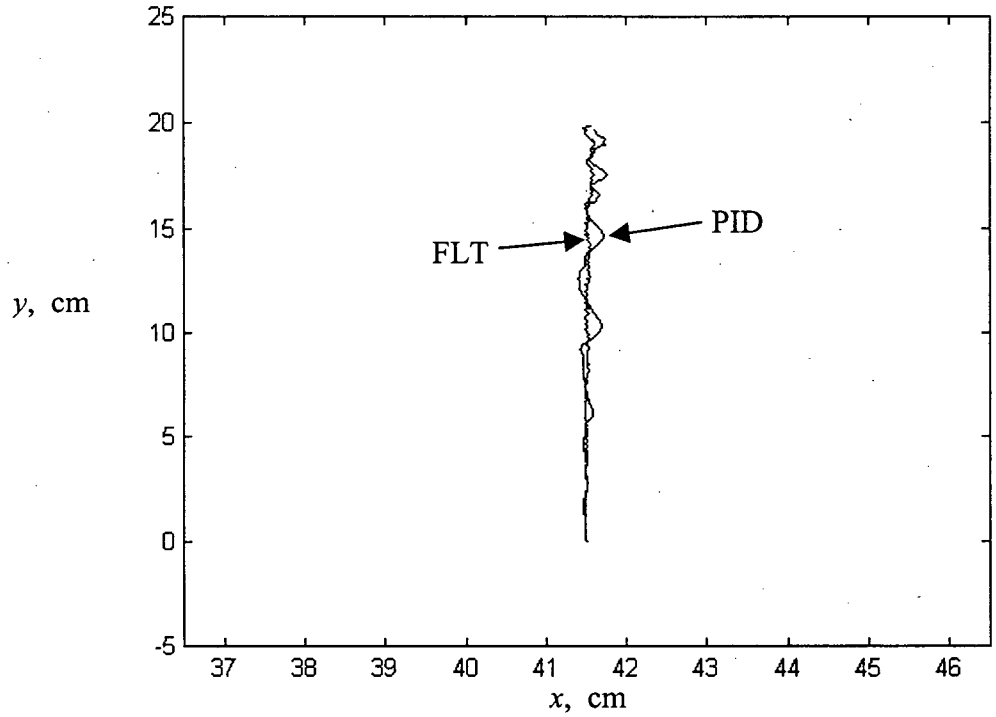

Figure 7-15 Straight line tracking: comparison of the FLT and PID using one revolute and one prismatic joint.

power, and does not depend on a model of the robot (the experimental, Ziegler-Nichols method is used here to tune the PID gains).

One is able to tune the FLT controller by incorporating a multiplicative confidence factor into the dynamical compensation term $\boldsymbol{F}$, and gradually increasing it as more experience is gained through experimentation. This approach is used for tuning the FLT controller of the prototype robotic system.

The tip trajectories of the robot under the control of PID and FLT separately, are plotted in Figure 7-15. It is clear that at the expense of the computation cost, FLT gives better tracking accuracy than PID. Note that towards the end of the tracking, both controllers produce larger errors. This is due to increased dynamical coupling that exists and the greater effort that is required for synchronizing the two joints at the end of the trajectory. Another

major source of error is the unmodeled friction. It causes steady-state error and stick-slip motion. These nonlinear effects reduce the tip position accuracy and cause vibrations.

7.6.2 Circular trajectory

In order to further investigate the system, tracking of a circular trajectory was undertaken as a typical test-case. To begin with, tracking is carried out under the PID control. Different trajectory speed profiles were employed to assess the effectiveness of the controller and influence of the speed profile. The circular profiles are defined as:

$$\begin{cases} P_x = 41.5 + r - r\cos(\omega t); \\ P_y = r\sin(\omega t); \end{cases} \tag{7.9}$$

where: P_x , P_y are tip positions in the x and y directions, respectively; r is the radius of the circle; and ω is the angular velocity of the circular motion. For instance, $\omega = 0.1\pi$ corresponds to a tip motion around the circle in 20 seconds. Figure 7-16 schematically shows the tracked circle and the corresponding manipulator configurations at different instants of tracking. The radius r is taken to be 10 cm for all the cases. Each circle is tracked twice to check the repetitiveness of tracking.

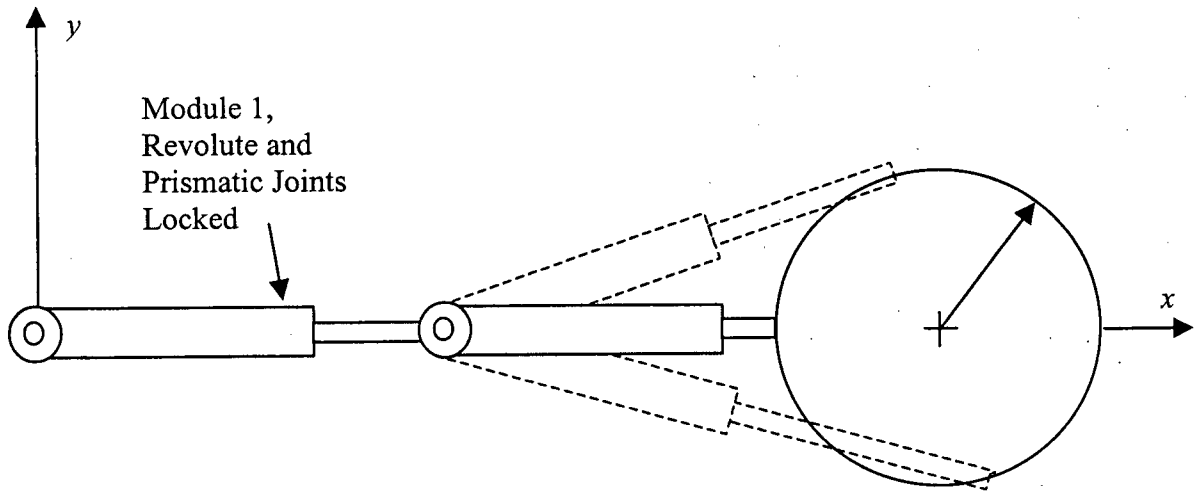

Figure 7-16 Schematic diagram showing tracking of a circular trajectory using module 2.

The first experiment of tracking a circular trajectory uses $\omega = 0.1\pi$; i.e. 20 seconds a circle. The results are shown in Figures 7-17. The maximum errors occur at locations where joints change their directions of motion. Due to Coulomb friction, the joints have nonlinear dead zones. The signal from the controller is generated based on the motion error. Once a joint stops, the error must be large enough to overcome the steady-state friction. This, in turn, causes a larger error. When the joint starts to move, the smaller dynamic friction results in a lower error. Of course, dynamical coupling also plays a role in causing the motion error. This can be seen when the speed of the profile increases from 20 seconds a circle to 10 seconds a circle (Figures 7-18). It is clear that with increased speed the tip trajectory is not as smooth as the one in Figure 7-17. This is mainly due to the dynamical coupling. The corresponding control effort also has increased. The repetitiveness of trajectory worsens as well due to the same reason. When the speed of the profile decreases from 20 seconds a circle to 30 seconds a circle (Figure 7-19), the repetitiveness improves but the error is slightly larger than that for the 20 seconds a circle. Here, dynamical coupling is lower, which makes the trajectory smoother and the level of repetition better. However, when desired trajectory moves slower, the error increases gradually and the control effort needed to overcome steady-state friction takes a longer time to accumulate. This causes the nonlinear dead-zone effect to worsen.

The FLT controller was also used in the case of 20 seconds a circle (Figures 7-20). As before, the performance of the FLT controller is better than that of the PID controller. It compensates for the dynamical coupling effect, which significantly reduces the error of the revolute joint. It is seen that, in area C, the tip error is low. In other areas (A, B, D), the

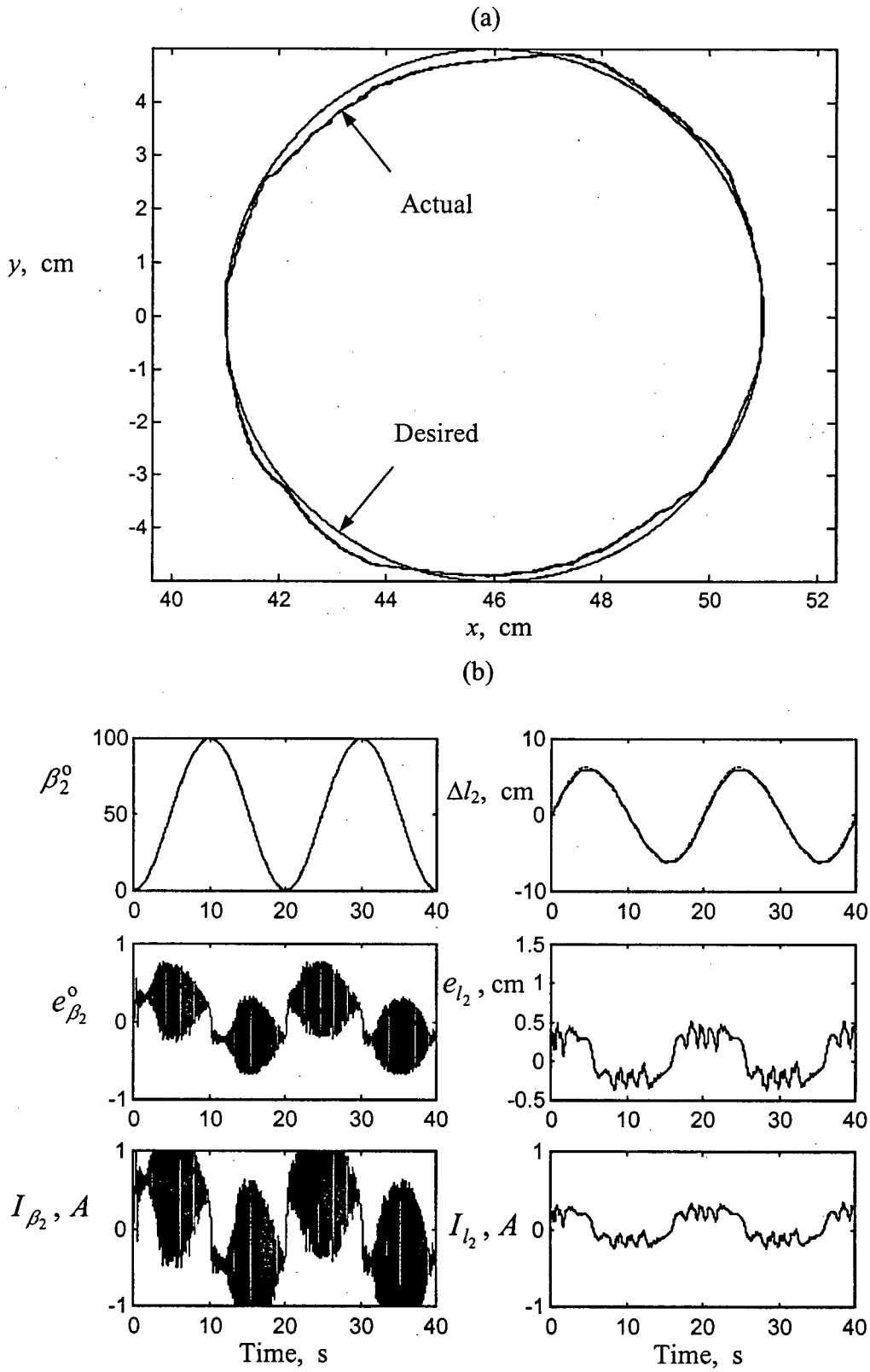

Figure 7-17 Tracking of a circle, at a speed of 0.314 rad/s, using the PID control: (a) tip trajectories; (b) joint dynamics and control signals.

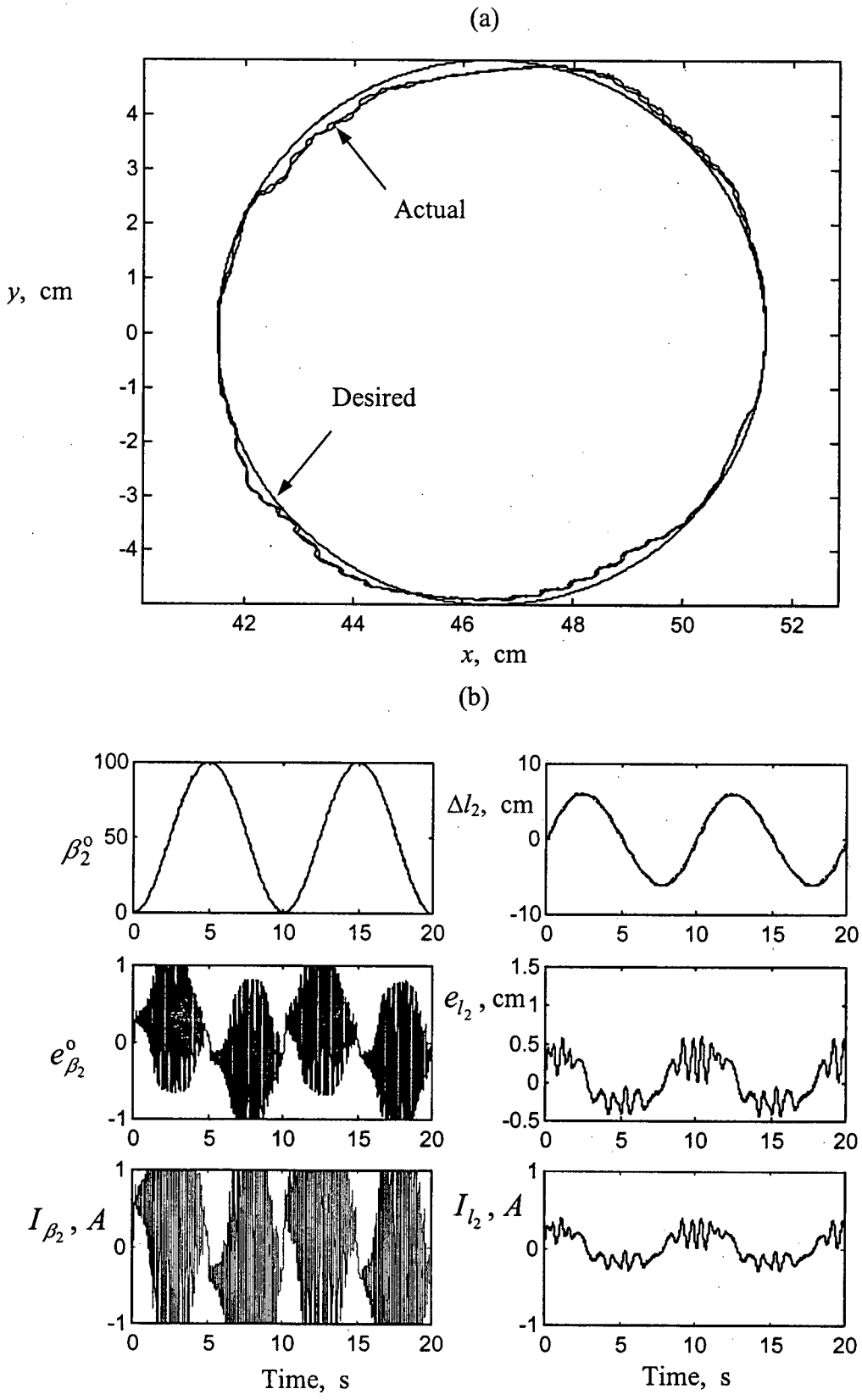

Figure 7-18 Tracking of a circle, at a speed of 0.628 rad/s, using the PID control: (a) tip trajectories; (b) joint motion and control signals.

(a)

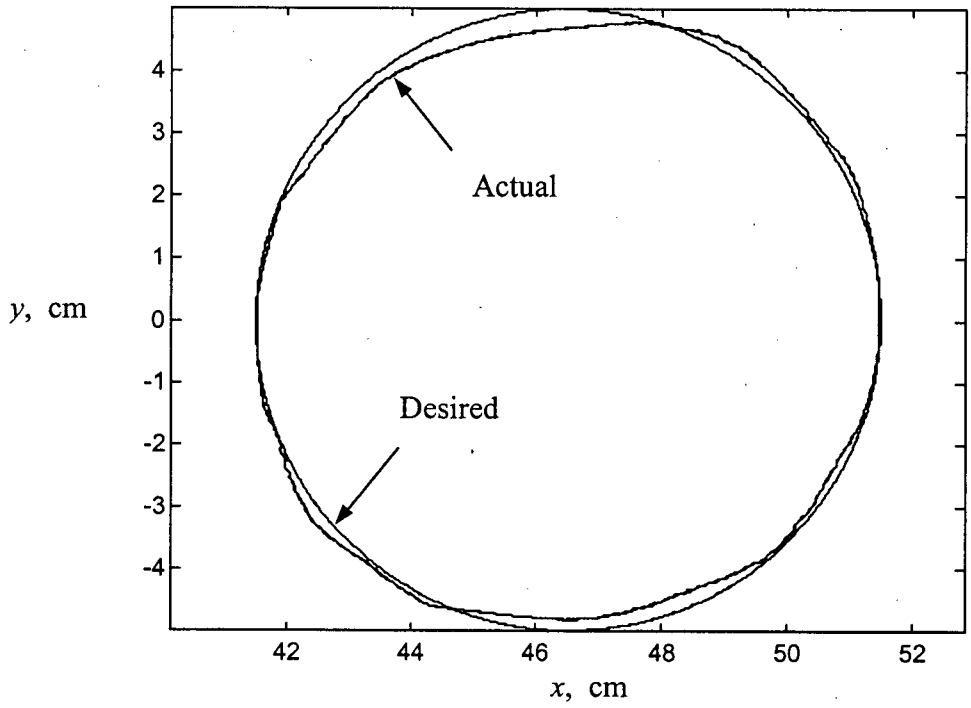

(b)

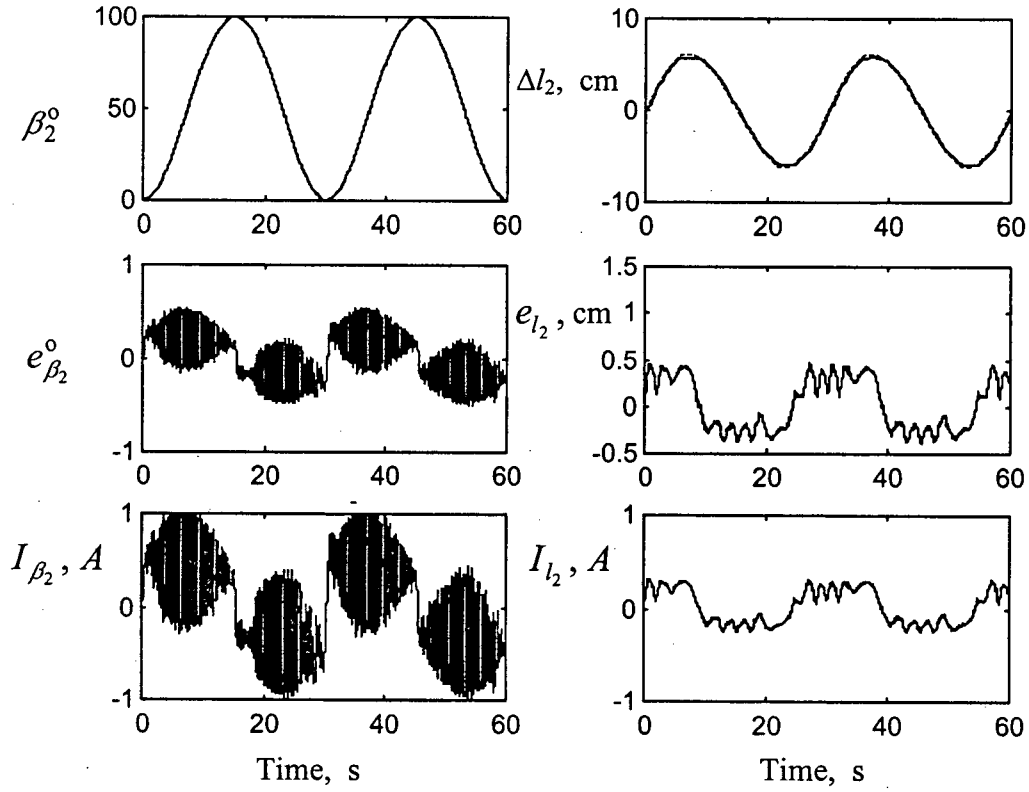

Figure 7-19 Circle tracking behavior under the PID control at a speed of 0.209 rad/s: (a) tip trajectories; (b) joint dynamics and control effort.

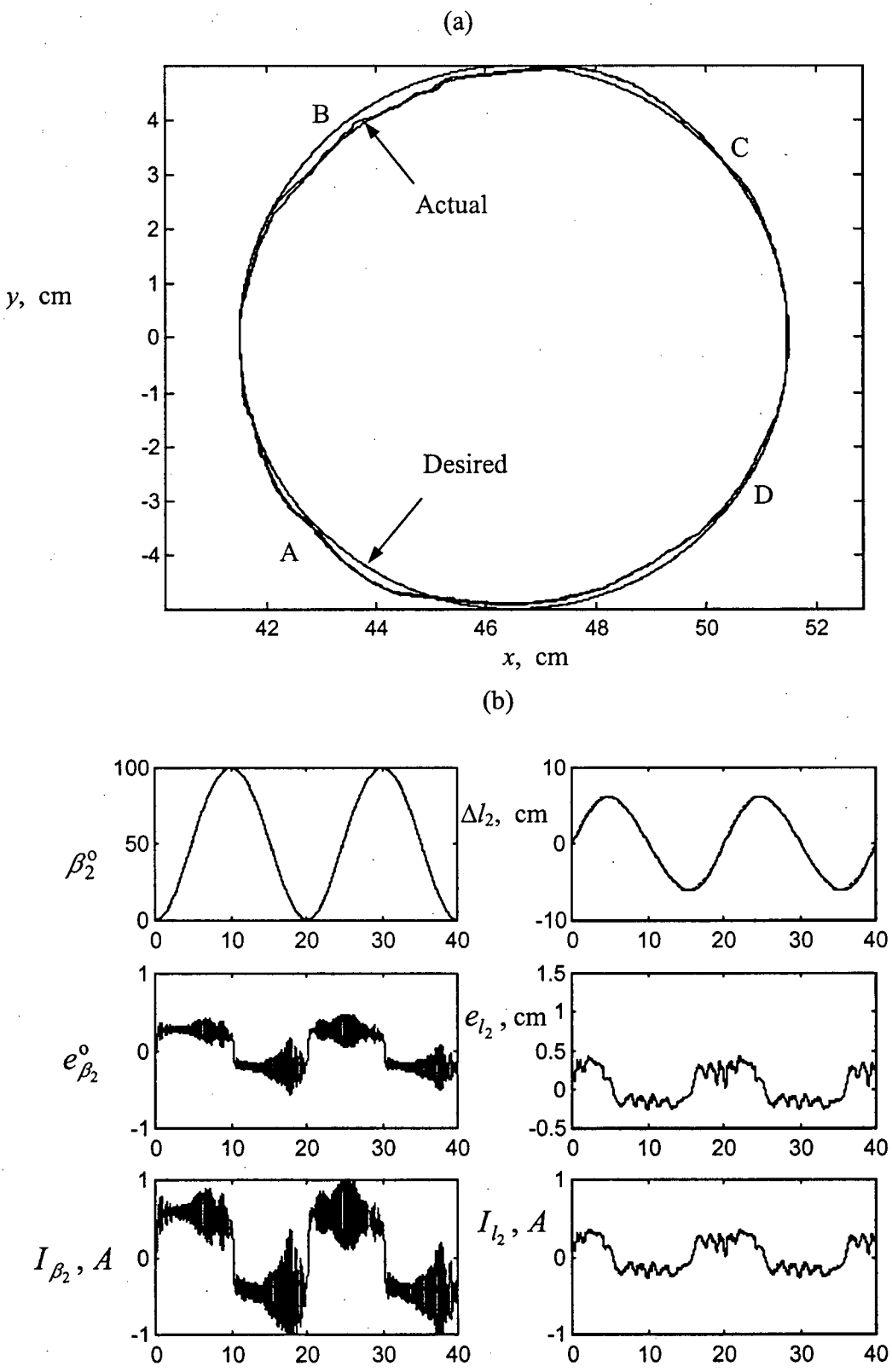

Figure 7-20 Tracking of a circle, at a speed of 0.314 rad/s, with the FLT: (a) tip trajectories; (b) joint dynamics and control effort.

dynamical compensation effort is evident. The FLT controller tries to compensate for the nonlinearity and dynamics, and consequently reduces the error and improves the repetitiveness. Again, it may be pointed out that the FLT needs a higher level of active control signal, and hence its bandwidth will be higher. The FLT controller will generate a higher frequency and a lower control magnitude.

The ground-based experiments verify several distinguishing characteristics of the variable-geometry manipulator system and its controllers:

- Prismatic joints have lower dynamical coupling, and are preferable for executing high precision tasks.
- Kinematic redundancy of a robot is useful in task planning to improve the tracking accuracy.
- The FLT controller is efficient, robust, and stable. It gives fine performance, but at a computational cost. It is suitable for the variable-geometry manipulator system.
- The PID controller is simple and fast. It works well with most trajectory following cases. Its parameters need to be fine tuned once they are assigned by a technique such as the Ziegler-Nicholes approach.
- Friction plays a significant role in causing tracking errors. It should be carefully modeled and compensated for. This is a difficult job, however, due to the highly nonlinear and time varying nature of friction. Even in presence of friction, the FLT is able to handle the control task in a robust manner. Modification of the FLT algorithm to account for friction should provide improved control performance.

8. CONCLUDING REMARKS

8.1 Contributions

The main contributions of the thesis can be summarized as follows:

(i) A relatively general formulation for studying three dimensional dynamics and control of a novel manipulator system, with slewing as well as deployable links, is developed. It is applicable to a large class of both space- and ground-based systems. Such a versatile approach has not been reported before. The nonrecursive O(N) character of the Lagrangian formulation for the three-dimensional system also represents a major step forward. Thus:

- Novel variable geometry manipulator;
- Three-dimensional character of the formulation; and
- Nonrecursive O(N) property of the equations

are innovative features of the thesis.

(ii) The planar dynamical study of a flexible, multimodule, space-based manipulator, involving up to 10 links in the present study, and that too accounting for orbital, librational and vibrational interactions, is indeed rare. Providing understanding of such complex interactions is indeed a contribution of importance.

(iii) In-plane control of this novel manipulator has received virtually no attention. The study lays a sound foundation to build on with the nonlinear FLT control of a single module orbiting manipulator.

(iv) Minimization of force and torque transmission to the platform supporting the manipulator is an important problem. The sequential conjugate gradient-restoration method has never been applied to this class of manipulators.

(v) It was indeed fortunate to have a two-module ground-based prototype manipulator designed and constructed by Chu [8]. This has made it possible to assess performance of control strategies not only through numerical simulation but also with ground-based experiments. Such correlation study, in horizontal plane, for the novel robotic system is an important contribution.

8.2 Summary of Conclusions

The project was so formulated as to emphasize development of methodology that may help understand complex dynamical interactions involved with the particular class of manipulators studied here. It was not intended to generate comprehensive design data, although the established methodology can be readily used to that end. The objective has been to assess versatility of the new tools developed through the study of a few representative cases and establish general trends. Based on the investigation, the following general conclusions can be made:

(a) The manipulator units act as payloads, and lower the natural frequency of those supporting them. The choice of shape functions used to model their flexibility can affect the speed of convergence. In general, the fundamental mode is sufficient to capture important features of the system dynamics.

(b) Significant coupling exists between the platform, link, and joint vibrations, as well as system libration. The most pronounced coupling was observed between the joint and link vibrations. In general, slewing and deployment maneuvers have a significant effect on the flexible degrees of freedom response.

(c) Motion of the manipulator modifies the system's inertia tensor and thus can induce considerable librational motion during the translation of the mobile base.

When the manipulator base is located near the platform's extremity, slewing and deployment maneuvers can also result in significant rigid body motion of the platform.

(d) Deployment alters the inertia and stiffness properties of each unit. This feature can be used to advantage to adapt the system's dynamic properties to given specifications.

(e) Excitation of the system's flexible degrees of freedom can deteriorate significantly the accuracy of the manipulator, particularly near the end of maneuvers.

(f) The system exhibits unacceptable response under critical combinations of parameters. The control strategy based on the FLT is found to be quite effective in regulating the rigid-body motion of manipulator links as well as the attitude motion of the platform. The unmodeled flexibility of the platform, joint, and manipulator links has virtually no effect on the performance of the FLT controller. It is able to regulate the elastic degrees of freedom rather well through coupling. The controller is remarkably robust.

(g) The optimization method based on sequential conjugate gradient-restoration algorithm is quite effective in minimizing transmission of forces and moments to the platform supporting the manipulator. Through a judicious choice of mass ratio of the modules for a given task, fine manipulations can be made without affecting dynamics of the gross manipulator. In the present study the mass ratio $R = 0.2$ was found to be adequate.

(h) The ground-based experiments generally validate trends indicated by the numerical simulation results. This is encouraging as the prototype system has limitations in terms of backlash, friction and, at times, less than smooth operation.

(i) Such a comprehensive study aimed at a general approach to this class of problems has not been reported before.

8.3 Recommendations for Future Work

Considering the diversity of research areas associated with the field of space robotics, the present thesis should be viewed as an initial step in the analysis and development of this particular class of space manipulators. The general formulation developed here can serve as a useful tool in future studies. However, there are several avenues which remain unexplored or demand more attention. Some of the more interesting and useful aspects include:

(i) extension of the present model to account for closed loops or contact dynamics.

(ii) modeling of system flexibility using various admissible functions, quasi-comparison functions, as well as system modes, and assessment of their effects on accuracy as well as convergence;

(iii) path planning and inverse kinematics with emphasis on obstacle avoidance, as well as minimization of structural vibrations and base reaction; effect of redundancy on system performance; completion of a given mission with one or more joints inoperational;

(iv) dynamics of satellite capture and release with the manipulator;

(v) comparative study of various optimal, adaptive, intelligent and hierarchical control strategies to regulate the rigid and flexible dynamics of single and multi-module systems;

(vi) more two-dimensional ground-based experiments to help validate numerical simulation results;

(vii) animation of simulation results for visual appreciation of the physics of the problem.

BIBLIOGRAPHY

[1] Evans, B., "Robots in Space," *Spaceflight*, Vol. 35, No. 12 1993, pp. 407-409.

[2] Canadian Science and Technology, O'Brien Publishing, Ottawa, Ontario, Fall 1995, p.11.

[3] Bassett, D.A., Wojik, Z.A., Hoefer, S., and Wittenborg, J., "Mobile Servicing System Assembly, Checkout and Operations," *46th International Astronautical Congress*, Oslo, Norway, October 1995, Paper No. IAF-95-T.3.04.

[4] Krukewich, K., Sexton, J., Cavin, K., Lee, N.E., and Cox, B., "The Systems Engineering Approach to the Integration of the Space Station Remote Manipulator System on the International Space Station (ISS)," *46th International Astronautical Congress*, Oslo, Norway, October 1995, Paper No. IAF-95-T.2.02.

[5] Kalaycioglu, S., "Robotics Evaluation and Characterization (REACH) of the SSRMS," *46th International Astronautical Congress*, Oslo, Norway, October 1995, Paper No. IAF-95-1.2.03.

[6] Chiun-Hogn, C., "Computer Vision System for Extravehicular Activity Helper/Retriever," *Applied Intelligence*, Vol. 5, No. 3, 1995, pp. 251-268.

[7] Lavery, D, "Perspectives on Future Space Robotics," *Aerospace America*, Vol. 32, No. 5, 1994, pp.32-37.

[8] Chu, M.S.T., *Design, Construction and Operation of a Variable Geometry Manipulator*, M.A.Sc. Thesis, University of British Columbia, Vancouver, B.C., Canada, October, 1997.

[9] Brereton, R. C., *A Stability Study of Gravity Oriented Satellites*, Ph.D. Thesis, The University of British Columbia, Vancouver, Canada, September 1967.

[10] Ambros, R.O., and Askew, R.S., "Experimental Investigation of Actuators for Space Robots," *Proceedings of the 1995 IEEE International Conference on Robotics and Automation*, Nagoya, Japan, 1995, Vol. 3, pp. 2625-2630.

[11] "Too much Sun gives Ulysses the Wobbles," *Electronics World and Wireless World*, Vol. 97, March 1991, p. 184.

[12] Caron, M., *Planar Dynamics and Control of Space-Based Flexible Manipulators with Slewing and Deployable Links*, M.A.Sc. Thesis, University of British Columbia, Vancouver, B.C., Canada, October 1996.

[13] Xu, Y., and Shum, H.Y., "Dynamic Control and Coupling of a Free-Flying Space Robot System," *Journal of Robotic Systems,* Vol. 11, No. 7, 1994, pp. 573-589.

[14] Modi, V.J., and Suleman, A., " Dynamical Study of the Proposed Space Station Type Configuration, " *Acta Astronautia*, Vol. 19, No. 5, 1989, pp. 377-391.

[15] Book, W.J., " Controlled Motion in an Elastic World," *Journal of Dynamic Systems, Measurement, and Control*, Vol.115, March 1993, pp. 252-260.

[16] Kelly, J.H., Glade, R.L., and Depkovitch, T.M., "Addressing the Issue of System Identification for Space Manipulators, " *Proceedings of SPIE - The International Society for Optical Engineering*, Vol. 1612, 1992, pp. 36-48.

[17] Kimura, S., Mivazaki, K., and Suzuki, Y., "Application of a Decentralized Autonomous Control Mechanism for Space Robotics, " *19th International Symposium on Space Technology and Science*, Yokohama, Japan, May 1994, Paper ISTS 94-c-02.

[18] Hirzinger, G., Landzettel, K., and Fagerer, C., "Telerobotics with Large Time Delays - the ROTEX Experience, " *Proceedings of the IEEE/RSJ/GI International Conference on Intelligent Robots and System*, Munich, Germany, 1994, Published by the IEEE, Piscataway. U.S.A., Vol. 1, pp. 571-578.

[19] Meirovitch, L., and Kwak, M.K., "On the Maneuvering and Control of Space Structures," *Proceedings of the First International Conference on the Dynamics of Flexible Structures in Space*, Cranfield, U. K., May 1990, Editors: C.L. Kirk, and J.L. Junkins, pp. 3-17.

[20] Roberson, R.E., "Two Decades of Spacecraft Attitude Control," *Journal of Guidance and Control,* Vol. 2, No.1, 1979, pp.3-8.

[21] Linkins, P.W., "Spacecraft Attitude Dynamics and Control – A Personal Perspective on Early Developments," *Journal of Guidance, Control, and Dynamics,* Vol. 9, No. 2, 1986, pp. 129-134.

[22] Modi, V.J., "Attitude Dynamics of Satellites with Flexible Appendages – A Brief Review," *Journal of Spacecraft and Rockets,* Vol. 11, 1974, pp. 743-751.

[23] Modi, V.J., and Shrivastava, S.K., "Satellite Attitude Dynamics and Control in the Presence of Environmental Torques – A Brief Survey," *Journal of Guidance, Control, and Dynamics,* Vol. 6, No. 6, 1983, pp. 461-471.

[24] Modi, V.J., "Spacecraft Attitude Dynamics: Evolution and Current Challenges," *Invited Address to the NATO/AGARD Symposium on the Space Vehicle Flight Mechanics*, Luxembourg, November 1989; also *Proceedings of the Symposium, AGARD-CP-489*, pp. 15-1 to 15-26; also *Acta Astronautica* Vol. 21, No. 10, 1990, pp. 698-718.

[25] Modi, V.J., "Man, the Unknown: Fleeting Impression of an Uncertain Mind," *Acta Astronautica*, Vol. 41, No.2, 1997, pp. 63-90

[26] Nagata, T., Modi, V.J., and Matsuo, H., "An Approach to Dynamics and Control of Flexible Systems," *A collection of Technical Papers, AIAA/AAS Astrodynamics Conference,* Scottsdale, Arizona, U.S.A, August 1994, Paper No. AIAA-94-3756CP, pp. 366-375.

[27] Dubowski, S., and Papadopoulos, E., "The Kinematics, Dynamics, and Control of Free-Flying and Free-Floating Space Robotic Systems," *IEEE Transaction on Robotics and Automation*, Vol. 9, No. 5, 1993, pp. 531-543.

[28] Papadopoulos, E., and Dubowski, S., "Dynamic Singularities in Free-Floating Space Manipulators" *Journal of Dynamic Systems, Measurement, and Control*, Vol.115, March 1993, pp. 44-52.

[29] Schebor, F.S., and Turney, J.L., "Realistic and Consistent Telerobotic Simulation," *Proceedings of the IEEE International Conference on Systems, Man, and Cybernetics*, Charlottesville, Virginia, U.S.A., 1991, Vol. 2, pp. 889-894.

[30] Bhatia, I.L., "Modeling of a Nonlinear Space Robotic System for Precision and Control, " *Proceedings of the SPIE - The International Society for Optical Engineering*, Vol. 1612, 1992, pp. 98-114.

[31] Bodley, C.S., Devers, A.D., Park, A.C., and Frisch. H.P., "A Digital Computer Program for the Dynamics Interaction Simulation of Controls and Structure (DISCOS), " Vol. I and II, NASA Technical Paper 1219, 1978.

[32] Singh, R.P., Vandervoort, R.J., and Likins, P.W., "Dynamics of Flexible Bodies in Tree-Topology - A Computer Oriented Approach, " *AIAIA/ASME/ASCE, 25th Structures, Structural Dynamics, and Materials Conference.* Palm Springs, California, U.S.A., 1984, Paper No. AIAA-84-1024.

[33] Pascal, M., "Dynamical Analysis of a Flexible manipulator Arm, " *Acta Astronautica*, Vol. 21, No. 3, 1990, pp. 161-169.

[34] Chan, J.K.W., *Dynamics and Control of an Orbiting Space Platform Based Mobile Flexible Manipulator*, M.A.Sc. Thesis, The University of British Columbia, Vancouver, Canada, 1990.

[35] Mah, H., *On the Nonlinear Dynamics of a Space Platform Based Mobile Flexible Manipulator*, Ph.D. Thesis, The University of British Columbia, Vancouver, Canada, 1992.

[36] Lilly, K.W., and Bonaventura, C.S., "Generalized Formulation for Simulation of Space Robot Constrained Motion, " *Proceedings of the IEEE International Conference on Robotics and Automation*, Nagoya, Japan. 1995, Vol. 3, pp. 2835-2840.

[37] Papadopoulos, E.G., "Large Payload Manipulation for Space Robots," *Proceedings of the IEEE/RSJ International Conference on Intelligent Robots and Systems,*

Yokohama. Japan, 1993, Published by the IEEE, Piscataway, U.S.A., pp. 208 I'-2094.

[38] Xavier, C., Jaar, G.J., and Misra, A.K., "Effect of Payload Impact on the Dynamics of a Space Robot," *Proceedings of the 1993 IEEE/RSG International Conference on Intelligent Robots and Systems,* Yokohama, Japan, 1993, Published by the IEEE, Piscataway, U.S.A., pp. 2070-2075.

[39] Yoshida, K., and Sashida, N., "Modeling of Impact Dynamics and Impulse Minimization for Space Robots," *Proceedings of the 1993 IEEE/RSG International Conference on Intelligent Robots and Systems*, Yokohama, Japan, 1993, Published by the IEEE, Piscataway, U.S.A., pp. 2064-2069.

[40] Cherchas, D.B., "Dynamics of Spin-Stabilized Satellites During Extension of Long Flexible Booms," *Journal of Spacecraft and Rockets*, Vol. 8, No. 7, 1971, pp. 802-804.

[41] Sellappan, R., and Bainum, P.M., "Dynamics of Spin-Stabilized Spacecraft During Deployment of Telescopic Appendages," *Journal of Spacecraft and Rockets,* Vol. 13. No. 10, pp. 605-610.

[42] Modi, V.J., and Ibrahim, A.M., "Dynamics of the Orbiter-Based WISP Experiment," *Acta Astronautica*, Vol. 26, No. 11. 1992, pp. 749-1-61.

[43] Modi, V.J., and Shen, Q., " On the Dynamics of Spacecraft with Flexible, Deployable and Slewing Appendages," *Advances in the Astronautical Sciences*, Editors: A.K. Misra, *et al.*, American Astronautical Society Publisher, San Diego, U.S.A., Vol. 85, Part III, 1993, pp. 2143-2162.

[44] Marom., I., *A Study of the Flexible Space Platform Based Mobile Deployable Manipulator*, Ph.D. Thesis, The University of British Columbia, Vancouver, Canada, 1993.

[45] Hokamoto, S., Modi, V.J., and A.K. Misra, "Dynamics and Control of Mobile Flexible Manipulators with Slewing and Deployable Links," *Advances in the Astronautical Sciences*, Editors: K.T. Alfriend *et al.*, American Astronautical Society Publisher, San Diego, U.S.A., Vol. 90, 1996, Paper No. AAS-95-322, pp. 339-357.

[46] Caron, M., Modi, V.J., Pradhan, S., de Silva, C.W., and Misra, A.K., "Planar Dynamics of Flexible Manipulators with Slewing Deployable Links," *Journal of Guidance, Control, and Dynamics*, Vol. 21, No. 4, 1998, pp. 572-580.

[47] de Silva, C.W., "Trajectory Design for Robotic Manipulators in Space Applications," *Journal of Guidance, Control, and Dynamics,* Vol. 14 No. 3, pp. 670-674.

[48] Hollerbach, J.M., "A Recursive Lagrangian Formulation of Manipulator Dynamics and Comparative Study of Dynamics Formulation Complexity," *IEEE Transactions on Systems, Man, and Cybernetics,* Vol. 10, No. 11, 1980, pp. 730-736.

[49] Keat, J.E., "Multibody System Order *N* Dynamics Formulation Based on Velocity Transform method," *Journal of Guidance, Control, and Dynamics*, Vol. 13, No. 2, 1990, pp. 207-212.

[50] Rosenthal, D.E., "An Order *N* Formulation for Robotic Systems," *The Journal of the Astronautical Sciences*, Vol. 38, No. 4, 1990, pp. 511-529.

[51] Suzuki, S., and Kojima, H., "Application of Order-n Formulation to Panel Deployment Problem of a Spacecraft," *Journal of Guidance, Control, and Dynamics*, Vol. 17, No. 3, 1994, pp. 634-636.

[52] Banerjee, A.K., "Order-n Formulation of Extrusion of a Beam with Large Bending and Rotation," *Journal of Guidance, Control, and Dynamics*, Vol. 15, No. 1, 1992, pp. 121-127.

[53] Jain, A., and Rodriguez, G., "Recursive Flexible Mlultibody System Dynamics Using Spatial Operators," *Journal of Guidance, Control, and Dynamics*, Vol. 15, No.6, 1992, pp. 1453-1466.

[54] Bae, D.S., and Haug, E.J., "A Recursive Formulation for Constrained Mechanical System Dynamics: Part I - Open Loop Systems," *Mechanics of Structures and Machines*, Vol. 15, No. 3, 1987, pp. 359-382.

[55] Pradham, S., Modi, V.J., and Misra, A.K., "Order *N* Formulation for Flexible Multibody Systems in Tree Topology: The Lagrangian Approach," *Journal of Guidance, Control, and Dynamics,* Vol. 20, No. 4, July-August 1997, pp. 665-672.

[56] Bainum,P.M., and Diarra, C.M., " The Dynamics and Control of the Orbiting Spacecraft Control Laboratory Experiment (SCOLE) During Station Keeping," *AIAA/AAS Astrodynamics Conference,* Minneapolis, Minnesota, August 1988, Paper No. 88-4252.

[57] Hirzinger, G., Brunner, B., Dietrich, J., and Heindl, J., "Sensor-Based Space Robotics-ROTEX and Its Telerobotic Features," *IEEE Transactions on Robotics and Automation,* Vol. 9, No. 5, 1993, pp. 649-661.

[58] Martin, E., Papadopoulos, E., and Angeles, J., " On the interaction of Flexible Modes and On-Off Thrusters in Space Robotic Systems," *Proceedings of the 1995 IEEE/RSG International Conference on Intelligent Robots and Systems,* Pittsburgh, Pennsylvania, U.S.A., 1995, Published by the IEEE, Piscataway, U.S.A., Vol. 2, pp. 65-70.

[59] Krishnan, S., and Vadali, S.R., " An Inverse-Free Technique for Attitude Control of Spacecraft using CMG's," *AAS/AAIA Spaceflight Mechanics Meeting*, Albuquerque, New Mexico, U.S.A., Feburary 1995, Paper No. AAS-95-139.

[60] Parlaktuna, O., Cook, G.E., Struss, A.M., and Fernandez, K.R., "Fine Attitude Control of Space Vehicles using Space Manipulators," *International Journal of Robotics and Automation*, Vol. 9, No. 1, 1994, pp.29-35.

[61] De Luca, A., " Dynamic Control of Robots with Joint Elasticity," *Proceedings of the IEEE International Conference on Robotics and Automation,* Philadelphia, U.S.A., 1988, Vol. 1, pp. 316-321.

[62] Bayo, E., "Computed Torque for the Position Control of Open-Chain Flexible Robots," *Proceedings of the IEEE International Conference on Robotics and Automation,* Raleigh, U.S.A., 1987, pp.923-928.

[63] Gebler, B., "Feed-Forward Control Strategy for an Industrial Robot with Elastic Links and Joints," *Proceedings of the IEEE International Conference on Robotics and Automation*, Raleigh, U.S.A., 1987, pp. 923-928.

[64] Bailey, T., and Hubbard, J.E., Jr, "Distributed Piezoelectric-Polymer Active Vibration Control of a Cantilever Beam," *Journal of Guidance, Control, and Dynamics,* Vol. 8, No. 5, 1985, pp. 605-611.

[65] Quinn, R.D., Chen, J.L., and Lawrence, C., "Base Reaction Control for Space-based Robots Operation in Microgravity Environment," Journal of Guidance, Control, and Dynamics, Vol. 17, No. 2, 1994, pp. 263-270.

[66] Hanson, M.L., and Tolson, R.H., " Reducing Flexible Base Vibration through Local Redundancy Resolution," *Journal of Robotic System*, Vol. 12, No. 11, 1995, pp. 767-779.

[67] Wang, D., "Comparison of Optimal and Nonoptimal Control Strategies for the Single Flexible Link," *International Journal of Robotics and Automation,* Vol. 9, No. 3, 1994, pp. 130-136.

[68] Craig, J.J., *Introduction to Robotics: Mechanics and Control*, Addison-Wesley Publish Company, Reading, Massachusetts, 2nd Edition, 1989, pp. 332-359.

[69] Fu, K.S., Gonzalez, R.C., and Lee, C.S.G., *Robotics: Control, Sensing, Vision, and Intelligence*, Mcgraw-Hill Book Company, New York, U.S.A. 1987, pp. 82-84, 103-124.

[70] Modi, V.J., Karray, F., and Chan, J.K., " On the Control of a Class of Flexible Manipulators Using Feedback Linearization Approach," *42nd Congress of the International Astronautical Federation*, Montreal, Canada, October 1991, Paper No. IAF-91-324; also *Acta Astronautica*, Vol. 29, No. 1, 1993, pp. 17-27.

[71] Ericsson, A.J., Bainum, P.M., and Quangqian, X., " The Optimal LQR Digital Control of a Free-Free orbiting Platform," *41st International Astronautical Congress,* Dresden, Germany, October 1990, Paper No. IAF-90-318; also *Acta Astronautica*, Vol. 29, No. 2, 1993, pp.69-81.

[72] Xu, J., Bainum, P.M., and Li, F., " Vibration Control of a Manipulator Tip on a Flexible Body," *Proceedings of the Eighth VPI & SU Symposium on Dynamics and Control of Large Structures*, May 1991, Blacksburg, Virginia, U.S.A., Editor: L. Meirovitch, pp. 703-714.

[73] Guangqing, X., and Bainum, P.M., "Optimal LQG Digital Control of Orbiting Large Flexible Beams," *The Journal of the Astronautical Sciences*, Vol. 37, No. 1, 1989, pp.59-78.

[74] Belloch, P.A., and Mingori, D.L., "Robust Linear Quadratic Gaussian Control for Flexible Structures," *Journal of Guidance, Control, and Dynamics*, Vol. 13, No.1, 1990, pp. 66-72.

[75] Meirovitch, L., *Elements of Vibration Analysis,* McGraw-Hill Book Company, New York, U.S.A., 2nd Edition, 1986, pp. 255-256, 282-290.

[76] Pradhan, S., Modi, V.J., and Misra, A.K., " Order N Formulation for Flexible Multibody Systems in Tree Topology – The Lagrangian Approach," *A Collection of Technical Papers, AIAA/AAS Astrodynamics Specialist Conference*, San Diego, California, U.S.A., July 1996, paper No. 96-3624, pp. 480-490.

[77] *IMSL Library Reference Manual*, Vol. 1, IMSL Inc., Houston, Texas, U.S.A., 1980, pp. DGEAR 1-DGEAR 9.

[78] de Silva, C.W., Modi, V.J., Chen, Y., "Dynamic Modeling and Control of a Variable Manipulator with Separation of Fine and Gross Manipulations," *Report on the IRIS Project MSA-1: Task Oriented, Sensor-Based Manipulations, Part II*, Institute for Robotics and Intelligent Systems, Department of mechanical Engineering, University of British Columbia, December 1996.

[79] Freund, E., "The Structure of Decoupled Nonlinear Systems, " *International Journal of Control,* Vol. 21, No. 3, 1975, pp. 443-450.

[80] Freund, E., "Fast Nonlinear Control with Arbitrary Pole-Placement for Industrial Robots and Manipulators, " *The International Journal of Robotics Research,* Vol. 1, No. 1, 1982, pp. 65-78.

[81] Slotine, J.E. and Sastry, S.S., "Tracking Control of Non-linear Systems using Sliding Surfaces with Application to Robot Manipulators, " *International Journal of Control,* Vol. 38, No. 2, 1983, pp. 465-492.

[82] Slotine, J.E., "Sliding Controller Design for Non-linear Systems, " *International Journal of Control,* Vol. 40, No. 2, 1984, pp. 421-434.

[83] Slotine, J.E., "The Robust Control of Robot Manipulators, " *International Journal of Robotics Research,* Vol. 4, No. 2, 1985, pp. 49-64.

[84] Slotine, J.E., and Li, W., "On the Adaptive Control of Robot Manipulators, " *International Journal of Robotics Research,* Vol. 6, No. 3, 1987, pp. 49-59.

[85] Beijczy, A.K., *Robot Arm Dynamics and Control,* JPL TM 33-669, California Institute of Technology, Pasadena, California, 1974.

[86] Singh, S.N., and Schy, A.A., "Invertibility and Robust Nonlinear Control of Robotic Systems, " *Proceedings of 23rd Conference on Decision and Control,* Las Vegas, Nevada, December 1984, pp. 1058-1063.

[87] Spong, M.W., and Vidyasagar, M., "Robust Linear Compensator Design for Nonlinear Robotic Control, " *Proceedings of IEEE Conference on Robotics and Automation*, St. Louis, Missouri, March 1985, pp. 954-959.

[88] Spong, M.W., and Vidyasagar, M., "Robust Nonlinear Control of Robot Manipulator," *Proceedings of the 24th IEEE Conference on Decision and Control,* Fort Lauderdale, Florida, December 1985, pp. 1767-1772.

[89] Spong, M.W., "Modeling and Control of Elastic Joint Robots, " *Journal of Dynamic systems, Measurement and Control,* Vol. 109, December 1987, pp. 310-319.

[90] Modi, V.J., Ng, A., and Karray, F., "Nonlinear Dynamics and Control of INSAT-II: Application of a General Formulation," *International Journal of Control,* Vol. 58, No.3, 1993, pp. 503 - 517.

[91] Miele, A., Cloutier, J.R., Mohanty, B.P., and Wu, A.K., "Sequential Conjugate Gradient-Restoration Algorithm for Optimal Control Problems with Nondifferential Constraints, " *International Journal of Control*, Vol. 29, No.2, 1979, pp. 189-211

[92] Clough, R.W. and Penzien, J., *Dynamics of Structures*, McCraw-Hill Book Co., New York, N.Y. 1975 pp. 281-326.

[93] Blevins, R.D., *Formulas for Natural Frequencies and Mode Shapes*, Van Nostrand Reinhold, New York, N.Y., U.S.A., 1979, pp. 101-170

[94] Kranklin, G.F., Powell, J.D., and Emami-Naeini, A., *Feedback control of Dynamics Systems*, Addison-Wesley Publishing Company, Inc., Massachusetts, U.S.A., 1986, pp. 103-106.

APPENDIX A: MODELING OF BEAM VIBRATION

For beam-type bodies, the Euler-Bernoulli beam theory, which does not model the effects of shear deformation and rotatory inertia, is employed in the formulation. The partial differential equation governing this type of beam flexure (v in the y direction) in the absence of external loading, is given as

$$\frac{\partial^2}{\partial x^2}\left(EI_{zz}\frac{\partial^2 v}{\partial x^2}\right)+m_b\frac{\partial^2 v}{\partial t^2}=0, \tag{A.1}$$

where m_b represents the beam mass per unit length, and EI_{zz} is the flexural rigidity in the y direction. An analogous expression can be written for beam deflections in the z direction. The boundary conditions can be of four types: related to the shear force, bending moment, deflection and rotation experienced by the beam at the boundaries. The former two are referred to as natural boundary conditions, while the latter two as geometric boundary conditions. The natural boundary conditions can be represented as

$$V_y^b(x)=-EI_{zz}\frac{\partial^3 v}{\partial x^3}, \tag{A.2}$$

and

$$W_y^b(x)=EI_{zz}\frac{\partial^2 v}{\partial x^2}, \tag{A.3}$$

where V_y^b and W_y^b denote the beam shear force and bending moments, respectively, in the directions indicated by the subscripts. Corresponding expressions can be written for flexure in the z direction.

Equation (A.2) can be solved exactly by taking the beam deflection $v(x, t)$ to be a function of both time, $Y(t)$, and the spatial domain, $\phi(x)$, as

$$v(x,t) = \phi(x)Y(t)\,. \tag{A.4}$$

Thus elastic deformations of the manipulator and platform can be discretized using assumed modes for each component of the system. Deformation of the i^{th} body is expressed as the product of spatially varying admissible shape functions (Φ_i) and time dependent generalized coordinates (δ_i). Now, the elastic displacement of the i^{th} body can be expressed as

$$\begin{bmatrix} u_i \\ v_i \\ w_i \end{bmatrix} = \begin{bmatrix} \Phi_{\mathrm{ix}} & 0 & 0 \\ 0 & \Phi_{\mathrm{iy}} & 0 \\ 0 & 0 & \Phi_{\mathrm{iz}} \end{bmatrix} \begin{bmatrix} \delta_{\mathrm{ix}} \\ \delta_{\mathrm{iy}} \\ \delta_{\mathrm{iz}} \end{bmatrix} = \Phi_{\mathrm{i}}\delta_{\mathrm{i}}, \tag{A.5}$$

where u_i , v_i and w_i correspond to the longitudinal and transverse elastic displacements, respectively, of an elemental mass located on the i^{th} body at $\boldsymbol{r}_i$. Similarly, the subscripts *x, y* and *z* refer to the longitudinal and transverse modes of vibration, respectively. Although the formulation accounts for the longitudinal elastic deformation, simulation results focus on the transverse displacements. The modules are considered to be Euler-bernoulli cantilever beams with tip masses. For the transverse vibration, in the *y* direction of the i^{th} body, the admissible shape functions for the k^{th} mode take the form [92]

$$\Phi_{iyk}(x_i, l_i) = A_{ik1}\sin\left(\frac{\lambda_{ik}x_i}{l_i}\right) + A_{ik2}\cos\left(\frac{\lambda_{ik}x_i}{l_i}\right) + A_{ik3}\sinh\left(\frac{\lambda_{ik}x_i}{l_i}\right) + A_{ik4}\cosh\left(\frac{\lambda_{ik}x_i}{l_i}\right), \tag{A.6}$$

where l_i is the length of the i^{th} body; x_i is the position along l_i ; and the parameters A_{ikj} and λ_{ik} depend on boundary conditions of the i^{th} body.

Of particular interest is the solution of Eq.(A.6), because the family of shape functions under various loading conditions will be used subsequently as admissible functions. These shape

functions are excellent candidates as admissible functions as, in a number of cases, the boundary conditions experienced by individual bodies in a multibody system approximate the fundamental loading conditions for which the exact shape functions can be found readily (e.g. free-free, clamped-free, etc.). Discarding the subscripts i, y, k in Eq.(A.6) for simplicity, the modal function can be written as

$$\Phi(x) = A_1 \sin ax + A_2 \cos ax + A_3 \sinh ax + A_4 \cosh ax, \qquad \text{(A.7)}$$

where: $a = \lambda / L$; $A_1, \ldots, A_4$ are constants which depend on the boundary conditions; λ, a multi-valued frequency parameter given by a transcendental equation, which depends on the boundary conditions, and L denotes the beam length. For several boundary conditions, these relations are summarized in Table A-1.

Table A-1 Euler-Bernoulli beam shape function parameters

Boundary Condition	Equation for λ	Formula for A_1
Free-Free	$\cos\lambda \cosh\lambda - 1 = 0$	$\dfrac{\cos\lambda - \cosh\lambda}{\sinh\lambda - \sin\lambda}$
Clamped-Free	$\cos\lambda \cosh\lambda + 1 = 0$	$\dfrac{\sinh\lambda - \sin\lambda}{\cosh\lambda + \cos\lambda}$
Clamped-Clamped	$\cos\lambda \cosh\lambda - 1 = 0$	$\dfrac{\cos\lambda - \cosh\lambda}{\sinh\lambda - \sin\lambda}$

The coefficients have the value:

$A_3 = A_1, \quad A_2 = A_4 = 1,$ free-free beam;

$A_3 = -A_1, \; A_2 = -A_4 = -1,$ clamped-free beam;

$A_3 = -A_1, \; A_2 = -A_4 = -1,$ clamped-clamped beam.

The mode shape function (admissible function) for the free cantilever beam with a tip mass payload has the form of [67]

$$\Phi(x) = (\sin kx - \sinh kx) - \frac{\sin\lambda + \sinh\lambda}{\cos\lambda + \cosh\lambda}(\cos kx - \cosh kx), \tag{A.8}$$

where k is the number of the mode and λ is the root of the characteristic equation

$$\cos\lambda\cosh\lambda + 1 = \frac{m_p}{\rho l}\lambda(\sin\lambda\cosh\lambda - \cos\lambda\sinh\lambda). \tag{A.9}$$

Here ρ is the linear density of the beam, l is the length of the beam, and m_p is the tip mass. The tip mass ratio is defined as $m_p/\rho l$.

This transcendental equation has infinite number of roots thus leading to an infinite number of mode shapes. The first five characteristic spatial frequencies λ_i (i = 1,2,...,5) for the cantilever beam with tip load mass ratio of one are shown in Table A-2 [93].

Table A-2. λ_i values for different modes

Number of Mode	λ
1	1.8751
2	4.6941
3	7.8548
4	10.996
5	14.137

APPENDIX B: ROTATION MATRIX AND ITS TIME DERIVATIVES

B.1 T Matrix

In the thesis the orientation of a body is defined using Euler angles with 1-2-3 order. In going from F_{i-1} to F_i, the first rotation is about x_{i-1}, the next about y_{i-1} and finally with respect to z_{i-1}. The following is the derivation of the rotation matrix T'. For the rotation in Fig. B-1, about x_i axis, y' and z' can be obtained as:

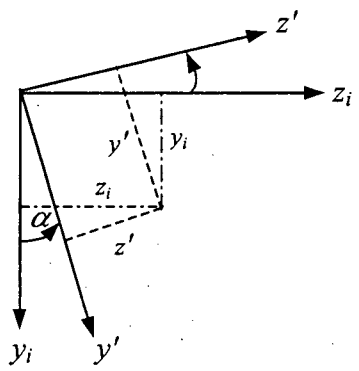

Figure B-1 Rotation about the x_i axis

$$\begin{aligned} y' &= y_i \cos\alpha + z_i \sin\alpha; \\ z' &= -y_i \sin\alpha + z_i \cos\alpha; \end{aligned} \tag{B.1}$$

thus

$$\begin{Bmatrix} x' \\ y' \\ z' \end{Bmatrix} = \mathbf{T}_x' \begin{Bmatrix} x_i \\ y_i \\ z_i \end{Bmatrix}; \tag{B.2}$$

where

$$\mathbf{T}_x' = \begin{bmatrix} 1 & 0 & 0 \\ 0 & \cos\alpha & \sin\alpha \\ 0 & -\sin\alpha & \cos\alpha \end{bmatrix}. \tag{B.3}$$

Similar procedure can be applied to the rotations about y_i and z_i axes. Corresponding matrices $\mathbf{T}_y'$ and $\mathbf{T}_z'$ can be given as

$$\mathbf{T}_y' = \begin{bmatrix} \cos\beta & 0 & -\sin\beta \\ 0 & 1 & 0 \\ \sin\beta & 0 & \cos\beta \end{bmatrix}; \tag{B.4}$$

and

$$\mathbf{T}_z' = \begin{bmatrix} \cos\gamma & \sin\gamma & 0 \\ -\sin\gamma & \cos\gamma & 0 \\ 0 & 0 & 1 \end{bmatrix}. \tag{B.5}$$

Here β and γ are the rotation angles with respect to y_i and z_i, respectively. The relation after three Euler rotation angles has the form

$$\begin{Bmatrix} x' \\ y' \\ z' \end{Bmatrix} = \mathbf{T}_z' \cdot \mathbf{T}_y' \cdot \mathbf{T}_x' \begin{Bmatrix} x_i \\ y_i \\ z_i \end{Bmatrix} = \mathbf{T}' \begin{Bmatrix} x_i \\ y_i \\ z_i \end{Bmatrix}. \tag{B.6}$$

In the thesis, the Euler angles are measured with respect to the initial frame. Furthermore, position of a mass element is also evaluated with respect to the initial frame. Hence the following relation

$$\begin{Bmatrix} x_i \\ y_i \\ z_i \end{Bmatrix} = \mathbf{T} \begin{Bmatrix} x' \\ y' \\ z' \end{Bmatrix} \tag{B.7}$$

is needed, where $\mathbf{T} = (\mathbf{T}')^{-1}$. As can be expected, $\mathbf{T}'$ is an orthogonal matrix thus

$$\mathbf{T} = (\mathbf{T}')^T = \begin{bmatrix} C_\gamma C_\beta & -S_\gamma C_\beta & S_\beta \\ C_\gamma S_\beta S_\alpha + S_\gamma C_\alpha & -S_\gamma S_\beta S_\alpha + C_\gamma C_\alpha & -C_\beta S_\alpha \\ -C_\gamma S_\beta C_\alpha + S_\gamma S_\alpha & S_\gamma S_\beta C_\alpha + C_\gamma S_\alpha & C_\beta C_\alpha \end{bmatrix}, \tag{B.8}$$

where C_x and S_x are abbreviations for cos(x) and sin(x), respectively.

B.2 $\dot{\mathbf{T}}$ Matrix

Taking derivative with respect to time gives

$$\dot{\mathbf{T}} = \begin{bmatrix} -S_\gamma C_\beta \dot{\gamma} - C_\gamma S_\beta \dot{\beta} & -C_\gamma C_\beta \dot{\gamma} + S_\gamma S_\beta \dot{\beta} & C_\beta \dot{\beta} \\ \begin{matrix}(-S_\gamma S_\beta S_\alpha + C_\gamma C_\alpha)\dot{\gamma} \\ +(C_\gamma C_\beta S_\alpha + S_\gamma C_\alpha)\dot{\beta} \\ +(C_\gamma S_\beta C_\alpha - S_\gamma S_\alpha)\dot{\alpha}\end{matrix} & \begin{matrix}(-C_\gamma S_\beta S_\alpha - S_\gamma C_\alpha)\dot{\gamma} \\ +(-S_\gamma C_\beta S_\alpha + C_\gamma C_\alpha)\dot{\beta} \\ +(-S_\gamma S_\beta C_\alpha - C_\gamma S_\alpha)\dot{\alpha}\end{matrix} & S_\beta S_\alpha \dot{\beta} - C_\beta C_\alpha \dot{\alpha} \\ \begin{matrix}(S_\gamma S_\beta C_\alpha + C_\gamma S_\alpha)\dot{\gamma} \\ +(-C_\gamma C_\beta C_\alpha + S_\gamma S_\alpha)\dot{\beta} \\ +(-C_\gamma S_\beta S_\alpha + S_\gamma C_\alpha)\dot{\alpha}\end{matrix} & \begin{matrix}(C_\gamma S_\beta C_\alpha - S_\gamma S_\alpha)\dot{\gamma} \\ +(S_\gamma C_\beta C_\alpha + C_\gamma S_\alpha)\dot{\beta} \\ +(-S_\gamma S_\beta S_\alpha + C_\gamma C_\alpha)\dot{\alpha}\end{matrix} & -S_\beta C_\alpha \dot{\beta} - C_\beta S_\alpha \dot{\alpha} \end{bmatrix} \tag{B-9}$$

In a simpler matrix form, this can be rewritten as

$$\dot{\mathbf{T}} = \mathbf{T}_\alpha \dot{\alpha} + \mathbf{T}_\beta \dot{\beta} + \mathbf{T}_\gamma \dot{\gamma}, \tag{B.10}$$

where:

$$\mathbf{T}_\alpha = \begin{bmatrix} 0 & 0 & 0 \\ C_\gamma S_\beta C_\alpha - S_\gamma S_\alpha & -S_\gamma S_\beta C_\alpha - C_\gamma S_\alpha & -C_\beta C_\alpha \\ -C_\gamma S_\beta S_\alpha + S_\gamma C_\alpha & -S_\gamma S_\beta S_\alpha + C_\gamma C_\alpha & -C_\beta S_\alpha \end{bmatrix}; \tag{B.11}$$

$$\mathbf{T}_\beta = \begin{bmatrix} -C_\gamma S_\beta & S_\gamma S_\beta & C_\beta \\ C_\gamma C_\beta S_\alpha + S_\gamma C_\alpha & -S_\gamma C_\beta S_\alpha + C_\gamma C_\alpha & S_\beta S_\alpha \\ -C_\gamma C_\beta C_\alpha + S_\gamma S_\alpha & S_\gamma C_\beta C_\alpha + C_\gamma S_\alpha & -S_\beta C_\alpha \end{bmatrix}; \tag{B.12}$$

and

$$\mathbf{T}_\gamma = \begin{bmatrix} -S_\gamma C_\beta & -C_\gamma C_\beta & 0 \\ -S_\gamma S_\beta S_\alpha + C_\gamma C_\alpha & -C_\gamma S_\beta S_\alpha - S_\gamma C_\alpha & 0 \\ S_\gamma S_\beta C_\alpha + C_\gamma S_\alpha & C_\gamma S_\beta C_\alpha - S_\gamma S_\alpha & 0 \end{bmatrix}. \tag{B.13}$$

For any vector $\boldsymbol{v}$,

$$\dot{\mathbf{T}}\boldsymbol{v} = \mathbf{T}_\alpha \boldsymbol{v}\dot{\alpha} + \mathbf{T}_\beta \boldsymbol{v}\dot{\beta} + \mathbf{T}_\gamma \boldsymbol{v}\dot{\gamma} \tag{B.14}$$

or

$$\dot{\mathbf{T}}\boldsymbol{v} = [\mathbf{T}_\alpha \boldsymbol{v} \vdots \mathbf{T}_\beta \boldsymbol{v} \vdots \mathbf{T}_\gamma \boldsymbol{v}\dot{\gamma}] \begin{Bmatrix} \dot{\alpha} \\ \dot{\beta} \\ \dot{\gamma} \end{Bmatrix} = \mathbf{P}(\boldsymbol{v})\{\dot{\eta}\}; \tag{B.15}$$

where $\mathbf{P}(\boldsymbol{v}) = [\mathbf{T}_\alpha \boldsymbol{v} \vdots \mathbf{T}_\beta \boldsymbol{v} \vdots \mathbf{T}_\gamma \boldsymbol{v}]$. This is the expression used in Eq. (2.8).

APPENDIX C: TIME DERIVATIVES OF VECTORS $f(r_i)$ AND $f(o_i)$

The time derivative of $f_i(r_i)$ is needed to evaluate kinetic energy of the body i,

$$\begin{aligned}\frac{d\, f_i(r_i)}{dt} &= \frac{d\Phi_i \delta_i}{dt} = \frac{d\Phi_i}{dt}\delta_i + \Phi_i \dot{\delta}_i\,, \\ &= \frac{d\Phi_i}{dl_i}\delta_i \dot{l}_i + \frac{d\Phi_i}{dr_i}\delta_i \dot{r}_i + \Phi_i \dot{\delta}_i\,.\end{aligned} \tag{C.1}$$

Let the deployable link of the manipulator have a telescopic type of motion as

$$\dot{r} = \frac{r}{l}\dot{l} \tag{C.2}$$

Now Eq. (C.1) becomes

$$\begin{aligned}\frac{d\, f_i(r_i)}{dt} &= \frac{d\Phi_i}{dl_i}\delta_i \dot{l}_i + \frac{d\Phi_i}{dr_i}\delta_i \frac{r}{l}\dot{l}_i + \Phi_i \dot{\delta}_i\,, \\ &= \left[\frac{d\Phi_i}{dl_i} + \frac{d\Phi_i}{dl_i}\frac{r}{l}\right]\delta_i \dot{l}_i + \Phi_i \dot{\delta}_i\,,\end{aligned} \tag{C.3}$$

or

$$\frac{d\, f_i(r_i)}{dt} = \Phi \mathbf{L}_i \delta_i \dot{l}_i + \Phi_i \dot{\delta}_i\,, \tag{C.4}$$

where

$$\Phi \mathbf{L}_i = \left[\frac{d\Phi_i}{dl_i} + \frac{d\Phi_i}{dl_i}\frac{r}{l}\right]. \tag{C.5}$$

This is the expression used in Eq. (2.8) of Chapter 2.

Similar approach can be used to obtain the time derivative of $\boldsymbol{f}\,(\mathbf{o}_i)$. From Eq. (A.5), $\mathbf{KA}(o_i)$ can be written as

$$\mathbf{KA}(o_i) = \begin{bmatrix} \Phi_{\mathrm{ix}}(o_i) & 0 & 0 \\ 0 & \Phi_{\mathrm{iy}}(o_i) & 0 \\ 0 & 0 & \Phi_{\mathrm{iz}}(o_i) \end{bmatrix} = \Phi_{\mathrm{i}}(o_i)\,, \tag{C.6}$$

where $\boldsymbol{o}_i = l_{i-1} + \boldsymbol{d}_i$. As both l_{i-1} and $\boldsymbol{d}_i$ are generalized coordinates, the time derivative of $\mathbf{KA}(\boldsymbol{o}_i)$ must account for them:

$$\frac{d\boldsymbol{f}_{i+1}(\boldsymbol{o}_i)}{dt} = \frac{d\mathbf{KA}_i(\boldsymbol{o}_i)\delta}{dt} = \begin{bmatrix} \frac{\partial \Phi_{ix}(\boldsymbol{o}_i)}{\partial \boldsymbol{d}_i}\dot{\boldsymbol{d}}_{i+1} & 0 & 0 \\ 0 & \frac{\partial \Phi_{iy}(\boldsymbol{o}_i)}{\partial \boldsymbol{d}_i}\dot{\boldsymbol{d}}_{i+1} & 0 \\ 0 & 0 & \frac{\partial \Phi_{iz}(\boldsymbol{o}_i)}{\partial \boldsymbol{d}_i}\dot{\boldsymbol{d}}_{i+1} \end{bmatrix} \delta_i$$

$$+ \begin{bmatrix} \frac{\partial \Phi_{ix}(\boldsymbol{o}_i)}{\partial \boldsymbol{l}_i}\dot{l}_i & 0 & 0 \\ 0 & \frac{\partial \Phi_{iy}(\boldsymbol{o}_i)}{\partial \boldsymbol{l}_i}\dot{l}_i & 0 \\ 0 & 0 & \frac{\partial \Phi_{iz}(\boldsymbol{o}_i)}{\partial \boldsymbol{l}_i}\dot{l}_i \end{bmatrix} \delta_i + \mathbf{KA}_i\dot{\delta}_i \; ; \qquad \text{(C.7)}$$

$$= \mathbf{KAD}_i[\delta_i]\dot{d}_{i+1} + \mathbf{KAL}_i[\delta]\dot{l}_i + \mathbf{KA}_i\dot{\delta}_i \cdot$$

Here:

$$\mathbf{KAD}_i = \begin{bmatrix} \frac{\partial \Phi_{ix}(\boldsymbol{o}_i)}{\partial \boldsymbol{d}_i} & 0 & 0 \\ 0 & \frac{\partial \Phi_{iy}(\boldsymbol{o}_i)}{\partial \boldsymbol{d}_i} & 0 \\ 0 & 0 & \frac{\partial \Phi_{iz}(\boldsymbol{o}_i)}{\partial \boldsymbol{d}_i} \end{bmatrix}; \qquad \text{(C.8)}$$

and

$$\mathbf{KAL}_i = \begin{bmatrix} \frac{\partial \Phi_{ix}(\boldsymbol{o}_i)}{\partial l_i} & 0 & 0 \\ 0 & \frac{\partial \Phi_{iy}(\boldsymbol{o}_i)}{\partial l_i} & 0 \\ 0 & 0 & \frac{\partial \Phi_{iz}(\boldsymbol{o}_i)}{\partial l_i} \end{bmatrix}. \qquad \text{(C.9)}$$

APPENDIX D: DERIVATIVES INVOLVED IN THE LAGRANGIAN PROCEDURE

As presented in equation (2-64),

$$\ddot{\boldsymbol{q}} = \mathbf{M}^{-1}\boldsymbol{Q} - \mathbf{M}^{-1}\left(\dot{\mathbf{M}}\dot{\boldsymbol{q}} - \frac{1}{2}\frac{\partial(\dot{\boldsymbol{q}}^T\mathbf{M}\dot{\boldsymbol{q}})}{\partial \boldsymbol{q}} + \frac{\partial P_e}{\partial \boldsymbol{q}} + \frac{\partial R_d}{\partial \dot{\boldsymbol{q}}}\right),$$

There are several derivatives to be evaluated. $\dot{\mathbf{M}}$ is the time derivative of coupled mass matrix $\mathbf{M}$ while $\dfrac{\partial(\dot{\boldsymbol{q}}^T\mathbf{M}\dot{\boldsymbol{q}})}{\partial \boldsymbol{q}}$ is a more complex derivative with respect to $\boldsymbol{q}$. Since $\mathbf{M} = (\boldsymbol{R}^v)^T\tilde{\mathbf{M}}\boldsymbol{R}^v$, the time derivative $\dot{\mathbf{M}}$ can be obtained as

$$\dot{\mathbf{M}} = (\dot{\boldsymbol{R}}^v)^T\tilde{\mathbf{M}}\boldsymbol{R}^v + (\boldsymbol{R}^v)^T\dot{\tilde{\mathbf{M}}}\boldsymbol{R}^v + (\boldsymbol{R}^v)^T\tilde{\mathbf{M}}\dot{\boldsymbol{R}}^v \tag{D.1}$$

The next derivative with respect to $\boldsymbol{q}$ is in the form

$$\frac{\partial(\dot{\boldsymbol{q}}^T\mathbf{M}\dot{\boldsymbol{q}})}{\partial \boldsymbol{q}} = \frac{\partial(\dot{\boldsymbol{q}}^T\boldsymbol{R}^{v^T}\tilde{\mathbf{M}}\boldsymbol{R}^v\dot{\boldsymbol{q}})}{\partial \boldsymbol{q}}\,. \tag{D.2}$$

Expanding the expression gives

$$\frac{\partial(\dot{\boldsymbol{q}}^T\mathbf{M}\dot{\boldsymbol{q}})}{\partial \boldsymbol{q}} = \begin{bmatrix} \dot{\boldsymbol{q}}^T\left(\dfrac{\partial \boldsymbol{R}^{v^T}}{\partial \boldsymbol{q}_{11}}\tilde{\mathbf{M}}\boldsymbol{R}^v + \boldsymbol{R}^{v^T}\dfrac{\partial \tilde{\mathbf{M}}}{\partial \boldsymbol{q}_{11}}\boldsymbol{R}^v + \boldsymbol{R}^{v^T}\tilde{\mathbf{M}}\dfrac{\partial \boldsymbol{R}^v}{\partial \boldsymbol{q}_{11}}\right)\dot{\boldsymbol{q}} \\ \vdots \\ \dot{\boldsymbol{q}}^T\left(\dfrac{\partial \boldsymbol{R}^{v^T}}{\partial \boldsymbol{q}_{ij}}\tilde{\mathbf{M}}\boldsymbol{R}^v + \boldsymbol{R}^{v^T}\dfrac{\partial \tilde{\mathbf{M}}}{\partial \boldsymbol{q}_{ij}}\boldsymbol{R}^v + \boldsymbol{R}^{v^T}\tilde{\mathbf{M}}\dfrac{\partial \boldsymbol{R}^v}{\partial \boldsymbol{q}_{ij}}\right)\dot{\boldsymbol{q}} \\ \vdots \\ \dot{\boldsymbol{q}}^T\left(\dfrac{\partial \boldsymbol{R}^{v^T}}{\partial \boldsymbol{q}_{Nn_u}}\tilde{\mathbf{M}}\boldsymbol{R}^v + \boldsymbol{R}^{v^T}\dfrac{\partial \tilde{\mathbf{M}}}{\partial \boldsymbol{q}_{Nn_u}}\boldsymbol{R}^v + \boldsymbol{R}^{v^T}\tilde{\mathbf{M}}\dfrac{\partial \boldsymbol{R}^v}{\partial \boldsymbol{q}_{Nn_u}}\right)\dot{\boldsymbol{q}} \end{bmatrix}. \tag{D.3}$$

Detailed derivation of this matrix is purposely omitted in order to keep the formulation more comprehensible. However, with the above information, one can readily go further to obtain the result either manually or using symbolic manipulation software, for example MAPLE V.